

Copyright © 1979, by the author(s).
All rights reserved.

Permission to make digital or hard copies of all or part of this work for personal or classroom use is granted without fee provided that copies are not made or distributed for profit or commercial advantage and that copies bear this notice and the full citation on the first page. To copy otherwise, to republish, to post on servers or to redistribute to lists, requires prior specific permission.

INFORMAL CONFERENCE ON
PARTICLE AND HYBRID CODES FOR FUSION

by

C. K. Birdsall and A. Friedman
(Coordinators)

Memorandum No. UCB/ERL M79/79

December 10 and 11, 1979

Napa, California

ELECTRONICS RESEARCH LABORATORY
College of Engineering
University of California, Berkeley
94720

Research sponsored by the Department of Energy Contract DE-AS03-76F00034-
DE-AT03-76ET53064.

INFORMAL CONFERENCE ON
PARTICLE AND HYBRID CODES FOR FUSION

December 10, 11, 1979
Napa, California

CONTENTS

- I Purpose
- II Attendees
- III Schedule
- IV Panel Discussion
- V Conclusions; Recommendations
- VI Papers

ACKNOWLEDGMENTS

This conference was conceived during a telephone call with David Nelson at DOE roughly two months ago. His suggestions as to purpose and focus, as well as his active participation in the meetings are acknowledged most gratefully.

My colleague, Alex Friedman, has been invaluable in all stages of conference preparation, from the suggestion of topics to be covered, and their grouping, consultation with many outside Berkeley, LBL, and LLL, the formulation of invitations, to many details of the meeting itself. I am most grateful for his help.

Ginger Fletcher, my part time assistant, devoted nearly all of her time for two months to finding a suitable meeting place near Berkeley (but far enough away to keep participants from straying to LBL, LLL, Stanford etc. during the meetings) for the meetings and a pleasant place for the conference dinner. She also did the typing, letter writing, and mailing to the potential and actual participants (with help from Steve Au Yeung on the initial computer mailing), made many phone calls to ensure that the details of the conference were handled properly, and arranged the get-together Sunday evening. We owe Ginger an immense vote of thanks for her help.

My thanks go to the speakers and panelists for their excellent presentations, which are already stimulating us to better work. The interchange of ideas that was sought was achieved; the interaction with David Nelson that was desired was also achieved.

PURPOSE

This conference was held in order to facilitate an exchange of ideas and results on plasma particle and particle-fluid hybrid codes in an informal, unpublished manner, with frank and open discussion among about fifty people. The only printed record is this collection of copies of transparencies used by the thirty-five speakers. In keeping with this informality, the results presented here are being distributed to the participants only and are not to be quoted without explicit permission from the author.

In December 1974 a similar unpublished conference was held in Berkeley at the request of Robert Price of ERDA. The present conference is a follow-up and is due in large part to the interest of David Nelson (Chief, Fusion Theory and Computer Services Branch, Div. Applied Plasma Physics, Office of Fusion Energy, DOE). Dr. Nelson presented his view from DOE of contributions by computation and simulation toward furthering plasma research leading to fusion reactors; he received considerable feedback from participants. We are most grateful to him for his active and stimulating participation.

The conference is also due to the pressure of accumulated interest among those who work with particle and hybrid codes, who wished to exchange new ideas, methods and results, in an informal setting. By no means was this meeting intended to conflict with the Ninth Conference on Numerical Simulation of Plasmas scheduled for June 30 - July 2, 1980 at Northwestern University, sponsored by Professors J. Denavit and G. Knorr, which covers a much wider area and is to be published.

Lastly, the particle-hybrid code community had concern that the very real contributions of particle and particle-fluid simulations to the understanding of fusion plasmas, in support of both theory and experiment, might just have been underestimated in Washington. This conference is, in part, a reaction to recommendations of the DOE committee for computer time allocations for FY80 which included: major labs receiving 63% of their requests, but universities receiving only 40%; the decision that large particle pushing or kinetic codes can be afforded only sparingly; basic plasma theory was given approximately a 20% absolute cut; ability to follow out unexpected results was cut to a bare minimum; studies of alternate concepts were cut more than were mainline studies. The challenges to the community are clear: make our contributions known; make our codes more efficient in terms useful physics per unit of computer time (optimize, use minimum number of dimensions and particles etc.); check code physics

PURPOSE (continued)

by analysis (time and spatial grid effects, fluctuations) and by comparison with known linear and nonlinear results so as to increase confidence in the simulations.

Editorially we note that the field has matured considerably from the early desk calculator work of Buneman and Hartree on magnetrons in the early 1940's, the one dimensional electrostatic plasma work on modern computers by Buneman and Dawson in the late 1950's, to the current 3d fully electromagnetic codes of Buneman and others. The early art has become more of a science. Simulation for magnetic fusion has now become strongly applications oriented, with DOE devoting the bulk of FY 80 computing resources to the direct support of existing experiments and the design of next generation devices, including calculations of transport, impurities, heating, stability, equilibrium, coil design etc., a milestone indeed. Coupled with this new emphasis is the current plateau in large computer time for magnetic fusion, with no relief planned until at least summer 1981. These factors present a challenge to all of us to be more efficient and more effective in our simulations.

Co-ordinators: C. K. (Ned) Birdsall Alex Friedman
U. C. Berkeley, December 17, 1979

Final Schedule for
Informal Conference on Particle and Hybrid Codes for Fusion
December 10-11, 1979, Napa, California

Conference coordinated by Charles K. (Ned) Birdsall, Alex Friedman, assisted by Ginger Pletcher, at the Electrical Engineering and Computer Science Department, University of California, Berkeley 94720

There will be four main sessions. Talks will be 20, 15 and 10 minutes with adequate time for discussion. If certain subjects draw great interest, additional time will be available.

Of general interest is the efficiency of particle and particle-fluid codes, in terms of physics output per unit of computer resource (time, memory, volume of output, etc.). Of comparable interest is the progress toward working at lower and lower frequencies, with larger mass ratios, etc.

MONDAY, DECEMBER 10

Session IA - 8:30 am to 12:00 noon Chairperson: C. Nielson

- * Long-time-averaging (LTA). Particle simulation of slow transport phenomena.
- * Particle MHD via a vis fluid MHD and other fluid codes.
- * Large time step problems ($m_i/m_e \gg 1$, $\omega \Delta t \gg 1$, digital filtering, stiff equation integrators).

<u>Paper</u>		<u>Page</u>
<u>1</u>	J. Denavit, T. L. Crystal, C. E. Rathmann, J. L. Vomvoridis, "Applications of Long-Time-Scale Particle Simulations."	<u>1</u>
<u>2</u>	B. Cohen, R. P. Freis, T. A. Brengle, "An Orbit-Averaged Particle Code."	22
<u>3</u>	W. Fawley, "Low Pass Filtering in Time."	44
<u>4</u>	D. Anderson, "Toward a Full 3d Hybrid Transport Code."	51
<u>5</u>	T. Tajima, J. M. LeBoeuf, F. Brunel, J. M. Dawson, "Recent Efforts in Particle MHD Code Development."	56
<u>7</u>	H. Okuda, "Steady State Drift Turbulence and Anomalous Diffusion, 3d."	101
<u>6</u>	C. K. Chu, "Vortex Ring Formation by Vortex-in-Cell Method."	93
<u>9</u>	C. Tull, "Code Exchange Mechanics."	121
<u>8</u>	B. McNamara, "Remarks on the Use of Integrals of Motion"	120

CONFERENCE ATTENDEES AND ADDRESSES

Dr. James R. Albritton L-477
Lawrence Livermore Laboratory
P.O. Box 808
Livermore, Ca. 94550

Dr. David Anderson
L-439
Lawrence Livermore Laboratory
Livermore, California 94558

Dr. Robert Berman
36-227
Massachusetts Institute of Technology
Cambridge, Ma. 02139

Dr. Oscar Buneman
ERL
Stanford University
Stanford, California 94305

Dr. Jack Byers
L-439, Bldg. 315, Rm. 285
Lawrence Livermore Laboratory
P.O. Box 808
Livermore, Ca. 94550

Dr. Frank Chambers
L-321
P.O. Box 808
Lawrence Livermore Laboratory
Livermore, Ca. 94550

Dr. C.Z. Cheng
Princeton Plasma Physics Laboratory
Princeton, New Jersey 08590

Dr. Chia K. Chu
Mechanical Engineering Dept.
Columbia University
New York, N. Y. 14850

Dr. Bruce Cohen
L-439, Bldg. 315, Rm. 277
Lawrence Livermore Laboratory
P.O. Box 808
Livermore, Ca. 94550

Dr. Jacques Denavit
Mechanical Engineering Dept.
Northwestern University
Evanston, Ill. 60201

Dr. Adam Drobot
Code 7750
U.S. Naval Research Laboratory
Washington D.C. 20375

Dr. Kent Estabrook
L-477
Lawrence Livermore Laboratory
P.O. Box 808
Livermore, Ca. 94550

Dr. William Fawley
L-439
Lawrence Livermore Laboratory
P.O. Box 808
Livermore, Ca. 94550

Dr. Charles Finan
L-22
Lawrence Livermore Laboratory
P.O. Box 808
Livermore, Ca. 94550

Dr. Bob Fries
L-439
Lawrence Livermore Laboratory
P.O. Box 808
Livermore, Ca. 94550

Dr. Brendan Godfrey
Mission Research Corporation
Santa Barbara, Ca. 94102

Dr. Dennis Hewett
Mail Stop 642
Los Alamos Scientific Laboratory
P.O. Box 1663
Los Alamos, New Mexico 87545

Dr. John Kulp
36-227
Massachusetts Institute of Technology
Cambridge, Mass. 02139

Dr. Bruce Langdon
L-477, Bldg. 381, Room 1228
Lawrence Livermore Laboratory
P.O. Box 808
Livermore, Ca. 94550

Dr. Barbara Lasinski
L-477, Bldg. 381, Room 1232
Lawrence Livermore Laboratory
P.O. Box 808
Livermore, Ca. 94550

Dr. Jae Koo Lee
P.O. Box 81608
General Atomic Company
San Diego, Ca. 92130

Dr. W.W. Lee
Princeton Plasma Physics Laboratory
Princeton, New Jersey 08540

Dr. Paulett Liewer
Physics Department
University of California, Los Angeles
Los Angeles, California 90024

Dr. Irv Lindemuth
Los Alamos Scientific Laboratory
P.O. Box 1663
Los Alamos, New Mexico 87545

Dr. Rodney Mason
Los Alamos Scientific Laboratory
P.O. Box 1663
Los Alamos, New Mexico 97545

Dr. Yoshi Matsuda
L-439
Lawrence Livermore Laboratory
P.O. Box 808
Livermore, Ca. 94550

Dr. Homer Meier
P.O. Box y, Bldg. 9201-2
Oak Ridge National Laboratory
Oak Ridge, Tennessee 37830

Dr. Barry Moore
Austin Research Associates
1901 Rutland Drive
Austin, Texas 78758

Dr. David Nelson
Magnetic Fusion Energy Division
Department of Energy
Germantown, Md. 20767

Dr. William Nevins
L-439
Lawrence Livermore Laboratory
P.O. Box 808
Livermore, Ca. 94550

Dr. Clair Nielson
Group CTR-6
Los Alamos Scientific Laboratory
P.O. Box 1663
Los Alamos, New Mexico 97545

Dr. Hideo Okuda
Princeton Plasma Physics Laboratory
Princeton, New Jersey 08540

Dr. Douglas Potter
Space Sciences Laboratory
University of California, Berkeley
Berkeley, Ca. 94720

Dr. J. W. Foukey
Division 5241
Sandia Laboratories
Albuquerque, New Mexico 87115

Dr. Jeff Quintenz
Division 5241
Sandia Laboratories
Albuquerque, New Mexico 87115

Dr. Abraham Sternlieb
Physics and Astronomy Department
University of Maryland
College Park, Md. 20740

Dr. T. Tajima
Physics Department
University of California, Los Angeles
Los Angeles, Ca. 90024

Dr. Carol Tull
L-402, Bldg. 219, Room 108
Lawrence Livermore Laboratory
P.O. Box 808
Livermore, Ca. 94550

Dr. Thomas Tumolillo
JOYCOR
P.O. Box 370
Del Mar, California 92104

Dr. Dan Winske
University of Maryland
College Park, Md. 20708

Dr. Wee Woo
Applied Science Department
University of California, Davis
Davis, Ca. 95616

YOUR HOSTS Yu Jiuan Chen
Vincent Thomas
Douglas Harned
Stephen Au Yeung
Niels Otani

Dr. C. K. Birdsall
EECS Dept, Cory Hall
University of California, Berkeley
Berkeley, California 94720

Dr. Alex Friedman
EECS Department
Cory Hall, University of California, Berkeley
Berkeley, Ca. 94720

Dr. Tony Lin
Department of Physics
University of California, Los Angeles
Los Angeles, California 90024

Dr. Viktor Decyk
Department of Physics
University of California, Los Angeles
Los Angeles, California 90024

Dr. Robert Huff
Department of Physics
University of California, Los Angeles
Los Angeles, California 90024

Dr. Thomas Oliphant
Los Alamos Scientific Laboratory
P.O. Box 1663
Los Alamos, New Mexico 87545

Dr. Brendon McNamara
L-439
Lawrence Livermore Laboratory
P.O. Box 808
Livermore, Ca. 94550

Dr. Tony Sgro
Los Alamos Scientific Laboratory
P.O. Box 1663
Los Alamos, New Mexico 87545

Thomas Brengle
L-440
Lawrence Livermore Laboratory
P.O. Box 808
Livermore, Ca. 94550

Session IB - 1:30 pm to 5:00 pm Chairperson: C. K. Birdsall

- David Nelson; view from DOE.
- Improvements in simulation 1974 to 1979, and future.
- Code production vs development running times; allocations and priorities.
- Hardware, e.g. array processors, graphics, class VII computers.
- Efficient 3d simulation; 3d grid vs 2d-Fourier representation.

C. K. Birdsall, Comments on 1974 Berkeley Meeting; hopes for this meeting.

Paper

10

D. Nelson, "Role of Particle and Hybrid Codes Present and Future; Computer Availability; Possibility of Adding Special Purpose Computers for Particle Codes."

Page
141

11

A. B. Langdon, "Tradeoffs Among Code Development vs Hardware Costs vs Elapsed Calendar Time; Future Hardware Needs; ZED Postprocessor."

145

12

J. Kulp, "High Performance Array Processor for LIST Machine; Architecture, Impact on Particle Simulation."

152

13

B. Moore, W. Drummond, "Particle Simulation on the VAP."

159

14

T. Brengle, N. Maron, G. Sutherland, "Use of an Array Processor With FDP-10."

165

15

R. Derman, "Macrocell Algorithms for Efficient Particle Pushing, for CRAY and AP in 2d, 2½d, 3d."

168

16

C. Y. Cheng, H. Okuda, "3d Simulation of Trapped Electron Instabilities in Toroidal Systems."

181

17

O. Buneman, "Data Management for a Million-mode 3-d e-m Code; Use of Tetrahedral Mesh."

196

18

T. Tumolillo, "HEEC-3D: Description of an Existing Self Consistent Particle Pusher."

210

TUESDAY, DECEMBER 11

Session IIA - 8:30 am to 12:00 noon Chairperson: J. Denavit

- Linearized codes.
- Modified particle codes (use of linear susceptibility or Boltzmann response, 1d stretched to 2d or 3d).
- Quasineutral, hybrid, and Darwin codes (applications to confinement, compression, equilibrium, stability, and transport).
- Buildup and plasma trapping, neutral beam injection, and wave heating (laser-pellet plasmas, pinches, mirrors, tokamaks).

Paper

Page

<u>19</u>	W. W. Lee, H. Okuda, "Particle Simulation Models for Low Frequency Microinstabilities, $\omega \leq \omega^*$."	233
<u>20</u>	A. G. Sgro, "Hybrid Simulation of Non-MHD Phenomena."	251
<u>21</u>	D. Hewett, "A Global Method of Solving the Electron Field Equations in a Zero-Inertia Electron Hybrid Simulation."	263
<u>22</u>	D. Winske, "Particle Simulation of Reversed Field Configurations."	281
<u>23</u>	R. Mason, "Monte Carlo (Hybrid) Model for Electron Transport in Laser Plasmas."	288
<u>24</u>	J. Byers, "1d Linearized Particle Model for Tandem Mirrors and Field Reversed Mirrors."	301
<u>25</u>	A. Friedman, J. Denavit, R. N Sudan, "Linearized 3d Hybrid Simulations; Ergodic Orbits in Simulation."	320
<u>26</u>	V. Decyk, "Diagnostics for Bounded Plasma, with Applications."	350
<u>27</u>	B. Cohen, N. Maron, G. R. Smith, W. M. Nevins, "DCLC Simulations with a Stretched 1d Code."	365
<u>28</u>	R. Huff, "Particle Hybrid Codes on the CHI Computer."	389

Session IIB - 1:30 pm to 4:00 pm Chairperson: O. Buneman

- Inhomogeneous plasmas (fluctuations, initialization techniques in 2d and 3d).
- Undesirable instabilities in warm plasma simulations (e.g. multi-beam and multi-ring).
- Grid effects (e.g. curvilinear coordinators, div B nonzero).

<u>20</u>	W. Nevins, "Fluctuations in Inhomogeneous Systems."	407
<u>30</u>	V. Thomas, C. K. Birdsall, "Alias Growth in Hybrid Oscillations due to Initiation at $k \Delta x = \pi$."	419
<u>31</u>	A. Drobot, A. Palevsky, "E-M Simulation of Strongly Radiating Systems."	427

<u>32</u>	B. Godfrey, "Electromagnetic Numerical Instabilities in Two-Dimensional Relativistic Beam Simulations."	440
<u>33</u>	A. Sternlieb, "Coupling of Particle Codes to Electric Circuits."	454
<u>34</u>	J. Poukey, J. P. Quintenz, "Preliminary Simulations of Ion Beam Neutralization."	490
<u>35</u>	Y. Chen, "Multi-Beam Instability Interference with Lower Hybrid Drift Instability."	503

4:00 pm to 5:00 pm Moderator: B. Cohen

• Panel Discussion: When to use a particle, fluid, or hybrid code (or none at all). All participants invited to contribute.

Panelists: J. Denavit, A. B. Langdon, B. McNamara, C. Nielson, H. Okuda

IV. Panel Discussion

Plasma simulation is one tool in the attack on understanding plasmas and eventually designing fusion reactors. Simulation using many particles vies for usefulness with simulation using fluids. Particle codes can deliver the full dynamics which is sometimes needed; fluid codes use parameters from theory, particle simulation, and/or experiment, and deliver average or long-term information. Particle-fluid hybrids attempt to use the best features of both, mixing fast and slow time scales. Particle codes, in some quarters, have gained a reputation for using much more computer time per unit of useful physics delivered than used by fluid codes. This reputation is considered undeserved by many particle simulators in most national labs and universities; the opinion may ring true occasionally. Fortunately, particle simulators, especially those with limited budgets, work very hard to optimize their codes, work in the least number of dimensions for the problem at hand, with the least number of particles necessary, and use as much fluid simulation and guide from theory as can be fit in and still do acceptable physics. Those with larger computing budgets, please follow. Generally speaking, the commitment is to the physics sought, and not to the local method or local code available.

Okuda addressed the progress made in understanding anomalous transport indigenous to tokamaks, moving from a early fully dynamic (hence, expensive) model to guiding center electron models in 3d, both electrostatic and magneto-static, with long time steps (less expensive), toward a 3d toroidal model for steady state, including turbulence and transport, poloidal divertors, and hybrid heating.

Denavit observed that hybrid codes, 3d particle codes, with time filtering, long time scales, all appear to be problem dependent. In conflict with this, there is the need for optimization via assembly language, which implies loss of flexibility. We are fortunate, in particle simulation, to be able to work on interesting problems and to obtain useful results. Simulation identifies physical mechanisms, suggests theoretical work and rejects ideas that do not fit.

Nielsen stated that simulation must continue in order to keep theorists honest; simulation is the only economical means of checking theory directly open

* This is a draft from my notes, to be checked over by the panelists before submitting formally to DOE for their internal use. The errors, omissions etc. are mine alone. C.K. Birdsall

Panel Discussion (Continued)

to them. The question is not whether, but how to continue, effectively. We must pay more attention to macroscopic work; as we do, we are likely to find that distinctions between particle and fluid work will disappear. The new hardware is revolutionary, but there still is an open question as to using one big computer or many small machines; his view is that special computers are still too small, too complicated to use.

McNamara presented a list of unresolved problems as follows:

Tokamaks

1. Anomalous electron transport
- is it really classical?
2. Nonlinear effects of ballooning and tearing

Field Reversal

1. Non-axisymmetric states in RFP
2. Equilibria and stability of large orbit FFM

Tandem Mirrors

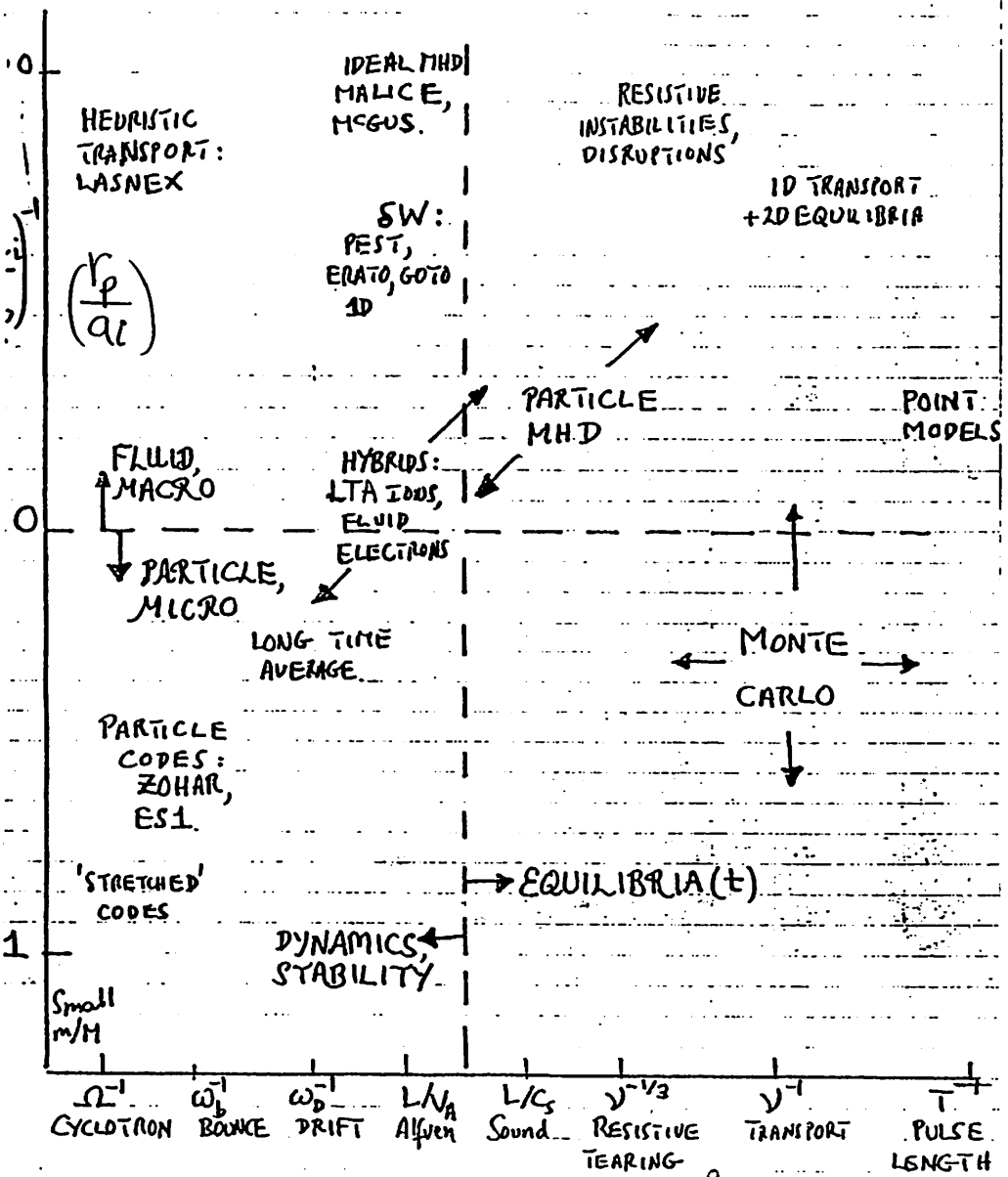
1. Nonlinear saturation of cyclotron modes
2. MHD stability and ballooning
3. Energy transport in tandems, thermal barriers, etc.

plus Computing - an Uppbeat View, as follows:

1. Simulation very effective and increasingly realistic. Therefore, push major design and physics efforts for fusion systems.
2. Provide more software and graphics support for designated activities. -Others benefit by fallout.
3. Encourage more collaboration - from three day advisory groups for new problems to joint efforts and publications.
4. Improve the numerical analysis input - without a \$200K tax to pay for it.
5. Write more reviews of the state of the art and advertise good results more vigorously.
6. LONG TERM GOALS - DESIGN A FUSION REACTOR ! Are we getting there??

plus the Computational Attack on Plasma Parameters, on the attached chart. Note the marriages of all kinds, across fuzzy boundaries: particle plus fluid; micro plus macro; dynamics plus equilibria, etc. McNamara ended with stressing the need for more advertising of accomplishments.

THE COMPUTATIONAL ATTACK ON PLASMA PARAMETERS.



Ω^{-1} CYCLOTRON
 ω_b^{-1} BOUNCE
 ω_D^{-1} DRIFT
 L/V_A Alfvén
 L/C_s Sound
 $\nu^{-1/3}$ RESISTIVE TEARING
 ν^{-1} TRANSPORT
 T PULSE LENGTH

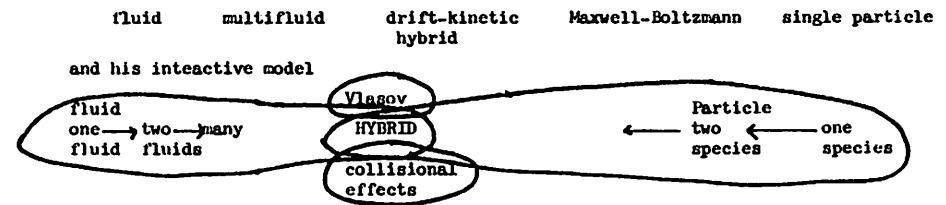
B. McKee

Panel Discussion (continued)

Langdon noted that the MFE computational effect has grown greatly in the last five years. He repeated his advice of the last meeting that, if we want to work with long time scales, then most time integrations will require implicit time averaging, which may not be attractive, but is needed, because explicit methods will end up unstable at large $\omega\Delta t$. He suggests turning to continuum methods for modeling kinetic physics - painful, but needed (Rod Mason has done some, with multigroup transport). He is interested in partially kinetic models.

Cohen concluded the panel discussion with the observations that scaled variables probably always be with us, that having computer variables match experiment is probably impossible in the foreseeable future. He presented a summary of his philosophy on hybrid simulations, attached. (Everyone, please note that Cohen has given good example in this move to more efficient computation.)

Birdsall sketched on the blackboard the DOE hierarchy of models, with increasing expense reading left to right,



making the point that these models interacting are mutually supportive and are seldom wholly independent: over emphasizing one tool or removing another might well reduce the effectiveness of the remaining system.

V. CONCLUSIONS: RECOMMENDATIONS

Many of these are already in the Panel Discussion.

The 1974 conference for the same purposes covered a number of topics which are now pretty well resolved, e.g., particle weighting battles are mostly past, with linear and quadratic weighting widely used and understood (multipole use isolated); hybrid codes were just starting then and now exist in a variety of forms; 3d codes, then done by one or two groups are now done by several; one special purpose computer was mentioned then, with many now.

However, several authors from 1974 gave up-dates in 1979 on problems still not fully resolved, such as linearized particle codes, long-time-scale particle simulations, the plea for use of implicit schemes for large time steps, and 3d economical codes. The 1974 conference called for more use of hybrids (happening), more emphasis on simulations including inhomogeneous density, magnetic field, temperature etc. (happening) and for honest use of two species, large m_i/m_e (happening somewhat). Perhaps the long term needed to resolve these problem areas indicates their toughness and raises the question of pursuing them further - some of them obviously must be.

David Nelson's view from DOE, paper #10, was provocative. The loud and clear messages were that magnetic fusion computing capability is fixed, with no relief expected before 1981, with increasing allocations to device specifics and less to large particle pushing or kinetic codes. His list of problem areas needing more attention was:

Divergors - axi + non axisymmetric sheaths, potentials, boundary layers, ambipolarity,

Plasma edge including shadow of limiter neutrals, atomic physics, reflux, metal surface,

Transport in non axisymmetric systems

RF heating including nonlinear effects

Optimization of gyrotron geometry

Stability of E B T ring-plasma

Formation + tearing problems in RFM, RFSP, spheromak

All the old unsolved problems including bump on tail (α particles)

His cost-hierarchy of models was repeated at the end of the panel write-up; this ranking, while possibly taken as self-evident in some quarters, was not readily accepted by the participants; or, even if accepted in a fuzzy way, it was considered highly undesirable to use in some form of cost-effectiveness argument for and against fluid versus particle simulations. That is, both kinds need the

Hybrid Simulations - Philosophy

Kinetic detail requires particles [or $f(\vec{v})$ description].

$$a_s/R_p = \mathcal{O}(1 \pm)$$

$$a_s \approx v_s/u_{ts}$$

large-orbit equilibrium & transport;
e.g., field reversal

$$a_s/\lambda_{\text{wave}} = \mathcal{O}(1 \pm)$$

$$\lambda_D/L_n = \mathcal{O}(1 \pm)$$

microinstability, e.g., drift waves
sheaths

$$\omega - k v_{||} + l \langle \omega_{ci} \rangle + p \omega_{\text{bounce}} = 0$$

Landau resonance

e.g. wave (\pm) dissipation, trapping
overlap of resonance

When kinetic detail is unnecessary, elimination of particles and fine time & space scales and adoption of fluid description can greatly extend computational power. $m_e/m_i \ll 1$ often separates ions & electrons.

$$\omega/\omega_{cs}, a_s/R_p \ll 1$$

drift approximation

$$\omega/\omega_{cs}, a_s/R_p \gg 1$$

unmagnetized, straight-line orbits

$$\langle v \rangle \ll \omega/k$$

hydro~~magnetic~~^{static}

$$\langle v \rangle \gg \omega/k$$

adiabatic

linear phenomena

linear dielectric, $\chi_s(\omega - i\nu_s, k)$.

Payoff: Analytic reduction of fluid description, appropriate to specific parameter regimes and problems, (1) result in large savings of computer memory & time, and (2) greatly extend the range of parameters accessible to simulation.

Directions: 1. simulation of transport with hybrid orbit-averaged code
2. Hybrid simulation of microinstabilities with more realistic parameters and geometries.

* This is a draft from my notes, to be checked over by the panelists before submitting formally to DOE for their internal use. The errors, omissions etc. are mine alone. CKH

other and the best is in the middle; indeed, the progress made in the past five years and noted in this conference was strong evidence that both kinds of simulations are moving toward particle-fluid hybrids.

A. Bruce Langdon, in Paper #11, made several strong suggestions about doing MFE computing more effectively and more efficiently. Optimization pays off very quickly (he gave experience with ZOHAR showing that optimization paid off almost as it was done!) Optimization must be done selectively, so as not to hurt in making changes (e.g. ZOHAR particle boundary conditions are handled in Fortran). He advocated use of monitor, intervening, postprocessing, and linking to other codes; these rely heavily on interactive codes, sharing the (large) data set of the simulation code, doing considerable computing and driving rapid graphic displays. Postprocessing is very helpful in evoking good physical understanding, such as spectra, filtering, finding spatial and temporal correlations etc. Fast graphic display, like LLL's TMDS, is extremely invaluable. The pitch to MFE was not only to update software, but also to update hardware.

Recommendations are both explicit and implicit in the Panel Discussion and in the above. To all: in computing be more effective, more efficient; in physics, make results better known. To DOE: be more aware of the interactions within the particle simulation-theory-experiment net; be more aware that most particle simulation workers have moved toward particle-fluid models to stay; plug, on your end, for more efficient equipment; include particle simulation people on your computer time allocations committee; reward inventions, like long-time averaging, orbit-averaging, hybrid codes, MHD-particle codes, use of global integrals of motion, use of macrocells, etc., when these result in real savings; keep alive support of the smaller university efforts, which in turn aid much in keeping honest the larger national lab efforts; penalize users with larger budgets who are slow to use new invention to save time (do away with "if you don't use it, you lose it" policy).

①
1. LONG-TIME-SCALE AND LOW-FREQUENCY SIMULATIONS

T.L. Crystal, J. Denavit, C.E. Rathmann, J.L. Vomvoridis
Northwestern University

OUTLINE

1. LONG-TIME-SCALE PARTICLE SIMULATIONS

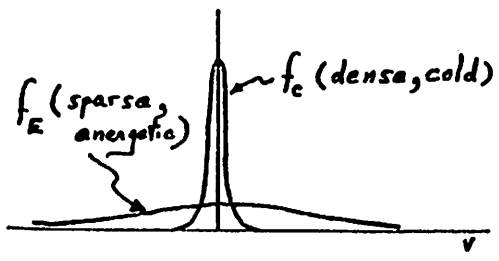
Algorithm
Bump-in-tail instability
Simulations in nonuniform media

2. LOW-FREQUENCY SIMULATIONS

Drift-kinetic equation
Electron trapping and trapped-electron modes
Frequency-domain simulations

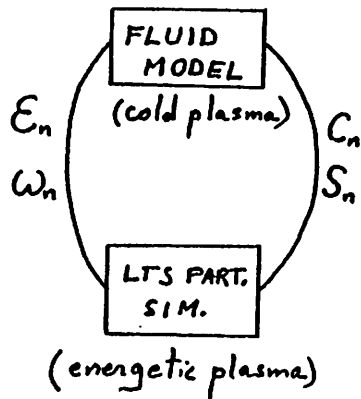
HYBRID REPRESENTATION

TWO-COMPONENT PLASMA



$$E(x,t) = \sum_n E_n \sin(k_n x + \alpha_n(t))$$

$E_n, \omega_n = -\dot{\alpha}_n$ are slowly varying functions of time
 $(\dot{E}_n \ll \omega_n E_n)$



SOURCE TERMS

$$= e \sum_i v_i \frac{\cos}{\sin} (k_n x_i + \alpha_n)$$

FREQUENCY SHIFT:

$$\tilde{\omega}_n = \omega_n - \omega_{pe} = -\frac{C_n}{2 E_n}$$

ENERGY: $S U_n = \frac{E_n}{8\pi} S_n \Delta t$

see: JCP 26, 408, 1978.

$$U_n = \left(\frac{\omega_{pe}^2}{\omega_n^2} + 1 \right) \frac{E_n^2}{8\pi}$$

LTS ALGORITHM

For particle i interacting with wave n :

$$v_i(t') = v_i(t) - \frac{e}{m} \int_t^{t'} E_n \sin \left\{ k_n [x_i(t) + (t''-t)v_i(t'')] + \alpha_n(t) - (t''-t)\omega_n(t) \right\} dt'' + O(E_n^2)$$

$$\Delta v_{in} = \frac{e E_n}{m} \Delta t \left[\cos \psi_{in} \frac{\cos \theta_{in} - 1}{\theta_{in}} - \sin \psi_{in} \frac{\sin \theta_{in}}{\theta_{in}} \right]$$

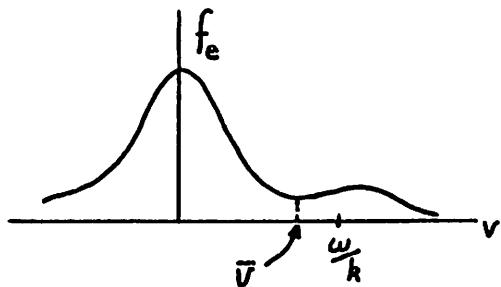
$$\Delta x_{in} = \frac{e E_n}{m} \Delta t^2 \left[\cos \psi_{in} \frac{\sin \theta_{in} - \theta_{in}}{\theta_{in}^2} + \sin \psi_{in} \frac{\cos \theta_{in}}{\theta_{in}^2} \right]$$

$$\theta_{in} = k_n \left(v_i - \frac{\omega_n}{k_n} \right) \Delta t, \quad \psi_{in} = \alpha_n - k_n x_i$$

$\omega_r \Delta t \ll 1$

$$\omega_r = \left(\frac{e E k}{m} \right)^{1/2} \ll \omega_p$$

NONLINEAR SATURATION OF BUMP-ON-TAIL INSTABILITY



$$\omega^2 = \omega_p^2 + 3k^2 V_{th}^2$$

$$\uparrow$$

$$n = n_0(1 + \Delta)$$

$$\Delta \ll 1.$$

$$\frac{E}{k} = \bar{v} \text{ for } \Delta = 0.$$

Saturation theories:

1. O'Neil (PF 14, 1204, 1971)

2. Simon-Rosenbluth (PF 19, 1567, 1976)

$$\omega_r \propto \gamma \quad \omega_r = \left(\frac{eEk}{m}\right)^{1/2}$$

$$\text{or } E \propto \Delta^2$$

$$E \propto \Delta^{1/2}$$

Simulation requirements: (resulting from $\Delta \ll 1$)

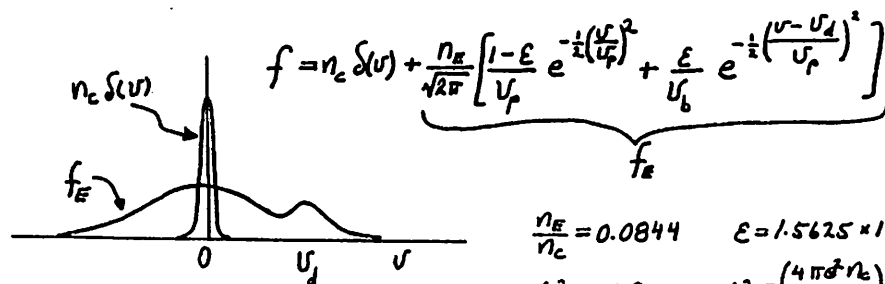
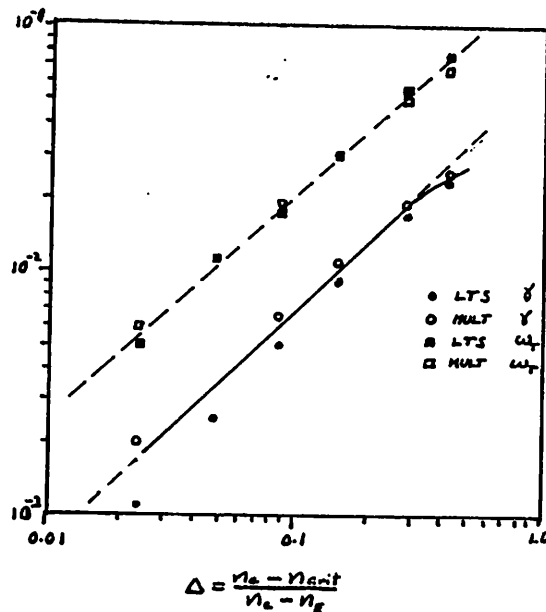
Long times $t_{max} \gg \gamma^{-1} \gg \omega_p^{-1}$ ($t_{max} \sim 10^4 \omega_p^{-1}$)

Low noise level

Fine velocity resolution $\frac{\gamma}{k}, \frac{\omega_r}{k} \ll V_{th}$

$$\Delta x = \frac{\lambda}{62} \quad \Delta v = \frac{V_{th}}{213} \quad \sim 8 \times 10^4 \text{ particles} \quad \Delta t = 2 \omega_p^{-1}$$

SATURATION AMPLITUDE (Collisionless)



$$f = n_c \delta(v) + \frac{n_E}{\sqrt{2\pi}} \left[\frac{1-E}{V_p} e^{-\frac{1}{2} \left(\frac{v}{V_p}\right)^2} + \frac{E}{V_b} e^{-\frac{1}{2} \left(\frac{v-v_d}{V_p}\right)^2} \right]$$

$$t \sim \omega_0^{-1}$$

$$x \sim L$$

$$v \sim v_0 = L \omega_0$$

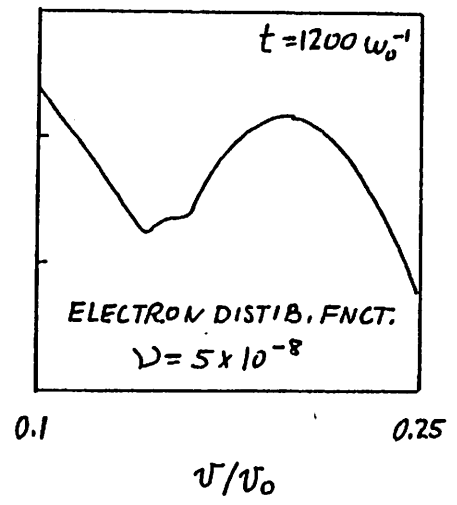
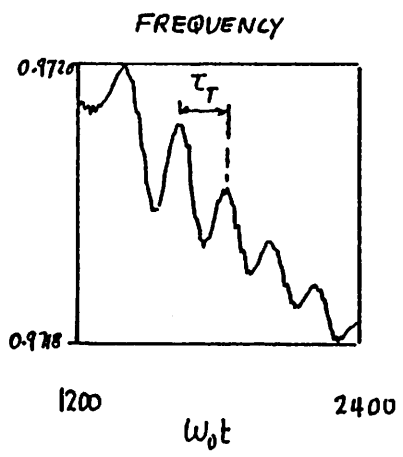
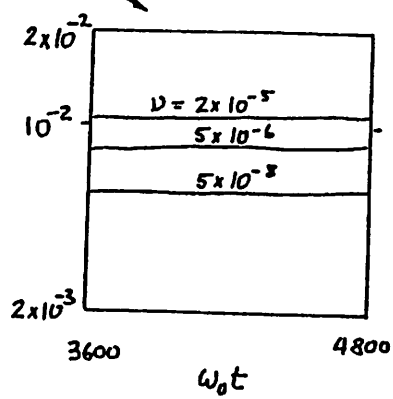
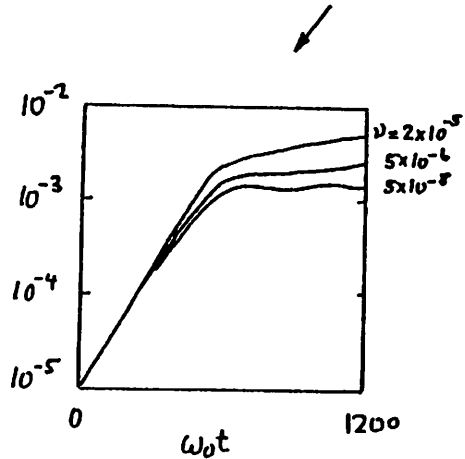
$$\frac{n_E}{n_c} = 0.0844 \quad E = 1.5625 \times 10^{-2}$$

$$\frac{\omega_r}{\omega_0} = 0.9 \quad \omega_c = \left(\frac{4\pi^2 n_c}{m_e}\right)^{1/2}$$

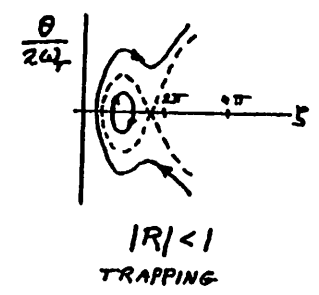
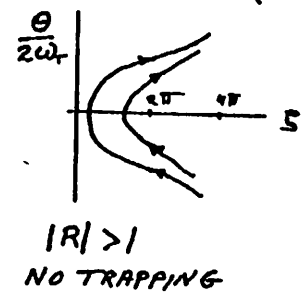
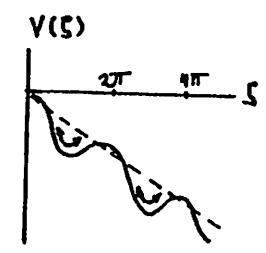
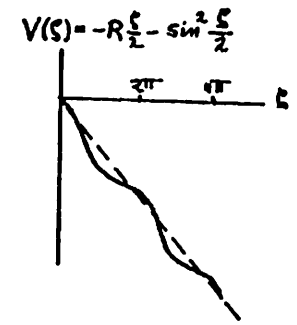
$$V_p = 4.26 \times 10^{-2} V_0 \quad V_b = 2.04 \times 10^{-2} V_0$$

$$v_d = 0.1974 V_0$$

AMPLITUDE VS. TIME



TRAPPING IN NON-UNIFORM MEDIUM
(Whistler mode example)



Inhomogeneity ratio $R = \left(3\nu_T - \frac{kV_z^2}{\Omega}\right) \frac{dQ/dz}{2\omega_T^2}$

NONLINEAR WAVE GROWTH WHEN $R < 1$



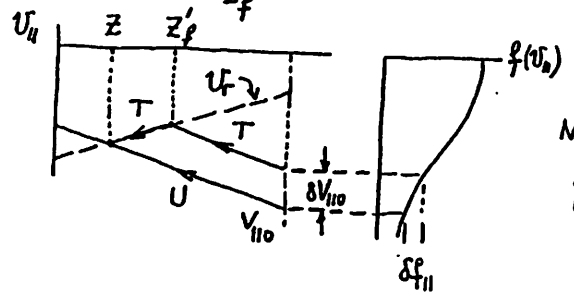
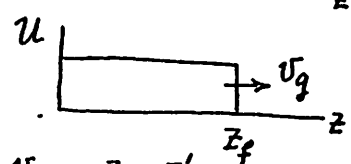
$R > 0$

Linear disp. relation

$$\frac{k^2 c^2}{\omega_p^2} = \frac{\omega}{\Omega - \omega}$$

Resonant velocity

$$v_r = \frac{\omega - \Omega}{k}$$



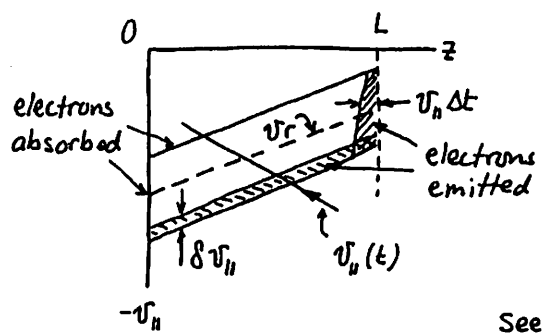
Nonlinear growth rate

$$\gamma_{NL} = \frac{1}{2} \gamma_e R K \omega_e t \sin \bar{s}$$

Simulation particles needed only in band

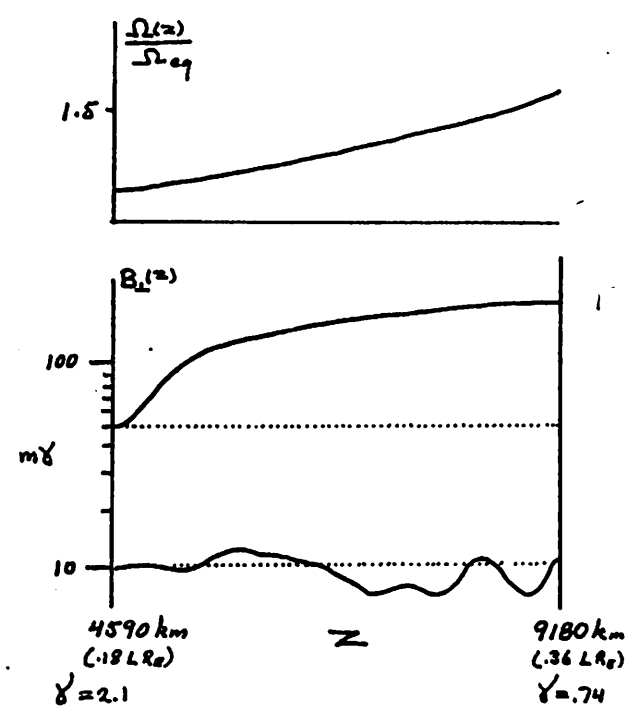
$$v_r \pm n v_t \quad n \sim 3$$

Note: For $\nabla \Omega \neq 0$ particles leaving resonant region do not return



See: PF 22, 367 (1979)
PF Jan 1980

EXAMPLE



$$\frac{\omega_p}{\Omega_0} = 8.25$$

$$\frac{nE}{n_0} = 5 \times 10^{-4}$$

$$\Delta t = 16.6 \Omega_0^{-1}$$

$$\frac{\omega}{\Omega_0} = 0.5$$

$$T_e = 30 \text{ keV}$$

$$t_{max} = 7207 \Omega_0^{-1}$$

$$T_{ii} = 6 \text{ keV}$$

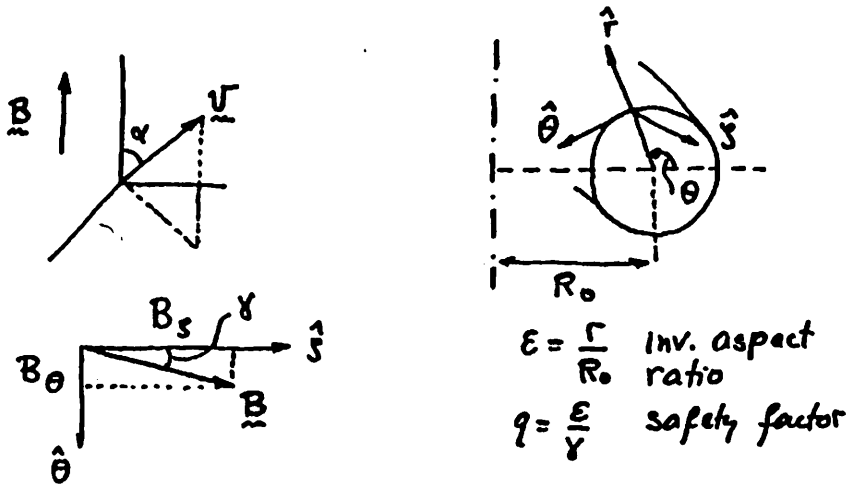
$$\Delta z = 180 \frac{c}{\omega_p}$$

$$\frac{\omega_T}{\Omega_0} = 4.85 \times 10^{-3} \quad (10.84)$$

$$\frac{\gamma_e}{\Omega_0} = 10^{-4}$$

$$\frac{\gamma_e}{\omega_T} = 0.02 \quad (10.01)$$

LINEARIZED DKE FOR ELECTRONS



$$\frac{\partial f}{\partial t} + v \cos \alpha \frac{1}{r} \left(\gamma \frac{\partial}{\partial \theta} + \epsilon \frac{\partial}{\partial s} \right) \left(f - \frac{e\varphi}{T_e} f^0 \right) + \frac{\epsilon v \gamma \sin \theta \sin \alpha}{r} \frac{\partial f}{\partial \alpha} + \frac{v_{th}^2}{L_n \Omega} \left[1 + \gamma \left(\frac{\epsilon}{T_e} - \frac{3}{2} \right) \right] f^0 \frac{\epsilon}{\gamma r} \frac{\partial}{\partial s} \left(\frac{e\varphi}{T_e} \right) + \frac{\epsilon v^2 (1 + \cos^2 \alpha)}{2 r^2 \Omega} \cos \theta \frac{\partial}{\partial \theta} \left(f - \frac{e\varphi}{T_e} f^0 \right) = \frac{\nu(v)}{\sin \alpha} \frac{\partial}{\partial \alpha} \left(\sin \alpha \frac{\partial f}{\partial \alpha} \right)$$

$$L_n = \frac{\nabla n}{n}, \quad \gamma = \frac{n}{T_e} \frac{\nabla T_e}{\nabla n}$$

FOURIER-TRANSFORMED DKE

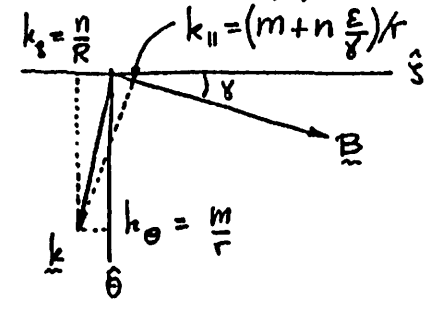
θ and s : $e^{i(m\theta + ns)}$

$$\frac{\partial f_m}{\partial t} = -i v u k_{||} g_m + i \frac{\epsilon v (1-u^2)}{4} \frac{\partial}{\partial u} (g_{m+1} - g_{m-1}) - i \frac{v_D}{\gamma} \left[1 + \gamma \left(v^2 - \frac{3}{2} \right) \right] (m - k_{||}) \varphi_m f^0 - i \frac{v^2 (1+u^2)}{4 \gamma} \left[(m+1) g_{m+1} + (m-1) g_{m-1} \right] \epsilon \frac{f_e}{r} + \nu \frac{\partial}{\partial u} (1-u^2) \frac{\partial g_m}{\partial u}$$

where:

$g_m = f_m - \varphi_m f^0$ (non-adiabatic part of electron d.f.)

velocity $\sim v_{th}$
length $\sim r/\gamma$
time $\sim r/\gamma v_{th}$
potential $\sim T_e/e$



See: P.F. 21, 1533 (1978)
also T.L. Crystal and J. Denavit
"Curvature and Gradient Drift Effects on Trapped-Electron Modes"
(Submitted to PF)

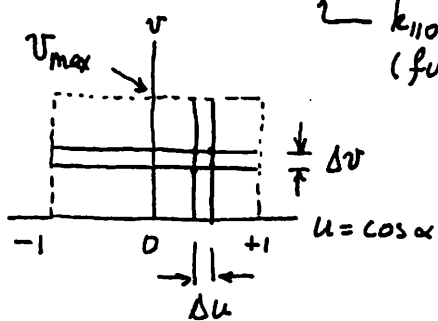
NUMERICAL SOLUTION

Single toroidal mode: n

Multiple poloidal modes: $m = m_0 + l$
 $l = 0, \pm 1, \dots, \pm l_{max}$

$$k_{||} = m_0 + n \frac{\epsilon}{r} + l$$

$k_{||0}$: const. for local approx
 (funct. of r in non-loc. comput.)

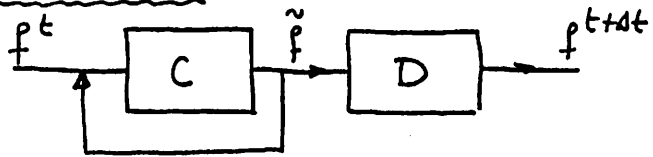


Trapping, drift, ψ -terms
 (iteration)

$$\frac{\partial f_m}{\partial t} = -i v u k_{||} f_m + C + D$$

← veloc. diffusim (collisions)

Split time step:



Collisionless Implicit diffusim algorithm

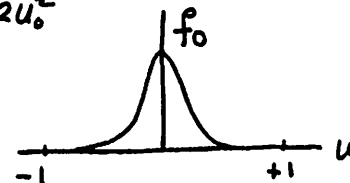
See J.C.P (Awaiting publication)
 "Computer Sim. of Trapped-Electron Modes in Tokamaks"

UNPERTURBED ELECTRON TRAPPING

$$(\psi_m = 0, n = 0, m_0 = 0)$$

Monoenergetic initial d.f.

$$f_0(v, u, t=0) = \frac{\delta(v-v_0)}{(2\pi)^{3/2} v^2} e^{-\frac{u^2}{2u_0^2}}$$



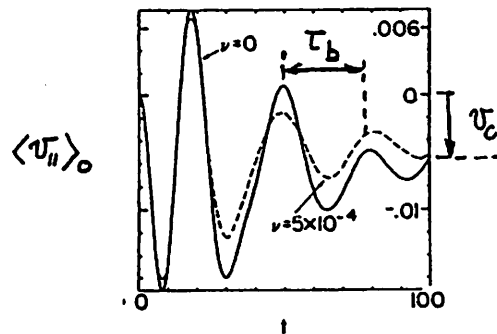
$f_m = 0$ for $m \neq 0$

$$u_0 = \frac{\epsilon^{1/2}}{2^{3/4}} \quad (\text{primarily trapped electrons})$$

$\gamma = 0.1$

$\epsilon = 0.1$

$\frac{\rho_e}{r} = 0.1$

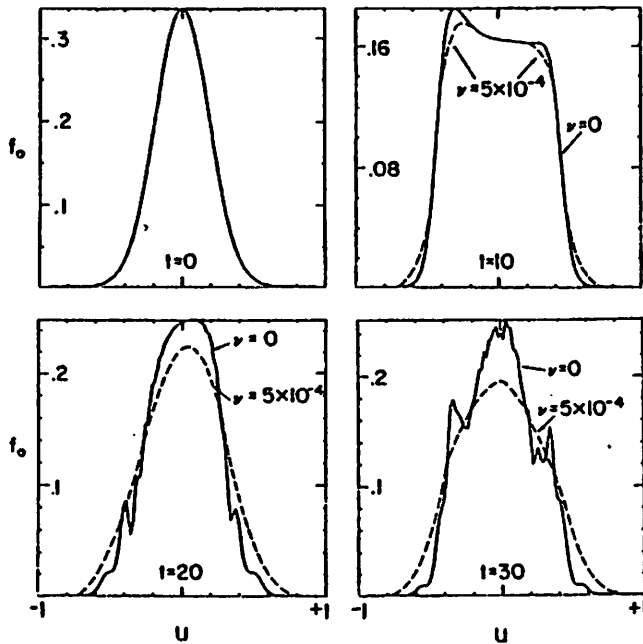


$$T_b = \frac{2\pi}{\omega_b} = 33.4$$

(theory)

Note: Collisionless comput. require $l_{max} \approx 10$
 For $\nu = 5 \times 10^{-4}$, convergence with $l_{max} = 4$.

PITCH-ANGLE DISTRIBUTION



$\epsilon = 0.1, \gamma = 0.1, \frac{P_e}{F} = 0.1$

SOLVING FOR THE POTENTIAL

Poisson eq.

$$\varphi_m = \frac{1}{k^2 \lambda_D^2} (N_m^i - N_m^e)$$

Ion drift motion ($\omega \ll \Omega_i$)

$$\vec{v}_i = \frac{c}{B} \frac{\partial \varphi}{\partial \theta} \hat{r} \Rightarrow \frac{dN_m^i}{dt} = -i \frac{m v_D}{\gamma} \varphi_m$$

or:

$$\frac{d\varphi_m}{dt} + \frac{i \gamma v_D}{m^2 \lambda_D^2} \varphi_m = \frac{i \gamma^2}{m^2 \lambda_D^2} [k_n \langle v_{||} \rangle_m - \frac{\epsilon}{k} (\langle v_{||} \rangle_{m+1} - \langle v_{||} \rangle_{m-1})] + i \frac{\epsilon f_e}{\gamma r} [(m+1)(W_{m+1} - \varphi_{m+1}) + (m-1)(W_{m-1} - \varphi_{m-1})]$$

$$\langle v_{||} \rangle_m = 2\pi \int u v^3 f_m dv, \quad W_m = \frac{1}{2} \int (1+u^2) v^4 f_m dv$$

High-frequency: $\omega_h = \frac{k v}{k} \omega_{pe}$

Convergence of iteration:

$$\delta = \frac{\omega_h \Delta t}{2} < 1$$

Numerical growth rate:

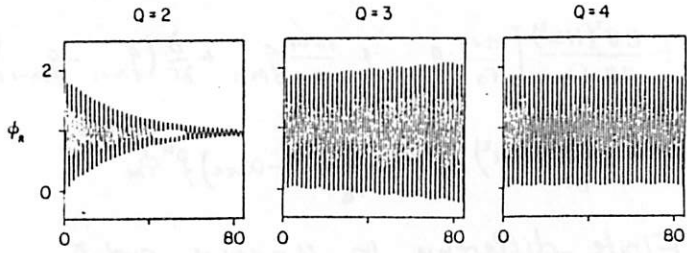
$$\Gamma_Q = -\frac{(-\delta)^Q}{\Delta t} : \begin{cases} \text{Stable for } Q = 2, 4, \dots \\ \text{Unstable for } Q = 1, 3, \dots \end{cases}$$

NUMERICAL STABILITY TESTS

$m = 10$
 $\gamma = 0.1$
 $\lambda_D = 2 \times 10^{-3}$
 $k_{||} = 1.0$
 $\Delta t = 0.2$



$\omega_h = 2.89$
 $\delta = 0.289 < 1$



$T_2 = -0.0347$

STABLE

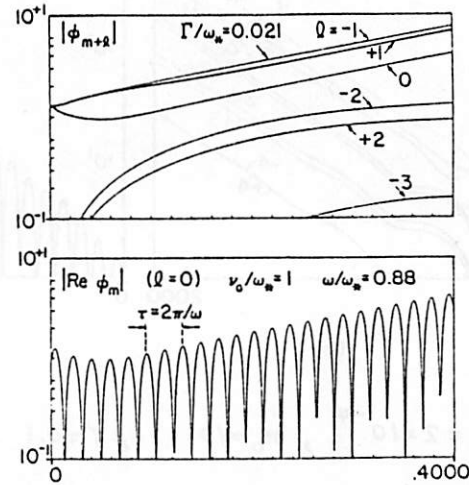
$T_3 = 0.0029$

UNSTABLE

$T_4 = -0.00024$

STABLE

DISSIPATIVE TRAPPED-ELECTRON INSTABILITY $(\beta_e / \Gamma = 0)$

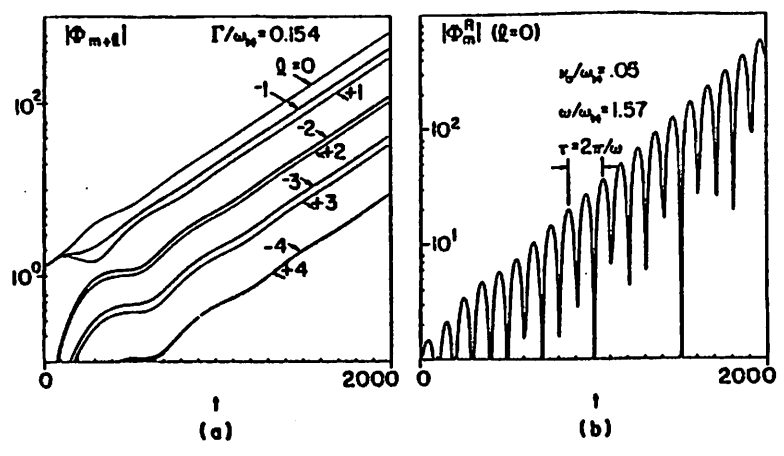


$v_D = 2 \times 10^{-4}$, $m_e = 10$, $\gamma = 0.1$, $\lambda_D = 2 \times 10^{-3}$

$k_{||0} = 0.1$, $q = 1$, $\epsilon = 0.2$, $l_{max} = 4$

$$v = \frac{v_D}{\left(\frac{1+v^2}{2}\right)^{3/2}} , \quad v_D = v_* = \frac{m_e v_D}{\gamma} = 0.02$$

MAGNETIC DRIFT INSTABILITY ($\beta_e / r = 7 \times 10^{-4}$)



$v_D = 2 \times 10^{-4}$, $m_0 = 10$, $\gamma = 0.1$, $\lambda_D = 2 \times 10^{-3}$
 $k_{H0} = 0.1$, $\eta = 1$, $\epsilon = 0.2$, $l_{max} = 4$
 $\nu = \frac{\nu_0}{(\frac{1+\nu^2}{2})^{3/2}}$, $\nu_0 = \omega_{ce} / 20$

FREQUENCY-DOMAIN COMPUTATIONS (including radial dependence)

Electron DKE:

Let $g_m = f_m - \frac{e}{T_e} \psi f_m^0$ Non-adiabatic part of distribution function

$$\begin{aligned}
 & [\omega - u v k_{||}(r)] g_m + \frac{(1-u^2) \delta \epsilon v}{4 r_0} \frac{\partial}{\partial u} (g_{m+1} - g_{m-1}) \\
 & + \frac{\epsilon v^2 (1+u^2)}{4 r_0 \Omega_e} \left[\frac{m+1}{r_0} g_{m+1} + \frac{m-1}{r_0} g_{m-1} + \frac{\partial}{\partial r} (g_{m+1} - g_{m-1}) \right] \\
 & + i \nu \frac{\partial}{\partial u} (1-u^2) \frac{\partial g_m}{\partial u} = \frac{e}{T_e} (\omega - \omega_{ce}) f_m^0 \phi_m
 \end{aligned}$$

Finite-difference in $u = \cos \alpha$ and δ

$g_m(k \Delta u, j \Delta v, r) = g_{j,p}(r)$

$p = (2l_{max} + 1)k + m - m_0$

Band-matrix sol

$$\begin{aligned}
 & \begin{matrix} \xrightarrow{2l_{max}+1} \\ \left[\begin{array}{c} 0 \\ \vdots \\ 0 \end{array} \right] \times \left[\begin{array}{c} g \\ g_m \end{array} \right] = \left[\begin{array}{c} \frac{e}{T_e} (\omega - \omega_{ce}) f_m^0 \phi_m \end{array} \right] \\ \xleftarrow{2l_{max}+1} \end{matrix} \Rightarrow \frac{N_m^e}{N_0} = \frac{e \phi_m}{T_e} + \underbrace{\int g_m dv}_{S_m}
 \end{aligned}$$

IONS: GYROKINETIC "SLAB" MODEL
(with $k_r \rho_i \ll 1$)

$$\frac{n_m^i}{N_0} = -\frac{e}{T_e} \left[T_0 + (T_0 - T_1) \rho_i^2 \frac{\partial^2}{\partial r^2} \right] (\tau S_i + S_{xi}) Z(s) \phi_m + \eta_i (\dots)$$

$$S_{xi} = \frac{\omega_{*i}}{\sqrt{2} |k_{ri}| v_i}, \quad \tau = \frac{T_e}{T_i}$$

$$S_i = \frac{\omega}{\omega_{*i}} S_{xi}, \quad T_0 = I_0(b_y) e^{-b_y}, \quad T_1 = I_1(b_y) e^{-b_y}, \quad b_y = \rho_i^2 k_\theta^2$$

Ion-point distance: $S_{xi} = 1 \Rightarrow \Delta r^{ion} = \frac{\tau}{\sqrt{2} \gamma_0} \frac{L_q}{L_n} \rho_i$

Note: $\frac{\Delta r^{ion}}{\Delta r^{rat}} = \frac{\tau}{\sqrt{2}} \frac{1}{\gamma_0} \frac{r}{L_n} \rho_i k_\theta$
 Rational surfaces separation

$$\left(L_q^{-1} \equiv \frac{1}{q} \frac{dq}{dr} \right)$$

$$\Delta r^{rat} = \frac{1}{m_0} \frac{1}{q}$$

RADIAL MODE EQUATIONS

$$\frac{d^2 \phi_m}{dr^2} = \frac{S_m + 1 + \tau + T_0 (\tau S_i + S_{xi}) Z(s_i)}{\rho_i^2 (T_0 - T_1) (\tau S_i + S_{xi}) Z(s_i)}$$

$$m = m_0 + l, \quad l = 0, \pm 1, \dots, \pm l_{max}$$

Symmetries:

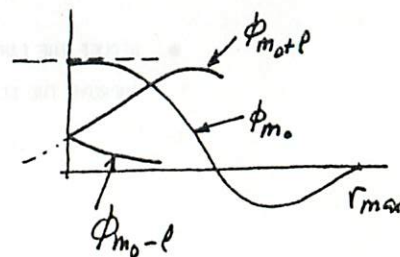
$$\phi_{m_0-l}(\delta r) = \phi_{m_0+l}(-\delta r), \quad \phi_{m_0+l}'(\delta r) = -\phi_{m_0+l}'(-\delta r)$$

Numerical integration in r by finite differences with two-point boundary conditions (SUPPORT code)

At $r=r_0$: $\phi_{m_0} = 1$, $\phi_{m_0-l} = \phi_{m_0+l}$, $\phi_{m_0+l}' = 0$ (all l 's)
 At $r=r_{max}$: $\phi_{m_0+l} = 0$ (all l 's)
 $\phi_{m_0}' = 0$, $\phi_{m_0-l}' = -\phi_{m_0+l}'$

Frequency determined to satisfy condition $\phi_{m_0}' = 0$

- (a) Iterations (Muller method)
- (b) Nyquist-type plots $\phi_{m_0}'(\omega)$ vs. $\text{Re } \omega$



2. ORBIT-AVERAGED PARTICLE CODES

BRUCE COHEN, TOM BRENGLE, AND BOB FREIS
LAWRENCE LIVERMORE LABORATORY
MFE

GOAL: PERFORM NUMERICALLY STABLE AND ACCURATE
PARTICLE SIMULATIONS OF VERY SLOWLY VARYING PHENOMENA
WITHOUT LOSS OF KINETIC DETAILS, I.E.

- FILTER HIGH FREQUENCY SELF-CONSISTENT FIELD CHANGES;
- FOLLOW PARTICLE ORBITS ON THEIR NATURAL TIME SCALE;
- AVERAGE PARTICLE CURRENTS AND CHARGE DENSITIES OVER MANY ORBIT TIMES; AND
- SOLVE FOR THE SELF-CONSISTENT FIELDS MUCH LESS OFTEN THAN ADVANCING THE PARTICLES SO AS TO
- REDUCE THE PARTICLE STATISTICAL REQUIREMENT AND IMPROVE THE ECONOMICS OF THE SIMULATION.

E.G. ORBIT-AVERAGED MAGNETO-INDUCTIVE CODES

2D SUPERLAYER AND ID MAGIC

- MAGNETO-INDUCTIVE PHYSICS MODEL

$$\nabla \times \vec{B} = 4\pi \vec{J} + \frac{\partial \vec{E}}{c \partial t} \quad n_i = n_e$$

$$\nabla \times \vec{E} = -\frac{\partial \vec{B}}{c \partial t}$$

$\vec{J} \approx \vec{J}_i$ ELECTRONS ARE COLD IONS: $\vec{f} = m_i \vec{a}$
OPEN MAGNETIC FIELD LINES TERMINATE ON
CONDUCTORS WHICH SHORT-OUT $\nabla \phi \perp \vec{B}_0$

IF MAGNETIC FIELD LINES CLOSE, AS IN FIELD-REVERSAL,
ELECTROSTATIC AND ELECTRON DYNAMICAL EFFECTS MUST BE
INCLUDED. \vec{J}_e MAY NO LONGER BE NEGLIGIBLE.

SUPERLAYER - J.A. BYERS, PHYS. REV. LETT. 39, (1977), 1476

MAGIC - T.A. BRENGLE & B.I. COHEN, UCID-17795 Rev.1 (1978)

Magneto-Inductive Algorithm

- Advance particles on micro time step Δt

$$\vec{v}^{n+1/2} = \vec{v}^{n-1/2} + \sum_j^{\text{grid}} \frac{e}{m} \Delta t S_j^n [\vec{E}_j + (\frac{\vec{v}^{n+1/2} + \vec{v}^{n-1/2}}{2c}) \times \vec{B}_j] - \text{drag} \pm RF \dots$$

$$r^{n+1} = [(r^n + v_r^{n+1/2} \Delta t)^2 + (v_\theta^{n+1/2} \Delta t)^2]^{1/2}$$

$$z^{n+1} = z^n + v_z^{n+1/2} \Delta t$$

where $S_j^n \equiv$ grid interpolation factor for \vec{x}^n and x_j^{grid} .

We use Boris' scheme - 2nd order, leapfrog

- Accumulate J_θ from ions at each Δt

$$J_{\theta j}^{n+1/2} = \frac{e}{2} \sum_i^{\text{ions}} (S_j^n v_{\theta i}^{n+1/2} + S_j^{n+1} v_{\theta i}^{n+1/2})$$

or

$$J_{\theta j}^n = \frac{e}{m} \sum_i^{\text{ions}} S_j^n (\mathcal{L}_{\theta i} - \frac{e}{c} \sum_l^{\text{grid}} S_l^n \psi_l) \approx \frac{e}{m} \sum_i^{\text{ions}} S_j^n (\mathcal{L}_{\theta i} - \frac{e}{c} \psi_j)$$

where $\mathcal{L}_{\theta i} \equiv$ canonical angular momentum

and $\psi \equiv r A_\theta \propto$ the magnetic flux

- Average J_θ in time over macro time step $\Delta T \gg \Delta t$

$$\langle J_\theta \rangle^{M+1/2} = \frac{\sum_{n'=0}^{N-1} W(n'-N/2) J_\theta^{M\Delta T + n'\Delta t}}{\sum_{n'=0}^{N-1} W(n'-N/2)}$$

$N \equiv \Delta T / \Delta t$

$W \equiv$ data window and digital smoothing factor

- Solve Maxwell's equations for \vec{E} and \vec{B} using $\langle J_\theta \rangle$

$$\left(\nabla_{r^2}^2 - \frac{1}{r^2} \right) \begin{bmatrix} \frac{\psi}{r}^{M+1/2} \text{ predictor} \\ \text{or} \\ \alpha \frac{\psi}{r}^{M+1} + (1-\alpha) \frac{\psi}{r}^M \text{ corrector} \end{bmatrix} = -\frac{4\pi}{c} \langle J_\theta \rangle^{M+1/2}$$

$$\vec{B} = \nabla \times (\psi \hat{e}_\theta / r) + \vec{B}_0$$

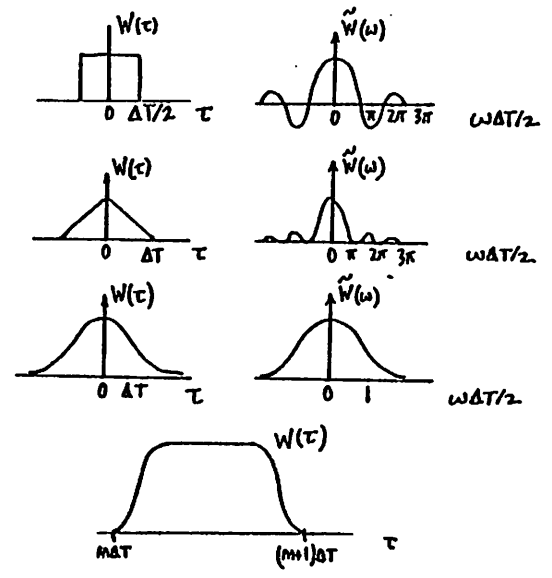
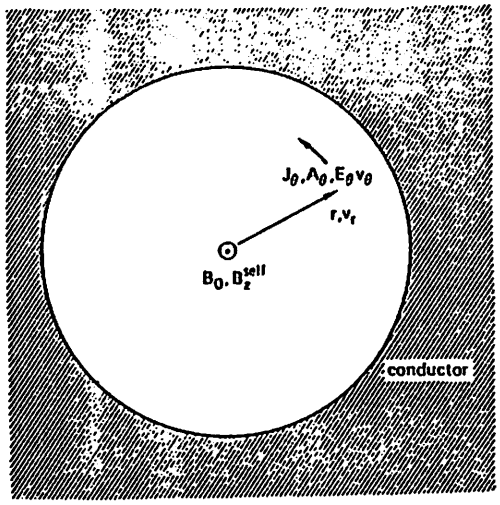
$$\beta E_\theta^{M+1/2} + (1-\beta) E_\theta^M = -\frac{1}{c\Delta T/2} (\psi/r^{M+1/2} - \psi/r^M) \quad \text{predictor}$$

$$\text{and } (M+1/2, \Delta T/2) \rightarrow (M+1, \Delta T) \quad \text{corrector}$$

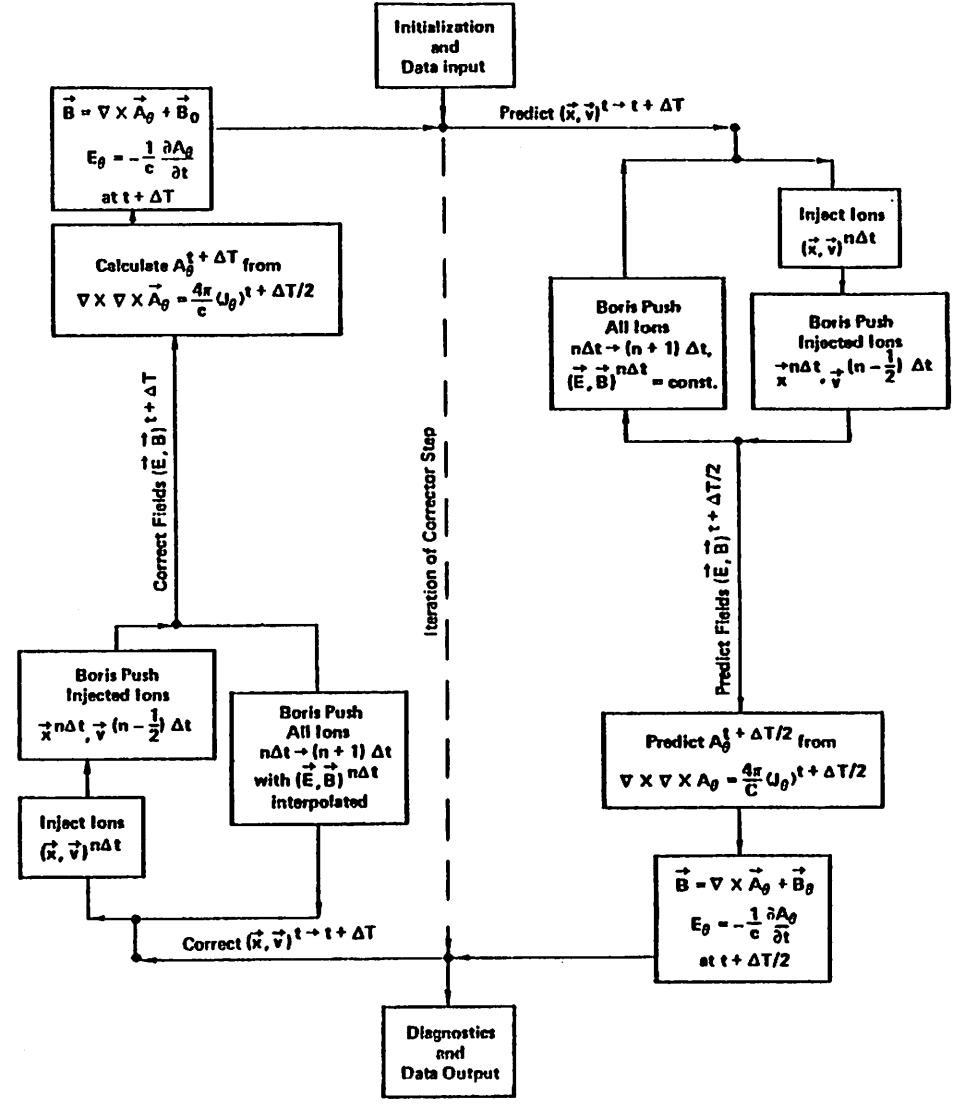
$\alpha, \beta \equiv$ centering parameters, $\frac{1}{2} \leq \alpha, \beta \leq 1$, control damping

- Advance particle velocities with $(\vec{E}, \vec{B})^{M\Delta T}$

$$(\vec{E}, \vec{B})^{M\Delta T} \xrightarrow{\text{interpolation/extrapolation}} (\vec{E}, \vec{B})^{n\Delta t}$$



Flow Chart for Magneto-Inductive Code with Orbit Averaging and Time Splitting



Finite Δt Considerations - Model Algorithms

Normal mode analysis, slab geometry, cold plasma and no averaging

- $J_y \propto v_y$ algorithm (linearized)

$$\partial_x^2 [\alpha A_y^{n+1} + (1-\alpha) A_y^n] = -4\pi n_0 e v_y^{n+1/2}$$

$$\beta E_y^{n+1} + (1-\beta) E_y^n = -\frac{1}{c\Delta t} (A_y^{n+1} - A_y^n)$$

$$v_x^{n+1/2} - v_x^{n-1/2} = \omega_{ci}^0 \frac{\Delta t}{2} (v_y^{n+1/2} + v_y^{n-1/2})$$

$$v_y^{n+1/2} - v_y^{n-1/2} = \frac{e\Delta t}{m_i} E_y^n - \omega_{ci}^0 \frac{\Delta t}{2} (v_x^{n+1/2} + v_x^{n-1/2})$$

Fourier transform $(x,t) \rightarrow (k,\omega)$ and ignore aliases

- i. $\omega_{ci}^0 \Delta t/2 \ll 1$, two branches

- compressional Alfvén wave: $\text{Re } \omega \sim \frac{\pm k v_A}{(1+k_x^2 c^2/\omega_{pi}^2)^{1/2}}$

damping for $\alpha + \beta > 1$, $\text{Im } \omega \sim -\frac{1}{2\Delta t} \frac{(\text{Re } \omega \Delta t)^2 (\alpha + \beta - 1)}{1+k_x^2 c^2/\omega_{pi}^2}$

- even-odd oscillation $\omega \Delta t = \pm \pi + i \ln \left[\frac{2-\alpha-\beta + \frac{\omega_{pi}^2}{(\alpha+\beta-1)k_x^2 c^2}}{\alpha+\beta-1} \right]$
 may be stable or unstable

- ii. $\alpha = \beta = 1/2$ (no damping) and $\omega_{ci}^0 \Delta t/2 \ll 1$

$$\tan^2 \omega \Delta t/2 \approx \begin{cases} \frac{k_x^2 v_A^2 \Delta t^2/4}{1+k_x^2 c^2/\omega_{pi}^2} & \text{Alfvén branch} \\ - (1+k_x^2 c^2/\omega_{pi}^2) & \text{even-odd instability} \end{cases}$$

- $J_y \propto \frac{e}{m} (P_y - \frac{e}{c} A_y)$ algorithm (linearized)

$$\partial_x^2 A_y^n = -\frac{4\pi n_0 e}{mc} (P_y - \frac{e}{c} A_y^n - \frac{e}{c} B_0 x^n)$$

$$v_y^{n+1} = v_y^n + \frac{e}{mc} (A_y^n - A_y^{n+1}) + \frac{e B_0}{mc} (x^{n+1} - x^n)$$

$$v_x^{n+1/2} = v_x^{n-1/2} + \frac{\omega_{ci}^0 \Delta t}{2} (v_y^{n+1/2} + v_y^{n-1/2})$$

$$x^{n+1} = x^n + v_x^{n+1/2} \Delta t$$

Normal modes satisfy

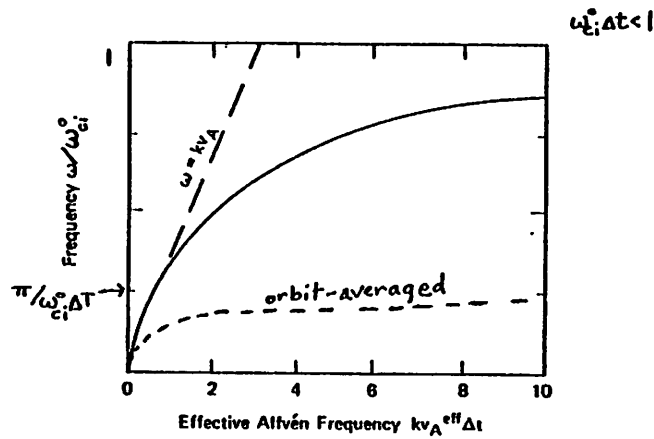
$$\tan^2 \omega \Delta t/2 = \frac{k_x^2 v_A^2 \Delta t^2/4}{1+(\omega_{ci}^0 \Delta t/2)^2 + k_x^2 c^2/\omega_{pi}^2} \quad \text{Alfvén branch}$$

§ no extraneous even-odd oscillation

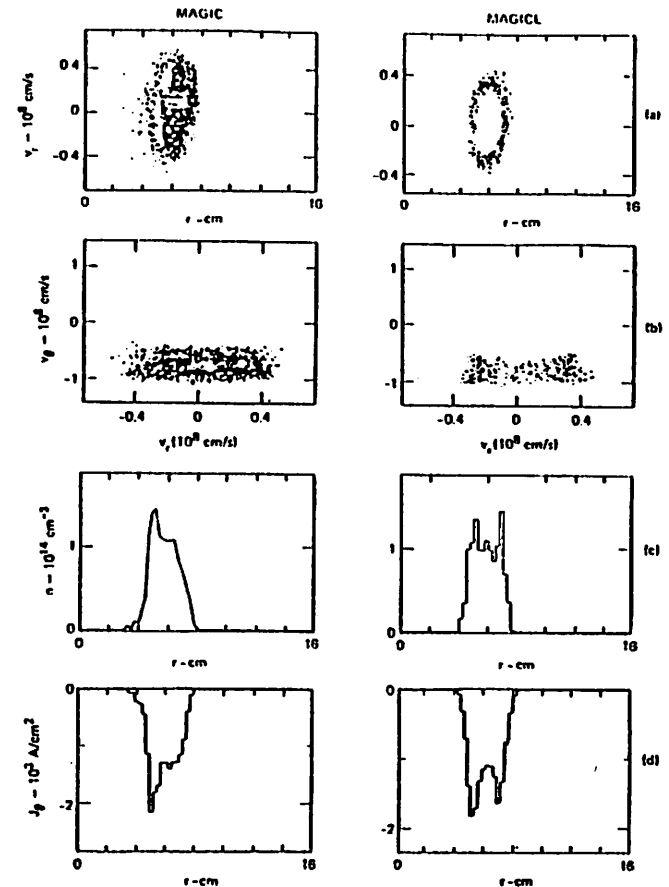
When both algorithms are orbit-averaged, the $J_y - P_y$ algorithm should be more stable than $J_y - v_y$.

1-D Magneto-Inductive Simulations (r, v_r, v_θ)
MAGIC and MAGICL (orbit-averaged)

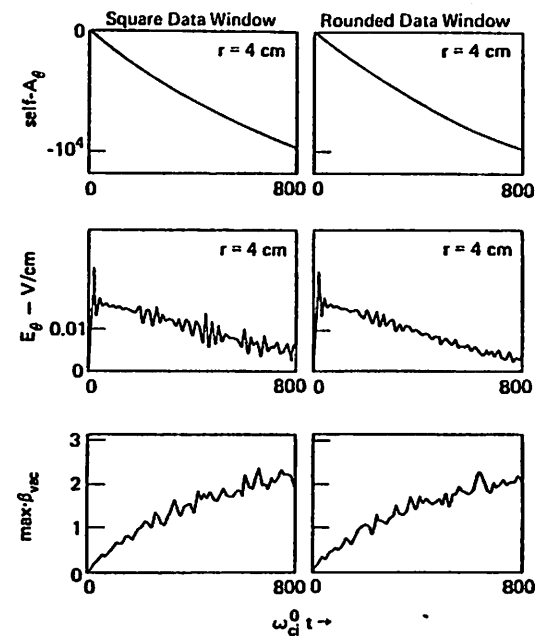
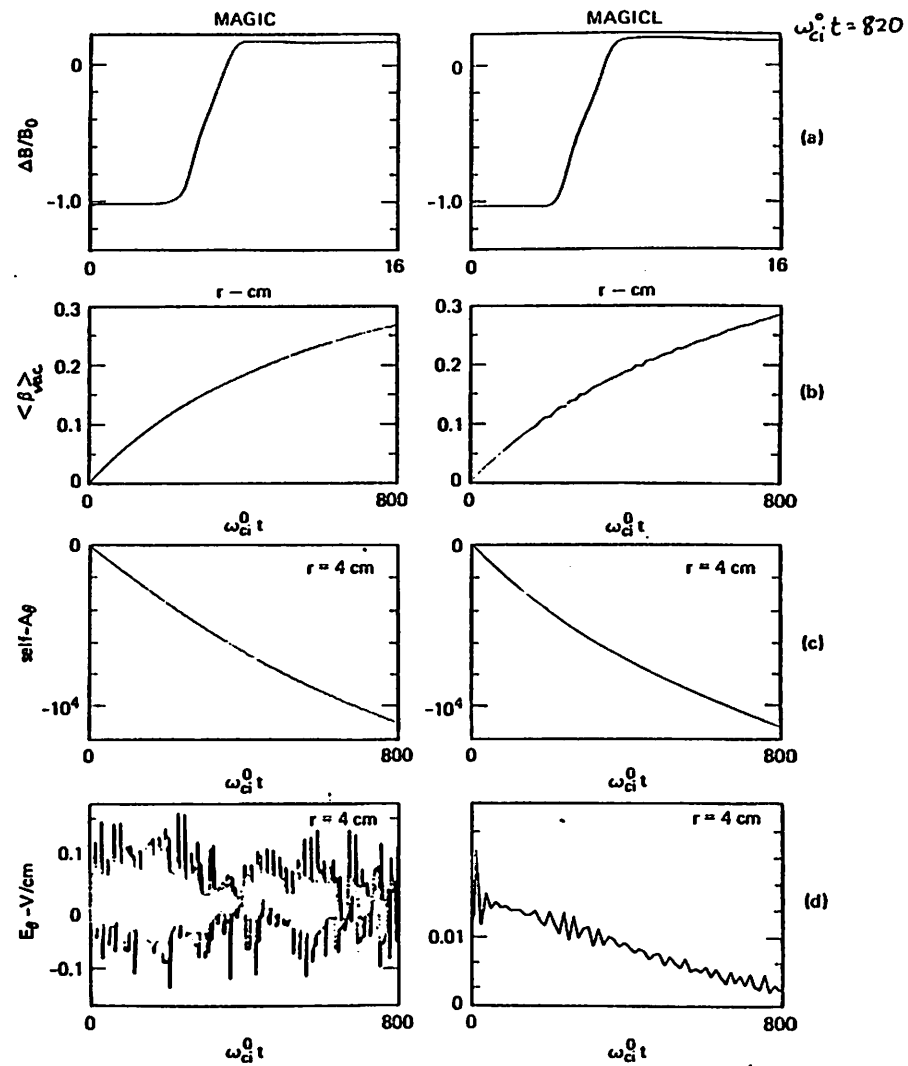
Compressional Alfvén Wave Dispersion Relation



- With orbit-averaging, modes with $\omega > \pi/\Delta T$ are suppressed. Modes with $\omega \ll \Delta T^{-1}$ are undistorted and undamped [$\text{Im } \omega \propto -(\text{Re } \omega \Delta T)^2$].
- Orbit-averaging quenches the even-odd instability and both $J_y \propto v_y$ and $J_y \propto P_y - eA_y/c$ algorithms work equally well.



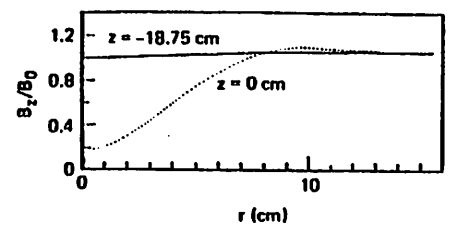
tangential injection: $E_{\text{beam}} = 12 \pm .6 \text{ keV}$ at $r = 5.5 \pm .5 \text{ cm}$
 $I = 50 \text{ A}$ $B_0 = 4500 \text{ G}$ conductor at 16 cm
 $\omega_i^0 \Delta t = .2$ $\Delta T / \Delta t = 64$ 1000 ions



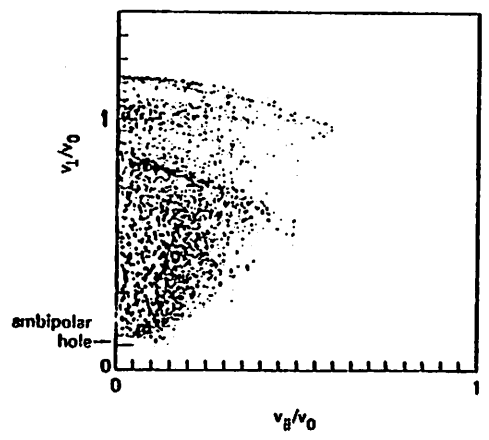
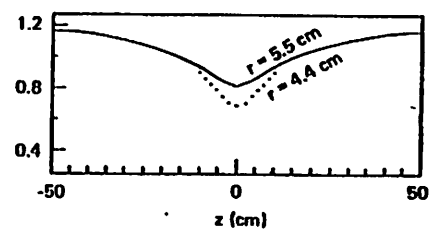
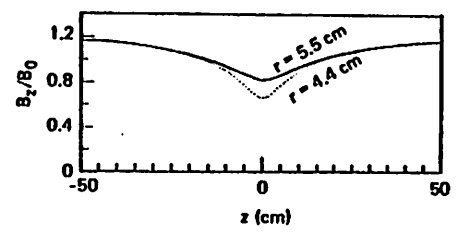
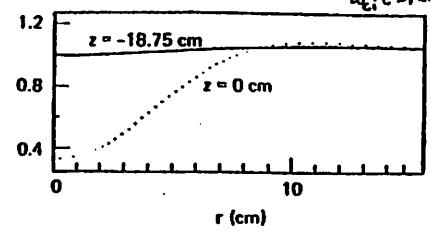
2-D Magneto-Inductive Simulations ($r, z; v_r, v_\theta, v_z$)

$\langle E_{beam} \rangle = 12 \text{ keV } D^+ \quad I = 300 \text{ A neutrals} \quad T_e \approx 50 \text{ eV} \quad R_{mirror} = 1.2 \text{ at } z = \pm 50 \text{ cm}$
 $v_{e0} \neq 0 \quad B_0 = 4350 \text{ G}$

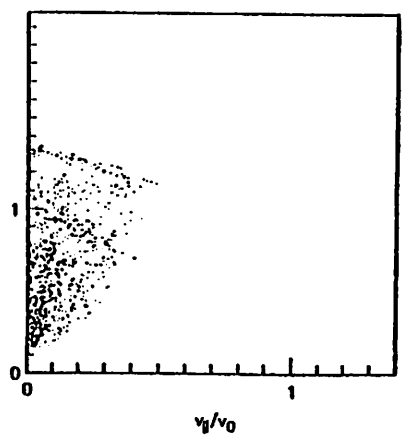
SUPERLAYER



SUPERAVERAGE $\omega_{ci}^0 t = 120$



$\omega_{ci}^0 \Delta t = 0.2 \quad \leq 19,200 \text{ ions}$

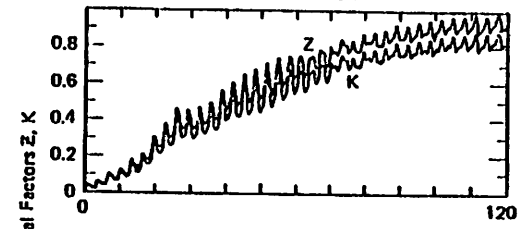


$\Delta T/\Delta t = 60 \quad \leq 6000 \text{ ions}$
 1 corrector iteration

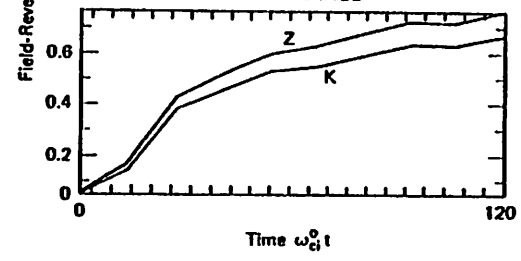
2XII B Buildup to Near Field Reversal

$$Z \equiv 1 - \frac{B_{min}}{B_{max}} \quad K \equiv 1 - \frac{B_{min}}{B_0}$$

SUPERLAYER



SUPERAVERAGE



CODE PERFORMANCE CHARACTERISTICS

OPTIMIZE ACCURACY, ENSURE STABILITY, AND REDUCE NUMBER OF SIMULATION PARTICLES BY ADJUSTING

- $\Delta T/\Delta t$ - AS LARGE AS POSSIBLE, LIMITED BY
E.G. 60 TO 1000
- α and β - ACCURACY: $\alpha, \beta \sim \frac{1}{2}+$ STABILITY: $0.6 \leq \alpha, \beta$
- NUMBER OF CORRECTOR ITERATIONS - FEWER THE BETTER FOR ECONOMICS.
STABILITY: $n_0 \geq 1$ ACCURACY IMPROVES: $n_0 > 1$
- INTERPOLATION/EXTRAPOLATION OF $(\vec{E}, \vec{B})^{nat}$ FOR PARTICLE PUSH -
PREDICTOR PASS: $\vec{E}, \vec{B} = \text{CONST.}$ IS ADEQUATE

CORRECTOR PASS: $\vec{E}, \vec{B} = \text{LINEAR INTERPOLATION \& EXTRAPOLATION NECESSARY TO REMOVE JERKS. BIASING INTERPOLATION BACKWARDS IN FAVOR OF OLD } \vec{E}, \vec{B} \text{ IMPROVES ACCURACY \& STABILITY. WITH BIAS ONE CORRECTOR PASS IS ENOUGH.}$
- NUMBER OF PARTICLES - REDUCTION POSSIBLE DEPENDS ON $\Delta T/\Delta t \gg 1$ AND PHASE-SPACE DISORDER, IS PROBLEM DEPENDENT BUT CAN BE QUITE DRAMATIC.
- DATA WINDOW W - ROUNDED "CORNERS" REDUCES E_{θ} NOISE BUT NOT DRAMATICALLY.

TIME-FILTERING IS ACCOMPLISHED; THERE IS SUBSTANTIAL SMOOTHING OF Δt DISCRETENESS NOISE. E.G. INJECTION NOISE; AND WAVES ARE DAMPED.

E.G. SIMULATION OF ZXIIB ON REALISTIC TIME SCALES

- SUCCESSFUL DEMONSTRATION OF SUPERAVERAGE SIMULATION OF BUILDUP AND TRANSPORT OVER LONG TIMES.
- SUPERAVERAGE ACCOMMODATES LARGE LARMOR RADIUS EFFECTS AND DISPARATE TIME SCALES:

PARTICLE ORBIT TIMES $\sim \omega_i^{-1} \sim 10^{-8}$ SEC.

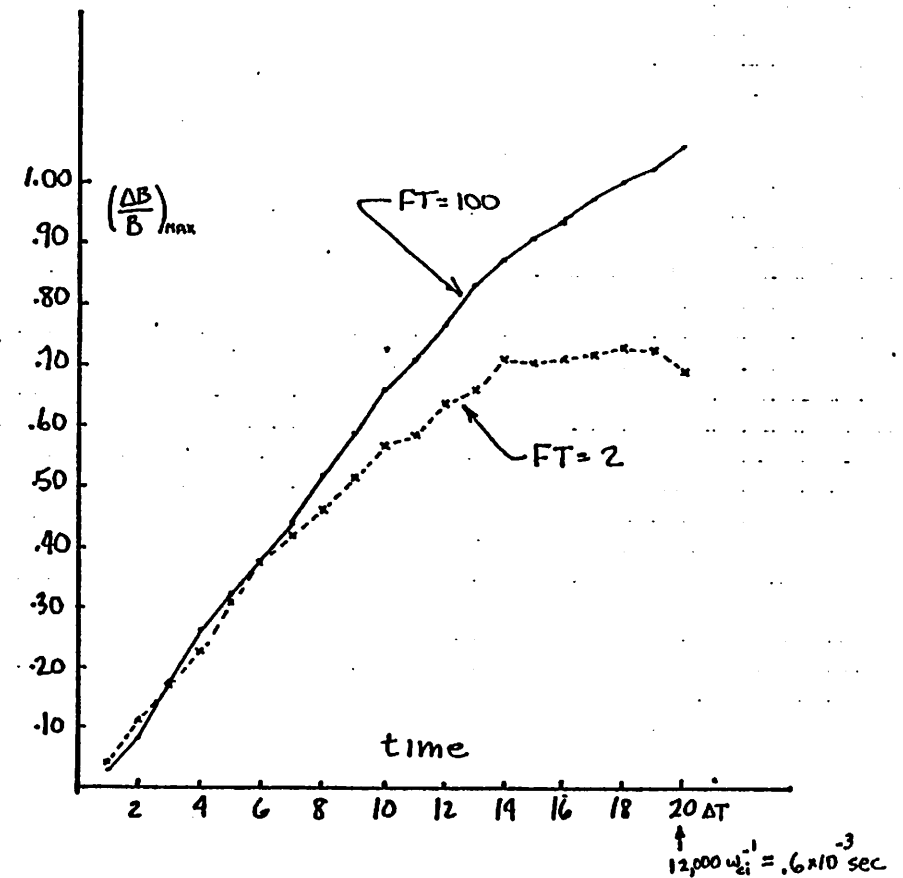
PLASMA BUILDUP TIMES 10^{-3} SEC.

- ORBIT-AVERAGING
 - (1) FILTERS OUT HIGH FREQUENCY FLUCTUATIONS,
 - (2) REDUCES THE NUMBER OF SIMULATION PARTICLES,
AND
 - (3) ELIMINATES ARTIFICIAL ACCELERATION OF SLOW PROCESSES, E.G., DRAG, RF DIFFUSION, AND INJECTION.
- NON-ADIABATIC ION LOSSES IN ZXIIB ARE REPRODUCED IN OUR SIMULATIONS, A NEW RESULT.

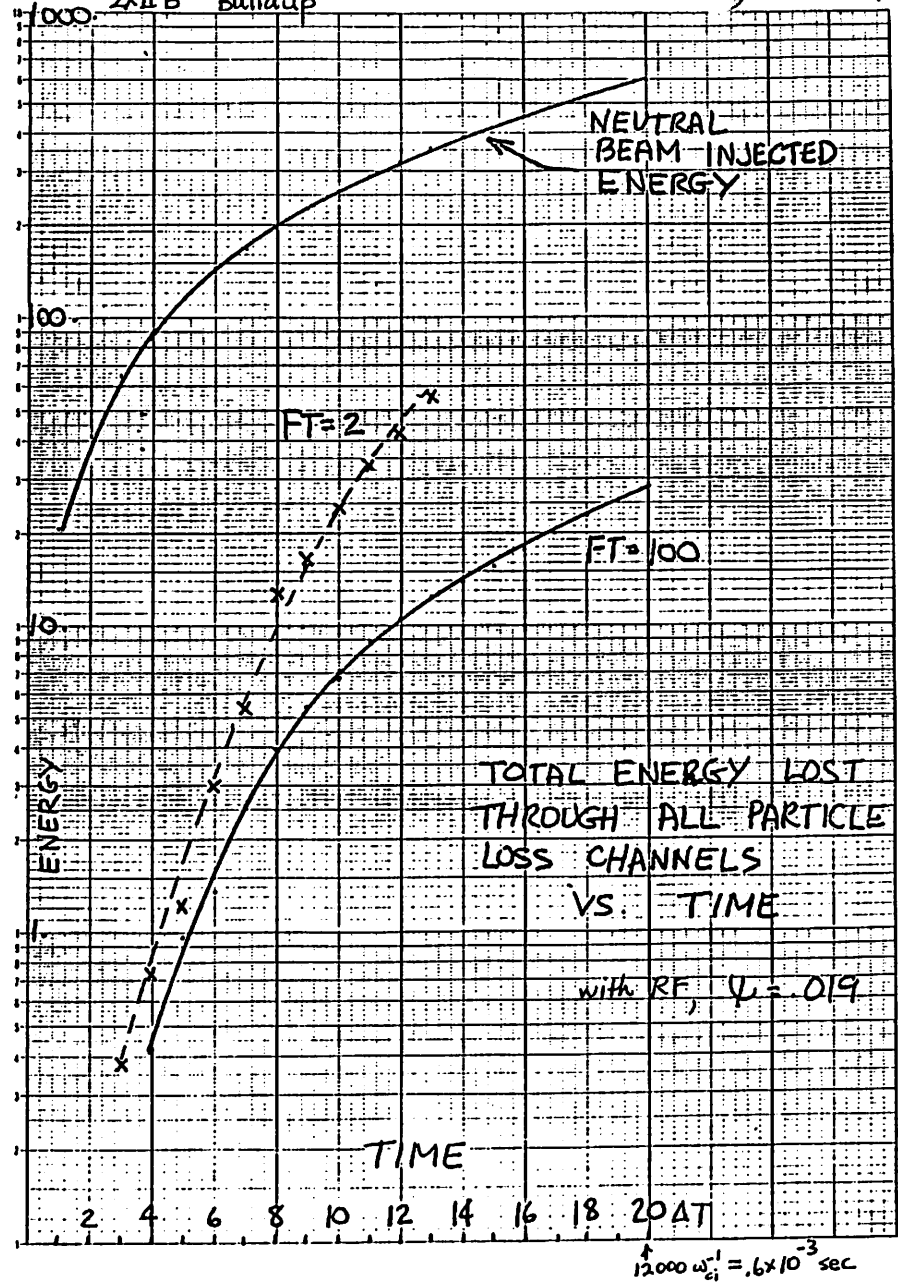
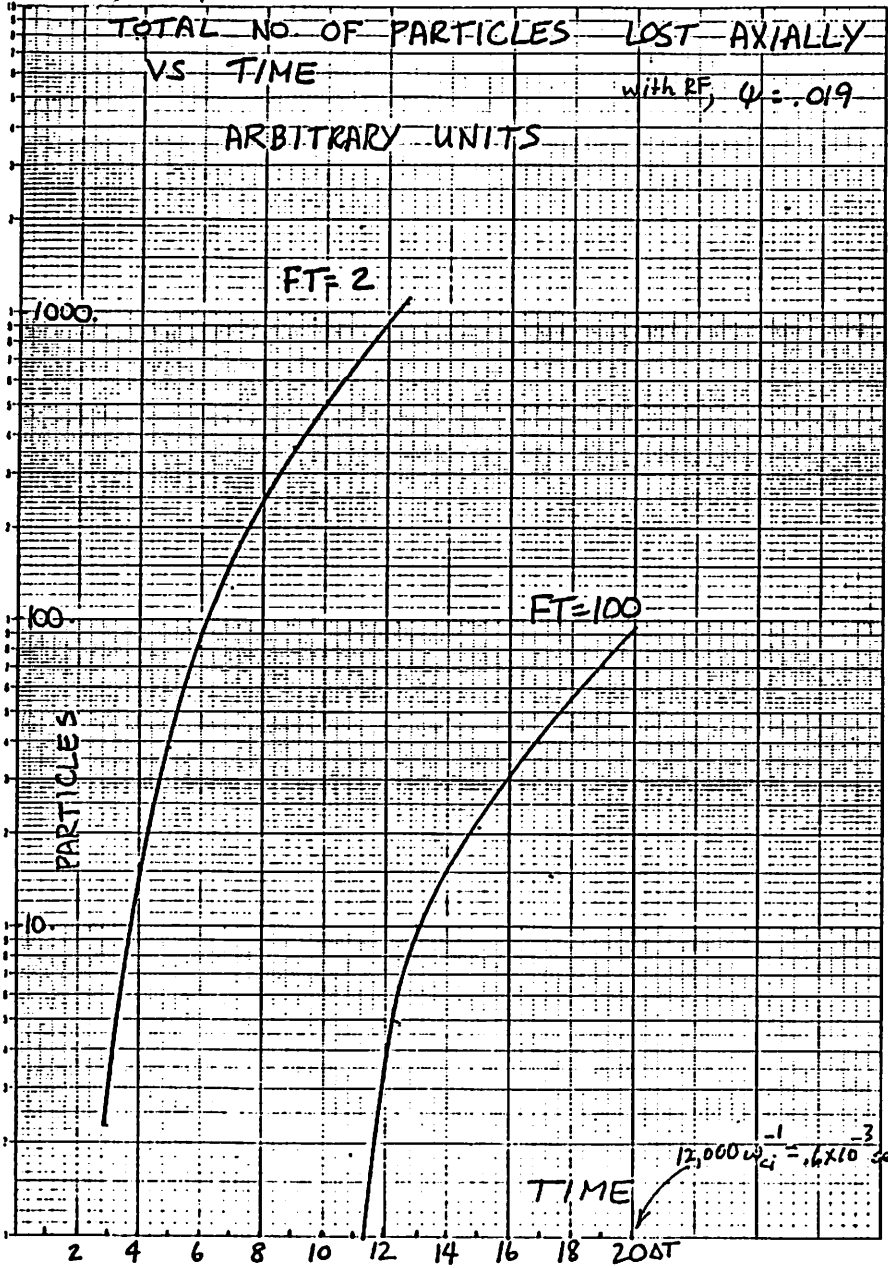
2XII B Buildup

SUPERAVERAGE PHYSICS MODEL

- 2-D (r,z) AXISYMMETRIC (v_r, v_θ, v_z)
- SELF-CONSISTENT B_r AND B_z , AND INDUCTION E_θ (DARWIN MODEL)
- CHARGE NEUTRAL AND $\vec{J}_e = 0$
- ELECTROSTATICS NEGLIGIBLE ON OPEN FIELD LINES FOR $\langle \frac{1}{2} m v_r^2 \rangle \gg T_e$
- 3-D DESCRIPTION OF NEUTRAL BEAM DEPOSITION INCLUDING CHARGE EXCHANGE AND IONIZATION
- RF TURBULENT DIFFUSION BASED ON QUASILINEAR THEORY
- IONS DRAG ON ELECTRONS (T_e IS AN INPUT PARAMETER)



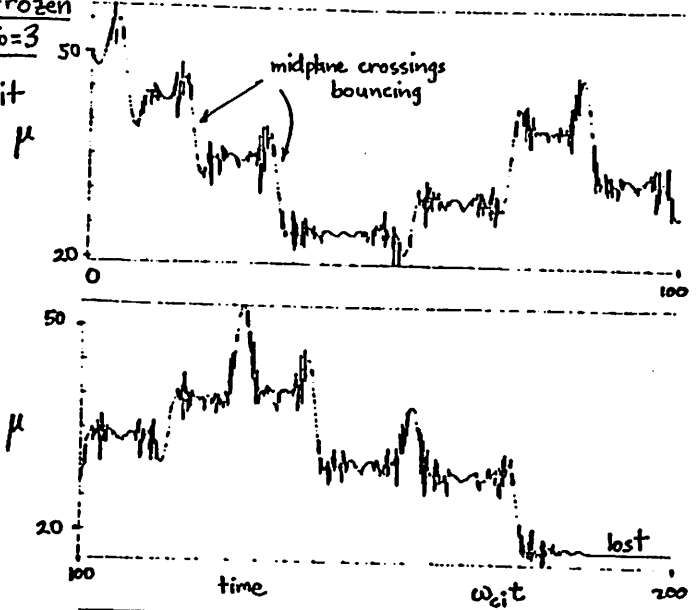
FIELD REVERSAL VS TIME
 COMPARED FOR TWO ACCELERATION
 FACTORS (FT).
 with RF, $\Psi_i = .019$



Particle Orbits in Frozen Fields Mirror Ratio=3

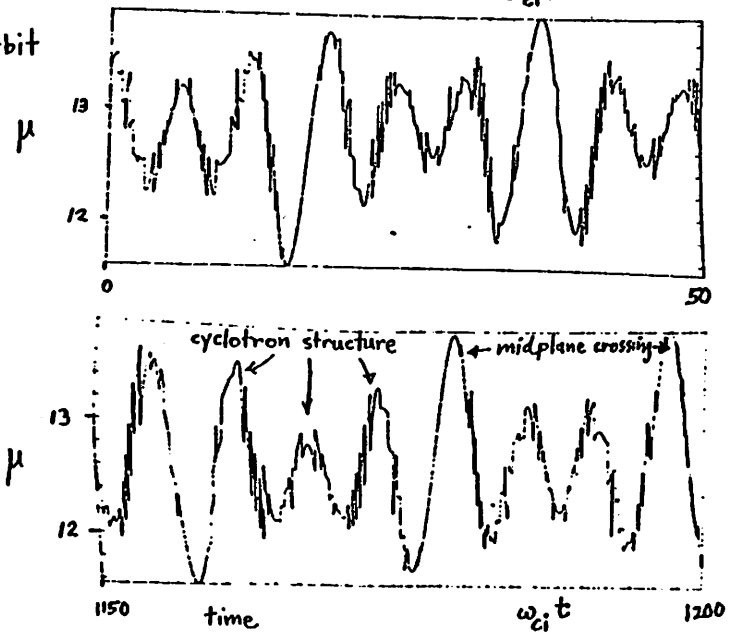
(a) Stochastic orbit

$\omega_b(t=0) \sim \omega_{ci}^0 / 4$



(b) Adiabatic orbit

$\omega_b \sim \omega_{ci}^0 / 8$



$\Delta P_{\theta}^{error} / P_{\theta} \leq 10^{-4}$
 $\Delta KE^{error} / KE \leq 10^{-6}$

SUPERAVERAGE Performance Characteristics on CRAY

τ (particle push / Δt timestep - particle) \sim 40-60 μ sec
 includes charge exchange, RF diffusion, drag, etc.
 (needs improvement)

$\omega_{ci} \Delta t \sim 0.1$ to 0.2

$\omega_{ci} t^{final} / \frac{2\pi}{2\pi} \sim \frac{2 \times 10^4}{2\pi} = 3.2 \times 10^3 \Rightarrow$ 100 min cpu CRAY time

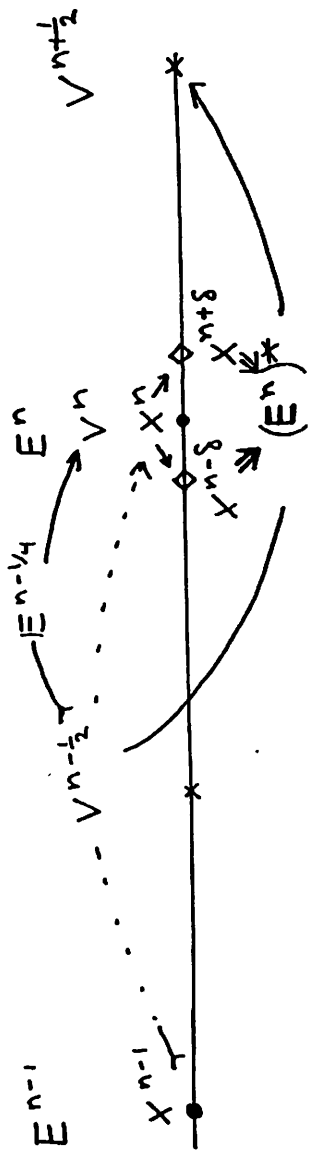
$\omega_{ci} = 2 \times 10^7 \text{ sec}^{-1}$ for $B_0 = 4300 \text{ G}$
 $t^{final} \leq 10^{-3} \text{ sec}$

$t^{final} / \tau_{bounce} \sim 300$ to 1000

$N_{ions} \sim 500$ to 1000 core = 300 K words

$n_{g,radial} = 29-57 \times n_{g,axial} = 65-130$

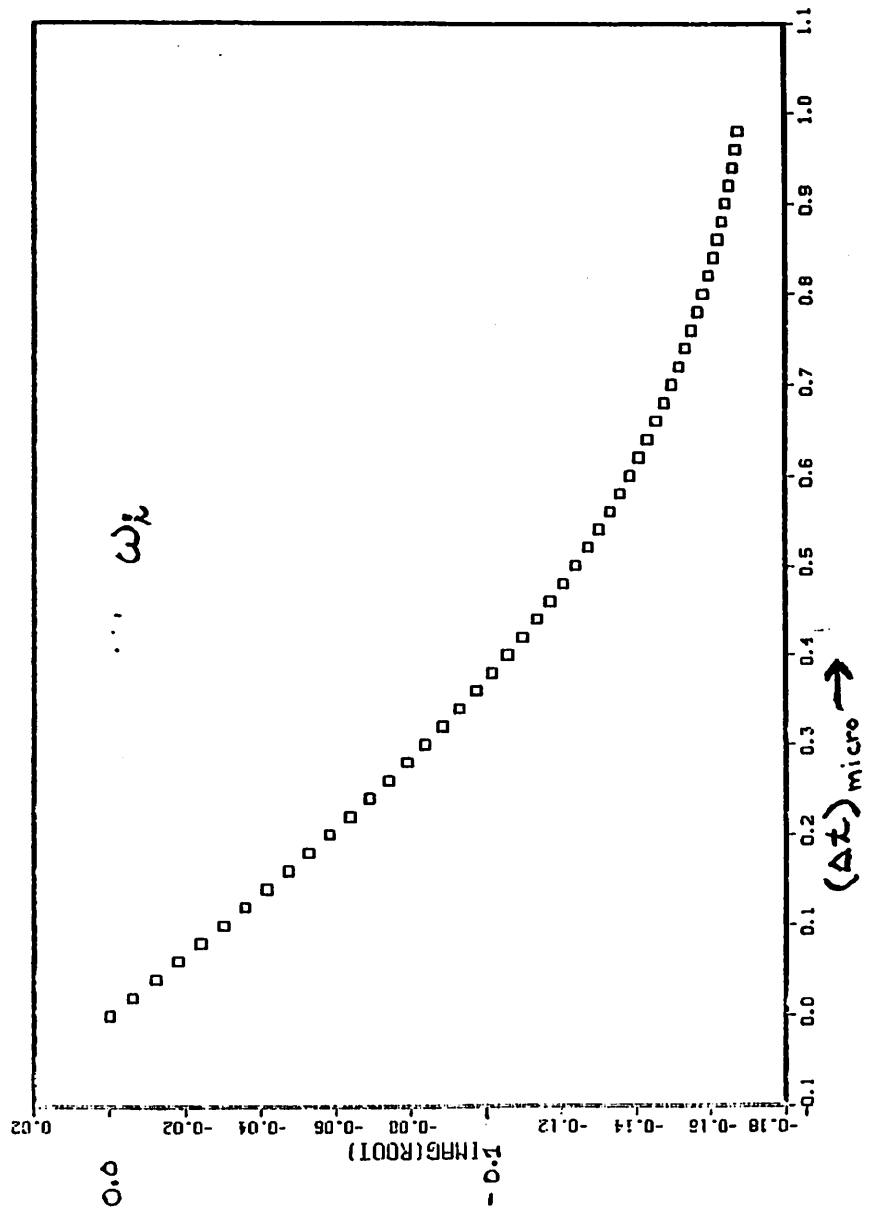
PARTICLE MOVER

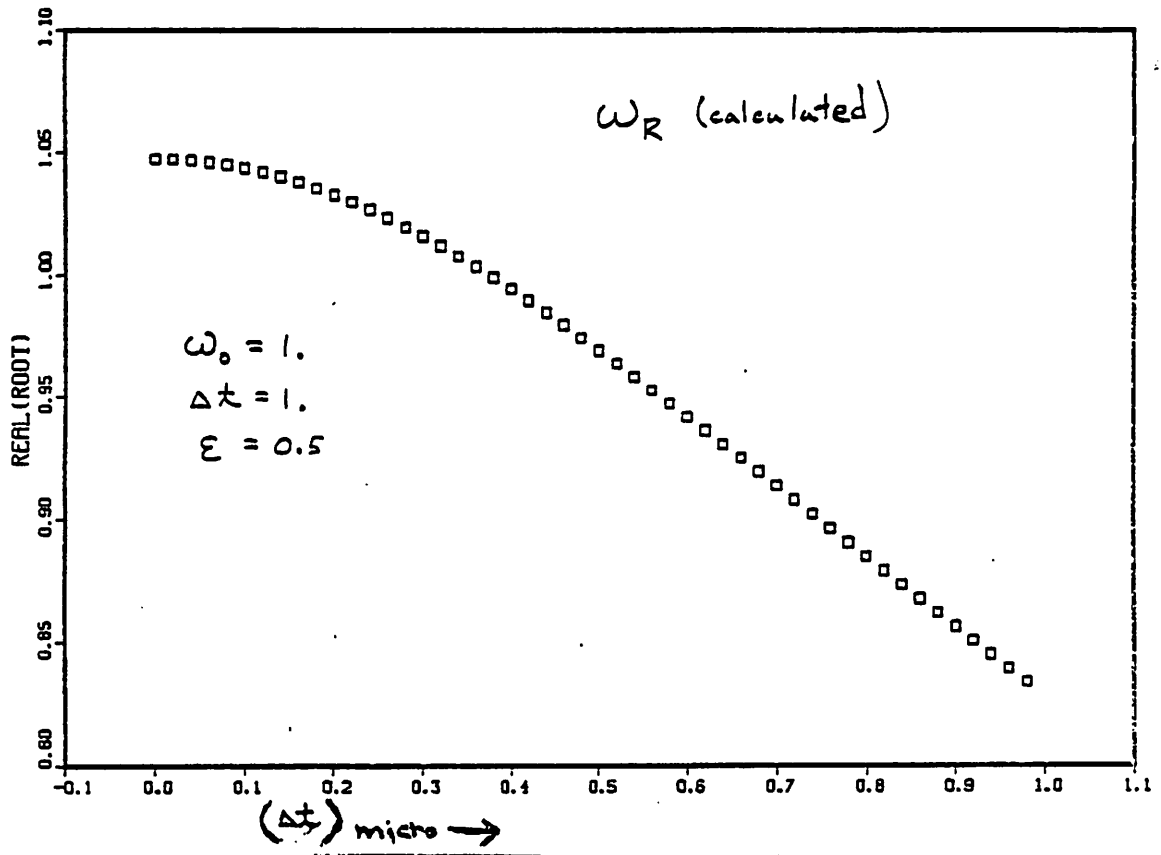


LOW PASS FILTERING IN TIME 44

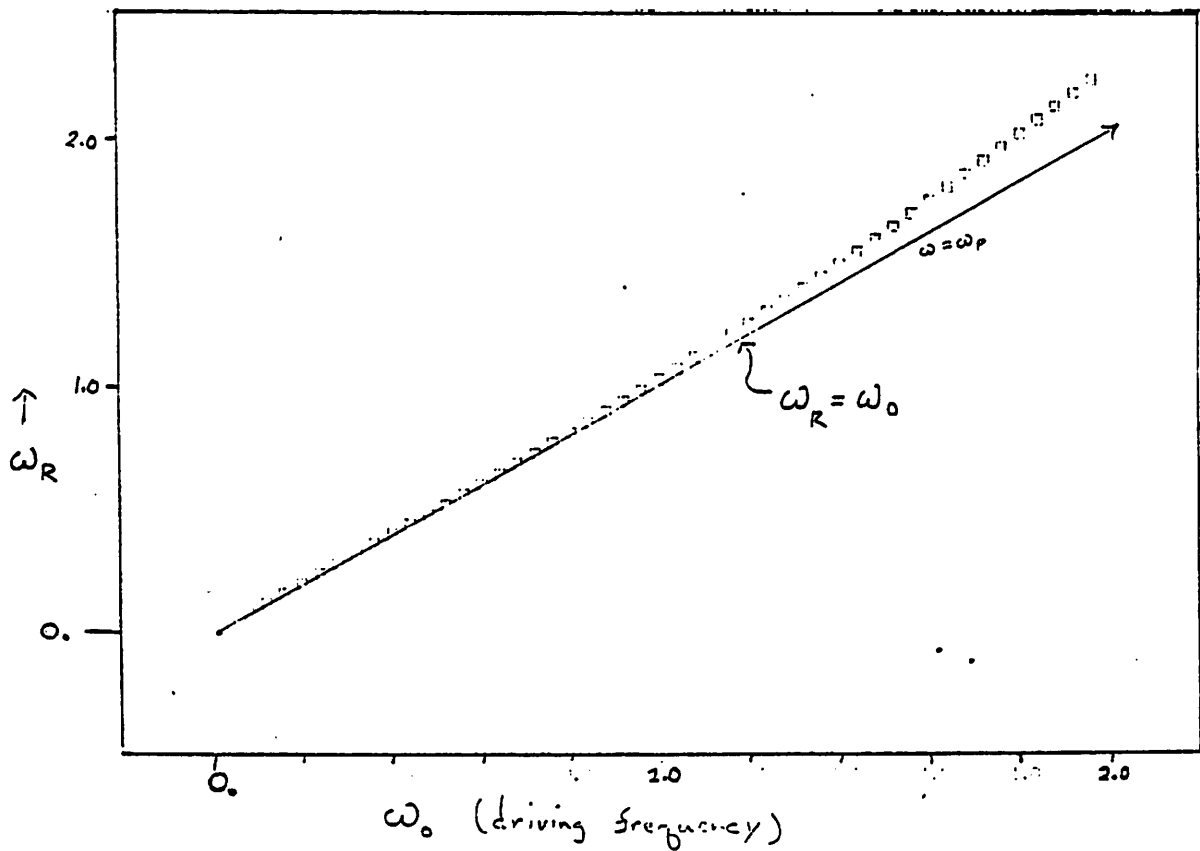
W.M. FAWLEY (UCB-LU)
C.K. BIRDSALL (UCB)

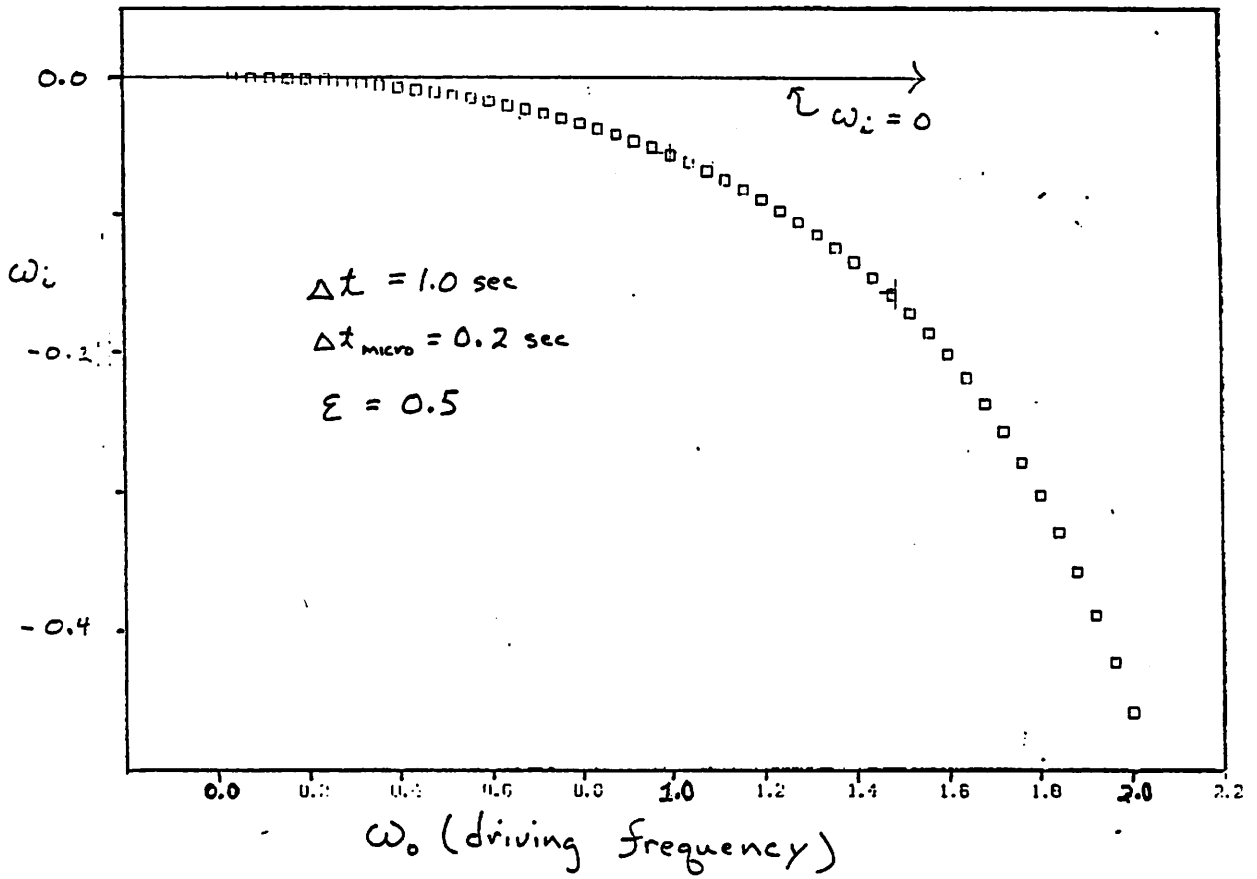
$$\begin{aligned}
 X^n &= X^{n-1} + V^{n-\frac{1}{2}} \cdot \Delta t \\
 V^n &= V^{n-\frac{1}{2}} + \left(\frac{q\Delta t}{2m} \right) \left(\frac{3}{4} E^n + \frac{1}{4} E^{n-1} \right) \\
 X^{n+\delta} &= X^n + V^n \cdot \delta \cdot \Delta t \quad ; \delta < 1 \\
 (E^m)^* &\equiv \frac{1}{2} \left\{ (1-\epsilon) E^{n-\delta} + (1+\epsilon) E^{n+\delta} \right\} \quad ; 0 \leq \epsilon \leq 1 \\
 V^{n+\frac{1}{2}} &= V^{n-\frac{1}{2}} + \left(\frac{q\Delta t}{m} \right) (E^n)^*
 \end{aligned}$$



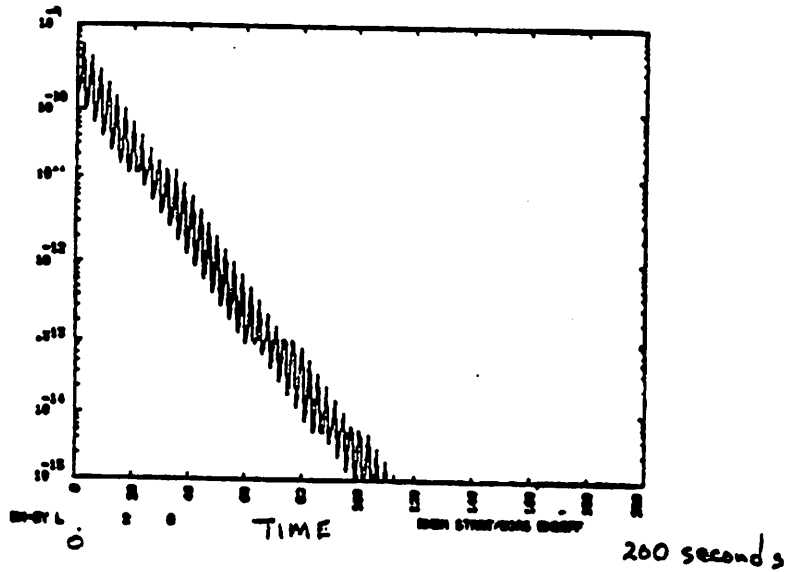


$$\Delta t_{\text{NORMAL}} = 1.0 \text{ sec} \quad \epsilon = 0.5 \quad \left(\frac{\Delta t_{\text{micro}}}{\Delta t_{\text{NORMAL}}} \right) = 0.2$$





$\omega_0 = 1$ $\Delta t (\text{micro}) = 0.2$
 $\Delta t = 1$ $\epsilon = 0.5$

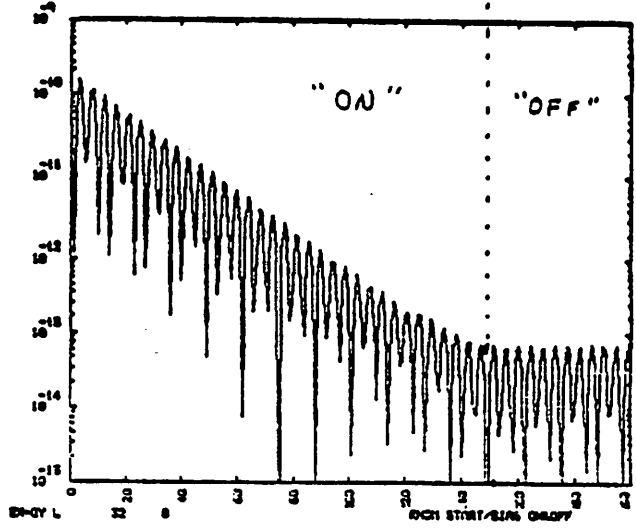


ELECTROSTATIC ENERGY (ESEK)

MODE 2

$\omega_p \approx 1$

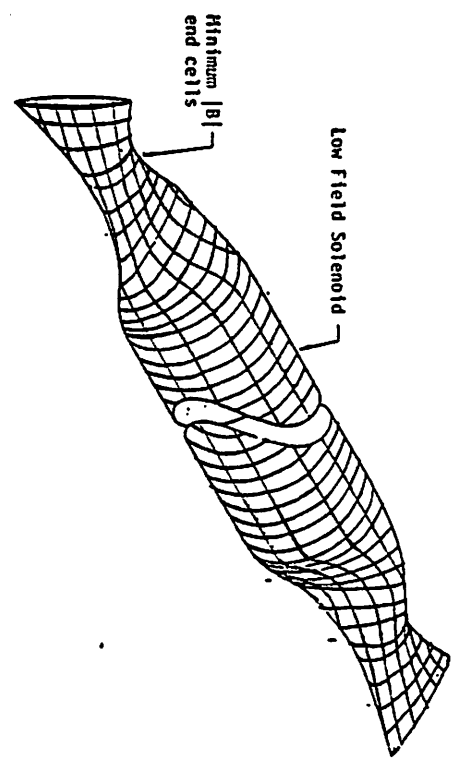
DAMPING



ESEK , MODE 32

$\omega_p \approx 0.7$ (finite grid effect)

This shows effect of turning damping off at $t = 150$ sec.



4. TOWARD A FULL 3D HYBRID TRANSPORT CODE:
A REACTOR SIMULATION CODE

David Anderson
LLL
Livermore

PRECURSORS AND FOUNDATIONS

FLUID CODES	{	3D MHD Fully Implicit Fixed Grid. Finan & Killeen
		3D MHD Implicit MALICE. Barnes & Brackbill
		3D MHD Semi Implicit Resistive MALICE. Brackbill
BIG Δt PARTICLE AND HYBRID CODES	{	1D Hybrid. Crystal, Rathmann, Vomvoridis, & Denavit
		1D Hybrid. Byers, Cohen, Condit, & Hanson
		2D Hybrid. Hewett & Nielson
		2D Superaverage. Cohen, Brenolds, Conley, & Freis
NUMERICAL ANALYTIC METHODS	{	2D FEM Galerkin. Gresho
		1D (& 2D) Moving Node FEM Galerkin. Gelinas
		ICCG. Meijerink & Vandervorst. Kershaw

THREE MODEL 3D TRANSPORT CODE

- THREE MODELS:
1. Long Timestep Transport on Full Time Interval
 2. Short Timestep 3D MHD Calculations at Occasional Sub-Intervals
 3. Short Timestep 3D Particle Simulation at Occasional Sub-Intervals

ONE GRID: All Simulations on 3D Almost Lagrangian Grid

REGIMES OF CODE OPERATION

1. Transient Start Up
2. Slow Evolution Near Steady State
3. Fast MHD Disruption
4. Fast Micro-Turbulent Disruption

ECONOMIC REGIMES

- A. Only 2. is Advantageous For Computer Economics
- B. Fusion Reactors Won't Work Unless in Regime 2

SUMMARY

1. Need 3D Transport As In TMR.
2. Keep Track Of MHD Stability.
3. Get Transport Coefficients From Particle Simulation.
4. Calculate All Of These On Same Grid.
5. Most Economical For Reactor Configurations.
6. Galerkin and ICCG Methods Developed.
7. MALICE Exists. Its Companion Particle Code Does Not.
8. Currently Available Computers Barely Adequate.

5MHD Particle Code

56

T. Tajima

UCLA

Collaborators

J. N. Leboeuf

F. Brunel

J. M. Dawson

C. C. Wu

1. Algorithm

2. Force free electron algorithm

3. Lax-Wendroff algorithm

Comparison of Various Versions

4. Comparison with Other Codes

5. Applications

57

Comparison (without vectorization)

1. Eulerian Leapfrog

2. Eulerian FCT 2-3 slower

3. MHD particle $\left\{ \begin{array}{l} 2-4 \text{ slower} \\ 2 \text{ memory} \end{array} \right.$

Shock 1. not appropriate

2, 3. O.K.

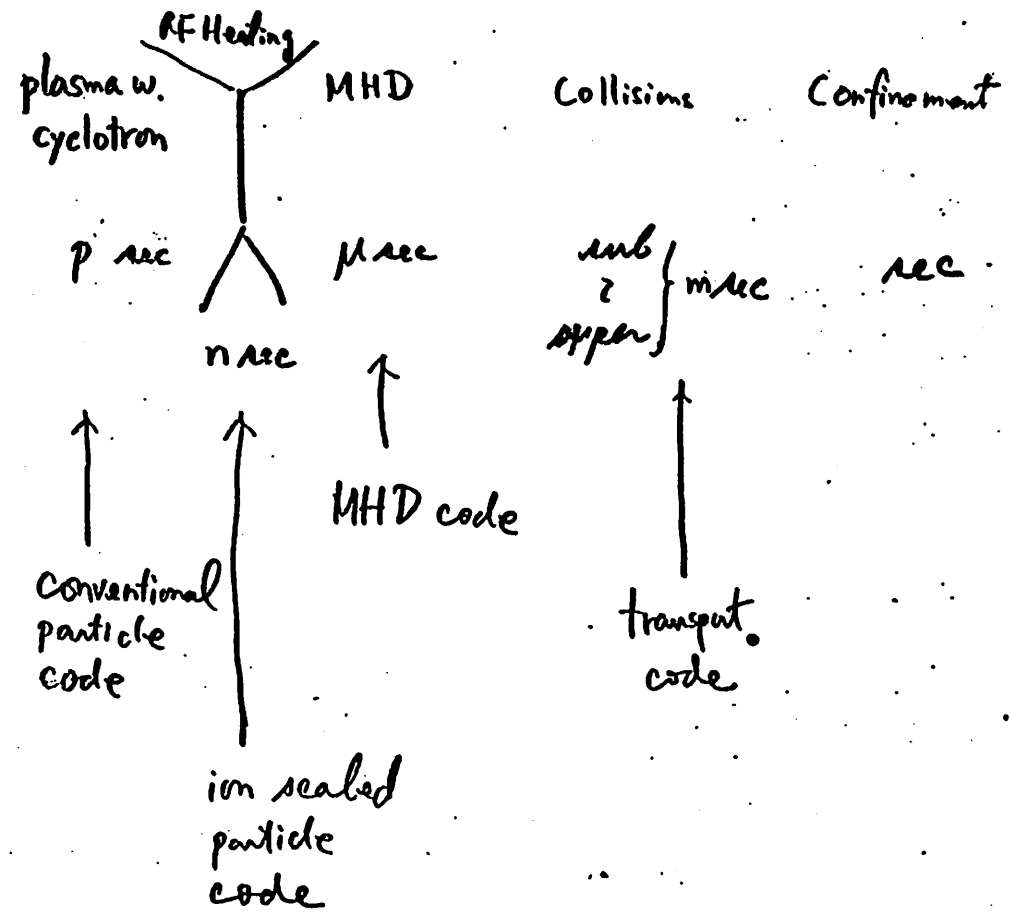
Magnetosphere 2, 3. O.K.

I'm not so sure

Churning fluid, turbulence, convection

Need

Fusion plasma has multiple time scales.



$$\frac{3 \times 10^{23} \times 3.5 \times 10^7}{10^{15}}$$

$$= \frac{10^{1+8+2}}{10^{15}} = 10^{11-15} = 10^{-4}$$

Difficulty in Eulerian MHD Codes

advective term \rightarrow e.g. negative density

$$\text{e.g. } \frac{\partial}{\partial t} \rho + \underline{v \cdot \nabla} \rho = 0$$

(curr: artificial)

v

$$P_0 \frac{u_1^2}{2c_s^2} = k (a_0 - a_1) \frac{B_e^2}{4\pi}$$

Difficulty in Lagrangian MHD codes

Complicated grid arrangements
(grid entanglement)

$$\left(\frac{u_1^2}{4c_s^2} = k (a_0 - a_1) \right)$$

$$\frac{c_s \sqrt{A_e} \sqrt{2\pi} \left(\frac{a}{L}\right)^{1/2}}{\left(c_s^2 + v_{Ae}^2 2\pi a/L\right)^{1/2}}$$

Removal of Difficulties of These Previous Codes

Introduction of Particles



- (i) Advection terms are automatically treated.
(No negative density (Mass conservation, momentum conservation: exact))
- (ii) Fixed uniform mesh
(no grid entanglement)

Some weaknesses

- Fluctuations
- More memory for computation

Philosophically

Divide the computational burden into subgrid structure (particles) and grid calculations (mesh).

Algorithm

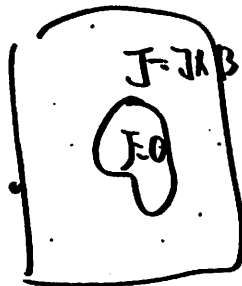
$$\left\{ \frac{d\vec{r}_i(t)}{dt} = \vec{v}_i(t) \right.$$

$$\left. \frac{d\vec{v}_i}{dt} = -\frac{1}{\rho} \nabla P - \frac{1}{4\pi\rho} \vec{B} \times (\nabla \times \vec{B}) \right.$$

← Grid quantities →

$$\rho = m \sum_{i \in q} f(\vec{r} - \vec{r}_i)$$

$$\langle \vec{v} \rangle = \frac{\sum_i \vec{v}_i f(\vec{r} - \vec{r}_i)}{\sum_i f(\vec{r} - \vec{r}_i)}$$



$$\left\{ \frac{\partial \vec{B}}{\partial t} = \nabla \times (\langle \vec{v} \rangle \times \vec{B}) \right.$$

← Grid Quantities →

64.

Variety of Applications of this code

65

Examples

• laser fusion "Magnetic Field Generation by the Rayleigh-Taylor Instability", Phys. Rev. Lett. 41, 1715 (1978).

• shocks "Double-Layer Forward Shocks in an MHD Fluid", Phys. Rev. Lett. 40, 652 (1978).

• space physics "Global Simulation of the Time-Dependent Magnetosphere", Geophys. Rev. Lett. 5, 609 (1978).

• CTR etc.

Fluid instability: "Kelvin-Helmholtz"
Instability in Supersonic and Supercavitic
Fluids" Physics of Fluid in press.

Hall Code Algorithm
or Force free electron algorithm

Electron eq.

$$c(\underline{\tilde{E}} + \frac{v_e}{c} \times \underline{\tilde{B}}) - m v_{ei} (\underline{\tilde{v}}_i - \underline{\tilde{v}}_e) + \frac{1}{n_e} \nabla \cdot \underline{\tilde{P}}_e = 0$$

Ion eq.

$$M \frac{d\underline{\tilde{v}}_i}{dt} = e(\underline{\tilde{E}} + \frac{v_i}{c} \times \underline{\tilde{B}}) - \frac{1}{n_i} \nabla \cdot \underline{\tilde{P}}_i - M v_{ie} (\underline{\tilde{v}}_i - \underline{\tilde{v}}_e)$$

\Rightarrow

$$nM \frac{d\underline{\tilde{v}}_i}{dt} = \frac{e}{c} n (\underline{\tilde{v}}_i - \underline{\tilde{v}}_e) \times \underline{\tilde{B}} - \nabla \cdot (\underline{\tilde{P}}_i + \frac{n}{n_e} \underline{\tilde{P}}_e)$$

\Rightarrow

$$\rho \frac{d\underline{\tilde{v}}_i}{dt} = -\frac{1}{4\pi} \underline{\tilde{B}} \times (\nabla \times \underline{\tilde{B}}) - \nabla \cdot (\underline{\tilde{P}}_i + \underline{\tilde{P}}_e)$$

(Quasi-neutrality)

Faraday's law

$$\frac{\partial \mathbf{B}}{\partial t} = c \nabla \times \left[\frac{\mathbf{v}_i}{c} \times \mathbf{B} + \frac{1}{4\pi n e} \mathbf{B} \times (\nabla \times \mathbf{B}) \right]$$

$$- \frac{m c v_i}{4\pi n e^2} \nabla \times \mathbf{B} + \frac{1}{n e} \nabla \cdot \mathbf{P}_0$$

The linear dispersion relation in this algorithm yields:

$$\omega = \pm \left[(k^2 v_A^2 / 2\Omega_i) \pm k v_A (1 + k^2 v_A^2 / 4\Omega_i^2)^{1/2} \right]$$

$$\frac{k v_A}{\Omega_i} \ll 1 \text{ case}$$

$$\omega \approx k v_A \left(1 \pm \frac{k v_A}{2\Omega_i} \right)$$

$$\frac{k v_A}{\Omega_i} \gg 1 \text{ case}$$

$$\omega \approx \Omega_i, \quad \frac{k^2 v_A^2}{\Omega_i}$$

With grid effects

$$\omega = v_A \sin d \pm 2 \frac{v_A^2}{\Omega_i} (1 - \cos d) - i \frac{1}{2} (1 - \cos d)$$

$$(d \equiv k_x \lambda_x)$$

Lax-Wendroff Algorithm

$$\frac{\partial B}{\partial t} = \nabla \times (v_f \times B)$$

direct leap-frog scheme impossible.

(i) Half step — Lax method

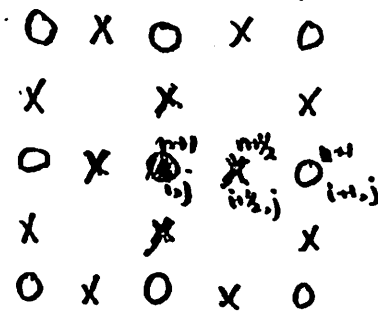
$$B^{n+1/2} = \langle B \rangle^{n+1/2} + \frac{\Delta t}{2} \nabla \times (v_f^{n+1/2} \times B^{n+1/2})$$

(ii) Full step — Leap-frog

$$B^{n+3/2} = B^{n+1/2} + \Delta t \nabla \times (v_f^{n+1} \times B^{n+1})$$

Various Implementations Grid Assignments

2 Grid - Area Weighting - Lax-Wendroff



e.g.

$$B_{i,j}^{n+1} = \frac{1}{4} (B_{i+1/2,j}^{n+1/2} + B_{i-1/2,j}^{n+1/2} + B_{i,j+1/2}^{n+1/2} + B_{i,j-1/2}^{n+1/2}) + \frac{\Delta t}{2\Delta x} \left[(v_f^{n+1/2} \times B^{n+1/2})_{i+1/2,j} - (v_f^{n+1/2} \times B^{n+1/2})_{i-1/2,j} \right]$$

Other examples tried:

Lax NGP

L-W NGP

1 Grid Area Weighting

2 Grid Area Weighting

Dipole FFT

Analysis of Numerical Stability, aliasing
and Finite-sized Particle Effects 73

2 Grid Area-Weighting Lax-Wendroff

$$\begin{cases} B_{i+\frac{1}{2},j+\frac{1}{2}}^{n+\frac{1}{2}} = \frac{1}{4}(B_{i+\frac{1}{2},j}^n + B_{i,j}^n + B_{i,j+\frac{1}{2}}^n + B_{i+\frac{1}{2},j+\frac{1}{2}}^n) - \frac{\Delta t}{2\Delta x}(F_{i+\frac{1}{2},j}^n - F_{i,j}^n) \\ B_{i,j}^{n+1} = B_{i,j}^n - \frac{\Delta t}{\Delta x}(F_{i+\frac{1}{2},j}^{n+\frac{1}{2}} - F_{i-\frac{1}{2},j}^{n+\frac{1}{2}}) \end{cases}$$

We assume $B \propto B \exp[i(k_x i \Delta x + k_y j \Delta y - \omega \Delta t)]$

Then

$$\begin{cases} B_{i+\frac{1}{2},j+\frac{1}{2}}^{n+\frac{1}{2}} = \left[\frac{1}{2}(\cos \alpha + 1) + i \theta_x \Delta t \sin \alpha \right] B^n \\ g B^n = B^n + (i \theta_x 2 \Delta t \sin \alpha) B^{n+\frac{1}{2}} \end{cases}$$

where

$$\alpha = k_x \Delta x ; \theta_x = \frac{v}{\Delta x}$$

$$g B^n = B^n + i \theta_x 2 \Delta t \sin \alpha \left[\frac{1}{N} (\cos \alpha + N - 1) + i \theta_x \Delta t \sin \alpha \right] B^n$$

(N: dimensionality)

$$g = 1 - 2 \theta_x^2 \Delta t^2 \sin^2 \alpha + i \frac{2 \Delta t \theta_x}{N} \sin \alpha (\cos \alpha + N - 1)$$

κ amplification factor

Stability

$$1 \geq |g|^2 = (1 - 2 \theta_x^2 \Delta t^2 \sin^2 \alpha)^2 + 4 \frac{\Delta t^2 \theta_x^2}{N^2} \sin^2 \alpha (\cos \alpha + N - 1)^2$$

$$|g|^2_{\alpha = \pi/2} - 1 = [-1 + \theta_x^2 \Delta t^2 + \frac{(N-1)^2}{N^2}] \theta_x^2 \Delta t^2 \leq 0$$

$$\Delta t \leq \left[1 - \frac{(N-1)^2}{N^2} \right]^{1/2} / \theta_x$$

similar to Courant-Friedrich-Lewy condition

Brillouin effect must reverse.

Finite-sized Particle Effect on Second Wave ⁷⁵

$$n = \sum_i f(r - r_i) = \langle f \rangle$$

$$-i \omega B = \nabla \times [\langle v \rangle \times B] \quad (1) \text{ induction eq.}$$

$$\text{, where } \langle v \rangle \equiv \frac{\langle v f \rangle}{\langle f \rangle}$$

$$-i \omega \langle f \rangle v = \langle f \nabla B^2 \rangle + \langle f \nabla n T \rangle \quad \text{Momentum eq.} \quad (2)$$

And effectively

$$-i \omega n + \nabla \langle f v \rangle = 0 \quad (3)$$

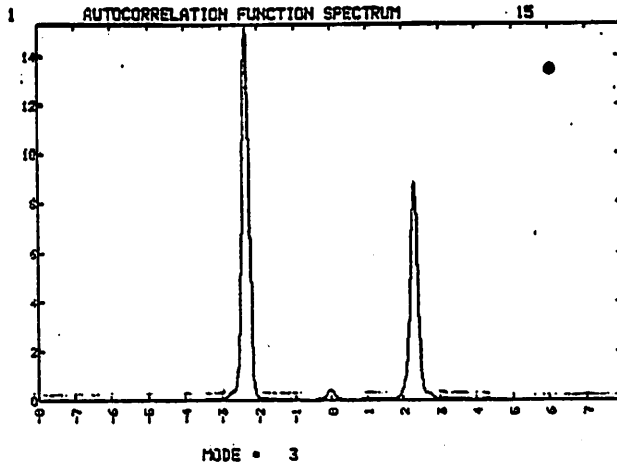
(2)+(3) \Rightarrow

$$(-i \omega)^2 n_k + k^2 c_s^2 \underline{f_k^2} n_k = 0 \quad (4)$$

(2)+(1) \Rightarrow

$$(-i \omega)^2 B_k = \frac{1}{\langle n \rangle} \left[\langle \underline{f_k^2} k B_k \rangle \times B \right]$$

where $f_k^2 = \exp(-k^2 a^2)$, if particle is a Gaussian



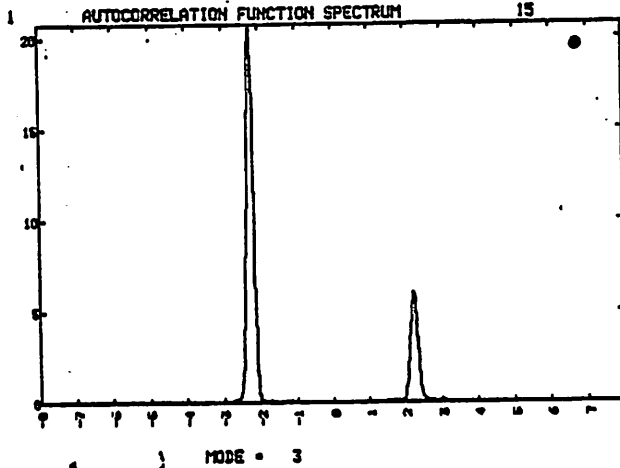
Magnetosonic

$k_z = 0$

2 grid
 $c-w$

Magnetosonic
wave

2 grid - Area Weighted - Lax Wendroff

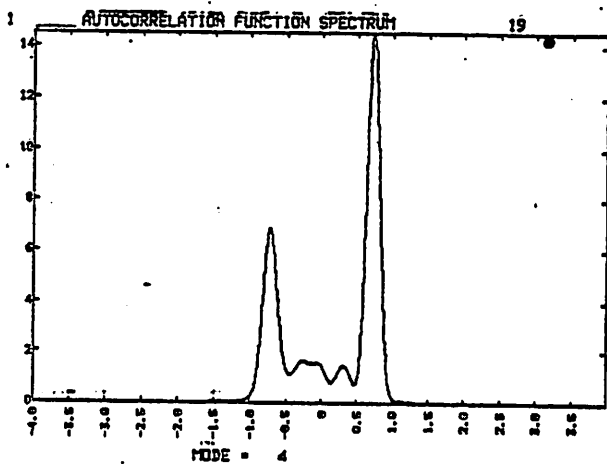
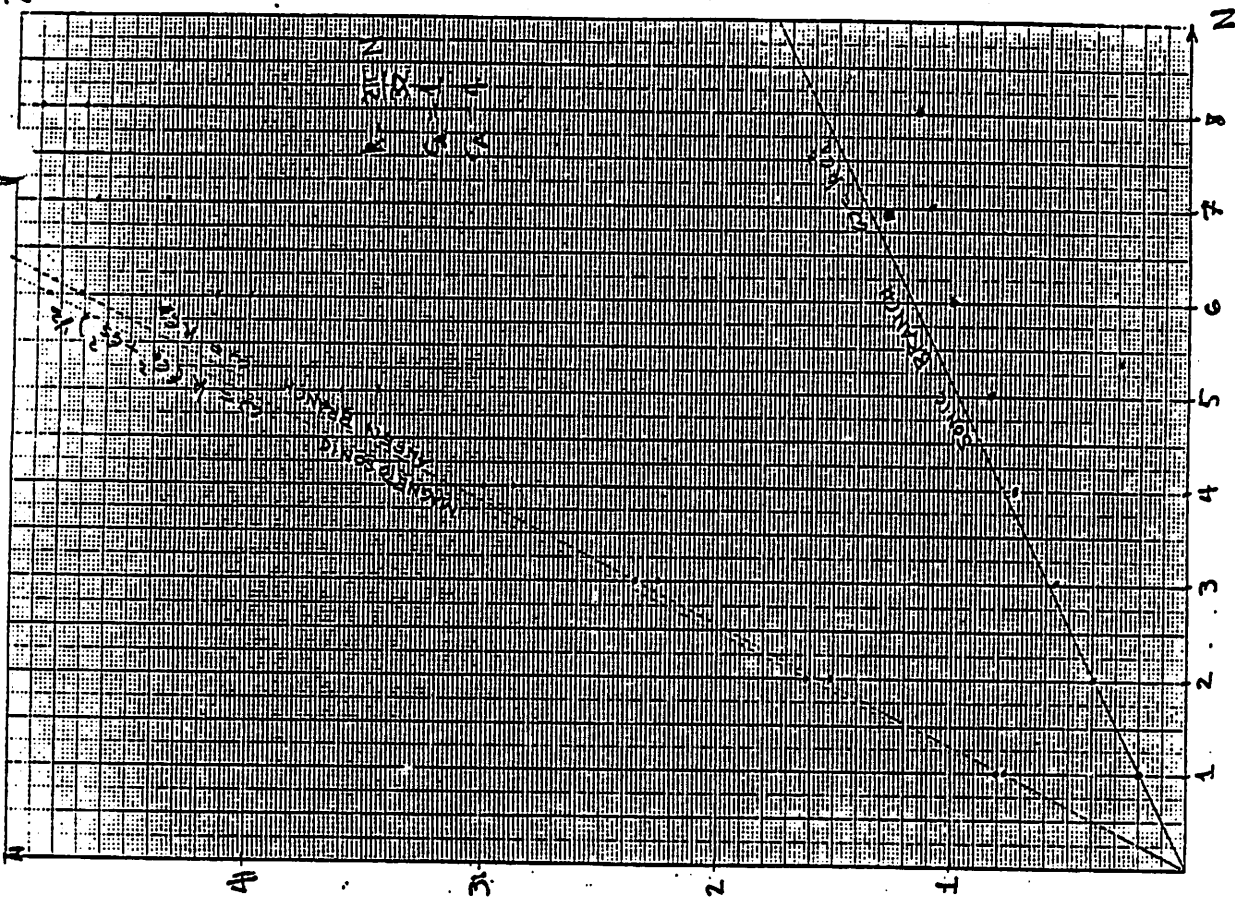


Alfven

2 grid
 $c-w$

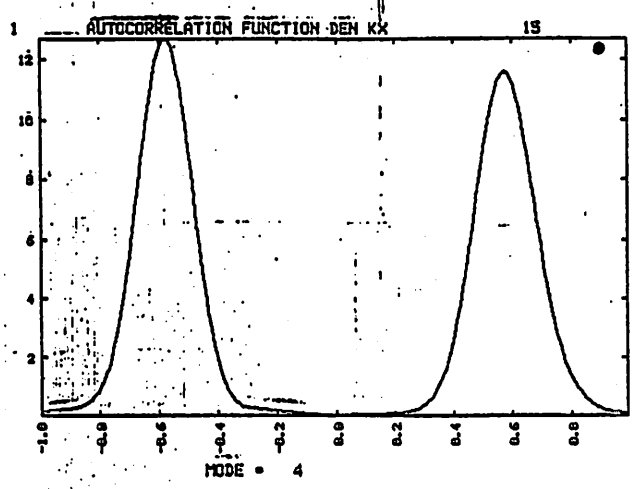
Alfven
wave

2 Grid - Area Weighted - Lax - Wendroff



Sound
Wave

2grid - Area Weighted - Lax Wendroff



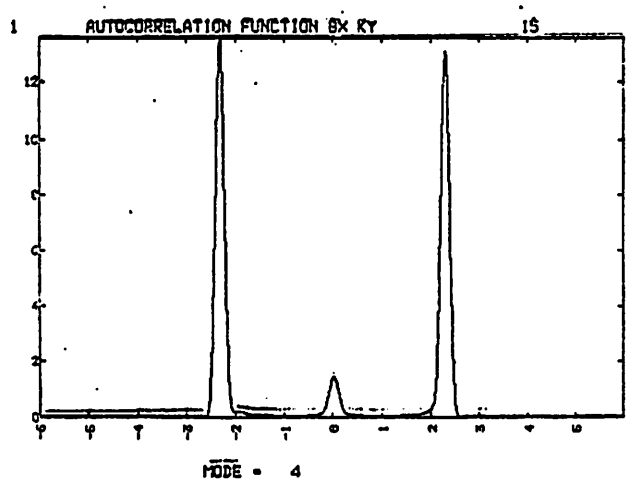
Sound wave
FFT

$C=1$
 $L=2 \times 32$
 $t=2$ steps

Sound wave

SUD-FFT-Lax Wendroff

659



Magnetosonic

FFT

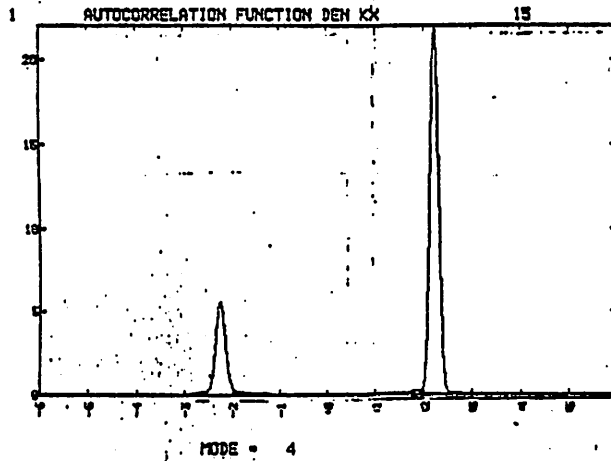
$t_1=...$
 $t_2=...$

Magnetosonic

SUD-FFT-Lax Wendroff

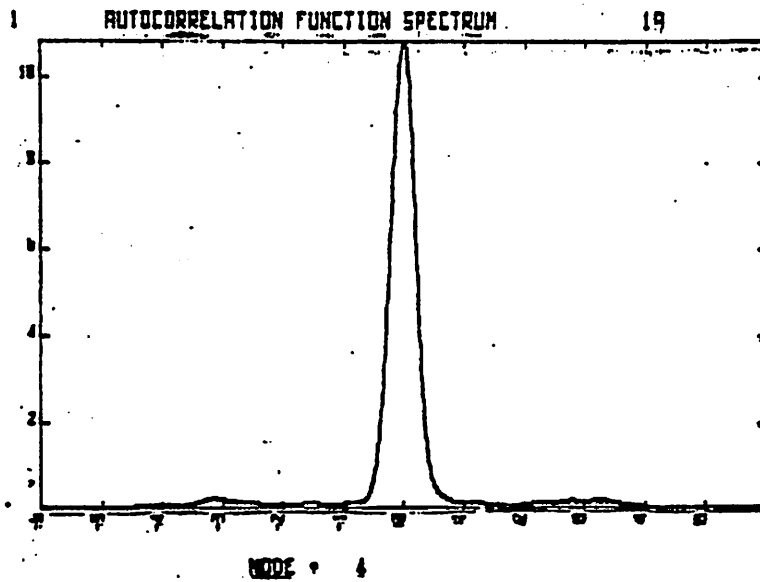
FFT

Alfron wave



Alfron wave

SUD - FFT - Lax-Wendroff



magnitud

Lax method

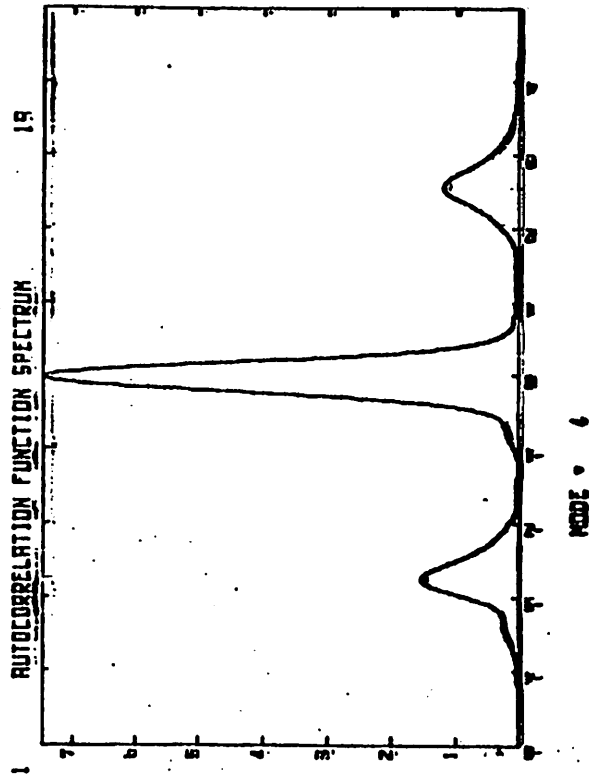
32-32

64-64 p. 1/2

$\bar{B}_2(t, k_1)$

$V_{1/2}$

1 grid - NGP - Lax method



Magnetosphere
 72726
 Lax-Wendroff
 Igrid
 (4x4x4)
 FCT
 Triangular
 mesh

Igrid - NGP F Lax Wendroff

12-2051

Comparison with Other Codes

1. Eulerian - Leapfrog
2. Eulerian - FCT
3. MHD particle
4. Lagrangian - Triangular mesh

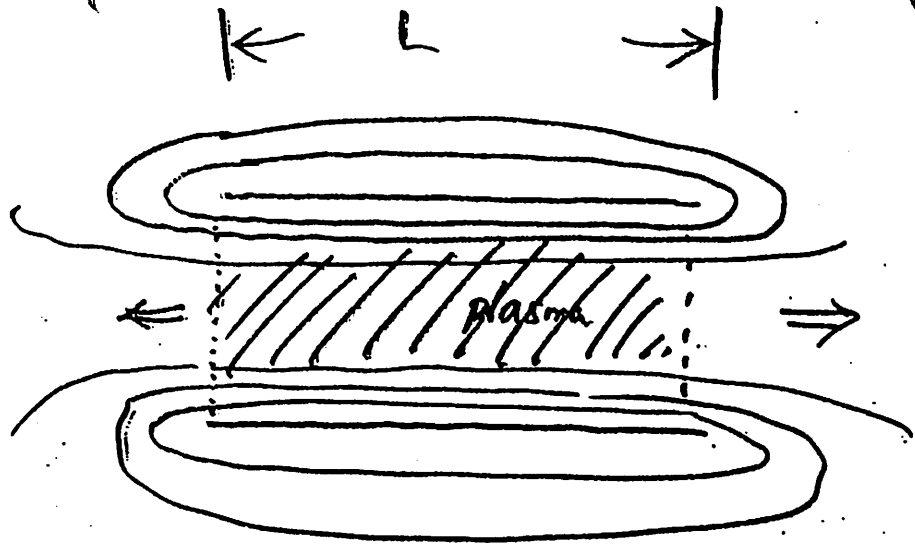
shock 1. not appropriate
 2, 3. OK

Magnetosphere 2, 3. OK

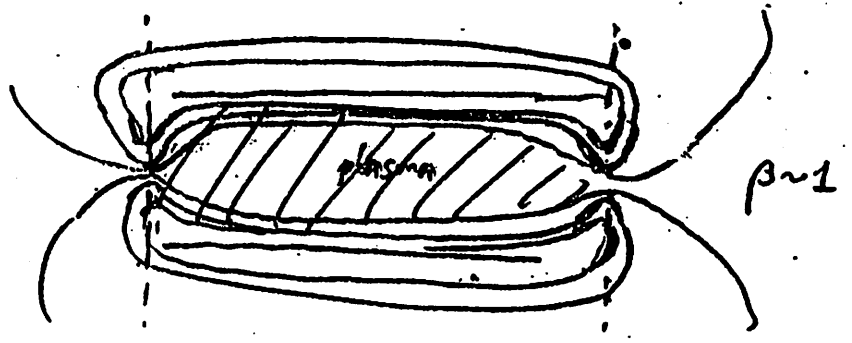
MHD particle code

Most advantageous for

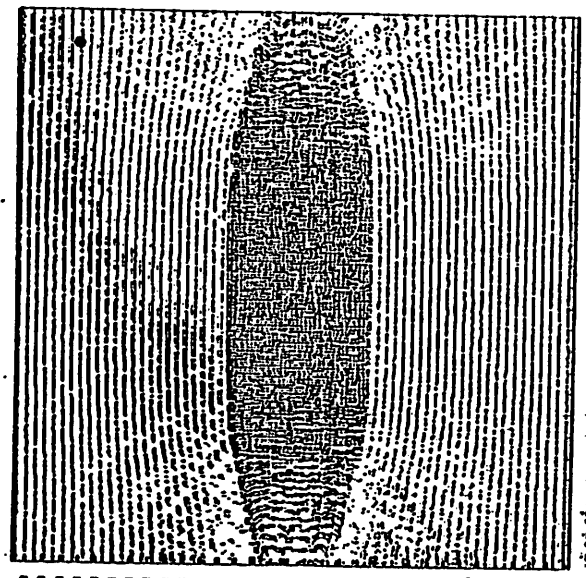
turbulence; convection; churning fluids



$$\tau = \frac{L}{2c_s} \quad (?)$$

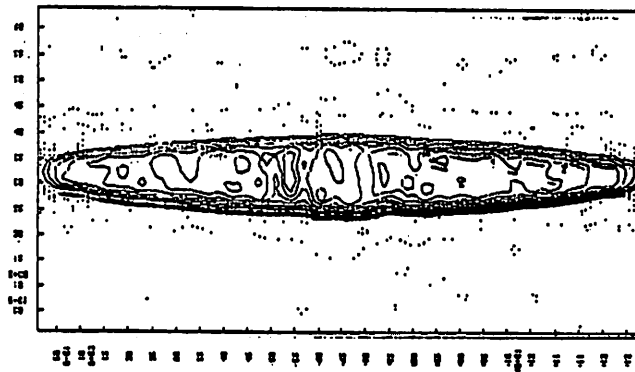
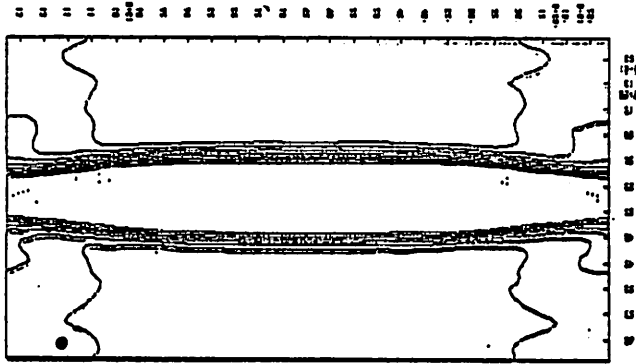


$$\tau \sim \infty \quad (?)$$



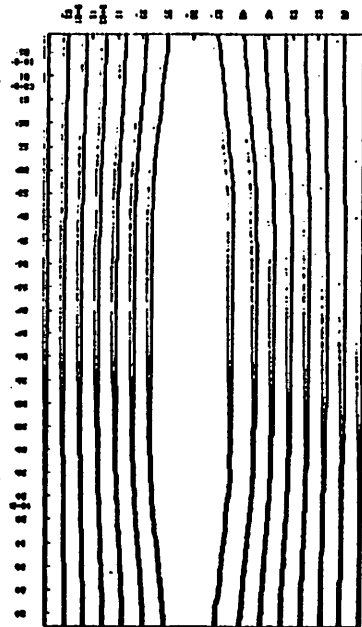
1. 40.00

PROBE 40 BTX T= 40.00 5.18217E-03 2.01570E+00



PROBE 05 DENSITY T= 100.00 3.00271E-01 8.77771E+00

PAGE 48
 TOT R2
 T. 48.88
 1.74576E+00
 9.97481E+01



90

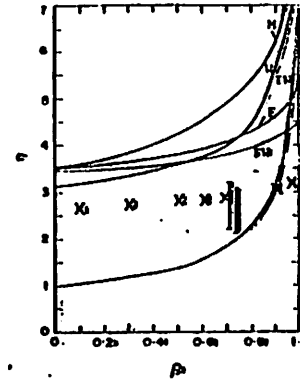


Fig. 2.

The elapsed problem-time in each case is enough for the rarefaction to propagate about 50 cm.

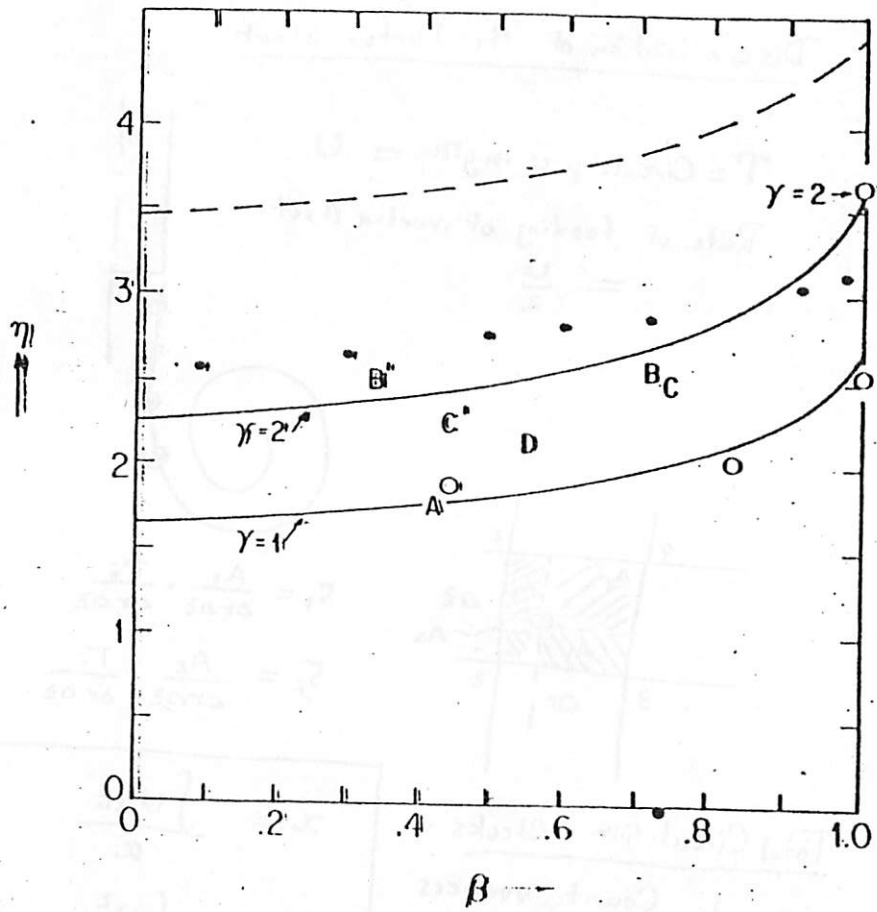
The more difficult computations with magnetic mirrors are being performed. A comparison of the mass decay rates from these calculations, obtained as suggested in (f), will give the crucial test of the ability of ideal MHD to describe endloss. The results for the straight case are very encouraging, however, not only because of their agreement with experiment but also because they suggest that some set of equations, even simpler than the MHD equations describe endloss.

References.

- [1] Freidberg, J. P. and Waltner, H. Nucl. Fusion **15**, 213 (1975).
- [2] Brachbill J. U. Numerical Magnetohydrodynamics for High Beta Plasmas, Maths. in Comp. Phys. **16**, Academic Press, N.Y. (to be published).
- [3] Brachbill J. U. and Barnes, D. C. Time-Dependent Calculations of Equilibrium and Stability Problems in Scyllac and Tokamak Geometries, Proc. of the Third Topical Conf. on Pulsed High Beta Plasmas, Culham (1975).
- [4] Freidberg J. P. and Wesson, J. A. Phys. Fluids **13**, 1117 (1970).
- [5] Waltner, H. (private communication).

(copies from Brachbill's paper.)
 High β Plasma Proc.

91



- solid-lines: our theory
- broken line: Freidberg et al. [Nucl. Fus. 15, 217 (1975)]
- : our simulation ($\gamma=1, 2$)
- : simulation of Brackbill et al. [Third Topical Conference on Pulsed High-Beta Plasmas, p. 315 (1976)]
- A : linear syllac [K.S. Thomas et al. Phys. Fluids 17, 1314 (1975)]
- B : scylla IV-3 [R.F. Gribble et al. Phys. Fluids 14, 2012 (1971)]
- C : scylla I-C [K.F. McEneaney et al. Phys. Fluids 20, 1556 (1977)]
- D : scylla IV-P [K.F. McEneaney et al. LANS report LAUR 78-1909 (1978)]

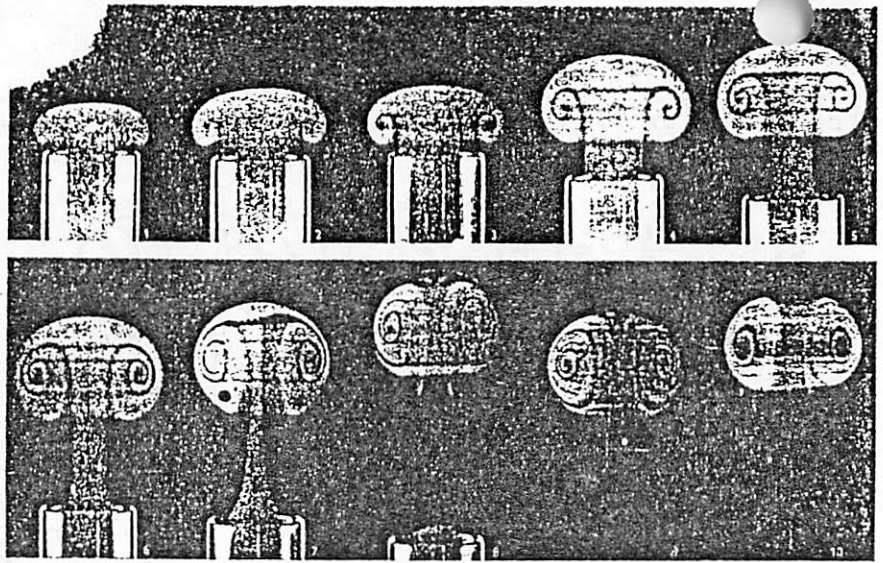


Figure 7.2.2. Different stages of vortex rings formed in water by the ejection of small quantities of coloured liquid (of approximately the same density as water) from the end of a circular glass tube with internal diameter 1.5 cm. There is clear water at the centre of the vortex ring in the last photograph, although it is not apparent from a side-view. (From Okabe and Inoue 1969.)

岡部淳 - OKABE JUN-ICHI

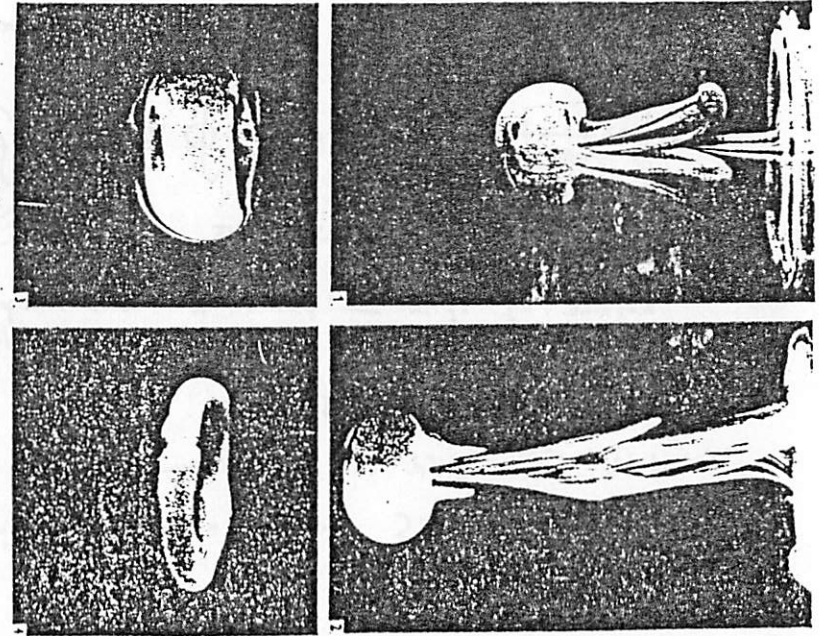


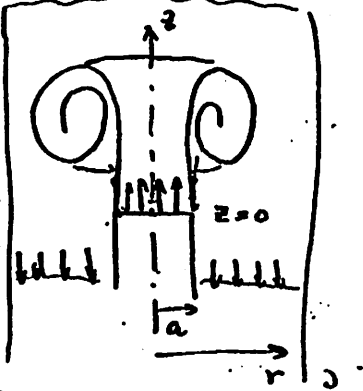
Figure 7.2.3. Different stages of vortex rings formed in water by allowing drops of coloured water to fall vertically from the end of a pipette 1 cm above a free surface. (From Okabe and Inoue 1961.)

6. FORMATION OF JET-HEAD VORTEX RING (CKChn, HCWu) T.T. Lee

$$\frac{D}{Dt} \zeta - \frac{\zeta U_r}{r} = \frac{D}{Dt} \left(\frac{\zeta}{r} \right) = 0$$

$$\nabla^2 \psi = -r \zeta$$

$$u_r = \frac{1}{r} \frac{\partial \psi}{\partial z} \quad u_z = -\frac{1}{r} \frac{\partial \psi}{\partial r}$$



I.C. $\underline{u} = 0$ everywhere

B.C. At jet exit $z=0, r \leq a$

$u_r = 0, u_z = U, \therefore \psi = \frac{1}{2} U r^2$

$z=0, r < a \quad \zeta = 0$

$z=0, r = a \quad \zeta$ prescribed as vortex sheet

$\Gamma = \iint \zeta dA = \oint \underline{u} \cdot d\mathbf{l}$



$\Gamma = U$ per unit length.

Replace by $\Gamma_i = \frac{U}{n}$ per vortex $n = \text{no. per unit length}$

Convert the vortices, keep Γ_i fixed.

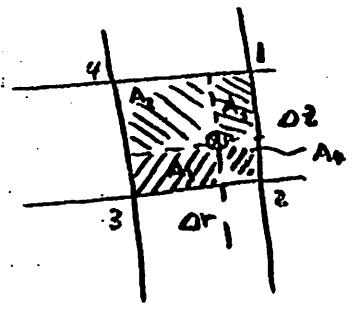
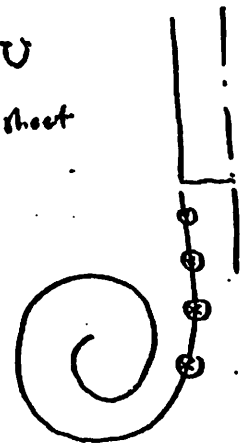
Distribute ζ on grid in $r-z$ plane

Solve $\nabla^2 \psi = -r \zeta$ as an elliptic PDE.

Discretization of the Vortex Sheet

$\Gamma = \text{Circul. p.u. length} = U$

Rate of feeding of vortex sheet
 $= \frac{U}{2}$



$\zeta_1 = \frac{A_1}{\Delta r \Delta z} \cdot \frac{\Gamma_i}{\Delta r \Delta z}$

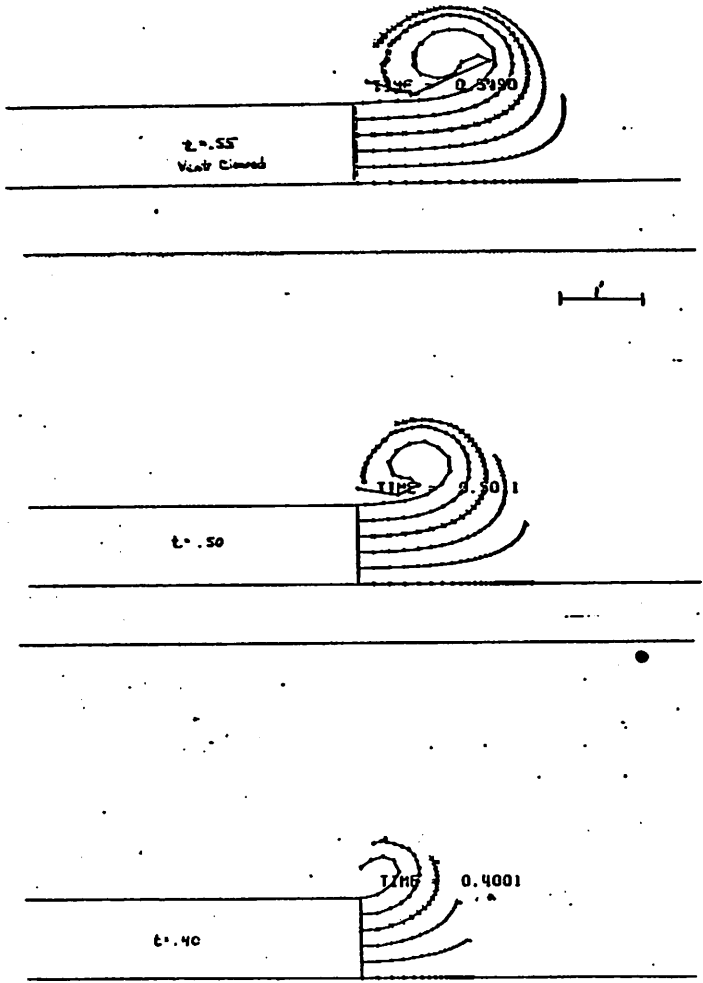
$\zeta_2 = \frac{A_2}{\Delta r \Delta z} \cdot \frac{\Gamma_i}{\Delta r \Delta z}$

Total Circulation Checks:

1. Count vortices
2. $\iint \zeta dA$
3. $\oint \underline{u} \cdot d\mathbf{s}$

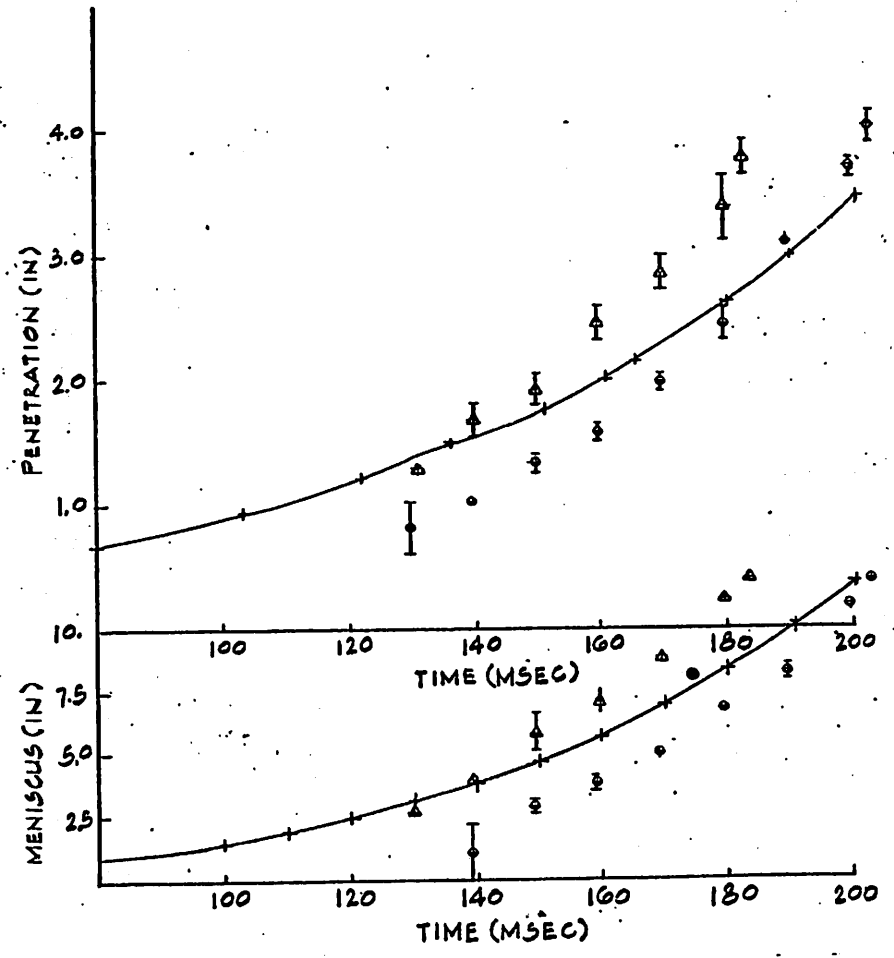
$\tilde{\zeta} = \frac{\int U dt}{a}$

$\tilde{\Gamma} = \frac{\int \frac{U^2}{2} dt}{U_{max} a}$



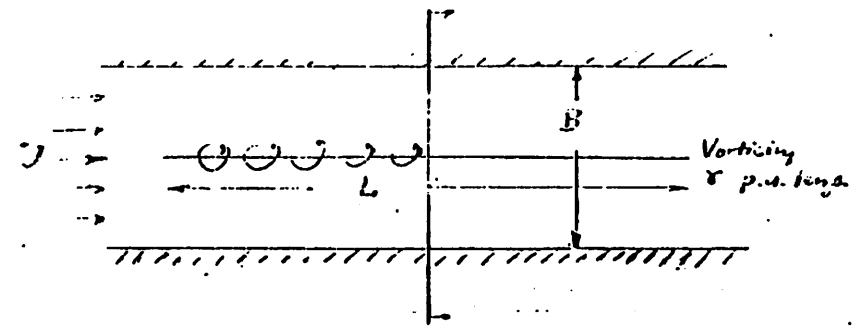
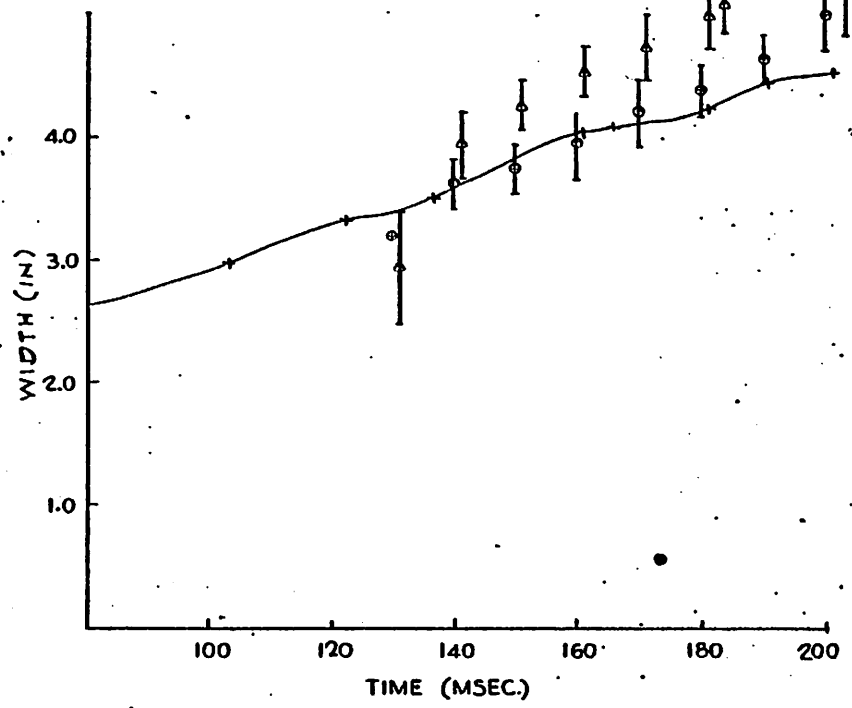
MUSHROOM GROWTH-PENETRATIONS VS TIME FOR 12" SUBMERGENCE

- - TEST 1
- △ - TEST 2
- + - CALCULATION



MUSHROOM GROWTH - WIDTHS V S TIME FOR 12" SUBMERGENCE

- - TEST 1
- △ - TEST 2
- + - CALCULATION



$L/B \gg 1$, Vortex sheet infinitesimal thickness

$$u = U + \frac{\gamma}{2} \quad \text{for } y \geq 0$$

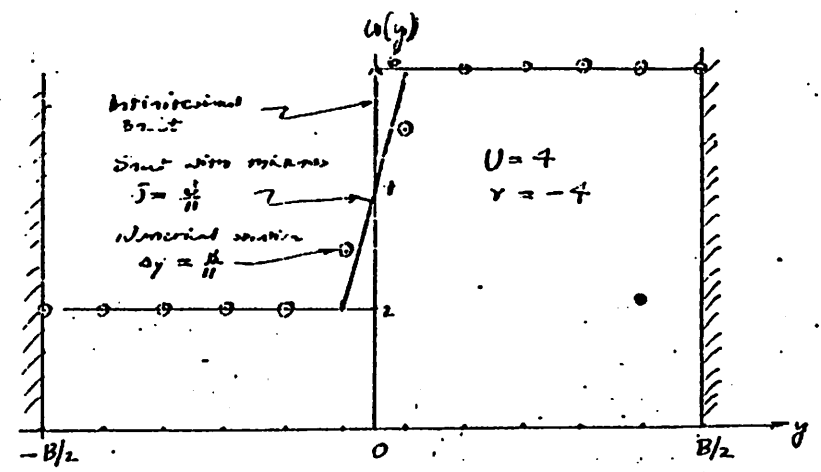
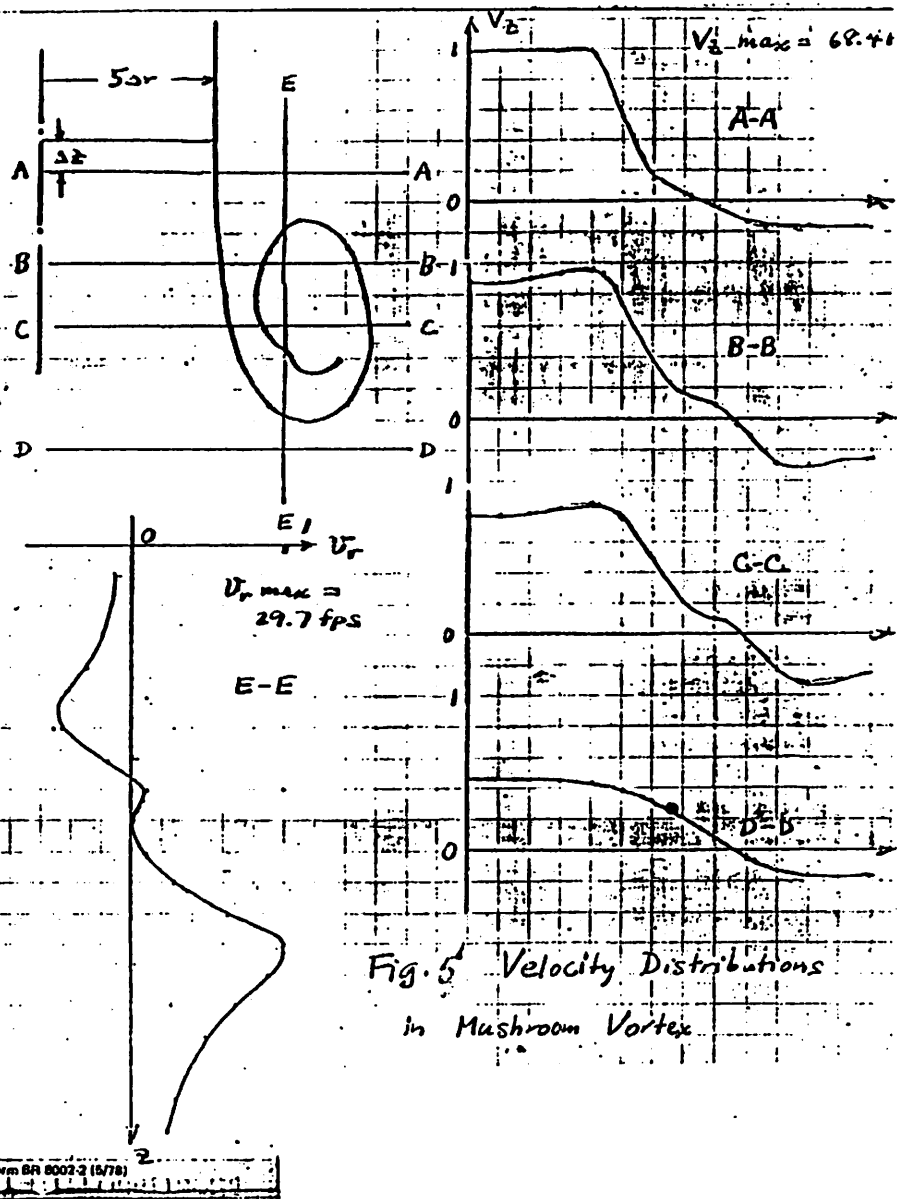


Fig. 4. Sample Vortex Sheet Problem



Form BR 8002-2 (4/78)

Steady State Drift Turbulence & Anomalous Diffusion (Electrostatic) low β

Exp

$$\tau_p, \tau_e \gg \gamma, \omega^*$$

Okuda, PPPL

$$\frac{\partial n}{\partial t} + \nabla \cdot \Gamma = S$$

$$\Gamma \approx D \nabla n$$

Simulations

initial value problem:



→ oscillation
vortex formation

mechanisms for anomalous diffusion

steady state problem: ionization & recycling

Experimental Observations (octupole experiments)

- Very small diffusion due to steady state Drift Turbulence (Drift, Trapped Particle Turbulence)
- Sensitive to q values
 - q : rational
 - q : irrational

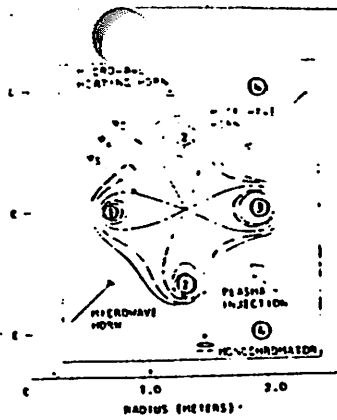


FIG. 1. Layout of the de octupole showing the location of the current rings and important flux surfaces. The symbol ψ_s indicates the separatrix, ψ_{min} is the surface with the minimum magnetic field, and ψ_c is the stability limit surface. The axis of symmetry is at left.

4341009D

© 1978 American Institute of Physics

434

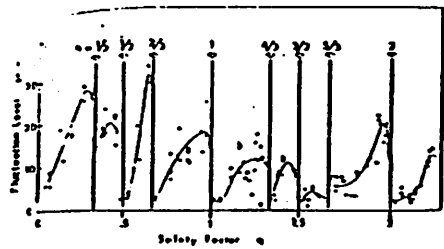


FIG. 6. Fluctuation amplitude as a function of safety factor q for lithium plasma ($T_e \approx 7$ eV).

Prater, Ejima, Ohkawa, Wong

PF 434, 21 (78)

collisions less plasma

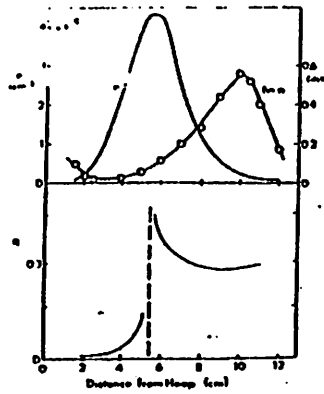


FIG. 2. (a) Density n and fluctuation amplitude $\delta n/n$ and (b) safety factor q , as a function of distance above the top internal octupole hoop.

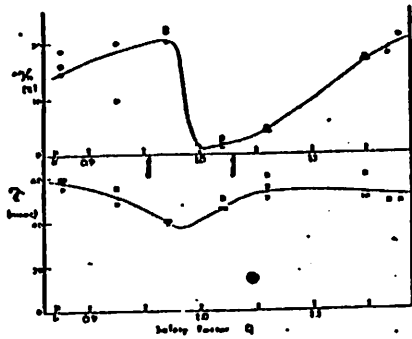


FIG. 7. (a) Fluctuation amplitude measured at 16 cm above No. 21 hoop as a function of q. (b) Plasma lifetime τ as a function of q.

Prater, Ejima, Ohkawa, and Wong

435

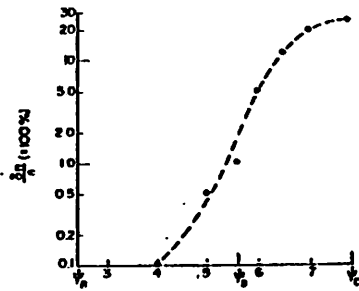


Fig. 1. The observed value of $\delta n/n$ as measured by Langmuir probes is plotted as a function of position, ψ_c .

waves propagated up the density gradient as well as perpendicular to it resulting in oblique propagation at roughly 45° to the direction of the density gradient. The parallel wavelength was measured to be about equal to the minor circumference of the torus or about 3.5 m resulting in a parallel phase velocity intermediate between ion and electron thermal speeds as expected for a drift wave. The observed values of $\delta n/n$ were approximately equal to $e\delta\phi/T_e$ and were observed to grow from about 0.1% inside ψ_c to about 25% at ψ_c as shown in fig. 1 for a value of $B_p \sim 750$ G.

Shown in fig. 2 is the time evolution of the density profile observed when $B_p \sim 750$ G compared with the predicted evolution due to classical diffusion using the $t = 0$ profile as an initial condition. The agreement was very good both in magnitude and in profile shape with the profile relaxing to a near normal mode shape [5] in 9 msec. It then decays with a decay time comparable to the 100 msec decay time of the magnetic field. This good agreement was obtained both in the quiescent region inside ψ_c and in the region with large amplitude fluctuations outside ψ_c . Clearly then the transport due to these drift modes was much less than that due to classical diffusion in this case, although anomalous transport due to this mode has been observed in other experiments [6]. Furthermore, over the range in magnetic field from $B_p \sim 250$ G to $B_p \sim 1.25$ kG the confinement time increased by over an order of magnitude while the value of $\delta n/n$ in the average-minimum-B regions actually increased somewhat.

224

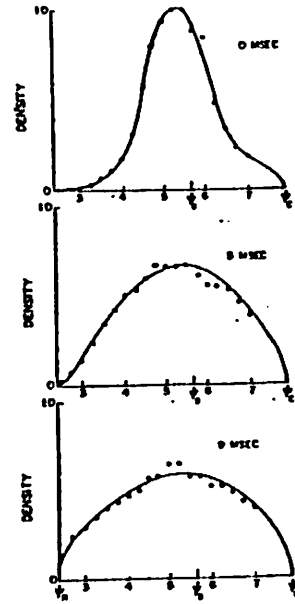
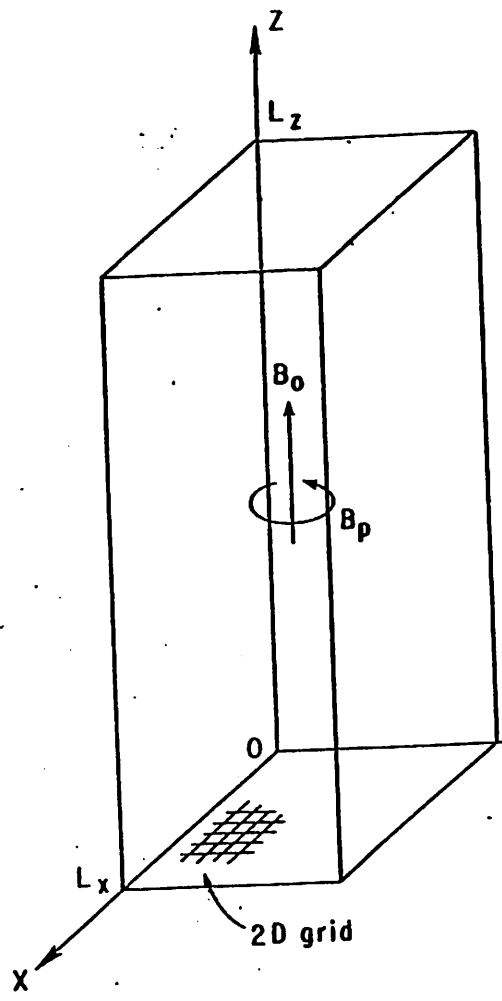


Fig. 2. The observed density profile with $B_p \sim 750$ G used as an initial condition at $t = 0$ and evolved for 9 and 90 msec in time by numerical solution to the diffusion equation using only classical diffusion. This predicted shape is compared with the experimental points at $t = 9$ msec and $t = 90$ msec. The density is normalized to 1.0 with the peak initial density equal to 1.2×10^{13} cm $^{-3}$. The scatter in the experimental points is due to digitizing errors in the data acquisition system and the δn fluctuations. The normal mode decay of the plasma relative to the magnetic field 9 msec after injection is 109 msec.

We conclude, therefore, that the diffusion due to the fluctuations, D_T , must be less than 10% of the magnitude of the classical diffusion or a significant difference in the time evolution of the density profile inside ψ_c and outside ψ_c would have been observed. This implies that $D_T < (1/250) D_{Bohm}$ for a fluctuation amplitude of $\delta n/n \sim 20\%$ in contradiction to the usual assumption of Bohm-like transport due to large

amplitude one must be able to transport them. The experiment does not guarantee the transport. In fact, anomalous presence of $\sim \Sigma_k k_{\parallel} \delta n$ fluctuation electrostatic interaction between the modes, $k_{\parallel} k_{\perp}$ factor, and the transport would give $\sin \psi_c \approx 0$. attempt was fluctuation ≈ 0.1 the δn larger than large transport [4, 8] or so

Slab Model



- free ions
- g.c. electrons

$\exp(ik_z Z)$ expansion
or higher order interpolat

$$\vec{B} = B_0 \hat{z} + B_p \cos \theta \hat{\theta}$$

$$\frac{B_p}{B_0} = \frac{2\pi r}{\ell L_0}$$

$$\begin{cases} \Delta x, \Delta y \sim \rho_i \\ \Delta z \gg \rho_i \end{cases}$$

$$\omega_{pi} \text{ at } \sim 0.5$$

$$v_{pi} \text{ at } \frac{1}{2}$$

772047

Fig. 1. A sketch of the simulation model. The plasma is imbedded in an external magnetic field. The model is periodic in z direction while the conducting walls are assumed in x, y directions.

typically $m_i/m_e \sim 4.60$
 $N \sim (\frac{1}{8} - \frac{1}{4}) M$

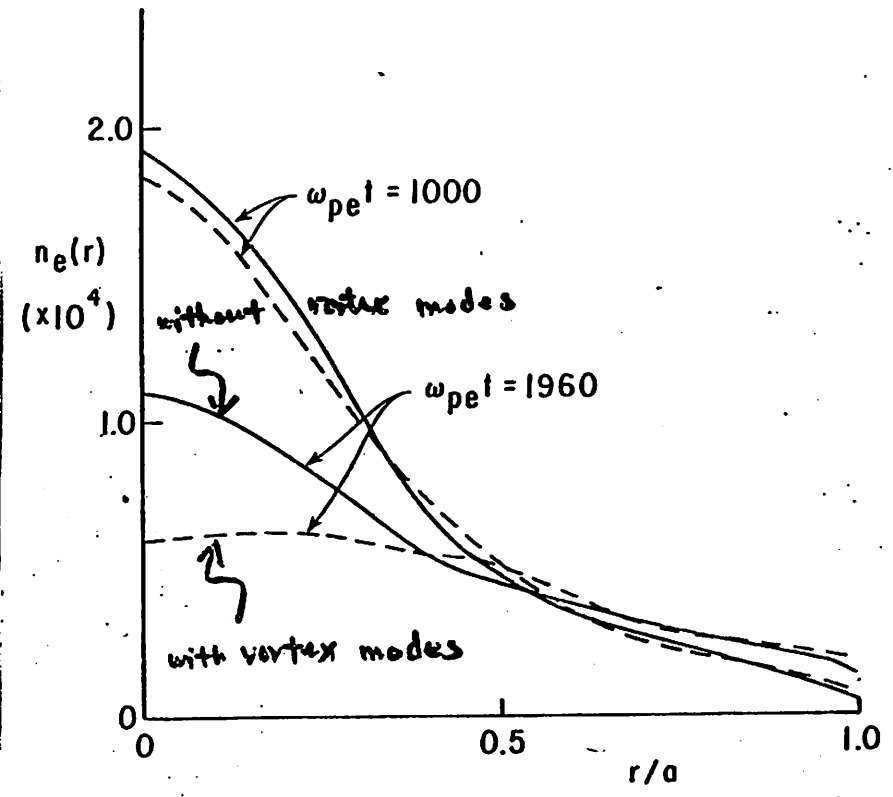
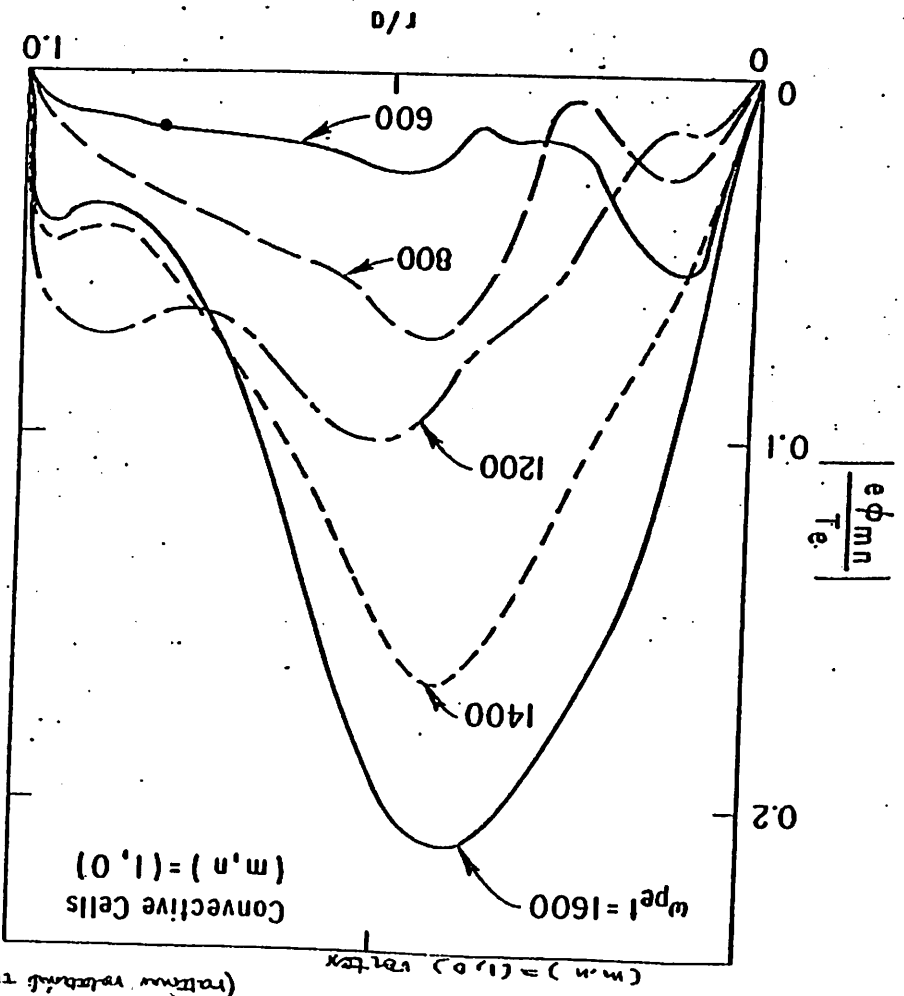


Fig. 13. Particle diffusion in the absence of convective cells. Fig. 11 is also plotted for comparison.

762384



772436
 Fig. 3. Radial mode structure of the largest convective cells and its time evolution. Case 1.

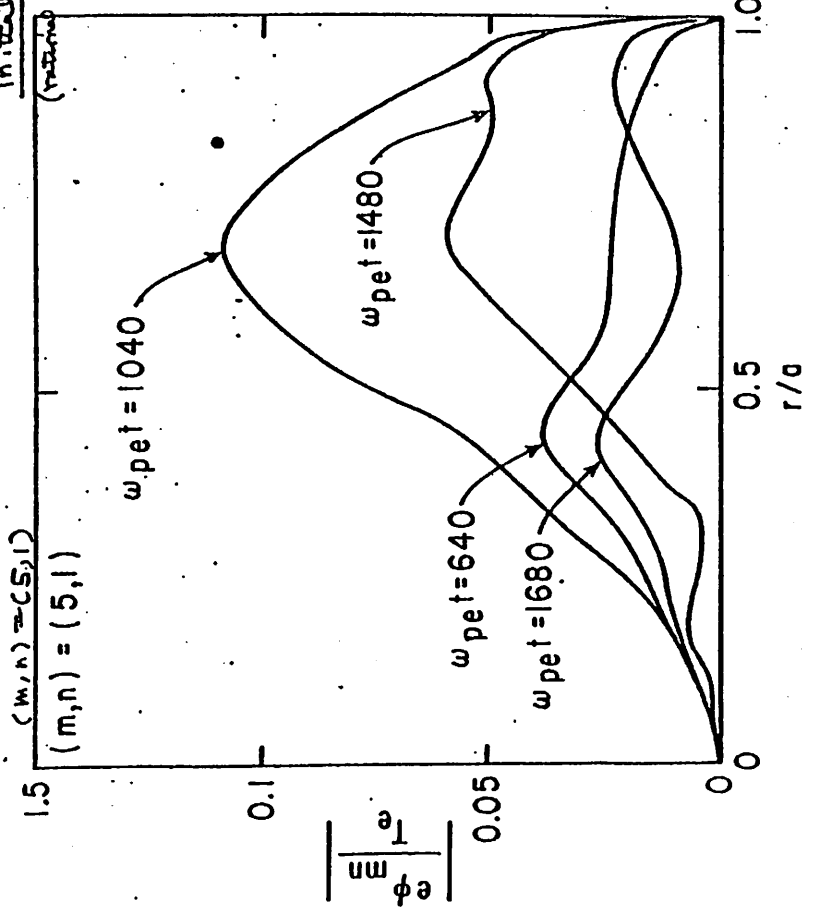
they predict

$$\frac{e\phi_m / T_e}{\omega_{pe} t} = \frac{r_i}{r_e} \frac{\omega_{pe}}{\omega_{ce}}$$

as that

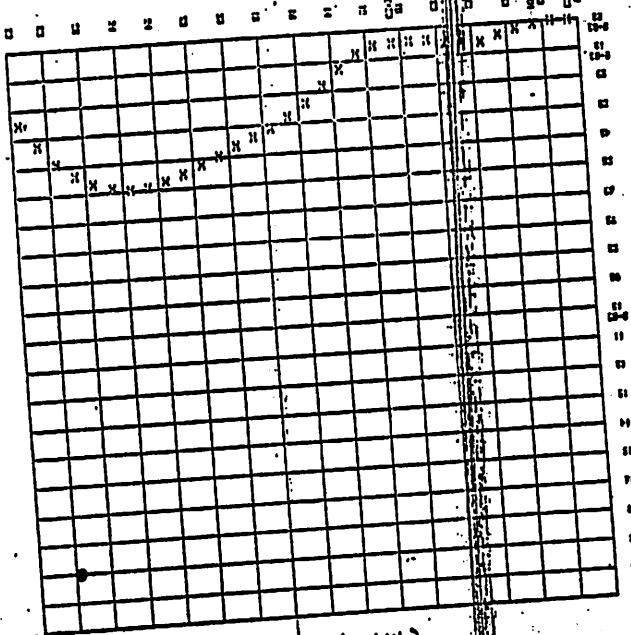
$$\frac{e\phi_m / T_e}{\omega_{pe} t} \ll r_i / r_e$$

Initial Value Problems
 (radial notational sumflow)



772445
 Fig. 4. Time development of the radial mode structure of the most unstable mode $(m, n) = (5, 1)$. Case 1.

POTENTIAL PROFILE OF THE 30-TH HARMONIC IN KTH AND THE 2-TH HARMONIC IN KZ



Drift wave

$$f = 800$$

(1, 1)

$$f = 1.2 \cdot 2.1$$

$$(m, n) = (-3, 1)$$

$$N = 800 \quad \gamma = 2$$

rational rotational transform
($\gamma = 2$)

Steady state turbulence

$$N = 400$$

$$(m, n) = (-3, 1)$$

$$N = 400$$

$$\gamma = 2$$

drift mode

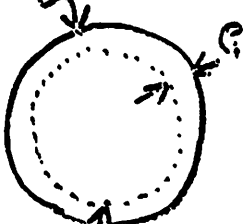
$$(m, n)$$

$$= (-3, 1)$$

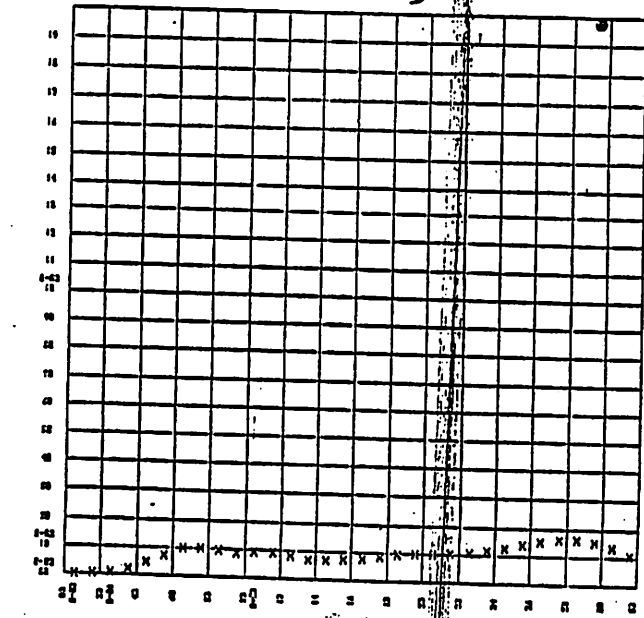
Drift mode

$$\frac{e\phi}{T_e}$$

ion boundary

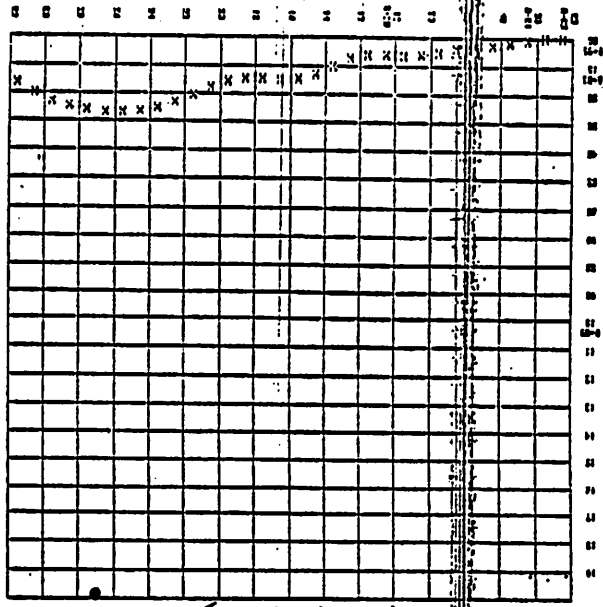


electron boundary



POTENTIAL PROFILE OF THE 30-TH HARMONIC IN KTH AND THE 2-TH HARMONIC IN KZ

POTENTIAL PROFILES OF THE 20-TH HARMONIC IN KTF AND THE 2-TH HARMONIC IN KZ



$\beta = 2$ $N = 1200$
 $(m/n) = (-3, 1)$

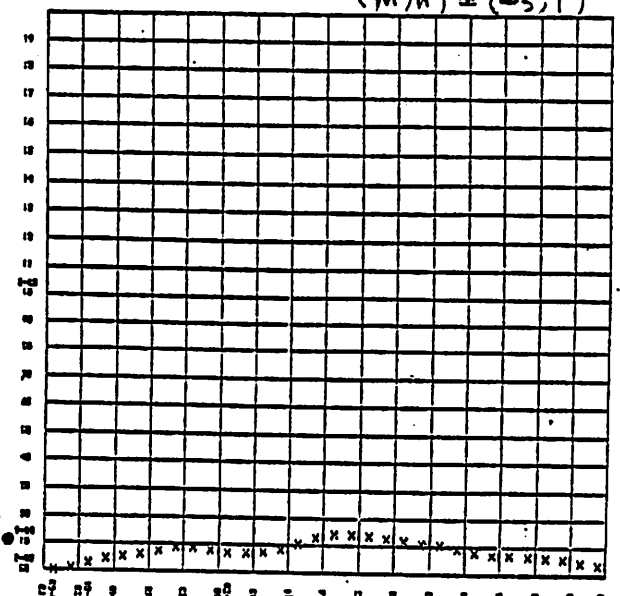
$t = 1200$
 Drift Wave

$t =$

110

$\beta = 2$ $N = 1200$
 $(m/n) = (-3, 1)$

$t = 1800$
 $(m/n) = (-3, 1)$



POTENTIAL PROFILES OF THE 20-TH HARMONIC IN KTF AND THE 2-TH HARMONIC IN KZ

111

Q. r 79

Steady state Turbulence

$\delta = 2$

$N = 410$

rational transform $\delta = 2$ (no skew) $\eta = 2$

vortex mode

$$R_n = \frac{R \cdot B}{B}$$

$$= \frac{f_2 B_2 + f_1 B_1}{B}$$

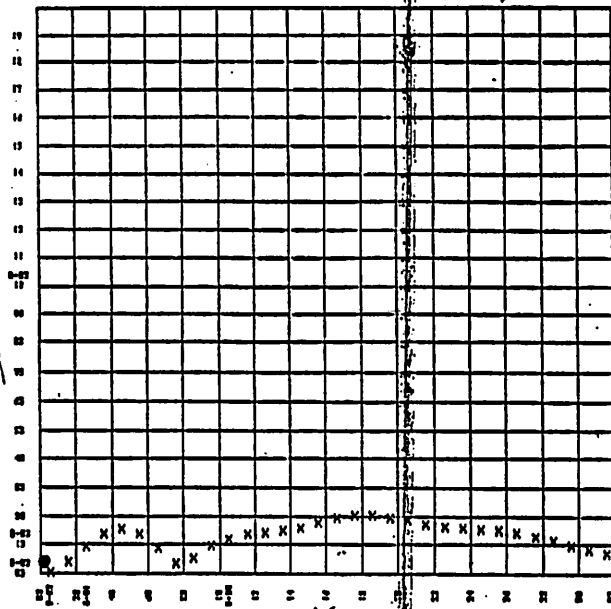
$$= \frac{f_2 B_2}{B} \left(1 + \frac{f_1 B_1}{f_2 B_2} \right)$$

$$= \frac{f_2 B_2}{B} \left(1 + \frac{2\pi r}{L} \frac{n}{m} \frac{B_1}{B_2} \right)$$

$$= \frac{f_2 B_2}{B} \left(1 + \frac{n}{m} \delta \right) \left| \frac{e\psi}{T} \right|$$

- $= 0$ for:
- $(m, n) = (-2, 1)$
 - $(2, -1)$
 - $(4, 2)$
 - $(-4, 2)$
 - etc
- vortex modes

$(m, n) = (-2, 1)$



POTENTIAL PROFILE OF THE 31-TH HARMONIC IN KTH AND THE 2-TH HARMONIC IN KZ

(m, n)
 $= (-2, 1)$
 $t = 400$

Vortex modes

112

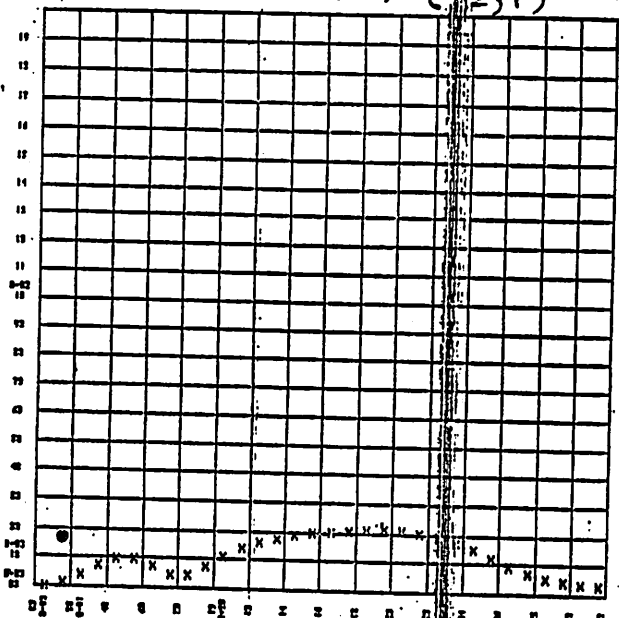
$N = 1000$

$N = 1000$

$\eta = 2$

$t = 1000$

$(m, n) = (-2, 1)$



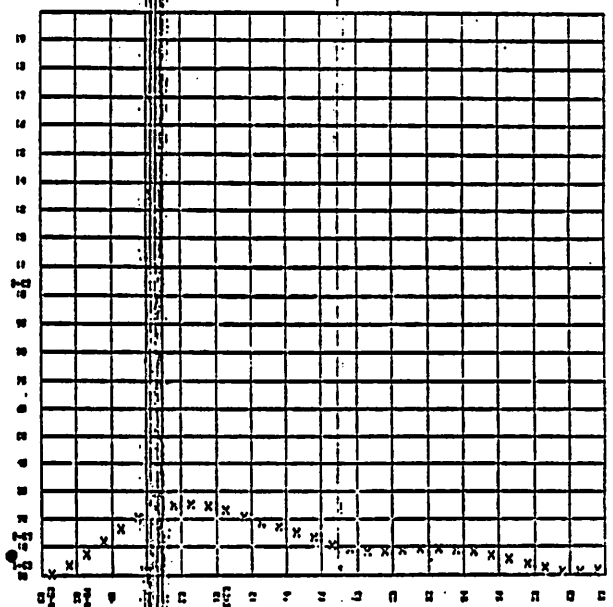
POTENTIAL PROFILE OF THE 31-TH HARMONIC IN KTH AND THE 2-TH HARMONIC IN KZ

113

6.00
 2
 100
 at

$t=1200$

$\eta=2$



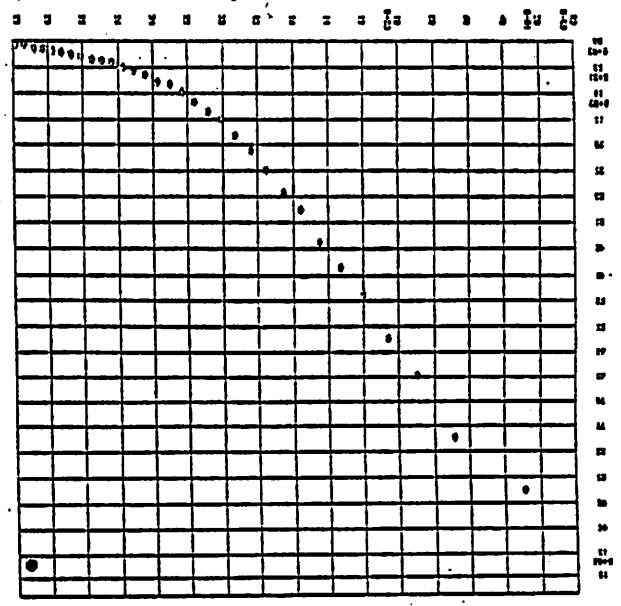
POTENTIAL PROFILE OF 1ST-TH HARMONIC IN KTM AND THE 2ND-TH HARMONIC IN KZ

(1, 0)
 (-3, 1)
 (5, 4)
 (-2, 1)

$R_{11} = 0$
 $R_{10} \delta_0 + R_{20} \delta_2 = 0$
 $2 = 8 = -\frac{m}{k}$

534

K-QUIDING CENTER DISTRIBUTION, $t=1600$



2

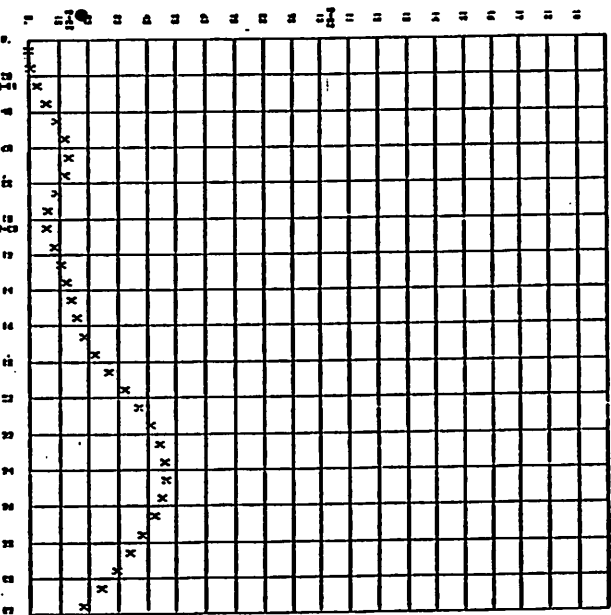
$t=1600$

Steak sub Tullu u

15
 (8=2)
 various potential harmonics

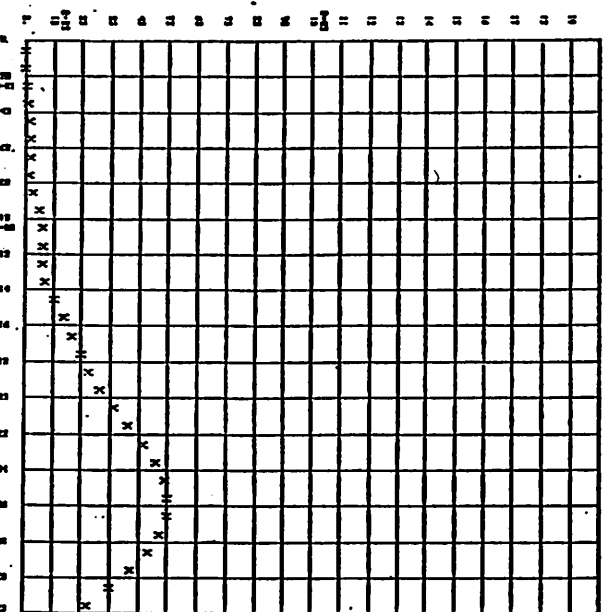
115
A17010

(m,n) = (-3, 1)



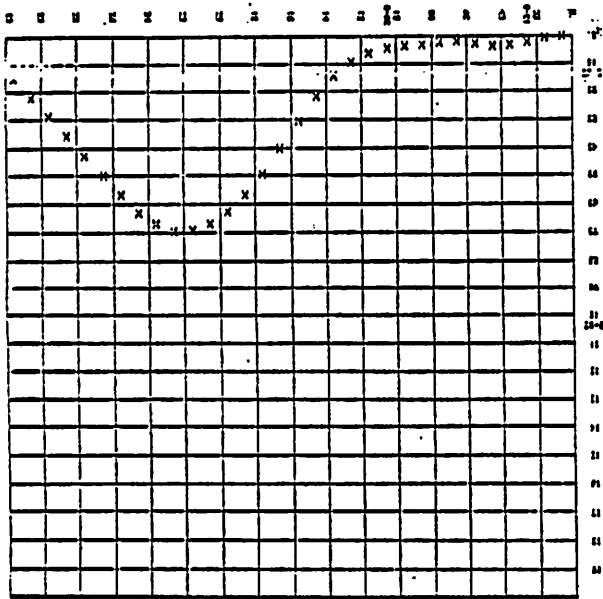
POTENTIAL PROFILE OF THE 30-TH HARMONIC IN KM RAD. THE 2-TH HARMONIC IN KZ

$f = 15$
 $N = 1200$
 $(m,n) = (-4, 2)$



POTENTIAL PROFILE OF THE 24-TH HARMONIC IN KM RAD. THE 2-TH HARMONIC IN KZ

POTENTIAL PROFILE OF THE 20-TH HARMONIC IN KTH AND THE 2-TH HARMONIC IN KZ

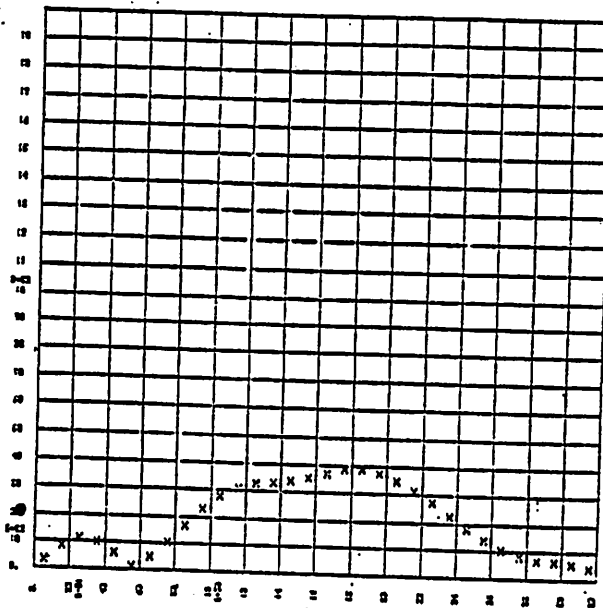


$(1.5) - (1.0)$

1.5

1.0

$\delta = 15$
 $N = 140$
 $(1.5) - (1.0)$



POTENTIAL PROFILE OF THE 20-TH HARMONIC IN KTH AND THE 1-TH HARMONIC IN KZ

119

119

8 REMARKS ON THE USE OF INTEGRALS OF MOTION.

B. MNATARA,
LLC. Dec. 1979.

Numerical modelling works best with careful choice of independent coordinates (flux surfaces, field lines, etc.) and dependent variables. Integrals of motion - μ , J , P_θ for particles, total mass, angular momentum, parallel flow, etc for fluids - are prime candidates.

GLOBAL INTEGRALS OF 1 FLUID MODEL:

$$N = \int n d^3x, \quad G = \int d^3x \vec{V} \cdot (\vec{B} + \frac{m}{2e} \nabla \times \vec{V}), \quad K = \int d^3x \vec{A} \cdot \vec{B}$$

$$\vec{L} = \int d^3x (\vec{r} \times \rho \vec{V}).$$

$$\text{Minimize } W = \int d^3x (B^2 + \frac{p}{\beta_1} + \frac{1}{2} \rho V^2)$$

with G, K, L, N as constraints to get equilibrium equations, & lowest energy states.

Relaxation of constraints \rightarrow instability.

AXISYMMETRY: GLOBAL \rightarrow SURFACE AVERAGES.

$$N(\psi) = \oint n \frac{d\ell}{R} / \oint \frac{d\ell}{R} = \langle n \rangle$$

$$g = \oint \frac{d\ell}{R} (\vec{V} \cdot \vec{B}) / \oint \frac{d\ell}{R}$$

$$K_0 = \langle A_\theta B_\theta \rangle \equiv q(\psi) \text{ in Tokamak.} \quad L = \langle \rho V_\theta \rangle$$

These are exact integrals, in the frame moving with ψ , for ideal plasma. The unaveraged part of the eqns. of motion allow for transport and wave propagation. Wave propagation can be completely eliminated, leaving only transport effects, by ensuring that equilibrium constraints are satisfied. These are Grad-Shafranov, a Bernoulli law for poloidal flow, charge neutrality, poloidal momentum - one constraint arising with from each integral of motion.

MULTISPECIES MODELS: Integrals + constraints can eliminate high frequency phenomena \rightarrow long time scales.

9. LIBRIS

FUNCTION-- AN ONLINE ABSTRACTING SYSTEM FOR COMPUTER SOFTWARE, E.G., PHYSICS CODES, ENGINEERING CODES, MATHEMATICAL AND GRAPHICS ROUTINES, UTILITIES, LIBRARIES, ETC.

ADVANTAGES OF AN ONLINE SYSTEM

- EASY TO EXCHANGE CODES ("RELEASE" ON MFE NET IS EQUIVALENT TO A "LOCAL" RELEASE)
- PUBLICITY-- MFECC BUFFER CONSULTING FROM MFECC ABSTRACT LISTINGS
- CONVENIENCE-- (NEW RELEASE ~ SPRING 1980)

NEW LIBRIS

NEW LIBRIS (CONT.)

LIBRIS REWRITE

- TECHNICAL PROBLEMS IN CURRENT VERSION
(FILE FORMATS, FILE STORAGE,
INFLEXIBLE OUTPUT)
- MORE HUMAN ENGINEERING NEEDED
- AVAILABILITY ON CRAY-1 AND 7600
(ULTIMATELY SHARED DATA BASE)
- MUCH IMPROVED RETRIEVAL

NEWLBRIS PROPOSAL IN DOCUMENT:

DOCUMENT PRINT NEWLBRIS DEVICE BOX NNN 1 D

COMMENTS TO CAROL TULL USER # 764

HIGHLIGHTS:

- NUMEROUS RETRIEVAL FIELDS, E.G.
AUTHOR DIVISION INSTALLATION
LANGUAGE SUBJECT
- INTERACTIVE SEARCHING THROUGH SUBJECT
CATEGORIES, E.G.

MATH PHYSICS (HANDOUT) ENGINEERING	→	ODE ROOTS FUNCTIONS LINEAR SYSTEMS PDE
--	---	--
- GRAPHICS
- ADD ABSTRACTS EITHER INTERACTIVELY
OR WITH TEXT FILES
- EDIT AND REVISE YOUR ABSTRACTS WITH
YOUR FAVORITE EDITOR

LIBRIS STATUS

PHYSICS + ENGINEERING CODES	33 ABSTRACTS
MATHEMATICAL ALGORITHMS AND COMPUTER SCIENCE	18 ABSTRACTS
MATHEMATICAL LIBRARIES	3 ABSTRACTS
UTILITY ROUTINES	11 ABSTRACTS

(SEE HANDOUTS FOR A BRIEF DESCRIPTION OF THE ABSTRACTS)

FUTURE WORK

PERIODIC MFECC PUBLICATION OF CODE LISTINGS TO ALL USERS

ADDITION OF MATHEMATICAL ROUTINES (K. FONG, ET. AL.)

ADDITION OF NESC ABSTRACTS

ONLINE PHYSICS CODE DOCUMENTATION ???

INFORMAL CONFERENCE ON PARTICLE AND HYBRID CODES FOR FUSION

December 10-11, 1979

CODE SYNOPSIS

Code Name: _____

Contact(s): _____

Machines: _____

Description: _____

Other Comments:

Return to:

Carol Tull
National Magnetic Fusion Energy Computer Center
P. O. Box 5509 L-402
Lawrence Livermore Laboratory
Livermore, California 94550

Fokker-Planck codes

No. 7 ISOTIONS - A. A. Mirin, NMFEEC CDC-7600

This is a one-dimensional multispecies code in which the distribution functions depend on speed only. Applications with this code include Q calculations for mirror reactors in which there is neutral beam injection.

No. 8 ISOLEGEND - A. A. Mirin, NMFEEC Cray-1 and CDC-7600

This is a two dimensional code in which the distribution functions depend on both speed and pitch angle (using a Legendre expansion). The code includes an axial electric field and models electrons and one ion species. The primary application for the code is to study runaway electrons and ions.

No. 9 THDSZ - A. A. Mirin, NMFEEC Cray-1 and CDC 7600

This is a three-dimensional multispecies code in which the particle distribution functions depend on speed, pitch angle, and one spatial co-ordinate. An electric field is computed self-consistently using a Poisson solver.

No. 10 HYBRID-II A. A. Mirin, NMFEEC Cray-1 and CDC-7600

This is a two-dimensional multispecies Fokker-Planck code in which the ion distribution functions depend on speed and pitch

angle. The electrons are taken as Maxwellian. Applications include mirror devices (both standard and tandem) and tokamaks. Various physical phenomena may be included.

No. 12 TDMFP - A. A. Mirin, NMFEEC, Cray-1 and CDC-7600

This is a two dimensional multispecies code which models two dimensional electrons and ions in the presence of a mirror loss cone. RF diffusion is included. Applications include modeling the effect that untrapped particles have on trapped particles in a tandem mirror device.

No. 56 FPPAC - M. G. McCoy and A. A. Mirin, NMFEEC Cray-1 and CDC-7600

This Fokker-Planck package is designed to be incorporated into large physics code drivers. It solves the full time dependent, nonlinear, multispecies equation in two dimensions, speed and pitch angle. The package is optimized for both the Cray-1 and the 7600 with the Cray version running up to 12 times faster than the 7600 version.

Transport codes

No. 11 FPT - A. A. Mirin, NMFEEC Cray-1 and CDC-7600

This is a transport code applicable to beam injected tokamaks. The energetic ions are described by two dimensional velocity space distribution functions which are time-integrated using the nonlinear Fokker-Planck operator. Applications include PLT, TFTR, PDX, and DITE.

Equilibrium codes

No. 18 ELLIPTI - J. C. Taylor, University of Glasgow (Scotland) PDP-10

This code is designed to solve nonlinear elliptic equations in two-dimensional regions.

No. 43 ORNLEQ - B. Dory, ORNL CDC-7600

This is the conducting shell version of the two-dimensional axisymmetric tokamak equilibrium code developed at ORNL for tokamak MHD calculations.

Magnetic field calculation codes

No. 13 MAFCO76 - C. Finan, NMPECC CDC-7600

This code computes magnetic fields for an arbitrary set of point conductors and calculates dI/B integrals.

No. 19 MSUPER - Larry Miller, UCLA CDC-7600

This is an interactive code for designing magnetic fields using Tektronix scopes. In this version, the code calculates magnetic fields due to point sources in systems with azimuthal symmetry.

No. 20 MFIELD - Larry Miller, UCLA CDC-7600

MFIELD is an interactive code for designing and plotting (on Tektronix scopes) magnetic fields for an arbitrary set of point current sources.

No. 37 EFFI - Steve Sackett, LLL Cray-1 and CDC-7600

This code calculates magnetic flux lines, fields, forces, and inductance for an arbitrary system of rectangular cross section conductors.

Dispersion equations and the plasma dispersion function

No. 21 ROOTS - Michael Gerver, Cornell CDC-7600

ROOTS calculates and plots the linear normal modes for electrostatic perturbations of a Vlasov plasma.

No. 36 ZETA - Bill Sharp, LLL CDC-7600

ZETA numerically computes the value of the Fried-Conte plasma dispersion function using three different approximation methods depending on the value of the argument of the function.

Hybrid codes

No. 14 FLUPA - Bill Hobbs, NRL CDC-7600

FLUPA is a particle-fluid hybrid code in which the thermal portion of the distribution function is represented as a fluid and the high energy tail of the distribution is represented by particles. Applications with this code include studies of the evolution of ion-acoustic waves, Landau damping, and nonlinear oscillations of the O'Neil analysis.

No. 25 GUIDON77 - C. G. Tull, NMFECC CDC-7600

This is a three-dimensional self-consistent guiding center particle model coupled with a plasma equilibrium calculation. Some particle collisional effects are included. Applications include neutral beam injection into toroidal systems.

Particle codes

No. 16 TIBROX R. Stephen Devoto, LLL CDC-7600

TIBROX computes single particle orbits for charged particles in magnetic fields. The fields may be computed analytically, input from other codes, or calculated internally using HAFCO76 type algorithms for a general set of point current sources. The code also performs field curvature, $d(\ln B)/ds$, and guiding center calculations.

No. 26 ESI A. Bruce Langdon, LLL Cray-1 and CDC-7600

This is a one-dimensional self-consistent electrostatic particle code with the provision for an external magnetic field. ESI has been used as a starting point in research applications as well as an introductory and experimental code.

No. 34 RINGA - A. Mankofsky, Cornell CDC-7600

RINGA is a self-consistent magnetostatic particle code (2.5 dimensional) used to study the behavior of strong axisymmetric ion rings.

No. 55 SPLASH - D. Nielsen and James Green, LLL and Stanford CDC-7600

SPLASH is a package of 9 codes used for three-dimensional self-consistent electromagnetic particle simulations. Several geometries and physical systems may be simulated with this code including uniform plasmas, columnar plasmas, RF plasma heating, mirror plasmas, and neutral beam injection into mirror systems.

Reaction rate calculations

No. 17 SIGMA*V - Kris Rothe, ORNL CDC-7600 and IBM 360/91

This subroutine package calculates reaction rates, $\langle \sigma v \rangle$, for 25 light elements for a specified temperature in the range from 1 to 1000 keV.

No. 65 SIGV - R. Stephen Devoto, LLL PDP-10

SIGV is a subroutine package for evaluating reaction rates, $\langle \sigma v \rangle$, for several commonly occurring distribution functions: 1). two Maxwellian species, 2). beam and Maxwellian species, 3). a cold gas distribution and a Maxwellian species, and 4). a beam and a mirror confined plasma.

Neutron and radiation transport codes

No. 5 ANISN-L - T. Wilcox and R. Herrick, LLL CDC-7600

ANISN-L solves the one-dimensional Boltzman transport equation for neutrons or gamma rays in slab, spherical, or cylindrical geometries. ANISN-L was designed to solve

deep-penetration problems in which angle dependent spectra are calculated in detail.

No. 6 MORSE-L - T. Wilcox and R. Herrick, LLL CDC-7600

This is a Monte Carlo multigroup transport code for neutron-gamma penetration problems in either a one-dimensional spherical geometry or a generalized three-dimensional model using quadratic surfaces as the interface between adjoining material media.

ENGINEERING CODES

Stress and thermal analysis codes

No. 40 SAP4C - Steve Sackett, LLL CDC-7600

This is a general structural analysis code for linear static and dynamic analysis of complex elastic structures. A large variety of both two dimensional and three dimensional structures may be modeled with this code.

No. 61 TACO - Bill Mason, LLL Cray-1 and CDC-7600

TACO is an implicit finite element code for heat transfer analyses. It performs linear and nonlinear analyses and is used for both transient and steady state problems.

No. 62 POSTACO - Bill Mason, LLL CDC-7600

This is a graphics post processor for scalar, two dimensional finite element codes. It was developed to process results from both the SAP4C and the TACO codes.

No. 64 GRAPE - Bruce Brown, LLL CDC-7600

GRAPE is a graphics display program for three-dimensional polygon and polyhedral models. It was developed specifically as a post processor for finite element and finite difference codes (e. g. SAP4C and TACO).

No. 68 SLIC - Michael Gerhard, LLL CDC-7600

SLIC is an interactive mesh generation program for two and three dimensional finite element codes. The user inputs co-ordinates for certain key points and enters commands which complete the description of the geometry. Entire surfaces and volumes are then generated from this geometric skeleton.

Electrical engineering

No. 27 EMTP - Waldo Magnuson, LLL CDC-7600

This network analysis code developed by the Bonneville Power Administration (Portland, Oregon) solves ordinary differential equations and/or algebraic equations for power distribution networks.

No. 66 SCEPTRE - Waldo Magnuson, LLL CDC-7600

SCEPTRE is a general-purpose electronic engineering program designed to assist the electrical engineer in determining the initial conditions and/or transient response of electronic circuits.

No. 67 SPICE-2 - Waldo Magnuson, LLL CDC-7600

SPICE is a general-purpose circuit simulation program for nonlinear DC, nonlinear transient, and linear AC analyses. Circuits may contain resistors, capacitors, inductors, mutual inductors, independent voltage and current sources, four types of dependent sources, transmission lines, and the four most common types of semiconductor devices: diodes, BJTs, JFETs, and MOSFETs.

MATHEMATICAL ALGORITHMS and COMPUTER SCIENCE

No. 3 ETBFCT and PRBFCT - Jay Boris, NRL CDC-7600

These two routines implement a flux-corrected transport algorithm and are designed for Eulerian, sliding rezone, or Lagrangian finite difference calculations.

No. 23 MOVELES - K. Estrabrook, LLL CCDC-7600

This is a COMPASS coded, one-dimensional electrostatic particle pushing algorithm employing integer arithmetic.

No. 28 MP - K. Fong, NMFECC CDC-7600

This is Richard Brent's multiple precision floating point arithmetic package which includes routines for evaluating elementary functions and the most commonly used special functions.

No. 29 Forsythe, Malcom and Moler codes - K. Fong, NMFECC CDC-7600

This is a package of ten numerical mathematical routines described in the authors' text on numerical methods. The package includes routines for solving linear systems of equations, a numerical integrator, spline interpolation routines, and a random number generator.

No. 30 Lawson and Hanson Least Square codes - K. Fong, NMFECC CDC-7600

This package consists of the Fortran codes described in Lawson and Hanson's text on least squares problems.

No. 41 GENIC and SOLIC - M. and G. Petravic, PPL PDP-10

The GENIC and SOLIC routines implement the ICCG algorithm to solve a sparse system of linear equations with a positive definite matrix of coefficients.

No. 42 ICLU - T. Cutler, LLL CDC-7600

This is a highly optimized subroutine for implementing the ICCG algorithm using only small core memory on the 7600.

No. 44 ILUCG - Alek Shestakov, NMFECC CDC-7600

This subroutine package solves the linear system of equations arising from a nine-point discretization of a two-dimensional partial differential equation over a rectangular domain. It uses the ICCG algorithm and is optimized for use in large physics codes.

No. 46 MPHP - Dale Nielsen, LLL CDC-7600

MPHP is an interactive multiple precision arithmetic package designed to emulate desk top calculators. It uses Richard Brent's multiple precision routines (No. 28) and includes elementary and special functions provided in the Brent package.

No. 47 ROOTSJY - Dale Nielsen, LLL

ROOTSJY calculates the roots of the complete Bessel function and its derivatives. This routine was used in a k-space field solver for a three-dimensional toroidal cavity problem.

No. 48 VECTOR-FFT - Oscar Buneman, Stanford Cray-1

This is a machine coded (CAL) vectorized Fast Fourier Transform routine.

No. 49 PACK-UNPACK - Oscar Buneman, Stanford Cray-1

These are vectorized CAL-coded routines for a 2:1 data compression and expansion. The routines were used to pack particle parameters in a three dimensional electromagnetic particle code.

No. 50 RCIPSQRT - Oscar Buneman, Stanford Cray-1

RCIPSQRT is a vectorized CAL-coded routine for computing reciprocal square roots. It was written for a relativistic particle code.

No. 52 Jordan's linear Algebra Routines - K. Fong, NMFECC Cray-1

This package consists of a limited number of highly optimized mathematical routines designed for the Cray-1 by Thomas Jordan from LASL. These routines mostly fall in the category of linear algebra.

No. 53 ZIO - A. Bruce Langdon, LLL Cray-1 and CDC-7600

The ZIO package is designed to perform efficient I/O for high performance production codes by providing the user with simple access to operating system features such as overlapped I/O, user error control, and user control over the assignment of disk units.

No. 54 DECSOL - Paul F. Dubois, LLL Cray-1

The DECSOL program consists of two highly optimized CAL routines to perform an LU decomposition and to solve a system of equations. It is limited to systems of 64 or less equations.

No. 58 INTRAN - Oscar Buneman, Stanford Cray-1

This is a vectorized CAL-coded routine to generate an array of random integers.

No. 63 SOLVER - H. S. AU-Yeung and A. Friedman, UCB Cray-1

SOLVER calculates roots of a user specified function using a simple version of Muller's method.

Mathematical Libraries

LASL Subroutine Library (LIBRIS ABSTRACT #24 CDC-6600)
 NCAR Subroutine Library (LIBRIS ABSTRACT #22) CDC-7600
 AELIB subroutine library (LIBRIS ABSTRACT #31) CDC-6600
 (From CHALK RIVER NUCLEAR LABORATORY)

HARWELL LIBRARY
 CERN "
 SANDIA "

- * IMSL (in public on the 7600)
- ** NAG (in public on the Cray-1)

- Kirby is negotiating to get
 NPL OPTIMIZATION LIBRARY
 PORT

- * Documentation available in Document
- ** Documentation being prepared

MATHEMATICAL ALGORITHMS AND COMPUTER
SCIENCE

EISPACK
 LINPACK
 FUNPACK

SEVERAL OTHER PACKAGES ARE ALREADY LISTED IN LIBRIS (e.g. BRENT'S package, LAWSON AND HANSON ROUTINES, etc.)

- KIRBY IS NEGOTIATING TO GET
 SPARSPAK

SOFTWARE TOOLS

TFORT

AUGMENT

FLECS

BRNANL

DAVE

POLISH

JPL TAPE EXCHANGE PACKAGE

10. VIEW FROM DOE

David Nelson

- VIEW FROM DOE \neq VIEW FROM CONGRESS
HOWEVER: i) DOE PROPOSES, CONGRESS DISPOSES
ii) SOMETIMES: VIEW FROM DOE = VIEW FROM CONGRESS
- DOE IS MISSION ORIENTED, BUT MISSION IS LONG TERM
FOR FUSION \therefore CONSIDERABLE BASIC APPLICABLE PHYSICS NEEDED

NSF PLASMA PHYSICS BUDGET (THEORY+EXP.)	< \$4M
DOE-OFF BUDGET IN APPLIED PLAS. PHYS.	~ \$60M
THEORY	\$17M
COMPUTING	\$10M

- EVEN CHOICE OF BASIC PROBLEMS SHOULD BE DICTATED
BY POTENTIAL APPLICATION TO FUSION, ESPECIALLY IF RESEARCH
IS EXPENSIVE
- COMPUTER COSTS AT MFECC: CRAY \$1000/CPU HOUR
7600 - \$300/CPU HOUR

- TIME REQUESTED FOR FY1980 : 42K 7600 HOURS
AVAILABLE : 28K 7600 HOURS
- IN FY1979 COMPUTER HOURS INCREASED 4X (UNUSUAL)
- MAY HAVE 7600 → CLASS V1 (CRAY?) IN JUNE 1981
NO RELIEF EXPECTED BEFORE THEN, AND EVEN THEN
SOME OF TIME WILL GO FOR NEW APPLICATIONS SUCH AS
ENGINEERING, NEUTRONICS, REACTORS, ...
- MFE BUDGET IS ESSENTIALLY STEADY STATE SINCE ~1977
- COMPUTER TIME AND MANPOWER COSTS MUST REFLECT THIS

PROBLEM AREAS NEEDING MORE ATTENTION:

- DIVERTORS - AXI + NONAXISYMMETRIC
SHEATHS, POTENTIALS, BDRY LAYERS, AMBIPOLARITY, ...
- PLASMA EDGE INCLUDING SHADOW OF LIMITER
NEUTRALS, ATOMIC PHYSICS, REFLUX, METAL SURFACE, ...
- TRANSPORT IN NONAXISYMMETRIC SYSTEMS
- RF HEATING INCLUDING NONLINEAR EFFECTS
- OPTIMIZATION OF CYROTRON GEOMETRY
- STABILITY OF EBT RING-PLASMA
- FORMATION + TEARING PROBLEMS IN RFM, RFOP, SPHEROMAK
- ALL THE OLD UNSOLVED PROBLEMS INCLUDING
BUMP ON TAIL (X PARTICLES)

BUT WE CAN'T WORK ON ALL PROBLEMS WITH ALL
TECHNIQUES FOR ALL TIME

HIERARCHY OF MODELS

FLUID

MULTIFLUID

DRIFT KINETIC

MAXWELL-BOLTZMAN

SINGLE PARTICLES

HYBRID

METHOD OR MODEL MUST BE APPROPRIATE TO PHYSICS

TECHNIQUES MUST BE EFFICIENT + ACCURATE

OVERKILL DOES NOT WIN FRIENDS, HOWEVER

COMPARISON BETWEEN MODELS IS TOO OFTEN NEGLECTED

II CODE OPTIMIZATION CAN PAY OFF VERY QUICKLY

A. B. Langford

ONE MAN-MONTH COSTS \approx \$6K

6 HOURS OF CRAY TIME COSTS \sim \$6K

example

\sim 1 man-year of optimization (machine language routines overlapped I/O) doubled the speed of ZOHAR

cost: \sim \$50K

At 400 hours/year (7600), 200 hours would be wasted

(and $\frac{1}{2}$ the work done)

cost: \gg 200 x \$500/hour \approx \$100K

This optimization paid off almost as it was done!

How CAN OPTIMIZATION HURT YOU?

Machine language segments should be delineated so that most physics alterations do not require changes to the machine language segments.

example: ZOHAR particle boundary conditions are handled in FORTRAN

-machine language "movers" just flag exiting particles
(a fortunate decision!)

If optimization is allowed to make a code become unyielding to minor changes in physics or problem specification then it may never be widely used.

example:

Does a change in mesh size from 64×64 to 32×128 require days of recoding?

Does a change to 96×96 force you off your home brew computer?

4

WAYS TO GET A BETTER BANG FOR YOUR
COMPUTATIONAL EFFORT

MONITOR

INTERVENE

POSTPROCESS

LINK TO OTHER CODES

} relies heavily on
interactive codes,
sharing the (large) data
set of the simulation code,
doing considerable computing,
driving rapid graphic displays.

ZED (Zohar Editor) Post-processor

Interactive code driving graphics terminal (+film)

Reads HISTORY file produced by ZOHAR (+ others)

At first (1974) produced only time plots of
requested variable(s) and linear combinations.

Then did spectra, filtering ...

Later (~1978), spatial cross-correlations
to reconstruct normal modes in inhomogeneous
plasmas (Nevins).

HOME-BREW HARDWARE

"TMDS" graphic display is extremely valuable.

Large backing store

$\approx 25 \times 10^6$ words ($\sim \$1M$)

$< 100 \mu s$ startup, ~ 1 word/ μs bandwidth

use for:

3D MHD, 2d multigroup diffusion....

system overlays + tables, swapping

disk "cylinder" buffer

Specialized CP Hardware (eg FPS array processor)
should be coupled to a viable general-purpose
computer, with software supported by a substantial
organization.

Comparison of speed & cost on special vs CRAY etc
computers should compare codes

- with similar optimization effort

- flexibility and growth potential

12 A High-performance Arithmetic Processor for the LISP Machine

R. Berman

T. Dupree

S. Orzag

J. Holloway

J. Kulp

Applications:

CPM (Computational Physics Machine)

Symbolic, numeric, graphics
INTEGRATED

Simulations (particle, fluid, IC)

Signal Processing (A.I.L.)

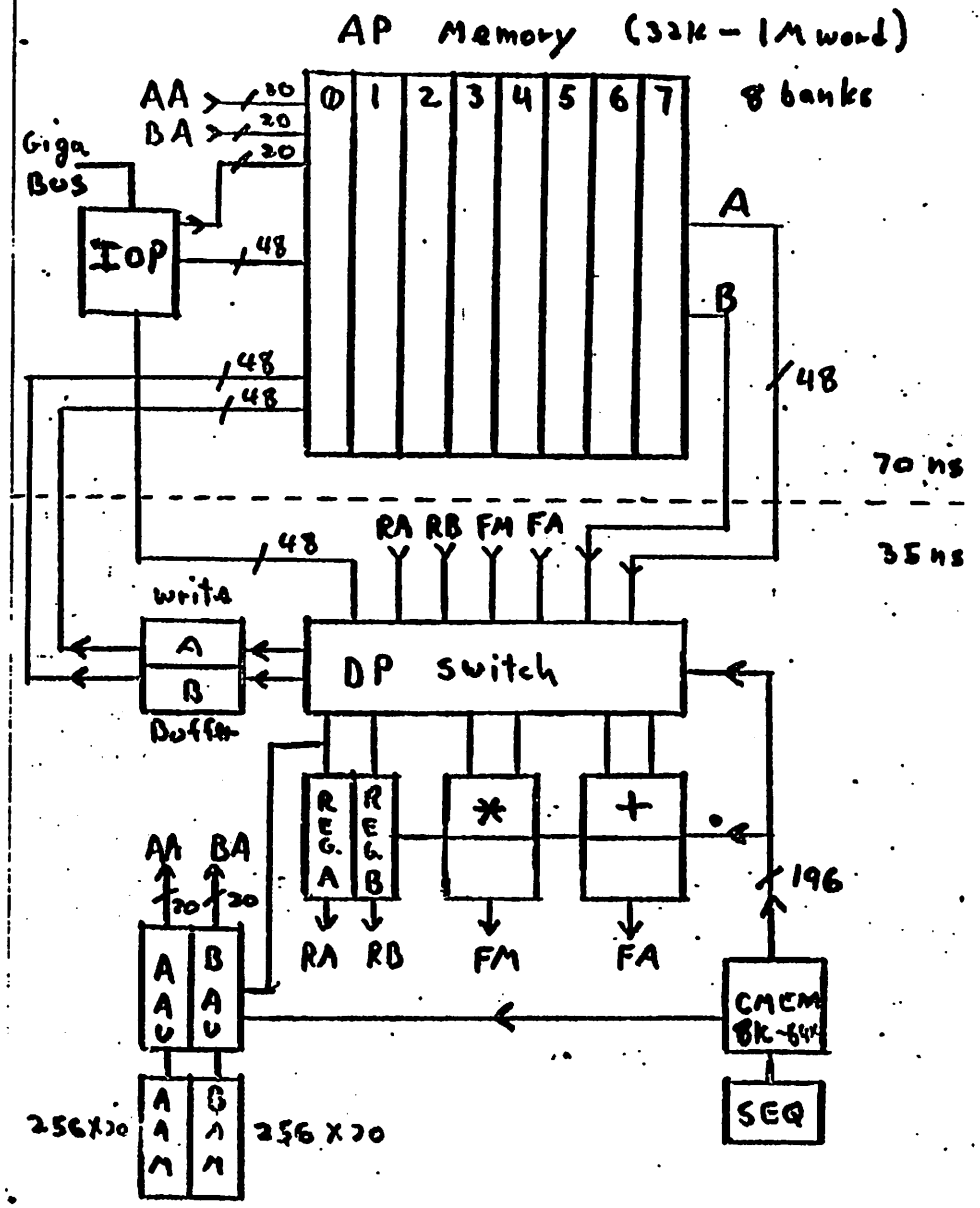
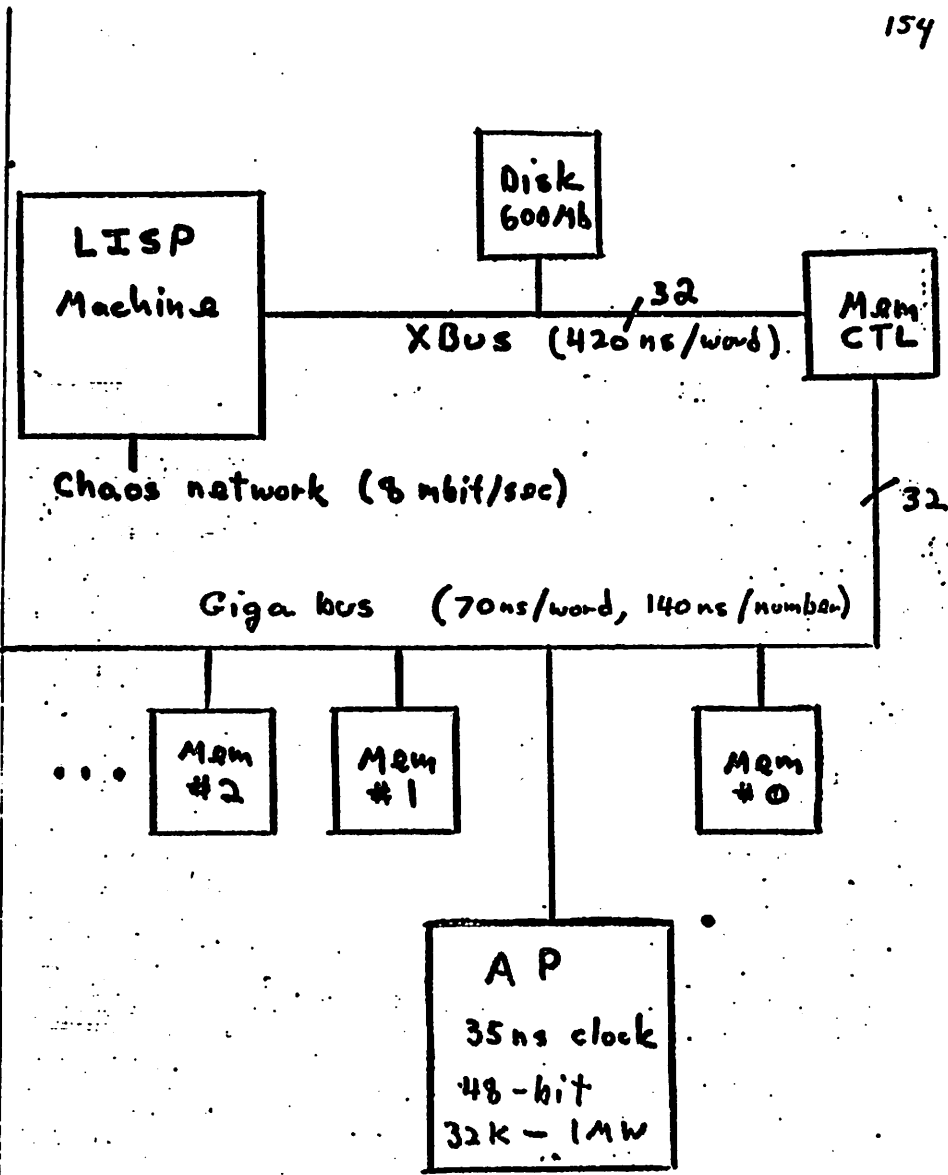
Goals: > 10 MFLOPS, Large memory
Software, < \$50k base

The LISP Machine

- Developed at the M.I.T.-A.I.L.
- 32-bit tagged architecture
- Large Virtual Memory for small machine (16 MWords)
- Integrated Disk (600 Mbytes), Displays (1000-line B+W, 4-bit color)
- Complex Functionality in Microcode
 - 16K words
 - VM support
 - High level Language interpreter (LISP)
 - Storage management
 - Type dispatch (generic ops)
 - data type ops
 - Message-passing (Smalltalk)
 - Micro compiler
- System software (window system)
- Single-user, single virtual machine, multiple processes
- MACSYMA

Why LISPM as a host processor?

Large VM + MACSYMA + availability
+ Software + Display features
+ \$35K system cost



AP Features

Technology: ECL F100K logic
 Wirewrap
 35 ns NMOS memory chips
 (4K, 16K) data, control mem's
 New CAD system

Number Formats: 48-bit floating point
 14-bit exp., 32 bit mantissa
 For I/O - small fp. 24bit
 packed integer 8, 12, 16

Memories: Gigabus - 1M - 16M words
 280 ns access/cycle
 70 ns transfer
 4-way interleave
 140 ns / number

AP memory - 32K - 1M words
 70 ns access/cycle
 8-4-2-1 way interleave
 3-port

Registers - 2 banks, 256 ea.
 read and write in 35 ns

Address - 2 x 256 20 bit
 2 x 16 20 bit

Control Memory - 8K - 64K
 196 bits, 70 ns, 2-way
 CM-cache - 256, 35 ns

Function Units

35 ns clock
 2 stage pipe
 57 MFLOPS (raw)
 No advance without push

Adder - +, -, ABS, Fix, Float, F, L,
 Boolean, shift, double precision,
 normalize
 Conditional operation

Multiplication - *, divide-step, double prec.

Address units - ALU ops
 table look-up for
 special func
 bit reverse
 2-0 arrays?

IOP (Input/output Processor)

Block transfers
 Format conversion

Sequencer - conditional branch, CALL,
 Return, LOOP count, etc.

AP Performance Estimates

20, ES, bilinear interpolation, v_x, v_y, E_x, E_y
Particle Push (incl. field interpolation)

16 cycles, .56 μ sec - fully overlapped, vectorized,
chained

26 cycles, .91 μ sec - fully overlapped, no
vectorizing, no chaining
↑
i.e. no explicit vectorizing

For no pipelining, multiply the times X 2

For no overlap, add 36 cycles for particle
72 cycles for fields.

1024 Complex FFT (vectorized): 1.5ms

Orszag et al have analyzed other computations
vector divide - 7 cycles

2 machines funded (NSF, MIT)

Operational summer of 1980?

W. E. Drummond and B. N. Moore
Austin Research Associates
1901 Rutland Drive
Austin, Texas 78758

ABSTRACT

A report will be given of the status of hardware and software development on the VAP. The VAP is designed as a floating point vector array processor of considerable power and will be able to execute large vector programs at high speed in a stand-alone mode. Other design features are multiple large fast data memories with independent data paths to a pipelined arithmetic unit. Four of these memories are vector (serial) memories with a maximum size of 8 million words. There is also a scalar (ram) memory with a total of 1 million words. Practical operation at speeds of 12 mflops will be possible. A software package is under development which will eventually make it possible to program at the Fortran level. Applications to plasma simulation will be discussed.

INTRODUCTION

Austin Research Associates is developing a floating point vector array processor, the VAP. This development was originally motivated by the need for an inexpensive high speed vector processor for large-scale plasma simulations. However, the architecture of the VAP provides an extraordinary degree of flexibility in vectorizing algorithms encountered in the solution of physical problems and, as a result, the VAP should have a fairly wide applicability.

The principal attributes of the VAP are:

1. It executes large vector programs at high speed.

For plasma simulation problems, it is expected to be approximately three times faster than a CDC-7600.

2. It has multiple, fast, data memories with independent data paths to the pipelined arithmetic units. Four of these memories are vector (serial) memories and one is a fast scalar (ram) memory. The initial configuration will have a total of 1.5 million words of fast memory and can be easily expanded to a much larger total memory.

For fully electromagnetic 2-1/2 D plasma simulation problems, the initial configuration handles 25,000 cells and 200,000 particles.

3. Programming is carried out using a subset of standard Fortran statements plus a few additional statements unique to vector programming.

4. It is inexpensive--less than 4 percent of the cost of a Cray I or a Star.

In the following sections, the organization of the VAP memories and data

flow logic will be described, together with certain features of the VAP software and utility packages.

MACHINE DESCRIPTION

The CPU of the VAP is a modified Floating Point Systems, Inc. AP-120B array processor. The AP-120B is a high-speed synchronous processor with a cycle time of 167 nanoseconds and executes one instruction per cycle. The instruction word provides the capability of overlapping 10 independent operations in each instruction, i.e., 10 independent instructions per cycle. The floating point arithmetic units consist of a pipelined multiplier and a pipelined adder, each of which can produce one result per cycle. Thus, the maximum execution rate for floating point operations is 12 megaflops.

To write and debug optimized code for the AP-120B requires assembly language programming which is extremely tedious because of the overlapping of multiple operations on each instruction. In addition, because of data path and memory conflicts, even carefully written assembly language code does not make very efficient use of the arithmetic pipelines. Finally, there is only one data memory which is limited to a maximum of a million words. Even with these restrictions, however, we have written plasma simulation codes on the AP-120B which execute at approximately the same speed as on the CDC-7600. Thus, the AP-120B is a cost-effective processor for many applications.

The VAP was designed to make use of the many attractive features of the AP-120B, while at the same time removing the memory size and data path conflict restrictions. The resulting hardware configuration lends itself to vector processing and the development of a vector Fortran compiler removes the need for assembly language coding. With this vector Fortran compiler, programming can be carried out as easily as on a

standard Fortran processor and programs execute approximately three times faster than on a CDC-7600.

The principal modifications to the AP-120B involve the addition of four high-speed data and control paths to the CPU, together with the expanded hardware logic to facilitate the flexible use of these additional data paths. The four high-speed data paths are connected through controllers to four high-speed ram memories which are used as vector (serial) memories. The use of ram memories avoids the latency problems associated with CCD or bubble memories.

The resulting VAP functional diagram is shown in Figure 1 and more details of the array processor section are given in Figure 2. In summarizing machine features and capabilities, it is convenient to distinguish between those characteristics of the conventional AP mode of operation given in Table 1 and the extended VAP mode given in Table 2. Under software control, the VAP can operate either as a vector array processor or in a conventional AP mode.

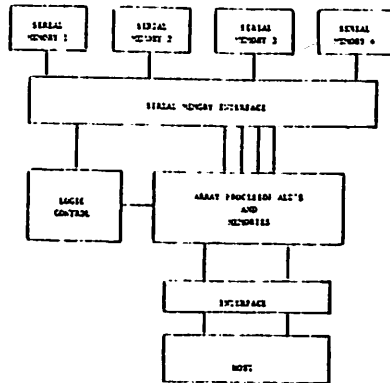


Fig. 1. VAP Machine Organization

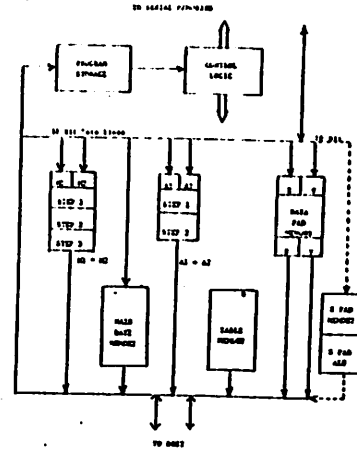


Fig. 2. Details of Array Processor CPU.

Table 1. AP mode features.

- * 167 nsec cycle time.
- * Independent pipelined floating adder and multiplier.
- * Pipelined access to as much as 512K words of ram data memory at rates up to 6 million words/second.
- * Sixteen 16-bit integer scratch registers with associated ALU.
- * 2K table memory rom.

For large vector programs, the execution speed is primarily limited by the maximum rate from the data memories to the ALU. The addition of the four fast data memories increases the data rate for the VAP to 30 million words per second as compared to 6 million words per second in the AP mode.

Table 2. VAP features.

- * All features of conventional AP available.
- * 4 (n x 64K) serial memories configurable under program control as inputs and outputs of arithmetic units.
- * Access rates of 6 million words/second to each memory giving total data flow rate of 30 million words/second.
- * Setup time for vector operations = 4 microseconds.

The additional control logic incorporated in the VAP takes advantage of the flexibilities provided by a mixture of vector and scalar memories so that scatter/gather operations which, in the past, were not thought to be vectorizable, are, in fact, easily vectorizable. For plasma simulation problems, the scatter/gather operations of interpolation and allocation are thus materially speeded up.

SOFTWARE

Parallel development of software and hardware is being undertaken in order that hardware design options may be realistically evaluated as they become apparent. The earliest possible useful production from the machine will also be obtained. VAP software items can be classified as support, e.g., compiler, assembler, linker, etc., or as utilities. Typical utilities include commonly used vector arithmetic operations, as well as specialized utilities for plasma simulation problems. Figure 3 is a block diagram indicating the stages required to convert VAP Fortran source code into an execution module. All of the support software items appear in Figure 3. All of the compiling, assembling, and linking

is done on the host computer and the complete binary execution module is shipped from the host to the VAP for stand-alone execution. Results and diagnostic data can be returned to the host during execution.

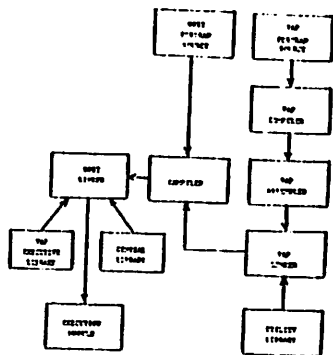


Fig. 3. Support software.

Programming is done principally in terms of a subset of standard Fortran statements with a few modifications unique to vector operations. Variables are declared as either vector or scalar variables and then used in the usual Fortran syntax.

For example, if B, C & D are vectors of the same length, located in different vector memories, the Fortran statement

$$A = B * C + D$$

multiplies each element of B times the corresponding element of C and adds the product to the corresponding element of D, to produce the resulting vector A, which is stored in the remaining vector memory.

Scatter/gather operations make use of additional symbols but the same Fortran syntax. E.g., if B, C & J are vectors located in different serial memories, the

Fortran statement

$$A = B * C + H \langle J \rangle$$

multiplies each element of B by the corresponding element of C and adds the product to the contents of the scalar memory at the address specified by the corresponding element of J to give the resulting vector A, which is stored in the fourth vector memory. This scatter/gather vector operation executes at the same speed as the pure vector operation discussed above.* Table 3 lists the execution rate of typical Fortran operations.

Table 3. Execution rates for VAP Fortran statements and utilities.^a

Pure Vector Operations	
1. $A = B * C$	6 Megaflops
2. $A = (B + C)$	6 Megaflops
3. $A = B * C + D$	12 Megaflops
4. $A = (B + C) * D$	12 Megaflops

Scatter/Gather Vector Operations	
1. $A = B * C + H \langle J \rangle$	12 Megaflops
2. $H \langle J \rangle = H \langle J \rangle + A * B$	4 Megaflops

Vector Utilities	
1. $A = \text{SQRT}(B)$	1.5 Megaflops
2. $A = 1/B$	1.5 Megaflops

^aIn this table, A, B, C and J are vectors located in different vector memory. $H \langle J \rangle$ is the contents of the scalar memory location whose address is the corresponding element of the vector J.

* Other scatter/gather operations, e.g., scatter/gather operation No. 2 in Table 3 may run more slowly for two reasons: The scalar memory is accessed twice for the operations on each element; and if adjacent elements of J have the same value, i.e., if the same memory location is addressed for two consecutive elements,

162

A critical element in any vector processor is the setup time for vector operations. For the VAP, this setup time is between three and four microseconds. Since the basic VAP cycle time is 167 ns, this means that the setup time for any vector operation consumes approximately 20 cycles. Since the most common vector operations execute one vector element per machine cycle, the overhead time, as a fraction of the execution time, is simply 20 divided by the number of elements in the vector. For vectors of length 200, the setup time is thus 10 percent of the execution time. For particle simulation problems, the typical vector length is 2,000, and thus setup time amounts to only 1 percent of the execution time. As a result, the utilization of the arithmetic pipelines approaches 100 percent in the VAP.

APPLICATIONS

Although the VAP is being developed because it is needed for a rather specific problem, it will be capable of quite general application. Some problems for which the VAP will be useful are listed in Table 4. Consideration of the 2-1/2 D plasma simulation problem will illustrate some of the features of the VAP. A 2-1/2 D fully-electromagnetic, fully-relativistic e-beam simulation code has been in production on the AP for some time and it will be the first major code to be implemented on the VAP. An estimated performance comparison is given in Table 5. The VAP can handle larger field arrays and particle tables because of the serial memory

the write to this memory location from the first of these elements would not be completed before the read of that same memory location for the next element. To guard against this possibility, the utility has been slowed. For plasma simulation codes, a special utility has been written for this operation which executes at 6 megaflops.

capacity, and the availability of optimized Fortran operations and efficiently coded vector utilities makes larger pieces of the code run at the 12 megaflop rate. With the VAP Fortran compiler, programs will also be more easily modified and debugged.

Table 4. Applications.

- * 2-1/2 D and 3 D plasma simulation.
- * Hydrodynamic and magnetohydrodynamic problems.
- * Simulation of diode operation.
- * General 2 D and 3 D partial differential equations.

OUTLOOK

An operating prototype of the VAP with reduced data path width and skeleton serial memory should be available by the end of the year to perform tests of the design. If all goes reasonably well at that point, it is anticipated that a fully operational machine will be working by the middle of next year.

Most of the software will be available before the prototype VAP is operational, and work will proceed on actual code development.

164
Table 5. Comparison of the capabilities of the AP mode and the VAP mode for a 2-1/2 D fully-electromagnetic, fully-relativistic, particle push program.

	AP	VAP
Number of particles	32K	200K
Number of cells	4K	25K
Execution time per particle ^a	81 μ sec/particle	21 μ sec/particle ^b
Ease of programming	Difficult	Same as Standard Fortran

^aFor purposes of comparison, standard Fortran programming of the CDC-7600 gives an execution time of about 80 microseconds per particle and standard Fortran programming of the Cray I initially achieved an execution time of approximately 12-1/2 microseconds per particle. However, more recent hand-optimized coding on the Cray I has led to a significant reduction in this push time. (Private communication - D. Forslund)

^bThis result is not a measured result. However, since the processor is a synchronous processor, it is believed to be accurate.



14

Comparing the Floating Point Systems, Inc. AP190L to Representative Scientific Computers: Some Benchmark Results

Thomas A. Brengle
Lawrence Livermore Laboratory
December 10, 1979

- What is the AP190L?

38 bit, 6 MHz clock, 64K Main Data Memory.
Microcoded.
2 way interleave memory.
2 cycle add pipe.
3 cycle multiply pipe.
Driven as peripheral by DEC PDP-10 Model KI.

- AP FORTRAN

Cross-compiler, runs on DEC-10.
First operable version.
Rudimentary optimization
(register-allocation, code foldback).

- Benchmark

MAGIC2 (Cohen, Brengle)
1D, cylindrical, magneto-inductive.
Speed bound by Boris mover
(about 85 floating point operations, including SQRT).



166
LAWRENCE LIVERMORE LABORATORY



167
LAWRENCE LIVERMORE LABORATORY

- Results

	FDP-10	AP190L	7600	CRAY
MIPS	1	18	36	80
Theoretical MFLOPS	.25	12	54-56	160-240
Elapsed time	5640	564	375	271
CPU	2559	276	99	50
MFLOPS	.14	1.3	3.5	7.0
<u>Realized MFLOPS</u> Theoretical MFLOPS	.56	.11	.06	.04
Megabucks/MFLOP	2	.08	1	1

Notes:

1. AP190L CPU time was inferred by counting cycles.
2. Priorities on 7600 and CRAY were set at 1.4.

- Comments

Effect of offloading code to AP190L was to reduce utilization of FDP-10 CPU by factor of 50. Enlargement of Program Memory will reduce overlaying. AP FORTRAN will get additional enhancements. New electron physics code shows problems with passing data as formal parameters instead of as COMMON data.

15 Macro cell Coding for Efficient Particle Movers

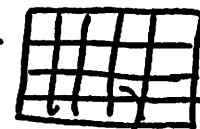
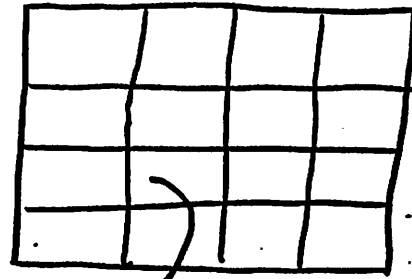
R.H. BERMAN
G.J. Carrette

A MACROCELL is a list-link programming technique to facilitate temporary vectors to make force interpolation and charge assignment run faster. This is intimately related to P³M technique.

Problems

Nonlinear - high gradients - transport
nonlinear phase space structures
- large N - small Δx

MACRO MESH



minimesh

minicell

Here an 80x80 mesh is broken into a 4x4 macro mesh.

Particle Descriptor

Cell Descriptor

$\underline{x}(i)$ at time t

HOL - head

$\underline{v}(i)$ at time $t + \frac{1}{2}$

NIL - #

$\underline{l}(i)$ - link coordinate

hol \rightarrow 17 \rightarrow 1034 \rightarrow 42
 NIL=3 \quad $\underline{l}(17)$ \quad $\underline{l}(1034)$ \quad $\underline{l}(42) \rightarrow 0$.

Force Interpolation

CIC

```

1 p = h0l
DO 10 i = 1, NIL
TX(i) = x(ip)          TVX(i) = vx(ip)
IT(i) = x(ip)          TVY(i) = vy(ip)
TY(i) = y(ip)
gT(i) = y(ip)
10 ip = l(ip)

```

```

DO 15 i = 1, NIL
fx(i) = TX(i) - IT(i)
15 fy(i) = TY(i) - gT(i)

```

```

DO 20 i = 1, NIL
W00 = fx(i) * fy(i)
W10 = (1 - fx(i)) * fy(i)

```

```

TVX(i) = W00 * EX00(i) + ...
TVY(i) = W00 * EY00(i) + ...

```

20

```

DO 16 i = 1, NIL

```

```

EX00(i) = phi(it(i)+1, gT(i)) - phi(it(i)-1, gT(i))

```

16

MOVE (leap frog)

```

DO 10 i = 1, NP
x(i) = x(i) + vx(i)
10 y(i) = y(i) + vy(i)

```

Check Boundary Conditions

1. Macro cells on perimeter
2. only check for outward motion

CHARGE ASSIGNMENT

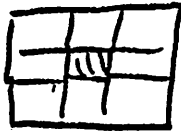
1. Calculate weights and cell coordinates as above with temp vectors.
2. Recalculate cell descriptor
Recalculate l.

Timings on Cray-1 give
 3X Mflops improvement in FORTRAN
 for 2d proof of principle. More
 with careful code. (< 6 ms/particle)

Extensions

1. P³M for P-P correction
 for short range force.

$i_p = hal \quad j_p = hal 2$



```

DO 10 i=1, N1L
DO 20 j=1, N1L2
TV(j) = V(j)
20 IT(j) = f*(|x(ip)-x(jp)|)
DO 30 q=1, N1L2
V(ip) = V(ip) + FOR(IT(j))
30 TV(j) = TV(j) - FOR(IT(j))
DO 40 q=1, N1L2
V(jp) = V(j)
40 jP = 2(jP)
10
```

$$\left\{ \begin{array}{l} \hat{u}(j) \\ \hat{v}(j) \\ \hline F(\hat{u}(j), \hat{v}(j)) \end{array} \right.$$

2. Non-Cartesian Meshes - geometry factors
3. Non-periodic BC
 WANDER-LISTS
4. Generalize.
 macro cell - independent processors
 augment cell descriptor
 natural unit for buffers - architecture
 problem. (macrocell uses physical
 information - not just
 code)
5. ideas of data abstraction are
 consistent with developing good
 code.
 More activities - disk - multiprocessors

15 Macrocell Coding for Efficient Particle Movers on Arithmetic Processors

Robert H. Herman*
George C. Carrette*

Plasma Fusion Center
Massachusetts Institute of Technology
Cambridge, Mass. 02139

To be presented at the Informal Conference on Particle And Hybrid
Codes for Fusion, Napa, California, December 1979

ABSTRACT

We discuss the use of a linked-list programming technique which we call macrocell coding to facilitate the introduction of temporary vectors to make the time step loops in particle-mesh simulations run faster on arithmetic processors. This extension to array processors of part of the PPM method of Eastwood and Hockney [1] represents a significant improvement in timings for code written in naive FORTRAN. The macrocell, as originally envisioned, promotes cost effective and more accurate calculation of short range forces, and therefore, permits longer simulations before numerical errors grow beyond reasonable bounds. Furthermore, these suggestions for macrocell usage provide efficient vectorization on machines like the Cray-1 in circumstances where large particle numbers or high spatial resolution is desired.

*This work was supported, in part, by the United States Department of Energy under Contract Number ET78-5-02-4082.

Some physical problems that are studied with particle-mesh simulation techniques demand efficient algorithms to allow complete investigations of the parameter spaces that are encountered. Our interest in problems in nonlinear plasma physics leads us to formulate model problems with millions of particles and meshes with high spatial resolution for long periods of time[2,9]. The typical time step loop in our electrostatic codes does: 1, a charge collection of the particles onto a mesh; 2, a potential solution; 3, integration of equations of motion. These steps may typically involve multilinear interpolation on or off the mesh. Higher order interpolation may be necessary for short-range accuracy. The particles move independently through the mesh in their self-consistent field and any external fields that are present. An array processor or pipeline machine like the LISP Machine A-Box[3,4] or the Cray-1 offers some promise to the particle simulator if he can customize his computation. The issue in the calculation is that, although the basic update of positions with velocities can be naturally vectorized, the computations of charge collection and force interpolation cannot. This occurs because typically, particles do not retain any association with each other as they wander throughout the mesh. The necessity to randomly access particle coordinates or equivalently, to access charge or field coordinates lessens the opportunity to be efficient in a pipeline environment. Efficient algorithms for the charge collection and force interpolation phases need to be found. We consider that efficient methods for potential solutions exist through vectorized FFT methods[5].

We can extend an idea of the PPM technique of Eastwood and Hockney[1] to write code that is amenable to vectorization on machines like the Cray-1. We call our implementation the macromesh mover for particles (macrocell in short). We will describe this conceptually in two dimensions with periodic boundary conditions. An $N \times N$ Cartesian mesh (the mini-mesh) with is covered with a macro-mesh of size $M \times M$. The particles, stored in random order in memory, have a macrocell coordinate L . This coordinate is a linked list. Thus, if there are NSP species of particles, an integer array $HOL(JMX, JMY, JSP)$ points to the first particle of species type JSP in a macro cell whose coordinates are (JMX, JMY) . Let $IP = HOL(JMX, JMY, JSP)$. Then, $X(L(IP))$ is the x-coordinate of the first particle, $Y(L(IP))$ is the y-coordinate, etc. The next particle number is $L(L(IP))$, and the total number of particles in the macrocell is $NIL(JMX, JMY, JSP)$. If $L(IP)$ is 0, the list terminates. It is more convenient for vectorization to use NIL then test for $L = 0$. Thus, DO loops, broken down into blocks of convenient length (64 on the Cray-1) or less, are possible.

The calculation proceeds as follows. First, we assume that the electric potential has been calculated and the linked list L has been prepared. We loop over the macrocells. Thus, particle coordinates and velocities, forces and geometrical interpolation factors are calculated and gathered into temporary vectors. This is facilitated by the macrocell

coordinate L . We use the time-centered leap-frog scheme to integrate the equations of motion. This can be performed in a vectorized mode on the Cray-1 using the temporary vectors as well as calculating the linear momentum and kinetic energy. Next, the particle spatial coordinates have to be reset to lie in the periodic mini-mesh. To do this, we need check only the macrocells that lie on the perimeter (surface) of the mesh. Furthermore, we need only check the particles which have moved in the outward normal direction. In terms of cells, we need only check the $4M$ macrocells on the perimeter of the mini-mesh for particles that moved outward, rather than the N^2 cells for all the particles. Finally, the charge collection can also be done using temporary vectors to calculate weighting factors. At the same time, the link coordinate L is recalculated. It is easier to recalculate the macrocell coordinates rather than trying to do some sort of garbage collection.

We must caution here that we do not advocate indiscriminate use of macrocells. The overhead in memory and computing may be too high a price to pay for small minimeshes and small numbers of particles. We believe that macrocell coding becomes an efficient alternative when there are a significant number of particles and a large number of macrocells. The efficiency of this scheme is optimized when there are an even number of particles per macrocell.

In Table I we present some timing studies on the Cray-1 using a two-dimensional mesh with $N=256$ and $M=64, 32, 16$. We are using a macrocell that contains $4^2, 8^2$ and 16^2 minimesh cells. We call the linear dimension of macrocell measured in minicells MC . We present results for 102400 particles. The times seem to be linear with particle number above 10240 particles. The critical issue in picking the macrocell size MC is to ensure that the macrocell contains a substantial number of particles. We have computed the time (TFORCE) for bi-linear force interpolation to update the velocities; the time (TPUSH) to update positions with the new velocities in the leap-frog time-centered integration algorithm and to reset the position coordinates on a spatially periodic mesh; the time (TRIIO) to collect the new charges with bilinear charge assignment. These operations include certain simulation overheads - zeroing certain arrays, moving coordinates, etc. and in the case of the macrocell methods, recomputing the macrocell coordinates. To compare the utility of macrocell coding, we also computed Mflops (Million floating point operations per second) by noting the number $N+$ and $N*$ of multiplications and additions in these cases, excluding the arithmetic necessary to reset the periodic mesh coordinates. The result shows that a factor of two in raw cycle time results over a naive method for coding the time step. It should be pointed out that the naive method is not too naive in that it uses the Cray vector commands for the push and for the remap to the periodic mesh. It is the non-vector character of the charge collection and force interpolation that slows down this

naive calculation.

We have employed several of the techniques advocated by Derman[8] for efficient FORTRAN coding in the particle push which accounts for the major difference in TPUSH for these two methods. We used initial coordinates randomly spread over the active mesh within a border. This accounts for in part for the difference in operation counts presented below. Listings in FORTRAN of this implementation are freely available from the authors.

Table I

Timings for Macrocell Coding				
	Naive FORTRAN	MC=4	MC=8	MC=16
N per cell	1.5	25	100	400
TFORCE (sec)	.9283	.4165	.3664	.3581
TPUSH (sec)	.0320	.0095	.0094	.0094
TRIIO (sec)	.5379	.2747	.2746	.2742
MFlops	3.827	10.743	11.529	11.678
TOTAL (sec)	1.498	0.701	0.650	0.642
RATIO (time)	1.0	.468	.434	.429
RATIO (Mflops)	1.0	2.8	3.0	3.1

We advocate the use of macrocell coding especially in the following when large particle numbers of high spatial resolution demand as much vectorization possible. The above table shows that even in naive FORTRAN, the extra coding necessary to perform macrocell management is compensated by increased vectorization as evidenced by the Mflops. We would suggest that this code be written seriously in assembler for production use.

This macrocell method can be extended with the following considerations:

1. The PPPM method can be used for short-range force correction, which is what originally motivated our thoughts this way. This technique can be vectorized to provide large accuracy for simulations running many time steps. The PPPM method consists of a Particle-Mesh calculated as we have outlined above followed by a Particle-Particle pair-wise correction for the short range force. The size of the macrocell then becomes a natural distance over which to do this correction. One processes the current macrocell applying a short range correction to the particles in the current macrocell and the

neighboring macrocells. Further optimization is possible if the particles are partly ordered within a macrocell.

2. Non-Cartesian coordinate systems can be treated with this technique. The macrocells, then, are more general than rectangles. It is still no more convenient to calculate geometrical factors, but the opportunity to vectorize exists.

3. Non-periodic boundary conditions on the particles can also be treated. Suppose we consider a bounded problem like a self-gravitating, isolated system or a bounded plasma. The particles that wander off the active mesh need to be processed separately. In the gravitating problem, a particle might move in a two-body approximation[7,8]. If a "wander-list" is created for these particles, they can be identified and processed quite speedily.

4. It is possible to extend the abstract structure of macrocells as suggested in (3) to contain more information. The particles within a macrocell are all independent of any other macrocell, and grouped together in space. It may be convenient to have the electric field or potential grouped into the macrocell configuration. It may also be desirable to do the charge collection in macrocell configuration as well. It needs only to guard the boundaries of the macrocells and fix them up later. This may be highly desirable if many independent parallel processors are present (e.g. Illiac IV, cf. [10]). It may also be desirable to tag the identity of particles by putting them in special macrocells, as might happen if it is necessary to identify particles in different regions of phase space that originally started close together. This is particularly important in measure phase space correlations in plasma turbulence or stochasticity[2,9].

In an two-dimensional electrostatic problem, say, the calculation for electric field proceeds by computing a mesh of potential values and using finite difference techniques to calculate the force. This is more efficient in storage than calculating extra meshes for the electric field. A space centered finite difference formula would cause 16 fpa (floating point operations) per particle for interpolation whereas it would cost $4N^2$ fpa to calculate the electric at all the points. Therefore, when the number of particles is much larger than $0.25N^2$, it is desirable to precalculate the electric field in a macrocell and use it for interpolation rather than differencing for each particle. The cost in extra storage is just $2MC^2$. A similar result obtains in three dimensions. Namely, when the number of particles is much larger than $.17N^2$, the electric field should be precalculated in a macrocell at a cost of $3MC^2$ memory locations.

6. Temporary vectors in macrocells can also be introduced for currents, magnetic fields, etc. for more general problems. We have typically used temporary vectors of

length 04 in our example.

7. A scheme of buffering particles in macrocells in main memory for an array processor can be envisioned. A large buffer of particles is read from disk, gathered into macrocells, processed, dispersed, and then written out. This procedure could be overlapped with reading and writing other buffers. We believe that the buffer sizes need to be carefully matched with the macrocell sizes and minimesh sizes for efficiency.

8. A final observation about coding styles and practices is appropriate here. We have used a FORTRAN implementation of the macrocell method to illustrate the technique for this discussion. Production codes would undoubtedly want this method in assembler or microcode. There is a significant problem in balancing the gains in formulating an algorithm and the ease of manipulating a data structure in a flexible high level language against the real-time problem of getting the maximal raw computing power from a machine. Our observation is that ideas of data abstraction (message-passing semantics, generalized data structures, data flow analysis) are consistent with developing efficient vector coding because they can use information about the vector structure of the data. But, unlike other models of vectorization (DO loops, expansions, temporary variables or vectors), properly chosen data abstractions can be used throughout the formulation of a problem (program) to recognize such activities as disk buffering, multi-processing environments (each assigned to a macrocell), or parallel machine processing (data movement over a network, another machine doing pre- or post-processing). Any data structure that the computational physicist wishes to impose on the calculation should be compatible with the technique for computing as well as the machine he computes with. We are finding the macrocell coding is amenable for these reasons.

In conclusion, we advocate the use of the macrocell as an efficient algorithm for particle mesh simulations on array processors. Coding in naive FORTRAN produces significant improvement in usage of the available resources. The macrocell concept, a hierarchical form of "divide-and-conquer", can be applied to other difficult problems that are studied on pipeline machines.

REFERENCES

1. J.W. Eastwood, R.W. Hockney, and D.N. Lawrence, "P3M3DP - The Three Dimensional Periodic Particle-Particle - Particle-Mesh Program," *Internal memo, Reading University, Department of Computer Science* (1978).
2. D.J. Tetrenault, R.H. Berman, and T.H. Dupree, "Computer Simulation of Nonlinear Phase Space Structure," *B.A.P.S.* 24, (1979), 942.

3. J.T. Holloway, "The LISP Machine ADOX," internal memo (May, 1979).
4. R.H. Berman and J.L. Kulp, "A Perspective on Environments for Computational Physics — The CPM — An Integrated Personal Computer System," Massachusetts Institute of Technology Plasma Fusion Center Computational Physics Working Paper 1 (1979).
5. O. Buneman, "VECFPT," in LIBRIS, NMFCECC (1979).
6. R.H. Berman, "Vectorizing a 1d Particle Push," *Buffer* 3, (1979), 12.
7. R.A. James and J. A. Sellwood, "Computer Simulation of Galaxies," *M.N.R.A.S.* 182, (1978), 331.
8. R.W. Hockney and D.R.K. Brownrigg, "Three Dimensional Computer Simulation of Galaxies," *M.N.R.A.S.* 167, (1974), 331.
9. R.H. Berman, "Criteria for Transition to Stochasticity," *B.A.P.S.* 24,, (1979), 942.
10. C.R. Jesshope and J.A.I. Craigie, "Some Principles of Parallelism in Particle and Mesh Modelling," internal memo, Department of Computer Science, reading University (1979).

16 3D Simulation of TEM in Tokamaks

by

C.Z. Cheng and H. Okuda

Princeton Plasma Physics Laboratory

THE NEED FOR NEW 3D PARTICLE MODEL

182

A) REALISTIC PLASMA DEVICE (E.G., TOKAMAK, Q-MACHINE)

AXIAL LENGTH \gg CROSS SECTIONAL LENGTH

FOR LOW FREQUENCY MICROINSTABILITIES ($\omega \ll \omega_{pi}$) *drift waves*
Alfven waves
lower hybrid waves
etc.

$$k_{\parallel} \ll k_{\perp}$$

$$\lambda_{\parallel} = \frac{2\pi}{k_{\parallel}} = \text{AXIAL LENGTH}$$

$$k_{\perp} \rho_i \sim 0(1)$$

Q-MACHINE PLASMA VOLUME

$$\begin{matrix} a \approx 1 \sim 2 \text{ cm} \\ l \approx 50 \sim 100 \text{ cm} \end{matrix} > \begin{cases} a \approx 100 \sim 200 \rho_i \\ l \approx 10^4 \lambda_D \end{cases}$$

$$v_T \sim 10^8 \lambda_D$$

FOR TOKAMAK $v_T > v_0$

B) FEATURE OF NEW 3D PARTICLE MODEL

KEEP ONLY FEW LONG-WAVELENGTH MODES IN THE AXIAL DIRECTION

MAKE EIGENFUNCTION EXPANSION IN THE AXIAL DIRECTION AND MULTIPLE

EXPANSION ON THE 2D SPATIAL GRID IN THE CROSS SECTION FOR

SOLVING MAXWELL'S EQUATIONS

183

Maxwell's Equations:

$$\begin{cases} \nabla \times \underline{B} = \frac{4\pi}{c} \underline{j}^T \Rightarrow \underline{B} & \textcircled{1} \\ \nabla \times \underline{E}^T = -\frac{1}{c} \frac{\partial \underline{B}}{\partial t} \Rightarrow \underline{E}^T & \textcircled{2} \\ \nabla^2 \phi = -4\pi \rho, \underline{E}^L = -\nabla \phi \Rightarrow \underline{E}^L & \textcircled{3} \end{cases}$$

Eq. ②:

$$\nabla^2 \underline{E}^T = \frac{4\pi}{c^2} \frac{\partial \underline{j}^T}{\partial t}$$

$$\frac{\partial \underline{j}^T}{\partial t} = \sum_j q_j \left[\frac{q_j}{m_j} (\underline{E} + \frac{1}{c} \underline{v}_j \times \underline{B}) f(\underline{r}-\underline{r}_j) - \underline{v}_j \cdot \nabla_j f \right]$$

$$\therefore -k^2 \underline{E}^T - \frac{4\pi e^2}{m_e c^2} (\eta \underline{E})^T = \underbrace{\left(\frac{4\pi e^2}{m_e c^2} \frac{\underline{J} \times \underline{B}}{c} - \frac{4\pi}{c} \sum_j q_j \underline{v}_j \cdot \nabla_j f \right)^T}_{\underline{\Sigma}^T}$$

where, solved by iteration method (UCLA)
(LASL)

$$\underline{J} = \underline{J}_e + \left(\frac{m_e}{m_i} \right) \underline{J}_i, \quad \eta = n_e + \left(\frac{m_e}{m_i} \right) n_i$$

Applications of 3D Models

- 1) Drift Wave Simulation
- Excitation of convective cells.

C.Z. Cheng and H. Okuda

① Phys. Rev. Lett. 38, 708 (1977)

② Nucl. Fusion 18, 587 (1978)

- 2) Trapped Electron Instabilities Simulation

C.Z. Cheng and H. Okuda

Phys. Rev. Lett. 41, 1116 (1979)

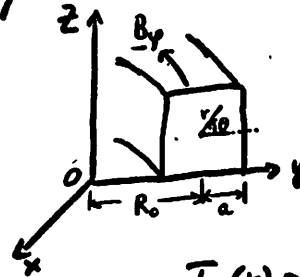
184

II)

3D Simulation of TEM in Toroidal Geometry (ρ)

(Cheng, Okuda)

the external magnetic field is



$$\underline{B} = \underline{B}_\varphi + \underline{B}_\theta, \quad B_\varphi = B_0 / (1 + \frac{r}{R_0})$$

$$B_\theta = B_0 \left(\frac{r}{R_0} g(r) \right), \quad g(r) = g_0 (1 + \lambda r^2/a^2)$$

$$T_e(r) \propto n(r) \propto \exp(-\lambda r^2/a^2)$$

$$\eta_e \equiv d \ln T_e / d \ln n_e = \text{constant in } r$$

Electrons are pushed by G.C. drift equations with

$\underline{E} \times \underline{B}$ drift, ∇B and curvature drifts.

$$\frac{d\underline{x}}{dt} = \underline{v}_\parallel + c \frac{\underline{E} \times \underline{B}}{B^2} - \frac{\pi c}{2B^3} (\mu_B/m + v_\parallel^2) \underline{B} \times \nabla B$$

$$\frac{dv_\parallel}{dt} = -eE_\parallel/m - \underline{B} \cdot \nabla (\mu_B/m_B) + c v_\parallel (\underline{E} \times \underline{B}) \cdot \nabla B / B^3$$

$$\mu \equiv m v_\parallel^2 / 2B = \text{adiabatic invariant}$$

Ion dynamics are exact.

Electron-ion pitch angle scattering is simulated with Monte-Carlo method with $\chi_{ei} \sim 1/\nu^3$.

Initial particle distribution is local Maxwellian.

185

(Critical Condition)
Radial Dependence of v_e^{*}

$$v_e^* = \frac{v_e}{\omega_{be}} = \frac{v_0 \left(\frac{v_e}{v}\right)^3 / (r/R_0)}{\sqrt{r/R_0} \frac{v}{qR_0}}, \quad v_0 = \frac{0.057}{T_0^{3/2}}$$

$$T_e = v^2 = T_{e0} \left(\frac{\alpha}{1-e^{-\alpha}}\right) \exp(-\alpha(r/a)^2)$$

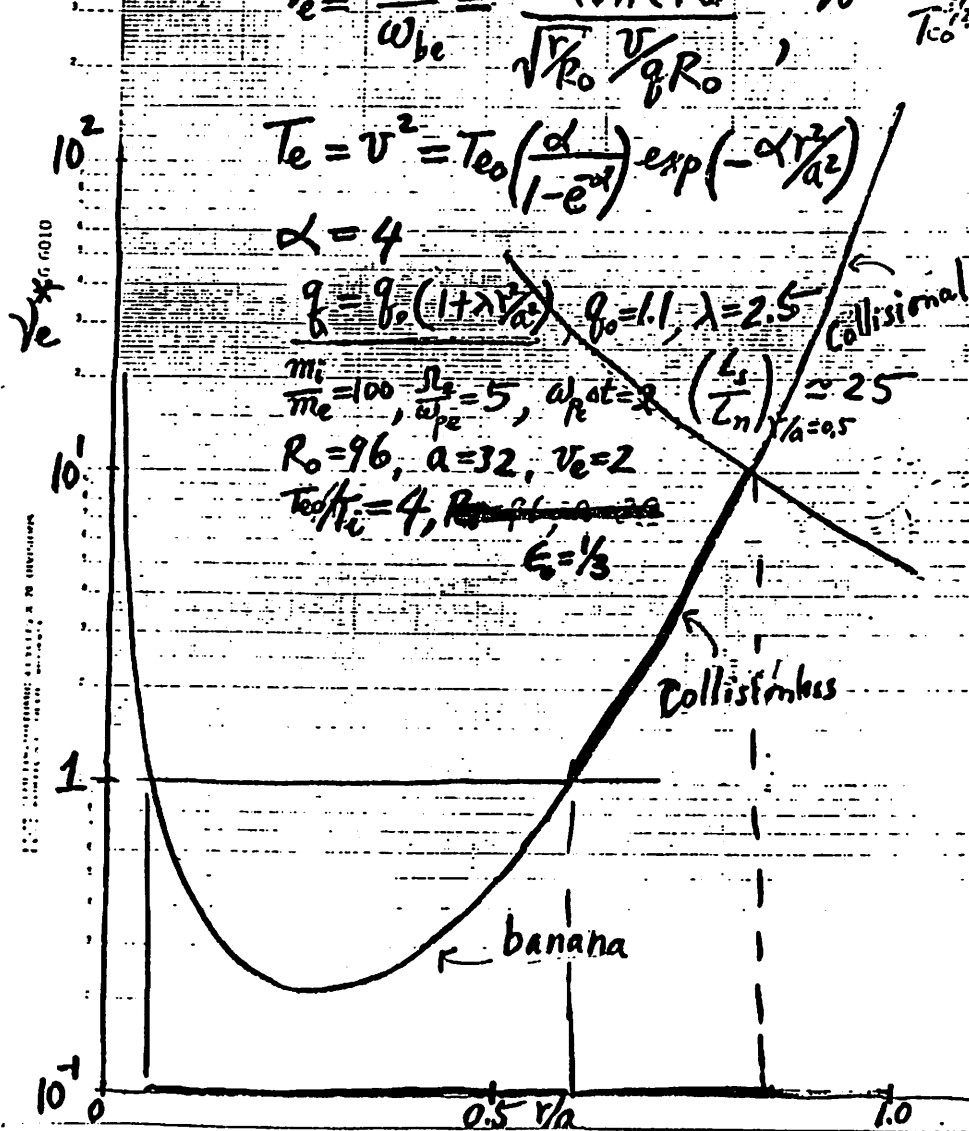
$$\alpha = 4$$

$$f = f_0 (1 + \lambda v_e^*), \quad f_0 = 1.1, \lambda = 2.5$$

$$\frac{m_i}{m_e} = 100, \frac{\Omega_i}{\omega_{pe}} = 5, a_{pe} = 2, \left(\frac{L_s}{L_n}\right)^{1/2} \approx 25$$

$$R_0 = 96, a = 32, v_e = 2$$

$$T_{e0}/T_i = 4, R_0 \approx 96, \epsilon_0 = 1/3$$



Neoclassical Transport

1) Particle Diffusion and Thermal Conduction

$$v_* = \frac{v_{ei}/\epsilon}{\omega_{be}}$$

In banana regime, $v_* < 1$

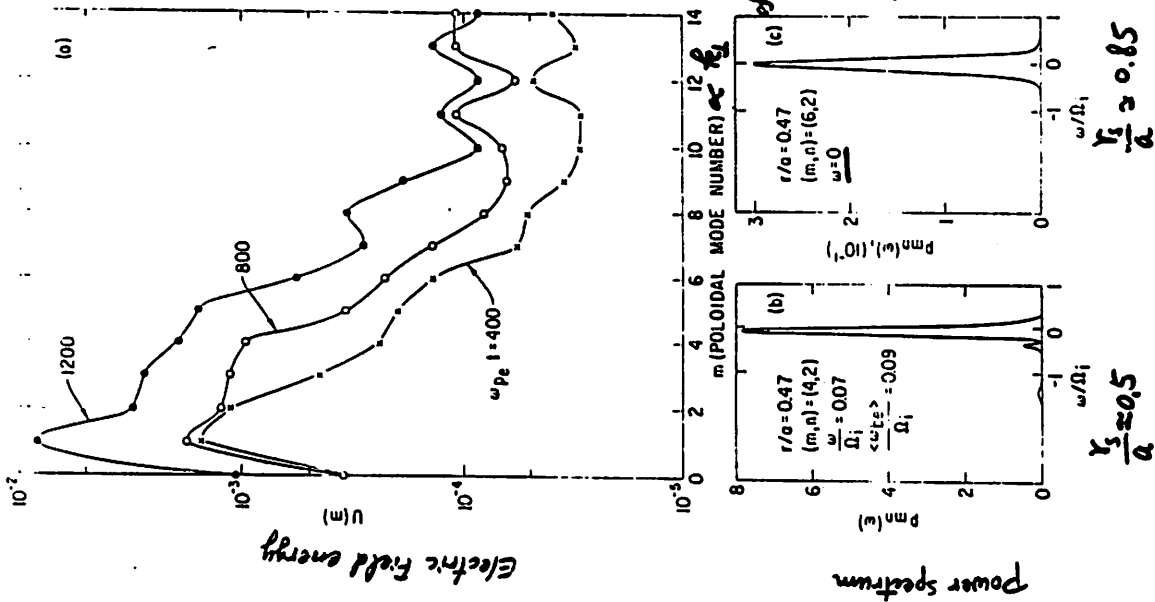
$$D_{\perp} \approx \rho_e^2 v_{ei} f^2 (R/r)^{3/2}$$

$$\chi_{e\perp} \approx D_{\perp}$$

$$\chi_{i\perp} \approx \rho_i^2 v_{ei} f^2 (R/r)^{3/2} \ll \chi_{e\perp}$$

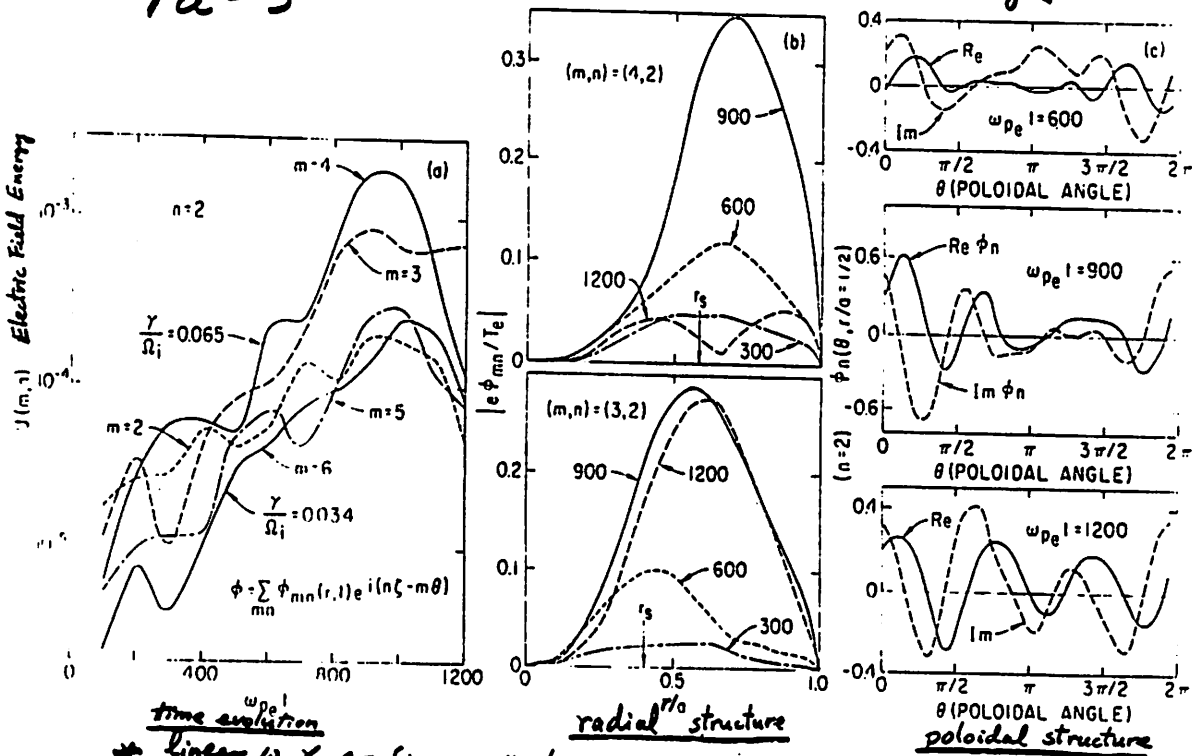
2) Bootstrap Current

$$J_S \approx \left(\frac{mc}{e\hbar_0}\right) \frac{\partial}{\partial r} \left(\frac{nT}{m}\right) \left(\frac{r}{R}\right)^{1/2} \quad \text{for } v_* < 1$$



Nonlinear excitation
of $\omega \approx 0$ modes
exist even in
the presence of
strong shear!

$R/a = 3$



Ballooning effect

* Linear ω, γ confirms with linear calculations by ① Rowoldt et al.

② Chong + Chen PPPL-1622

PLT & ATC EXP.

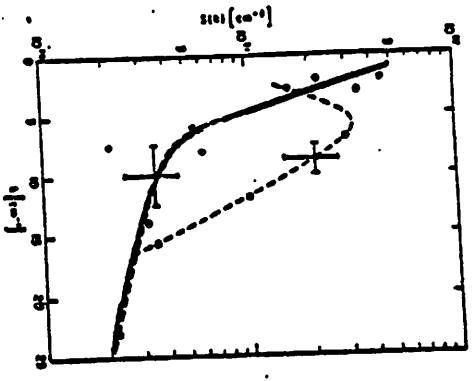


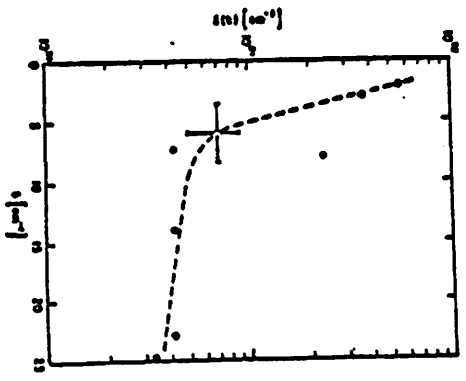
Fig. 7. Spectral density of fluctuations in PLT (at $\theta = 90^\circ$) \circ - PLT (at $\theta = -54^\circ$ and $\theta = -135^\circ$) \bullet - ATC.

773650

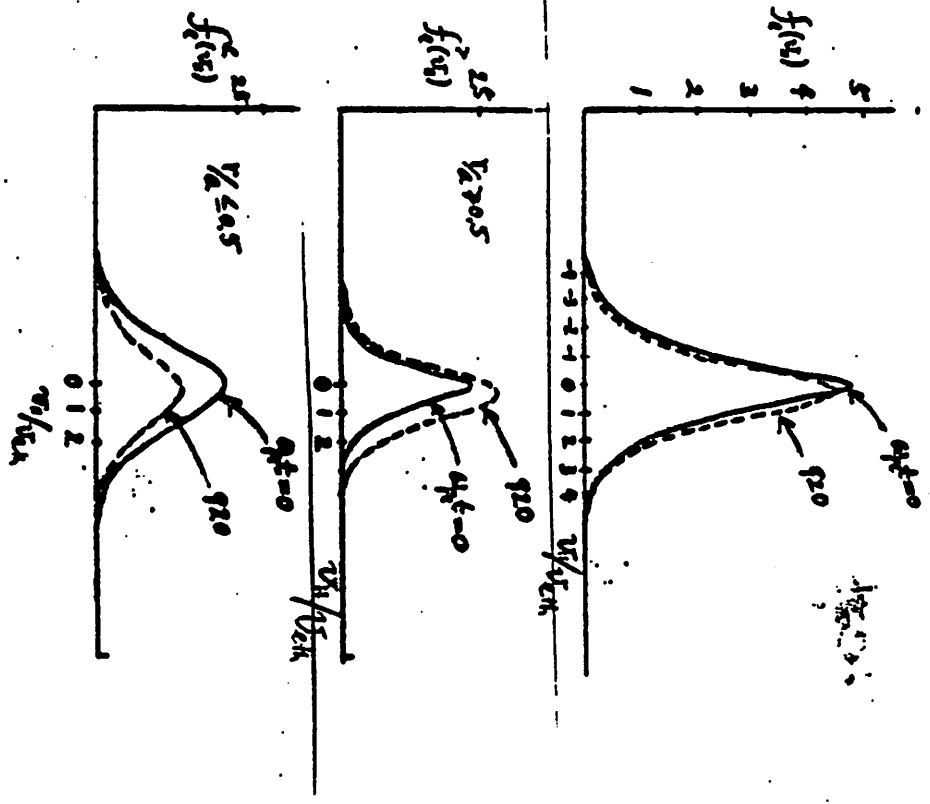
190

Fig. 8. Spectral density of fluctuations in PLT with hollow T-rod filaments (larger amplitude) and $\theta = -135^\circ$ (smaller amplitude).

773648



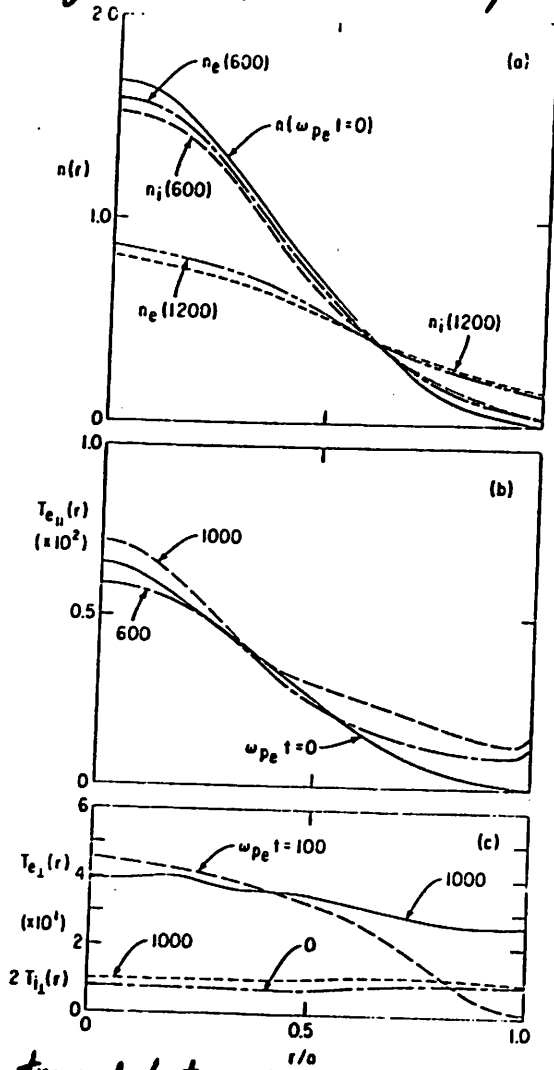
Electron Velocity Distribution



The bootstrap current

$$I \approx \frac{mc}{4\pi e} \frac{\partial}{\partial t} \left(\frac{nT}{m} \right) \left(\frac{R}{L} \right)^2 \approx v_p = V_{th} \delta \left(\frac{R}{L} \right)^2 \cdot \rho \left(\frac{1}{N} \frac{\partial n}{\partial t} + \frac{1}{T} \frac{\partial T}{\partial t} \right)$$

191



$$D_{\perp} \approx 2 \times 10^{-2} \rho_s^2 \omega_{pe}^2$$

$$\approx \left(\frac{cT_e}{eB}\right) (\rho_s / L_n)$$

$$D_{\perp}^{NC} \approx 10^{-3} \rho_s^2 \omega_{pe}^2$$

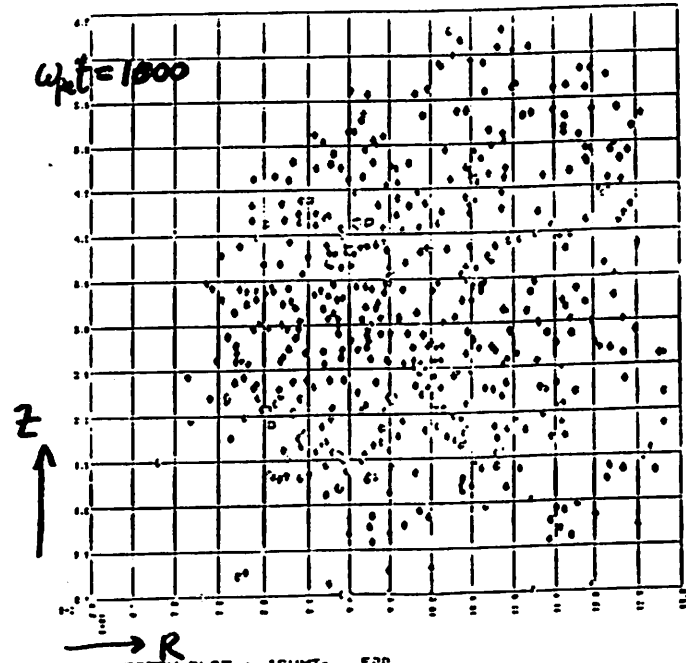
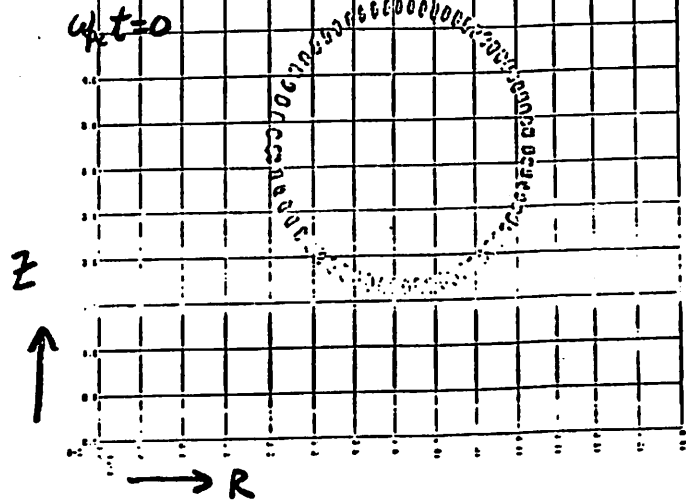
~~$\chi_{\perp}^e \approx 3D_{\perp}$~~

$$\chi_{\perp}^e \approx 3D_{\perp}$$

trapped electrons ($v_{\perp} > \bar{v}_{\perp}$)

FIG. 3

Electron Test Particles



ELECTRON TEST PARTICLES PLOT - 15MHT - 5BP

Summary for TEM Simulation

- 1) Check linear theory with η_e .
 $\gamma \propto (C_1 \eta_e + C_2)$, for $\eta_e = -1$, $\gamma < 0$
- 2) Observe ballooning behavior of TEM in the linear stage and its disappearance in the NL stage.
- 3) Generation of strong turbulence feature with $\Delta \omega \approx \omega^*$ and convective cells ($\omega \neq 0$) like structure.
- 4) Check neoclassical transport behavior, eg. bootstrap current.
- 5) Anomalous heat conductivity and density transport observed.

$$\chi_{\perp}^e \approx 3 D_{\perp}, \quad D_{\perp} \gg D_{\perp}^{\text{Neoclass}}$$

Future Plans

- 1) In neutral beam heated PLT plasma with $T_i > T_e$, $\eta_i > 1$, experimental results show that $\left(\frac{\delta n}{N}\right)^{\text{NB}} > \left(\frac{\delta n}{N}\right)$ but $\chi_{\perp}^{\text{eNB}} \approx \chi_{\perp}^e$.

This may be related to η_i mode which is an ion drift wave and doesn't require electron non-adiabatic response to make it unstable.

TEM also co-exists with η_i modes.

$\therefore \chi_{\perp}^e$ may be due to TEM only?

This can be simulated by 3D toroidal code!!

- 2) Develop finite- β 3D toroidal code to study transport due to magnetic fluctuations associated with small scale drift-tearing modes, finite β modified drift waves, stochastic magnetic fields, etc.

17.3 - D E-M RELATIVISTICPARTICLE MOVE

TIMINGS MICROSECONDS PER
PARTICLE STEP
ON THE CRAY

QUADRATIC SPLINE
INTERPOLATIONTETRAHEDRAL
INTERPOLATION

WEIGHTS 1

WEIGHTS $\frac{1}{2}$ FIELD COLLECT
& INTERPOLATION 9FIELD COLLECT
& INTERPOLATION $1\frac{1}{4}$ MOVE $1\frac{1}{4}$ MOVE $1\frac{1}{4}$

NEW WEIGHTS 1

C-C ACCUM.
OLD POS'N $1\frac{1}{4}$ CHARGE-CURRENT
ACCUMULATION 1NEW WEIGHTS $\frac{1}{2}$ AT OLD & NEW
POSITIONS $12\frac{1}{2}$ C-C ACCUM
NEW POS'N $1\frac{1}{4}$ TOTAL $24\frac{1}{2}$

TOTAL 6

AUXILIARIESPACK & UNPACK (LIBRIS)

sign bit + 7 bits biased exponent
+ 24 bit mantissa

SQUASH & BLOWUP

32-bit integer * 10^{-6} (2^{-20})

between -2048.000000 and 2047.999999
(allows half-word adds & subtracts)

VECFIT (LIBRIS)

64 complex arrays, each length 2^n , Fourier-
transformed in parallel ($n \leq 11$).

TETRAHEDRAL INTERPOLATION
(linear from only 4 table entries)

OVERLAP of I/O with COMPUTATION:
Z10 (LIBRIS)

HALF - WORD ARITHMETIC ON THE CRAY

189

200

TEST: SUM OF TWO NUMBERS BTWN -1024.000000 & +1023.999999

```

DIMENSION X(128),Y(128),N(64),U(128),M(64)
EQUIVALENCE (X(1),N(1)),(U(1),M(1))
CALL LINK("UNIT6=(OUTPUT,CREATE,MC)"/)
CALL PANVC(U)
CALL PANVC(U(65))
CALL PANVC(X)
CALL PANVC(X(65))
DO 4 I=1,128
U(I)=2048.*U(I)-1024.
X(I)=2048.*X(I)-1024.
Y(I)=X(I)+U(I)
CALL SQUASH(U)
CALL SQUASH(X)
DO 1 I=1,64
N(I)=N(I)+M(I)+100000000020000000000
CALL BLOWUP(N)
DO 2 I=1,126,6
WRITE(6,99)X(I),X(I+1),X(I+2),X(I+3),X(I+4),X(I+5)
WRITE(6,99)Y(I),Y(I+1),Y(I+2),Y(I+3),Y(I+4),Y(I+5)
WRITE(6,98)(10000000.*(X(I)-Y(I)),I=1,128)
FORMAT(1X,26F3.0)
FORMAT(6F13.6)
CALL EXIT
END
    
```

RED OUTPUT TOP LINE : 32-BIT ARITHMETIC
47 LINES. (A) OUTPUT BOTTOM LINE : REGULAR FLOAT ARITHMETIC
-L-N

-595.328590	51.818355	1129.000351	438.655076	447.515160	-997.062448
-595.328590	51.818354	1129.000351	438.655077	447.515160	-997.062447
-414.927875	529.901539	1323.802226	616.002561	-237.524015	314.578135
-414.927875	529.901539	1323.802227	616.002561	-237.524016	314.578135
791.967134	20.541625	231.625631	-59.944667	-236.859705	920.256655
791.967133	20.541625	231.625631	-59.944667	-236.859705	920.256655
1069.551678	1150.071316	567.232296	-1011.479963	-346.475391	-183.337484
1069.551677	1150.071316	567.232295	-1011.479963	-346.475391	-183.337484
16.832857	-804.246475	-1834.306370	110.013324	603.967479	887.716554
16.832857	-804.246475	-1834.306370	110.013323	603.967479	887.716554
-1238.059412	-87.466410	-124.182793	148.043823	852.710708	187.285010
-1238.059413	-87.466409	-124.182793	148.043823	852.710708	187.285010
1013.569518	1795.684489	1129.144354	-397.310045	843.630754	-407.792184
1013.569517	1795.684489	1129.144355	-397.310045	843.630755	-407.792183
-275.603466	73.268896	174.493128	-718.747376	427.593359	536.964971
-275.603466	73.268897	174.493127	-718.747377	427.593359	536.964970
-748.388295	200.710372	910.437201	-379.573199	208.709394	5.544247
-748.388296	200.710372	910.437201	-379.573200	208.709393	5.544247
-11.965263	374.433164	474.990366	-532.540940	-1159.915384	-932.544399
-11.965263	374.433164	474.990366	-532.540941	-1159.915385	-932.544399
397.804895	-1239.050673	602.123966	-677.832448	-116.629913	-896.434620
397.804896	-1239.050672	602.123966	-677.832448	-116.629913	-896.434620
-1224.904542	-182.478872	-1595.778546	795.549807	615.059140	961.825091
-1224.904543	-182.478873	-1595.778547	795.549807	615.059140	961.825091
-640.895184	-1879.690872	-1746.564226	744.070167	-276.863503	374.498011
-640.895184	-1879.690871	-1746.564226	744.070167	-276.863502	374.498010
17.730875	1343.560247	-1046.947722	30.805865	57.251193	264.720605
17.730875	1343.560247	-1046.947723	30.805866	57.251192	264.720605
-545.515934	897.848199	647.887833	-1065.233297	799.237789	-854.122472
-545.515934	897.848199	647.887833	-1065.233298	799.237789	-854.122472
-585.397239	1631.729687	-1195.383575	-73.658769	641.817876	-148.852828
-585.397240	1631.729686	-1195.383575	-73.658769	641.817876	-148.852828
-294.106311	619.626160	1440.468412	-644.459601	-552.896686	-1005.357639
-294.106311	619.626160	1440.468412	-644.459601	-552.896687	-1005.357639
1134.044845	-338.388642	-1399.604600	990.210764	38.510056	925.905988
1134.044845	-338.388642	-1399.604600	990.210763	38.510056	925.905988
-215.810184	635.532150	-941.459043	-957.497978	-1298.412893	-166.672716
-215.810183	635.532150	-941.459043	-957.497978	-1298.412894	-166.672715
-1378.893709	-1317.907406	1294.349863	430.550515	-303.045161	-339.350916
-1378.893709	-1317.907406	1294.349863	430.550515	-303.045161	-339.350916
-443.001930	-1182.102284	573.150744	683.660011	399.540341	158.593394
-443.001930	-1182.102284	573.150744	683.660011	399.540341	158.593394
7.5.-1.-8.-1.-1.0.1.-5.-4.4.0.4.0.-0.1.-0.-2.4.-6.5.-6.-3.0.3.-5.					
4.9.-2.-4.6.-6.1.2.-1.2.6.-0.-7.-4.-3.-5.4.-4.6.2.1.2.6.-2.3.6.					
2.-2.-2.-2.5.7.2.-2.-1.-8.6.-2.-3.-3.6.7.2.-2.2.7.7.-0.1.-2.-4.2.					
0.1.-3.9.-4.-4.-0.-4.3.4.-3.8.4.-3.-5.-6.0.-0.-1.2.-8.5.-6.-1.-4.					
5.5.5.-2.-6.-0.7.-3.3.-7.3.2.-2.-1.2.-4.0.5.1.-2.3.-4.-1.-0.					

END

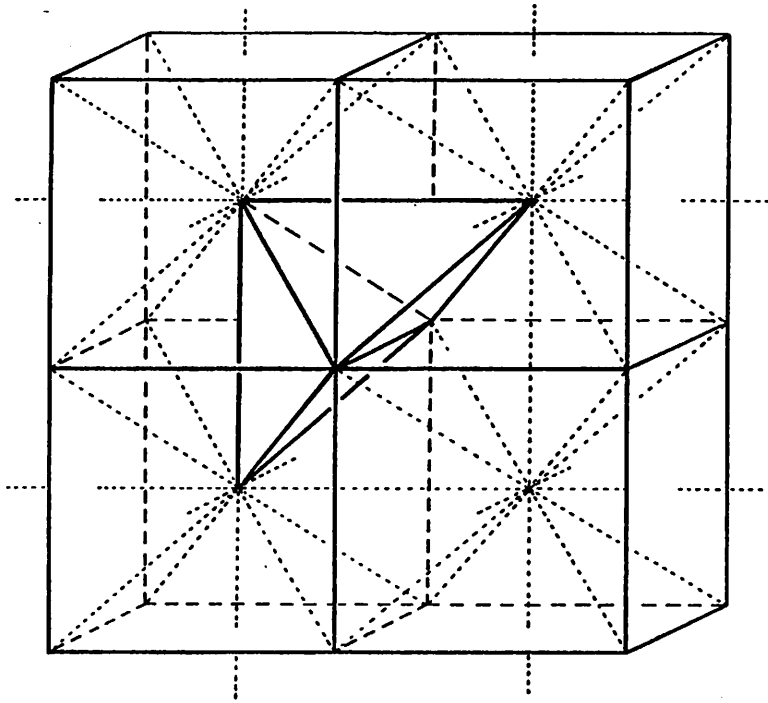


Figure 3. Tetrahedral mesh connecting cube centers and cube corners, with two of the tetrahedra emphasized.

DATA FLOW BETWEEN

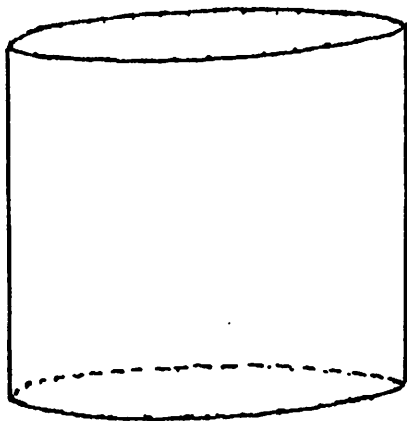
CDRE AND DISCS

$2 * 128^3$ INTERLEAVED

PARTICLE SIMULATION,

ELECTRO-MAGNETIC

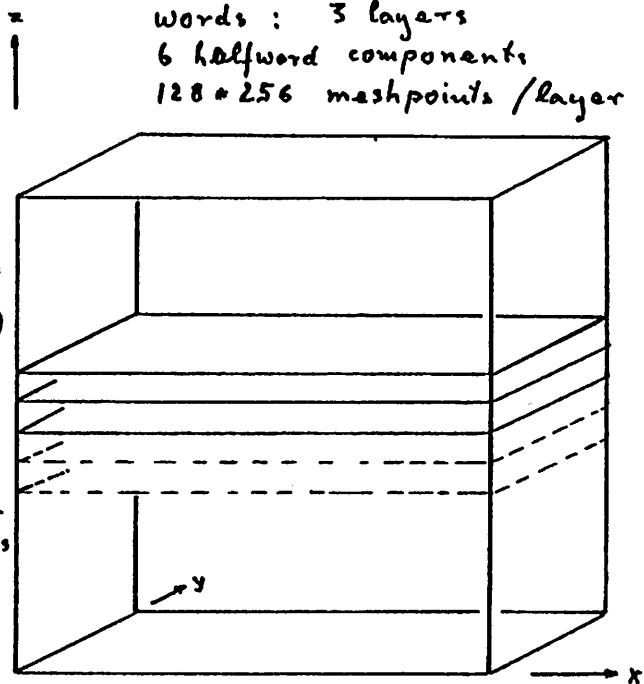
DISC SPACE
typically 4 million
words



2 million particles,
packed 3:1, sorted
by layers (pairs of) :

particle move phase

288 K packed field
words : 3 layers
6 halfword components
128 * 256 meshpoints / layer



320 K packed charge-
current words : 5 layers
4 halfword components
128 * 256 meshpoints / layer

(lowest two layers
catch the drop-downs)

CORE:

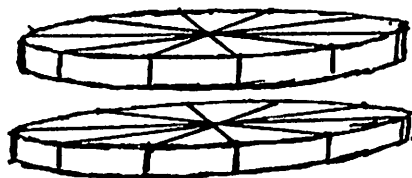
op's between layers during particle move phase

105 K packed field words, 2-z-layers

rs: d field words forming from

zeros ← unpack

c-c words: FT in x & y, repack (ers)



70 K packed charge-current words, 2 z-layers
Divided into 10 sectors

→ k_x 10 1/2-K words of fields read from each sector
←
7 K words of charge-currents written to each sector

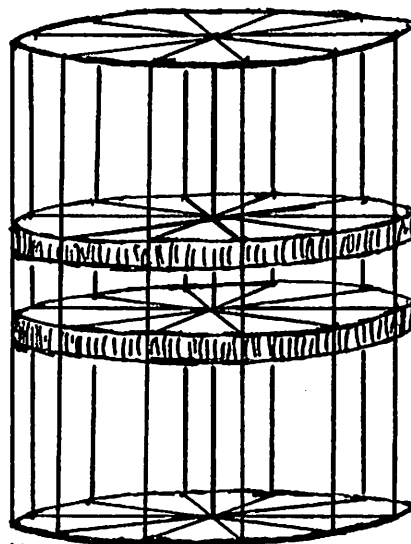
DISC SPACE

6.6 million words, packed

10 separate disc areas, different drives

z ↑

Write one sector of 67 field words



records contiguous in each sector

read one sector of 448 charge-currents

4.4 M packed charge-current words overwritten by 6.6 M packed field words after field update. (Partially transformed)

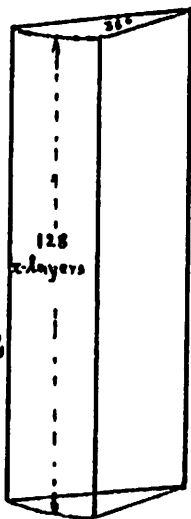
CORE:

207

op's between sectors during field update

2 K packed

z ↑



Disperse to four different disc areas on different drives so this I/O can proceed via four channels

K packed words

448 K packed charge-current words

overwritten by 672 K packed field words

repack ← FFT in k_x , ← pad with zeros fields
(work from inside out)

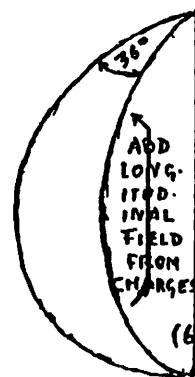
unpack, FFT in z , truncate, charge-currents
(work from outside in)

CORE:

208

Field update phase

630 K unpacked field words



MAXWELL UPDATE FIELDS FROM CURRENTS

Write updated harmonics to

read in 16 K word E of transverse field

420 K unpacked charge current words overwritten by field words

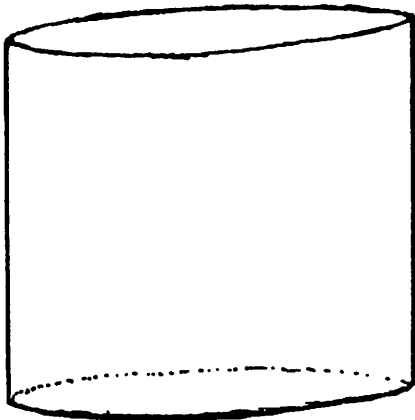
105 K harmonics

(k_x, k_y, k_z space)

$\frac{1}{10}$ sector of sphere of $\frac{4\pi}{3} 64^3 = 1.05$ million admitted harmonics

DISC SPACE

1.05 million
field harmonics



2.1 million packed
words transverse
field harmonics
("photons")
4 halfwords per
harmonic

ck to disc

TRIPLE
BUFFERING

atches
harmonics



NEEC-3D

18. A SELF-CONSISTENT PARTICLE AND FIELD SIMULATION CODE

T. A. Turno1110

December 10, 1979

SGEMP ANALYSIS

- ELECTROMAGNETIC RESPONSE OF STRUCTURES EXPOSED TO A PULSE OF HIGH-ENERGY PHOTONS
- SYSTEMS OF INTEREST
 - SATELLITES, MISSILES, AIRCRAFT
 - GROUND-BASED COMMUNICATIONS FACILITIES
 - SILOS
- PHYSICAL PHENOMENA
 - PHOTON TRANSPORT
 - ELECTRON GENERATION
 - ELECTRON MOTION - EM FIELD GENERATION
 - ELECTRONIC CIRCUIT RESPONSE

211

UNCLASSIFIED

PHENOMENA

- RELATIVISTIC PRIMARY ELECTRONS GENERATED AT SYSTEM SURFACES AND IN THE GASEOUS MEDIUM
- SECONDARY ELECTRONS & POSITIVE IONS GENERATED BY THE PRIMARY ELECTRONS
- ELECTRON TRAJECTORIES DETERMINED BY INDUCED ELECTROMAGNETIC FIELDS AND IONIZATION ENERGY LOSS FORCES
- FIELDS DETERMINED BY PRIMARY ELECTRON CURRENTS AND TIME DEPENDENT CONDUCTIVITY DUE TO PLASMA GENERATED BY IONIZING PRIMARIES
- COMPLEX BOUNDARY VALUE PROBLEM

UNCLASSIFIED

212

APPROACH

- ELECTROMAGNETIC FIELDS - FINITE DIFFERENCE TIME DOMAIN SOLUTION OF MAXWELLS CURL EQUATIONS

$$\vec{\nabla} \times \vec{E} = - \frac{\partial \vec{B}}{\partial t}$$

$$\vec{\nabla} \times \vec{H} = \vec{J} + \sigma \vec{E} + \frac{\partial \vec{D}}{\partial t}$$

- PRIMARY ELECTRONS - DISTRIBUTIONS REPRESENTED BY MACROPARTICLES TRAJECTORIES DETERMINED FROM

$$\frac{d(m\vec{v}\gamma)}{dt} = q(\vec{E} + \vec{v} \times \vec{B}) - \frac{F(v)\vec{v}}{v}$$

$$\frac{d(mc^2\gamma)}{dt} = q(\vec{v} \cdot \vec{E}) - F(v)v$$

UNCLASSIFIED

- PLASMAS USED IN THE CODE
- OHMIC - 3 SPECIES AIR CHEMISTRY USEFUL FOR NEAR ATMOSPHERIC PRESSURES
 - MACROPARTICLES FOR ELECTRONS IMMOBILE IONS NO COLLISIONS
 - SECONDARY IONIZATION AT LOW PRESSURES TREATED AS MACROPARTICLES. IMMOBILE IONS.

UNCLASSIFIED

- PLASMA - THREE SPECIES AND OHMIC

$$\sigma = e(\mu_e n_e + \mu_+ n_+ + \mu_- n_-)$$

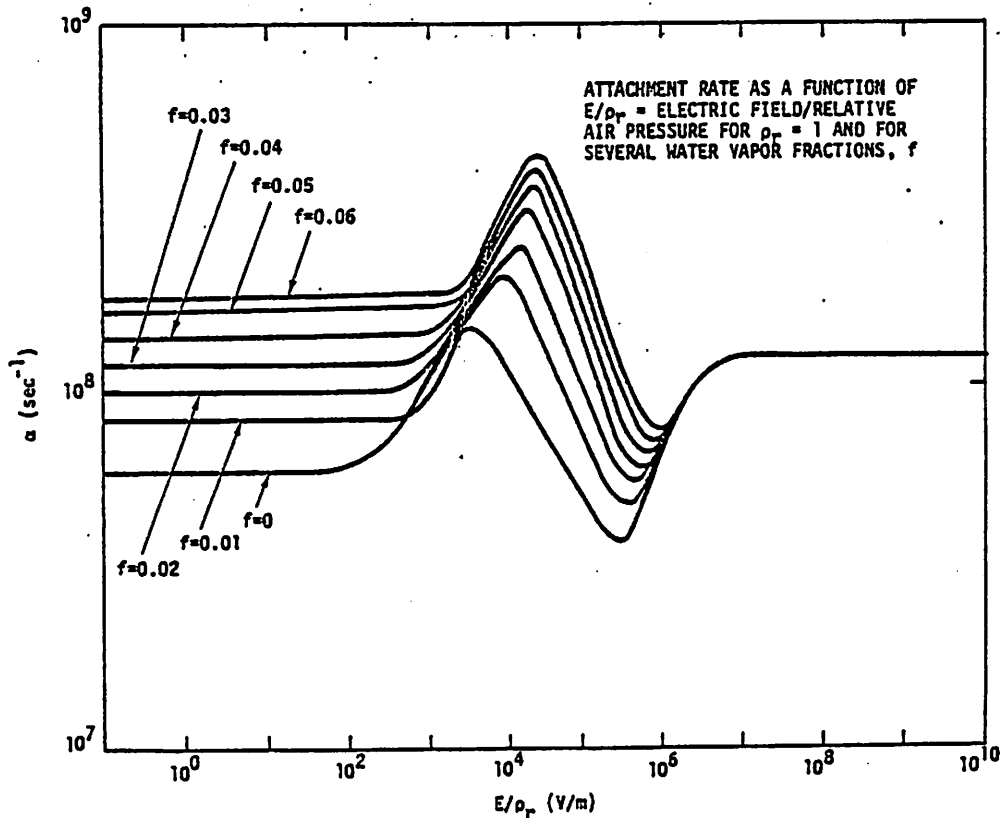
- AIR CHEMISTRY RATE EQUATIONS

$$\frac{dn_e}{dt} = Q - (\alpha - g) n_e - \beta n_+ n_e$$

$$\frac{dn_-}{dt} = \alpha n_e - \gamma n_+ n_-$$

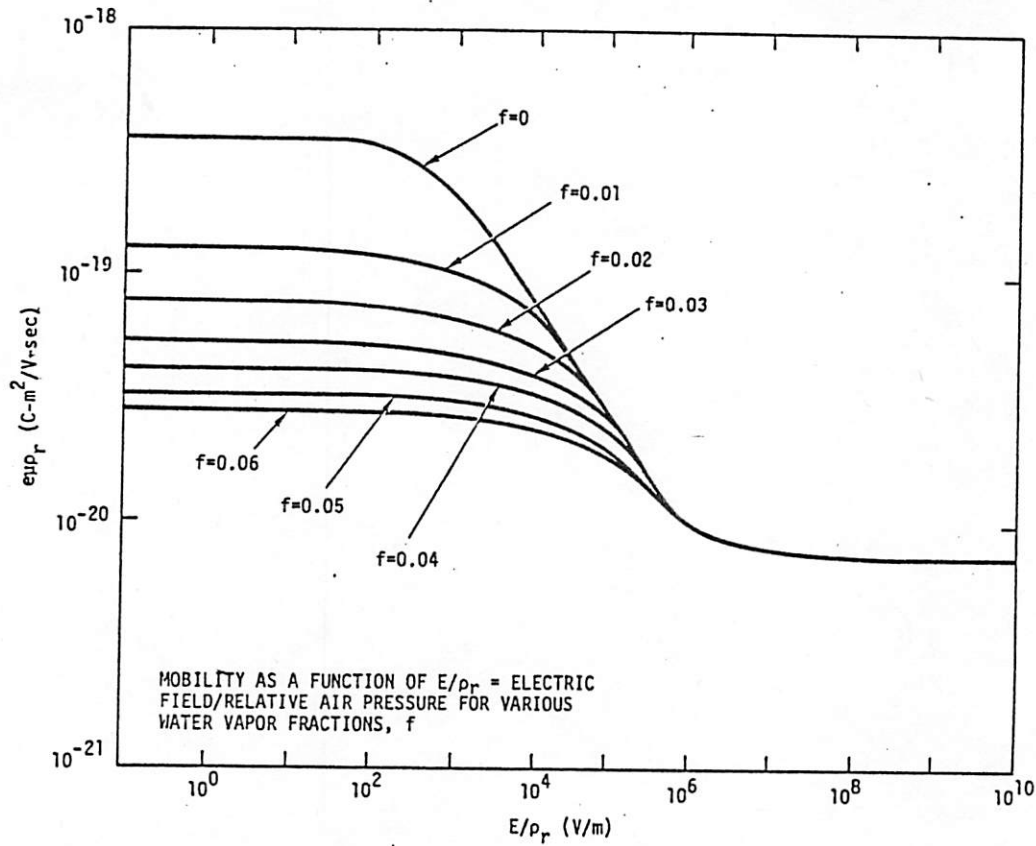
$$n_+ = n_- + n_e$$

UNCLASSIFIED



215

216



27

217
8

THREE-SPECIES RATE EQUATIONS

$$\frac{dn_e}{dt} = S - (\alpha - g)n_e - \beta n_+ n_e$$

$$\frac{dn_-}{dt} = \alpha n_e - \Gamma n_+ n_-$$

$$n_+ = n_- + n_e$$

THESE EQUATIONS MUST BE DIFFERENCED AND INTEGRATED FORWARD IN TIME AT EVERY ZONE OF THE ELECTROMAGNETIC SIMULATION AT EVERY TIME STEP. AT THE N^{TH} ZONE AND AT THE L^{TH} TIME STEP, USE:

$$n_{eN}^{L+1} = n_{eN}^L \exp(-\alpha_N^L \delta t) + [1 - \exp(-\alpha_N^L \delta t)] \frac{S_N^L + g_N^L n_{eN}^L}{\alpha_N^L} - \beta \delta t n_{+N}^L n_{eN}^L$$

$$n_{-N}^{L+1} = \alpha_N^L \delta t n_{eN}^L + n_{-N}^L (1 - \Gamma \delta t n_{+N}^L)$$

218

UNCLASSIFIED

UNCLASSIFIED

$$C = \begin{bmatrix} \frac{\partial y_j \partial z_k}{\partial x_1} & c_{1jk} \frac{\partial x_1 \partial z_k}{\partial y_j} & c_{1jk} \frac{\partial x_1 \partial y_j}{\partial z_k} \end{bmatrix} ;$$

$$L = \begin{bmatrix} \frac{\partial y_j \partial z_k}{\partial x_1} & b_{1jk} \frac{\partial x_1 \partial z_k}{\partial y_j} & b_{1jk} \frac{\partial x_1 \partial y_j}{\partial z_k} \end{bmatrix} ;$$

$$R = \begin{bmatrix} \frac{1}{a_{1jk}} \frac{\partial x_1}{\partial y_j \partial z_k} & \frac{1}{a_{1jk}} \frac{\partial y_j}{\partial x_1 \partial z_k} & \frac{1}{a_{1jk}} \frac{\partial z_k}{\partial x_1 \partial y_j} \end{bmatrix} ;$$

$$V = \begin{bmatrix} -\Delta z_k E_x \left| x_1, y_j, z_k + \Delta z_k \right. & -\Delta y_j E_y \left| x_1 + \Delta x_1, y_j, z_k + \Delta z_k \right. & \end{bmatrix} ;$$

$$I = \begin{bmatrix} \Delta x_1 H_x \left| x_1 + \Delta x_1, y_j, z_k \right. & \Delta y_j H_y \left| x_1, y_j + \Delta y_j, z_k \right. & \Delta z_k H_z \left| x_1 + \Delta x_1, y_j + \Delta y_j, z_k \right. \end{bmatrix} ;$$

$$S = \begin{bmatrix} \Delta x_1 \Delta y_j \Delta z_k \left| x_1 + \Delta x_1, y_j + \Delta y_j, z_k \right. & \Delta y_j \Delta z_k \Delta x_1 \left| x_1, y_j + \Delta y_j, z_k + \Delta z_k \right. & \Delta x_1 \Delta z_k \Delta y_j \left| x_1 + \Delta x_1, y_j, z_k + \Delta z_k \right. \end{bmatrix} ;$$

UNCLASSIFIED

UNCLASSIFIED

$$I_{x1jk}^{n+3/2} = I_{x1jk}^{n+1/2} + \frac{\partial c}{\partial x_1} \left\{ V_{z1jk}^{n+1} - V_{z1j-k}^{n+1} - V_{y1jk}^{n+1} + V_{y1j-k-1}^{n+1} \right\} ;$$

$$I_{y1jk}^{n+3/2} = I_{y1jk}^{n+1/2} + \frac{\partial c}{\partial y_j} \left\{ V_{x1jk}^{n+1} - V_{x1j-k-1}^{n+1} - V_{z1jk}^{n+1} + V_{z1-j+k}^{n+1} \right\} ;$$

$$I_{z1jk}^{n+3/2} = I_{z1jk}^{n+1/2} + \frac{\partial c}{\partial z_k} \left\{ V_{y1jk}^{n+1} - V_{y1-j+k}^{n+1} - V_{x1jk}^{n+1} + V_{x1j-1+k}^{n+1} \right\} ;$$

$$V_{x1jk}^{n+1} = \left(1 + \frac{\partial c}{\partial x_1} \right)^{-1} \left[V_{x1jk}^{n+1} + \frac{\partial c}{\partial x_1} \left(S_{x1jk}^{n+1/2} - I_{z1j+k}^{n+1/2} \right) \right] ;$$

$$I_{x1jk}^{n+1/2} + I_{y1j+k+1}^{n+1/2} - I_{z1jk}^{n+1/2} \left. \right] ;$$

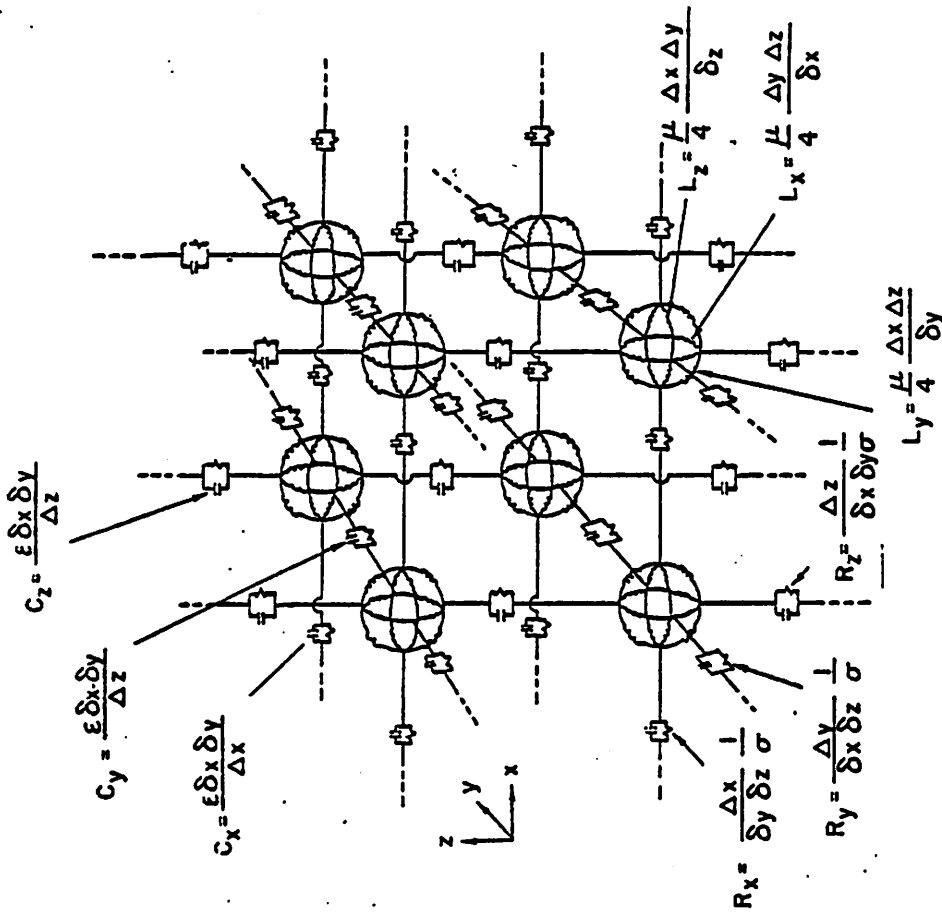
$$V_{y1jk}^{n+1} = \left(1 + \frac{\partial c}{\partial y_j} \right)^{-1} \left[V_{y1jk}^{n+1} + \frac{\partial c}{\partial y_j} \left(S_{y1jk}^{n+1/2} - I_{x1j-k}^{n+1/2} \right) \right] ;$$

$$I_{y1jk}^{n+1/2} + I_{z1+j+k}^{n+1/2} - I_{x1jk}^{n+1/2} \left. \right] ;$$

$$V_{z1jk}^{n+1} = \left(1 + \frac{\partial c}{\partial z_k} \right)^{-1} \left[V_{z1jk}^{n+1} + \frac{\partial c}{\partial z_k} \left(S_{z1jk}^{n+1/2} - I_{y1+j+k}^{n+1/2} \right) \right] ;$$

$$I_{z1jk}^{n+1/2} + I_{x1j+k}^{n+1/2} - I_{y1+j+k}^{n+1/2} \left. \right] ;$$

UNCLASSIFIED



UNCLASSIFIED

221 2



APPROACH

- ASSEMBLY LANGUAGE CODING FOR INTEGRATION OF FIELD AND PARTICLE EQUATIONS

- WORD PACKING CDC 60-BIT WORDS

$$(V_x, V_y, V_z)$$

$$(n_x, n_y, n_z)$$

$$(r=1, Q, N)$$

$$(C_{xk}, C_{yk}, C_{zk})$$

$$(L_{xk}, L_{yk}, L_{zk})$$

$$(S_{xk}, S_{xk+1}) (V_{xk}, V_{xk+1}) (I_{xk}, I_{xk+1})$$

$$(S_{yk}, S_{yk+1}) (V_{yk}, V_{yk+1}) (I_{yk}, I_{yk+1})$$

$$(S_{zk}, S_{zk+1}) (V_{zk}, V_{zk+1}) (I_{zk}, I_{zk+1})$$

OVERLAY STRUCTURE FOR THE CODE

- INPUT PROCESSOR
- EM SOLVER
- PARTICLE PUSHER
- AIR CHEMISTRY
- OUTPUT REQUESTS



CODE CHARACTERISTICS

- CARTESIAN COORDINATES - 3D
- ONE OR TWO PLANES OF SYMMETRY
- VARIABLE ZONING ALL AXES
- NUMBER OF SPATIAL ZONES UNLIMITED
- SIMULATION BOUNDARY CAN BE ALLOWED TO MOVE AT SPEED OF LIGHT
- RESTART/REZONE CAPABILITY
- STATIC FIELDS CAN BE ADDED TO TIME DEPENDENT FIELDS
- NUMBER OF MACROPARTICLES UNLIMITED
- SPECIALIZED INPUT LANGUAGE TO DEFINE SYSTEM GEOMETRY, EMISSION SURFACES OR VOLUMES, OUTPUT REQUESTS, RUN CONTROLS, PARTICLE ENERGY, ANGLE, AND TIME DISTRIBUTIONS



- SYSTEM GEOMETRY DESCRIBED AS A SEQUENCE OF LINES, SURFACES, OR VOLUMES WITH SPECIFIED MATERIAL CONSTANTS
- EMISSION SURFACES INDEXED TO PRESPECIFIED ELECTRON INTENSITY, ENERGY, AND ANGULAR DISTRIBUTIONS
- NEAREST GRID POINT CURRENT ALGORITHM
- SECONDARY ELECTRON PRODUCTION AT SURFACES WHERE PRIMARY ELECTRONS IMPACT CAN BE INCLUDED
- EXECUTION TIMES
 - 5.5 μ sec/EH ZONE TIME STEP
 - 19.0 μ sec/PARTICLE TIME STEP

502

225

226

INPUT LANGUAGE EXAMPLES

CV (X₁, X₂, X₃) TO (X'₁, X'₂, X'₃)
DV () () EPS = VALUE
LV () () SIG = VALUE
MV () () MU = VALUE

OUTPUT REQUESTS

- ANY FIELD QUANTITY AT ANY MESH POINT

EET I J J K K , HY I J J K K , JZ I J J K K , PLOT
SIG I J J K K , NEL I J J K K , PLOT

- POYNTING VECTOR AND COMPONENTS

PVX I J J K K , PVM I J J K K

- LINE INTEGRALS OR AVERAGES OVER CELLS

AVG(LABEL) = SUM OF ANY ALLOWED OUTPUT REQUEST
SUM(LABEL) = " " "

- REQUESTS ON PARTICLES
 - .. CHARGE IN SPACE, PLOT
 - .. Q, N, E BETWEEN Z_1 AND Z_2
 - .. NON RELATIVISTIC ENERGY DISTRIBUTION BETWEEN Z_1 AND Z_2
- ETC.

- PARTICLE DISTRIBUTIONS

ENERGY DISTRIBUTION 1 = list of dn/dE vs E

ANGLE DISTRIBUTION 1 = list of $dn/d\Omega$ vs θ

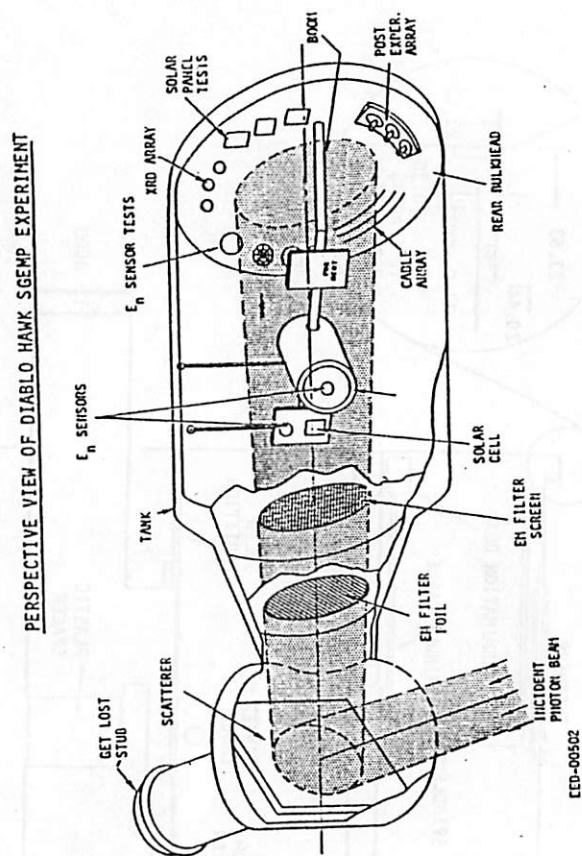
EMISSION INTENSITY 1 = list of J vs t

- PARTICLE EMISSION

(X_1, X_2, X_3) TO (X'_1, X'_2, X'_3) INT 1 /
 DELAY _____ TIMES _____, ED 1, AD 1, ADQ3 2, /
 N = _____

- RUN CONTROLS
- AIR CHEMISTRY PARAMETERS

UNCLASSIFIED

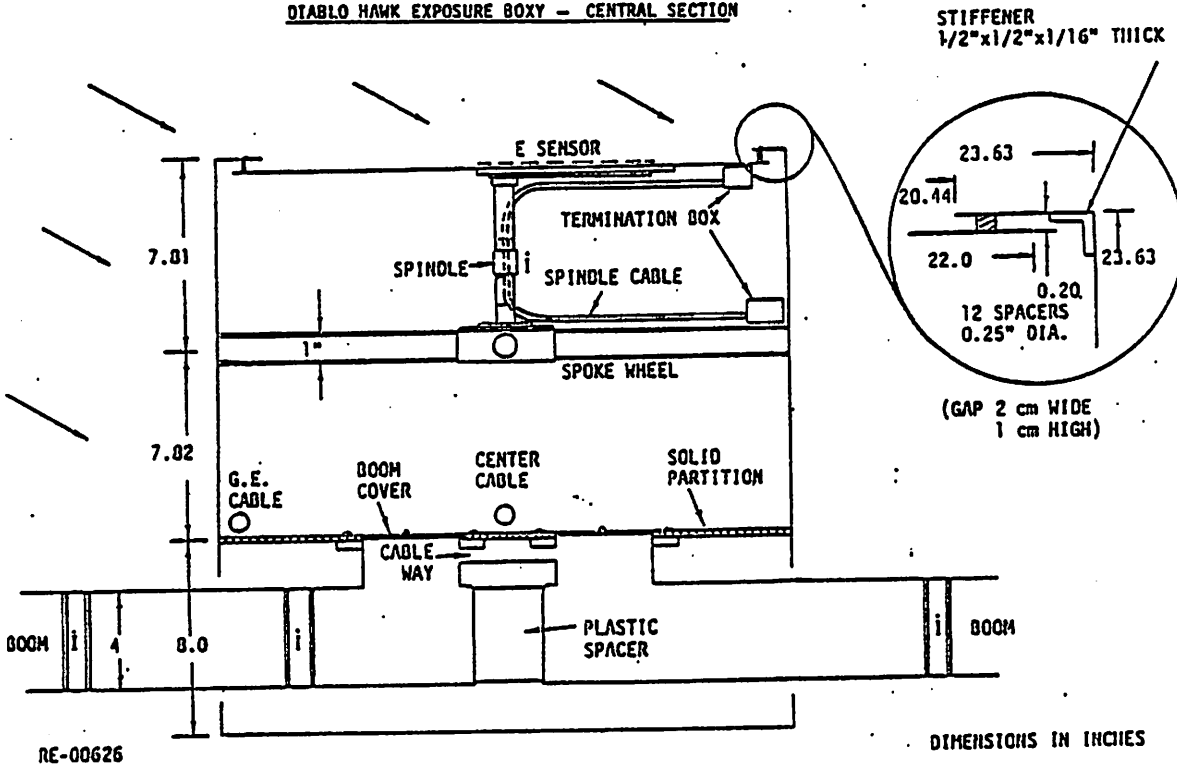


UNCLASSIFIED

UNCLASSIFIED

16

DIABLO HAWK EXPOSURE BOXY - CENTRAL SECTION



UNCLASSIFIED

229

UNCLASSIFIED

17

SGEMP EXPERIMENT SIMULATION PROCEDURE

- BOUNDARY CONDITIONS IMPOSED ON THE MESH
- X-RAY TRANSPORT THROUGH THE MODEL
- e⁻ DISTRIBUTIONS
- TIME-PHASED EMISSION
- OUTPUT REQUESTS
- FIT IT ALL ON THE COMPUTER

UNCLASSIFIED

230

ASSUMPTIONS

- . INDUCTIVE ISOLATION NOT MODELED BUT ASSUMED TO HOLD CURRENT FROM FLOWING TO CHAMBER WALLS FOR AT LEAST 20 ns
- . ONE PLANE OF SYMMETRY IMPOSED ON THE MODEL (QUITE A GOOD APPROXIMATION CONSIDERING THE MODEL GEOMETRY AND THE X-RAY FLUENCE CONTOURS)
- . TIME-DOMAIN FINITE-DIFFERENCE SOLUTION OF THE MAXWELL-LORENTZ EQUATION SET IN THREE DIMENSIONS IS USED AS THE PREDICTION TOOL
- . ELECTRON DISTRIBUTIONS DERIVED FROM X-RAY DISTRIBUTIONS UTILIZING THE QUICKE CODE

ELECTROMAGNETIC

- . SIMULATION TIME - 20 ns
- . EM TIME STEP - 8 psec
- . SMALLEST ZONE DIMENSION - 0.5 cm
- . NUMBER OF EM ZONES - 124,740

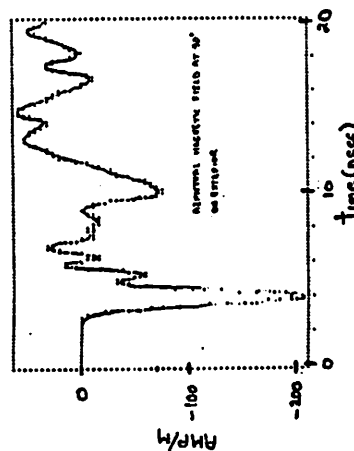
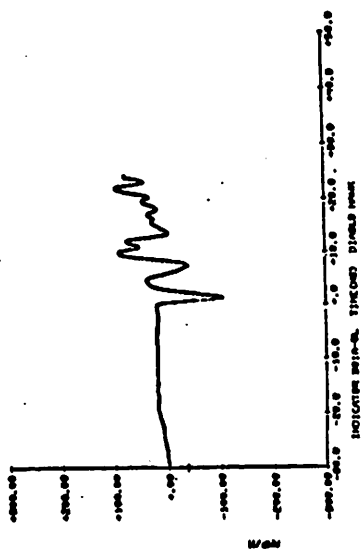
MACROPARTICLES

- . NUMBER OF EMISSION SURFACES - 511
- . TOTAL NUMBER OF INJECTED PARTICLES - 900,600
- . MAXIMUM NUMBER OF PARTICLES IN SPACE - 198,800
- . NUMBER OF ELECTRON ENERGY DISTRIBUTIONS - 45

INPUT-OUTPUT-EXECUTION

- . 2694 FIELD REQUESTS INTO 241 PLOTS
- . INPUT DECK LENGTH - 2580 CARDS
- . CPU TIME - ~3.56 HOURS
- . RAW OUTPUTS DIGITALLY FILTERED

UNCLASSIFIED



UNCLASSIFIED

19. $2\frac{1}{2}$ D PARTICAL SIMULATION MODELS

W. W. Lee and H. Okuda

PPPL

Purpose

To develop suitable models for studying microinstabilities in a tokamak plasma

Models - $2\frac{1}{2}$ D (x, y, v_x, v_y, v_z)

1. Electrostatic (ES)

a. Guiding Center Electron Model

b. Adiabatic Electron Model

2. Electromagnetic (Darwin)

a. Guiding Center Electron Model

Applications

Electron drift waves

Ion drift waves

Shear Alfvén waves

Limitations on Particle Models

$\Delta t \sim \omega_{pe}^{-1}$ or ω_{ce}^{-1} to resolve the highest frequency in the system

$\Delta x \sim \lambda_{De}$ to avoid grid instabilities

Therefore,

Using small mass ratios to reduce computer running time

Simulating a small system limited by the computer capacity

Characteristics of a tokamak plasma

$$\omega \sim \omega^* \ll \omega_{pe}$$

$$h_{||} \ll h_{\perp}$$

Guiding Center Electron Model (electrostatic) 236

[Lee + Ohmde, JCP 26, 139 (1978)]

1. Basic Formulations

a.)
$$\underline{v}_\perp = c \frac{\underline{E} \times \underline{B}}{B^2} \quad \left. \vphantom{\underline{v}_\perp} \right\} \text{electron}$$

$$\frac{dV_y}{dt} = -\frac{e}{m_e} E_{||}$$

$$\frac{d\underline{v}}{dt} = \frac{e}{m_i} \left(\underline{E} + \frac{\underline{v} \times \underline{B}}{c} \right) \quad \text{— ion}$$

$$\frac{d\underline{x}}{dt} = \underline{v}$$

b.) Poisson Eqn

$$\nabla^2 \varphi = \underbrace{4\pi \sum_a \rho_a \sum_j S(\underline{x} - \underline{x}_j)}_{-4\pi e (n_i - n_e)}$$

$$\underline{E} = -\nabla \varphi$$

2. Dispersion relation (fluid)

$$1 - \frac{\omega_{pi}^2}{\omega_i^2 - \omega^2} \frac{k_\perp^2}{k^2} - \frac{\omega_{pe}^2}{\omega^2} \frac{k_\perp^2}{k^2} = 0$$

for $k_{||} \rightarrow 0$, $\omega = \omega_{UH} \equiv (\omega_{pi}^2 + \omega_{ci}^2)^{1/2} = \omega_{pi}$ — highest freq.

$\Rightarrow \Delta t \sim \omega_{pi}^{-1}$ with realistic mass ratios

Adiabatic Electron Model (electrostatic) 237

[Ohmde, Dawson, Lin and Lin, Phys. Fluids 21, 476 (1978)]
 [Lee, Tang and Ohmde, PRL 1599 (1979)]

$$\frac{\Delta n_e}{n_e} \approx \frac{e\varphi}{T_e} \quad \text{when } v_{te} \gg \frac{\omega}{k_{||}} \sim v_{ti}$$

1. Basic Formulations

- Push ions exactly
- Ignore electron dynamics
- Poisson eqn

$$\nabla^2 \varphi - k_{oe}^2 \frac{n_e(x)}{\langle n \rangle} \varphi = -4\pi e [n_i(x, y) - n_e(x)]$$

where

$$n_e(x) = \langle n_i(x, y) \rangle_y \quad \text{high electron mobility model}$$

$$n_e(x) = n_e(x, t=0) \quad \text{low electron mobility model}$$

2. Dispersion relation (fluid ion)

$$1 - \frac{\omega_{pi}^2}{\omega^2} \frac{k_{||}^2}{k^2} + \frac{\omega_{pi}^2}{\omega_i^2 - \omega^2} \frac{k_\perp^2}{k^2} + \frac{k_{oe}^2}{k^2} = 0$$

$$k_{||} \rightarrow 0, \quad \omega = (\omega_{ci}^2 + k^2 c_s^2)^{1/2} \quad \text{— highest frequency}$$

$$\omega \ll \omega_{ci}, \quad \omega = k_{||} c_s$$

$$\Rightarrow \Delta t \sim \omega_{ci}^{-1} \quad \text{and} \quad \Delta x \gtrsim \lambda_{oe} \quad \text{also} \quad \frac{\sum \frac{L^2 E_k^2}{k} \frac{1}{8\pi}}{nT} \ll \frac{1}{n\lambda_{oe}^2}$$

Guiding Center Electron Model (Darwin)

[Lee, Okuda & Nevins, Proc. of 8th numerical simulation conference, 1978, paper PD-7]

1. Basic assumptions

$$\Delta B_z \approx 0$$

$$k_{\parallel} \ll k_{\perp}$$

2. Formulations

- Guiding center electrons
- Exact dynamics for ions
- Field Eqs

$$\nabla^2 \psi = -4\pi \sum_{\alpha} q_{\alpha} \sum_j S(\underline{x} - \underline{x}_j)$$

$$\nabla^2 A_z = -\frac{4\pi}{c} \sum_{\alpha} q_{\alpha} \sum_j V_{zj}^{\alpha} S(\underline{x} - \underline{x}_j)$$

$$\nabla^2 E_z^{\perp} = \frac{1}{c^2 n_0} [\omega_{pe}^2 n_e(\underline{x}) + \omega_{pi}^2 n_i(\underline{x})] [E_{\parallel}^{\perp}(\omega) + E_z^{\perp}(\omega)] \\ - \frac{4\pi}{c^2} \sum_{\alpha} q_{\alpha} \nabla \cdot \sum_j V_{zj}^{\alpha} \underline{v}_j^{\alpha} S(\underline{x} - \underline{x}_j)$$

$$\underline{E}^{\perp} = -\nabla \psi$$

$$\underline{B} = \nabla \times \underline{A}_z$$

3. Dispersion relation (Fluid)

$$\epsilon = 1 - \frac{\omega_{pi}^2}{\omega^2 - \omega_{ci}^2} \frac{k_{\perp}^2}{k^2} - \frac{1}{1 - \frac{k_{\parallel}^2 v_{te}^2}{\omega^2} - \frac{\omega_{pe}^2}{k^2 c^2}} \frac{\omega_{pe}^2}{\omega^2} \frac{k_{\parallel}^2}{k^2} = 0$$

for $\omega \gg \omega_{ci}$

$$\omega = \omega_{UH} \equiv \left[\omega_{pi}^2 + \frac{\omega_{pe}^2}{1 + \frac{\omega_{pe}^2}{k^2 c^2}} \frac{k_{\parallel}^2}{k^2} \right]^{1/2} \quad \text{-- highest frequency}$$

for $\omega \ll \omega_{ci}$

$$\omega = \omega_A \equiv k_{\parallel} V_A \left[\frac{1 + k^2 \rho_s^2}{1 + \frac{c^2 k^2}{\omega_{pe}^2}} \right]^{1/2} \quad \text{-- Alfvén wave}$$

$\Rightarrow \delta t \sim \omega_{pi}^{-1}$ and with realistic mass ratios

$$\beta \sim m_e/m_i$$

Electron Drift Waves in a sheared slab 240

[Lee, Nevins, Ohuda + White, PRL 43, 347 (1979)]

1. Convectively unstable drift waves have been observed in the simulation
2. Marginally stable eigenmodes predicted by the theory have not been detected
3. More theoretical understanding is needed

Ion Temperature Drift Instabilities in a sheared slab

[Lee, Tang and Ohuda, PPL-1599 (1979)]

1. Confirm the existence of the η_z -driven eigenmodes
2. Large ion energy transport has been observed
3. Nonlinear saturation is caused by the quasilinear diffusion of the ion temperature profile
4. Enhanced fluctuations associated with the marginally stable eigenmodes have been observed. They are probably caused by the re-distribution of the field energy. More theoretical work is in need.

Shear Alfvén Eigenmodes in a sheared slab

[Lee, Chencu etc. in progress]

1. Confirm the existence of shear Alfvén eigenmodes of the tearing type (odd ℓ + even A_{11})
2. Enhanced fluctuations associated with the weakly damped eigenmodes have been observed. They are probably caused by the re-distribution of the field energy. Need theoretical work
3. Shear Alfvén eigenmodes induce a 2nd order y -independent eddy current. A surprising result. Nonetheless, this observation has been verified by the quasilinear theory.
4. The induced current widens the shear free region near the rational surface and causes the formation of magnetic islands
5. As a result, large electron energy transport has been observed. This mechanism may be very important in understanding anomalous transport in tokamaks.

Tony Sgro

Tony Sgro

251

20. Implosive formation of a Pinched Plasma.

if $\frac{\tau_{ii}}{\tau_{implosim}} \geq 1$, a kinetic description of the ions is required.

ie, if $E_i \sim 100 \text{ kV}$, $n \sim 10^{15} \text{ cm}^{-3}$, $\tau_{ii} \sim 2 \mu\text{s}$, $\tau_{implosim} \sim 1 \mu\text{s}$.

Electrons: inertialless, charge neutralizing fluid [ie Quasineutrality] to eliminate short length and timescales of λ_D , ω_{pe} .

⇒ Simulations of macroscopic phenomena are possible.

Electron Microdynamics influences macroscopic plasma evolution through "anomalous" transport coefficients.

252

1D Hybrid Model "AURORA"

1 space component r , 3 velocity comp. w_1, w_2, w_3

$$m_i \frac{dw_i}{dt} = e(E + w \times H/c) - P + \text{anomalous ion heating} + S'$$

E and H : macroscopic fields

P : (anomalous) momentum transferred to e^- from i^+ in 1st approximation assumed independent of w_i .

Anomalous heating term (due to microturbulent fields) has some magnitude for all particles, but has random direction.

S' = source and sinks due to ionization and charge exchange with neutrals

$$n_i = \int f d^3w \quad (= n_e)$$

$$V_{ir} = \int w_r f d^3w \quad (= V_{er})$$

Electrons: inertialess fluid (1.0)

$$m_e n_e \frac{dv_z}{dt} = -en(E + v_z \times H/c) - \nabla_{\parallel} p_e + nP$$

$\hat{e}_z \cdot \nabla$ determine field diffusion (anisotropic σ)

$$\begin{pmatrix} \sigma_{\parallel} & \sigma_x & \sigma_z \\ \sigma_x & \sigma_{\perp} & 0 \\ \sigma_z & 0 & \sigma_{\perp} \end{pmatrix} \begin{pmatrix} E_0 - v_r H_z/c \\ E_z + v_r H_{\theta}/c \\ J_{\theta} \\ J_z \end{pmatrix} = \begin{pmatrix} J_{\parallel} \\ J_{\perp} \\ J_{\theta} \\ J_z \end{pmatrix}$$

with $E_{\theta} = -\frac{1}{c} \dot{A}_{\theta}$ $H = \text{curl } A$, solution is found

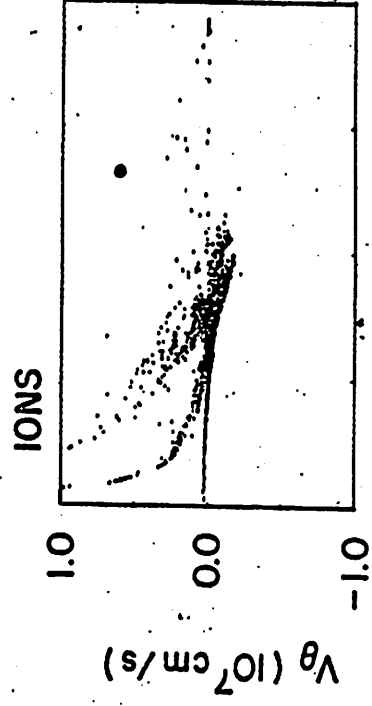
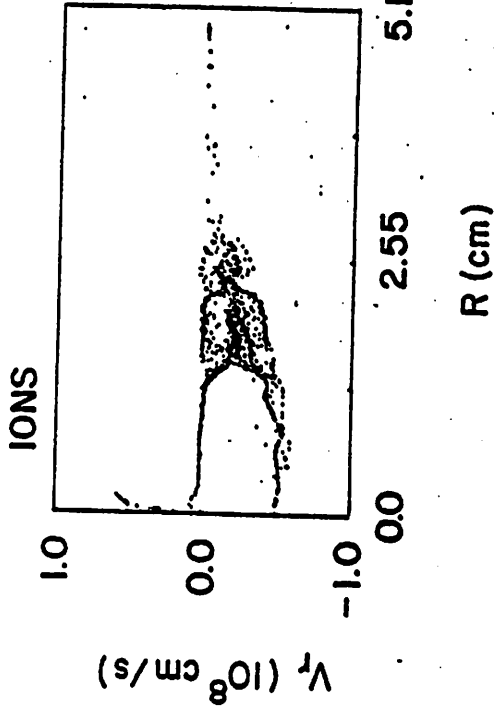
a vacuum region between pinched plasma and the wall may be represented by setting $\bar{\sigma} = 0$

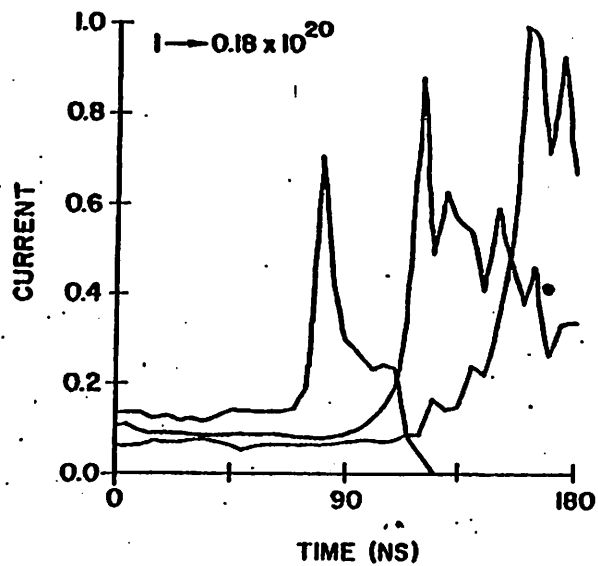
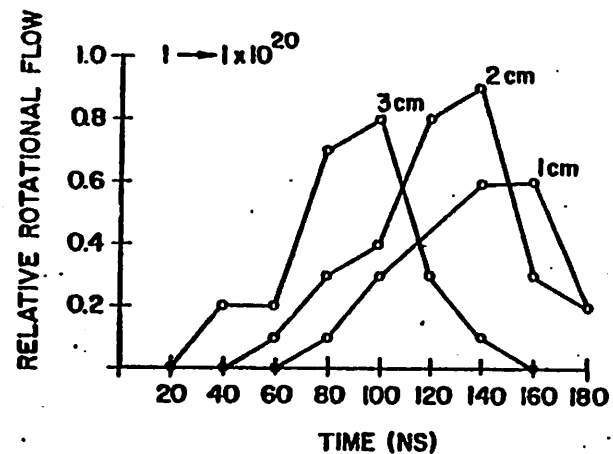
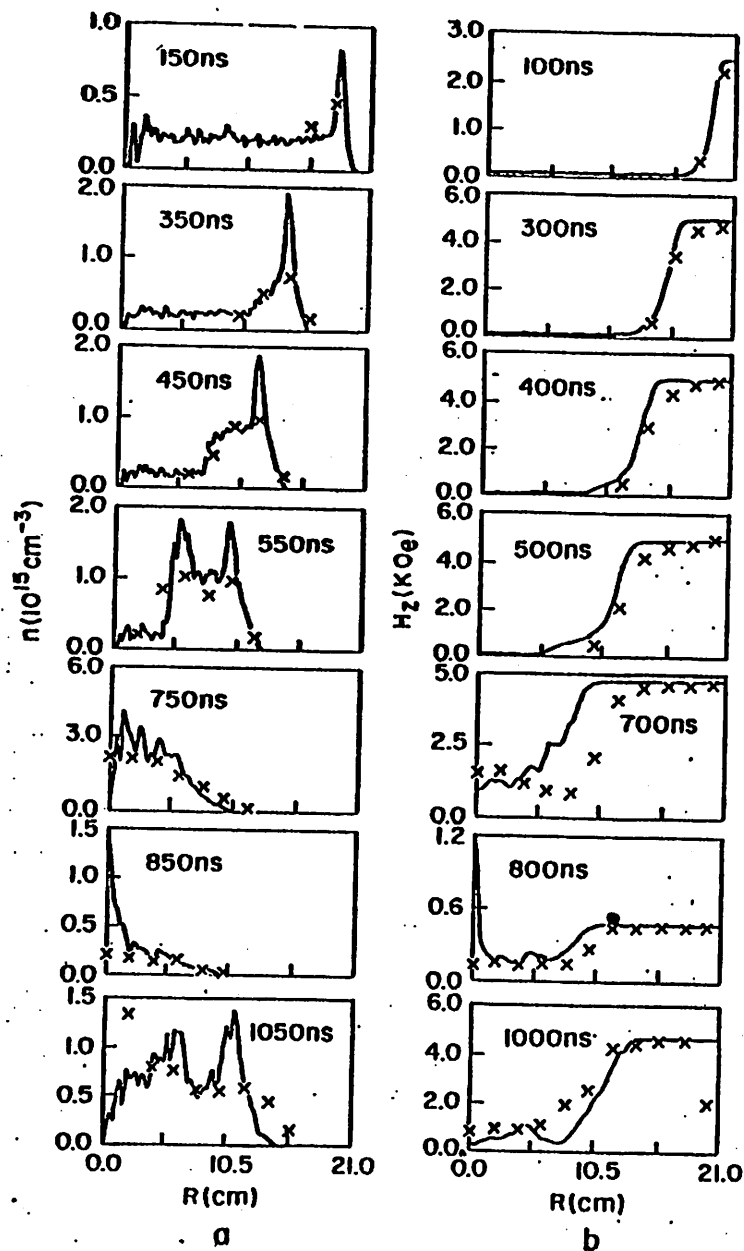
Then a single solution on the interval $0 \leq r \leq r_{\text{wall}}$ is found.

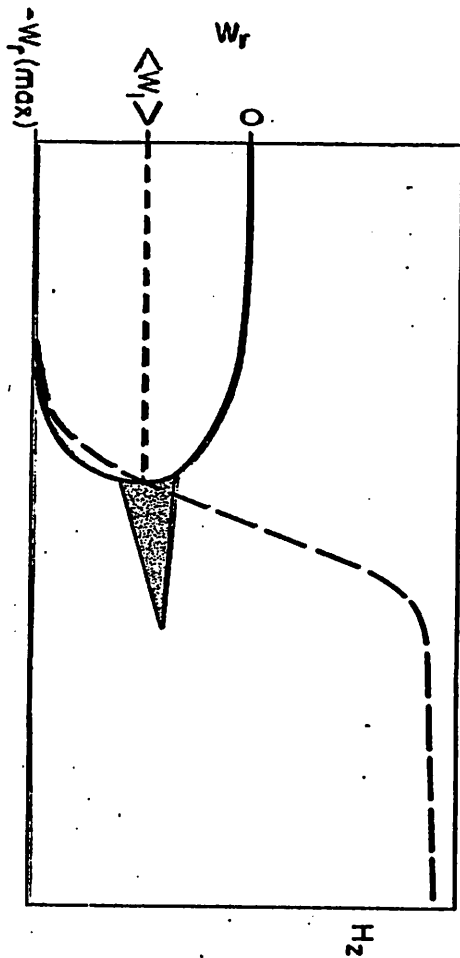
\hat{r} determines E_r

Energy eqn determines p_e includes:
 Joule heating
 ionization losses
 impurity losses
 Thermal cond. (α field)
 Equilibration

Transport Coef: Quasilinear or Quasiempirical







Since $f_i(w)$ is known,
neutron emission rate may be calculated

$$R = \frac{1}{2} \int dw_1 \int dw_2 \sigma(|w_1 - w_2|) |w_1 - w_2| f(w_1) f(w_2)$$

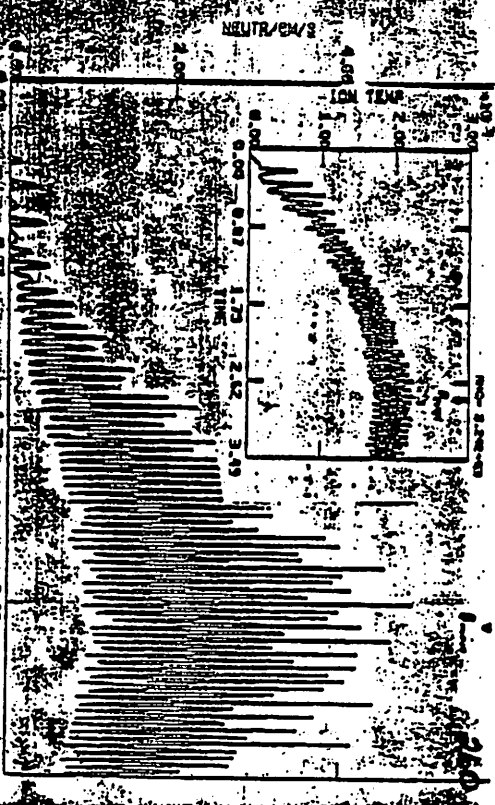
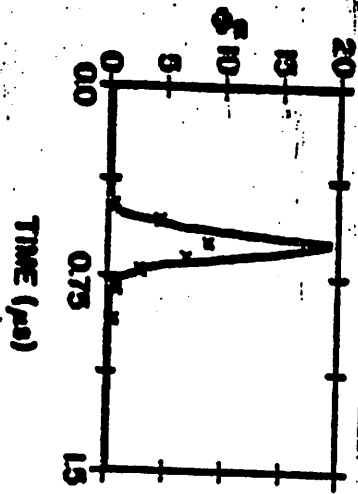
Can reflect non Maxwellian nature
of ions.

IHX

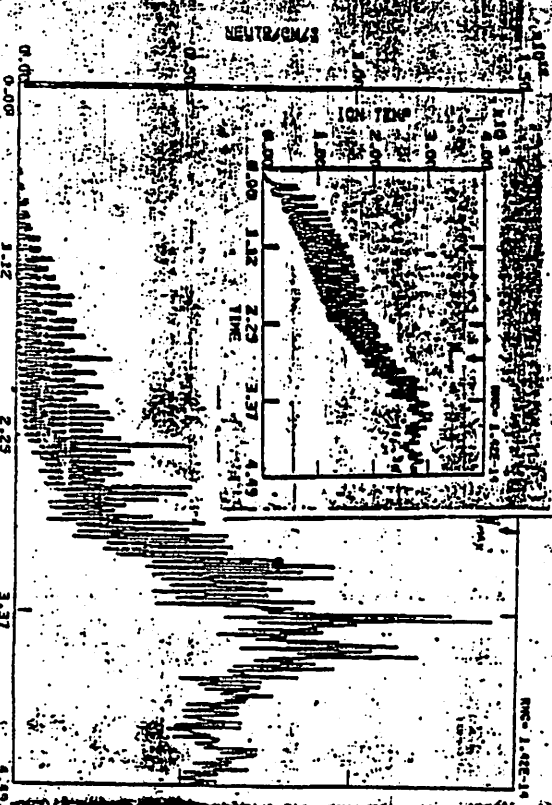
259

Calculated emission rate within a factor of 2 of experimental value.

$T_1 \sim$ few hundred eV. Neutron production calculated very sensitive to energy at these energies. If in this region were instantaneously magnified for the purpose of calculating neutron emission, the resulting fictional high energy ions would cause the emission rate to be 10 times higher.

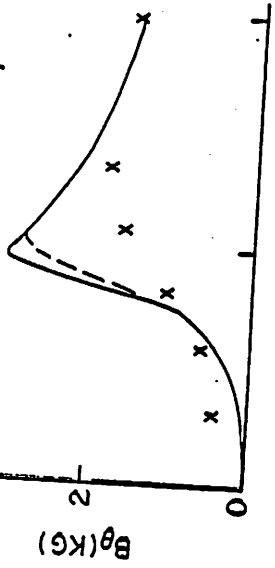


T = 4.500E-06 SECS

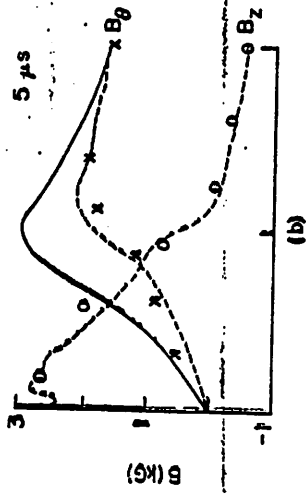


T = 4.500E-06 SEC

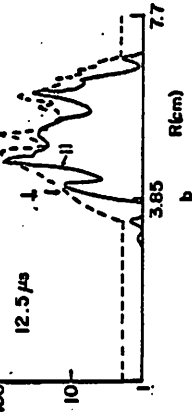
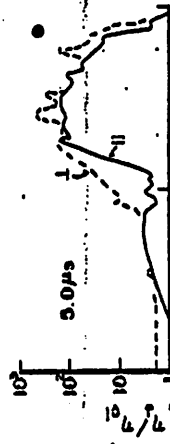
4 μ s



5 μ s



(b)



Conclusion

Hybrid model represents physics well in a regime of relevance to experiment which is not well described by MHD

Other Current and future Applications

- 1D - Implosive C.T. formation to a few implosion times (Simulation represents behavior at midplane in θ)
- 2D - C.T. formation to the equilibrium state.
- 1D and/or 2D: RSTP chip

21 A Global Electron-Field
Algorithm for an
Axisymmetric Hybrid
Simulation Code

D. W. Hewett, LASL

Assumptions

Quasi-Neutral

$$\nabla \cdot \vec{J} = 0$$

Darwin (nonradiative) Transverse Fields

$$\nabla \times E_{\perp} = \frac{1}{c} \dot{B}$$

$$\nabla \times B = \frac{4\pi}{c} J_{\perp}$$

neglects $\frac{\partial E_{\perp}}{\partial t}$

Inertia-less Electron Thermal Fluid

$$E_{\perp} = -\frac{\nabla P_e}{eN} - E_L - \frac{u_e \times B}{c} + \eta \cdot J$$

Two-Dimensional (R-Z) Eulerian
Grid

Model

In Coulomb Gauge

$$\dot{A}_\theta = -cE_{+\theta}$$

$$\dot{B}_\theta = -c [\nabla \times E_+]_\theta$$

and since $E_{L\theta} \equiv 0$, we have

$$\begin{aligned} \ddot{A}_\theta - \frac{c^2}{4\pi} \eta_{\theta\theta} \nabla^2 A|_\theta + u_{er} \frac{(rA_\theta)'}{r} + u_{ez} \frac{\partial A_\theta}{\partial z} \\ = \frac{c^2}{4\pi} \left[\eta_{\theta r} \frac{\partial B_\theta}{\partial z} - \eta_{\theta z} \frac{(rB_\theta)'}{r} \right] \end{aligned}$$

and

$$\begin{aligned} \dot{B}_\theta - \frac{c^2}{4\pi} \left[\frac{\partial}{\partial r} \eta_{zz} \frac{\partial (rB_\theta)}{\partial r} + \frac{\partial}{\partial z} \eta_{rr} \frac{\partial B_\theta}{\partial z} \right] \\ + \frac{\partial}{\partial r} (u_{er} B_\theta) + \frac{\partial}{\partial z} (u_{ez} B_\theta) \\ + c \left[\frac{\partial}{\partial z} (\eta_{r\theta} J_\theta + \eta_{rz} \frac{c}{4\pi} \frac{(rB_\theta)'}{r}) \right. \\ \left. + \frac{\partial}{\partial r} (\eta_{zr} \frac{c}{4\pi} \frac{\partial B_\theta}{\partial z} - \eta_{z\theta} J_\theta) \right] \\ = -\frac{c}{eN} \left[\frac{\partial N}{\partial z} \frac{\partial T_e}{\partial r} - \frac{\partial N}{\partial r} \frac{\partial T_e}{\partial z} \right] \\ + B_r r \left(\frac{u_{e\theta}}{r} \right)' + B_z \frac{\partial u_{e\theta}}{\partial z} \end{aligned}$$

with

$$B_r = -\frac{\partial A_\theta}{\partial z} \quad B_z = \frac{(rA_\theta)'}{r}$$

$$J_r = -\frac{c}{4\pi} \frac{\partial B_\theta}{\partial z} \quad J_z = \frac{c}{4\pi} \frac{(rB_\theta)'}{r}$$

$$J_\theta = -\frac{c}{4\pi} \nabla^2 A|_\theta$$

$$J = eN (u_i - u_e)$$

Electron Temperature Equation

Any method with the functional form

$$T_e = f(\rho, T_e, \vec{u}_e, \vec{B}, \vec{\eta})$$

is consistent with the preceding equations.

Considering the large time steps used, the algorithm for T_e must correctly describe $T_e = \text{constant}$ along \vec{B} .

not-yet included self-consistently

Solution Method

"Global ADI" for Electron/Field Eqs.

PIC for Ion

With a minimum density cutoff, the method will handle arbitrary plasma-vacuum intermixing without monitoring plasma-vacuum interface positions.

Vacuum Equations

$$\nabla^2 \vec{A}|_0 = 0$$

$$\left[\frac{(rB_\theta)'}{r} \right]' + \frac{\partial^2 B_\theta}{\partial z^2} = 0$$

Large η limit of preceding equations!

Advantages of this method.

Eases low density problems

- 1) without adding cold background
(which impedes proper vacuum signal propagation.)
- 2) with defining separate plasma and vacuum regions (which requires monitoring of plasma-vacuum interface location.)
- 3) with signal speed disparity between adjacent plasma-vacuum cells.

Method handles arbitrary plasma-vacuum intermixing with the application of BC's only on the outside of the simulation box.

Applications + Tests

One-Dimensional Implosions

- a) θ -pinch
(tests A_0 solution)
- b) z -pinch
(tests B_0 solution)

Anisotropic Plasma Instabilities (with A. G. Sgro + T. E. Cayton)

- a) Ion Cyclotron Instability
 - Ion trapping saturation
- b) Mirror Instability
 - Oblique propagation
 - correct linear growth rate

Bumpy θ -pinch Implosion

Fig 1a

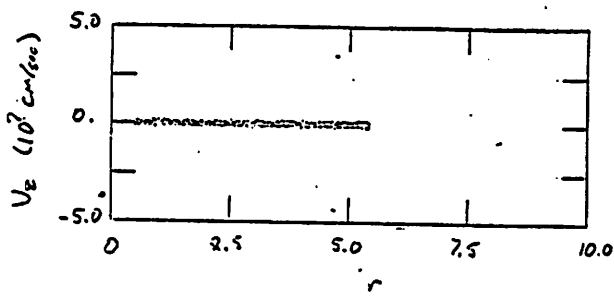
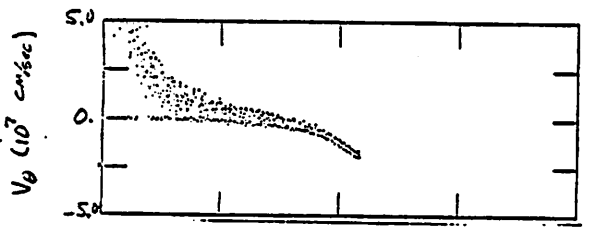
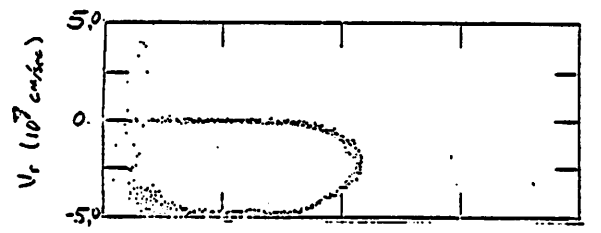
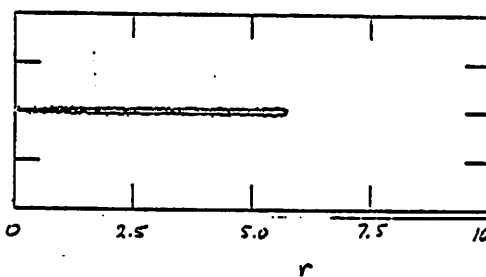
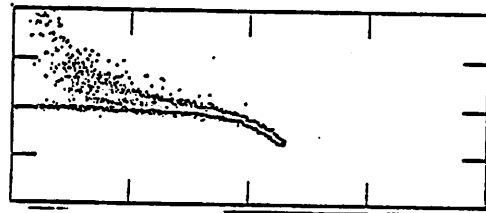
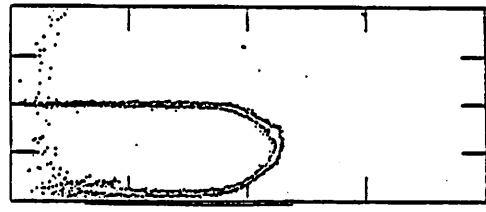


Fig 1b



271

Fig 2a

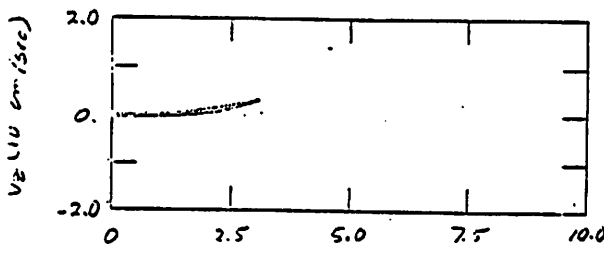
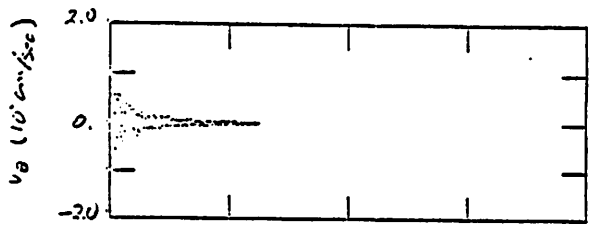
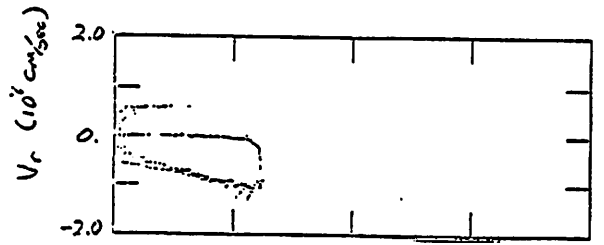
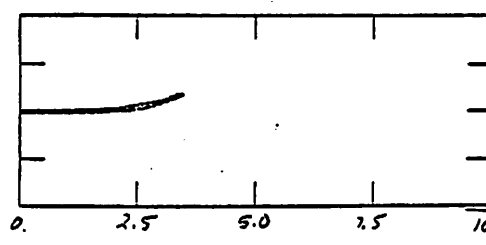
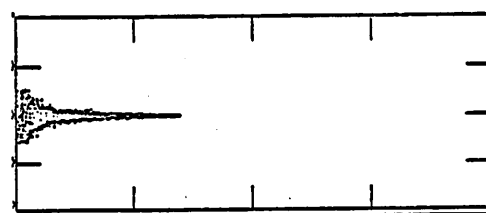
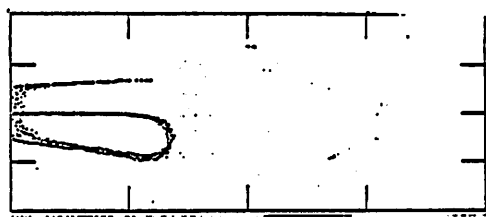


Fig 2b



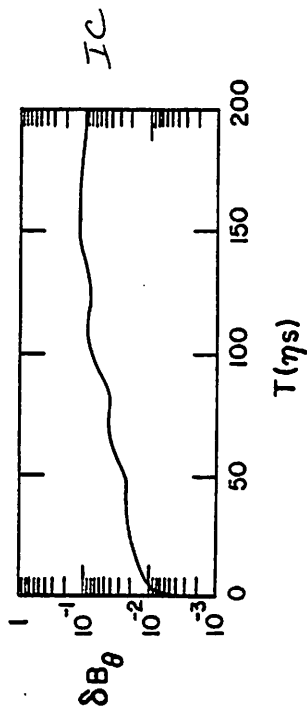
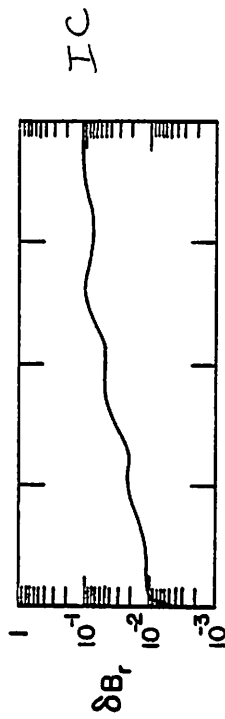
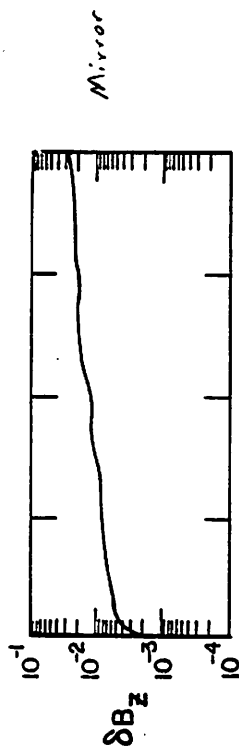
272

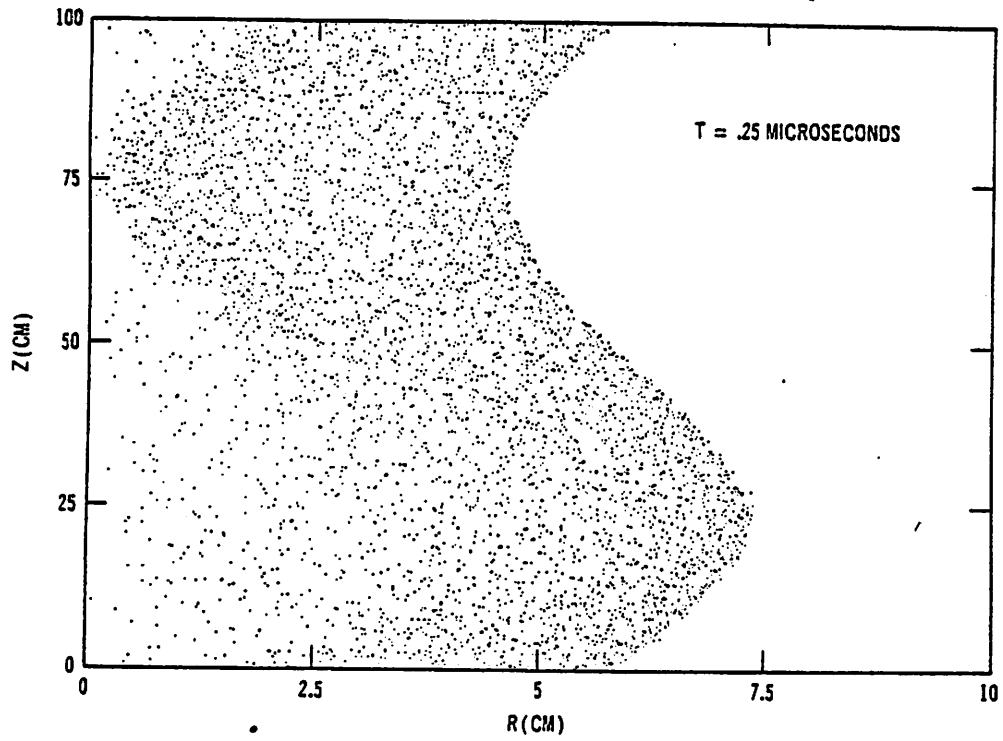
Bumpy θ -pinch Implosion

Implosion caused by

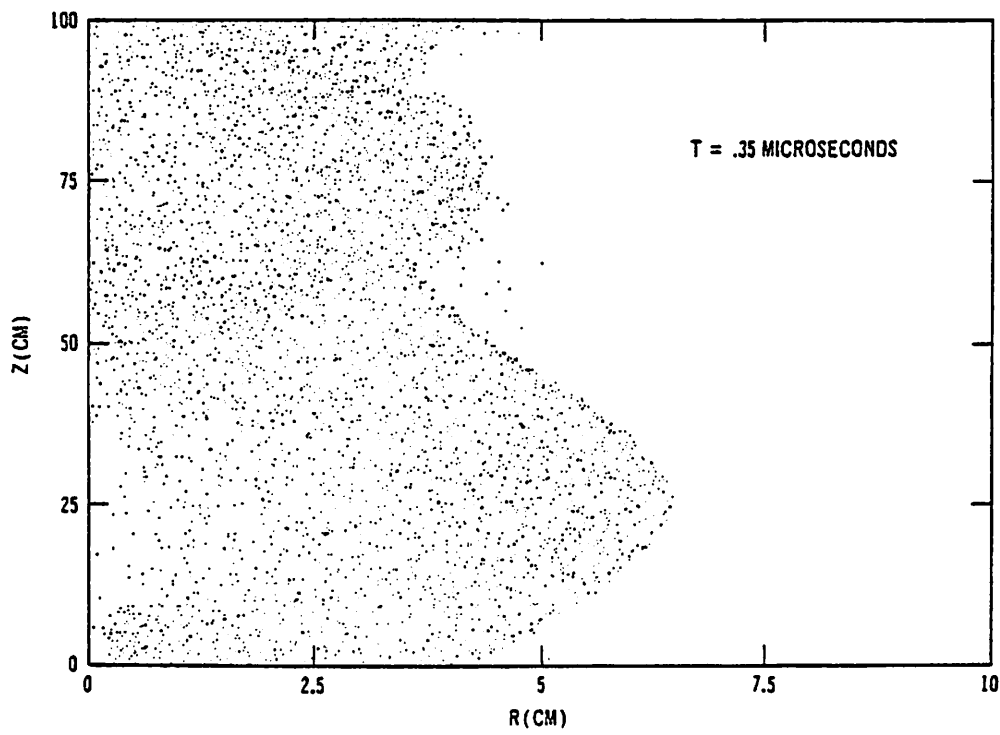
$$B_z(r=r_w, t) = 5 \left(1 + 5 \sin \frac{2\pi r}{L_z} \right) \text{ KG}$$

- strong 2-D effects
- arbitrary plasma-vacuum interface mixing





275



276

FRX Formation Study

FRX \equiv Field Reversed \ominus -pinch

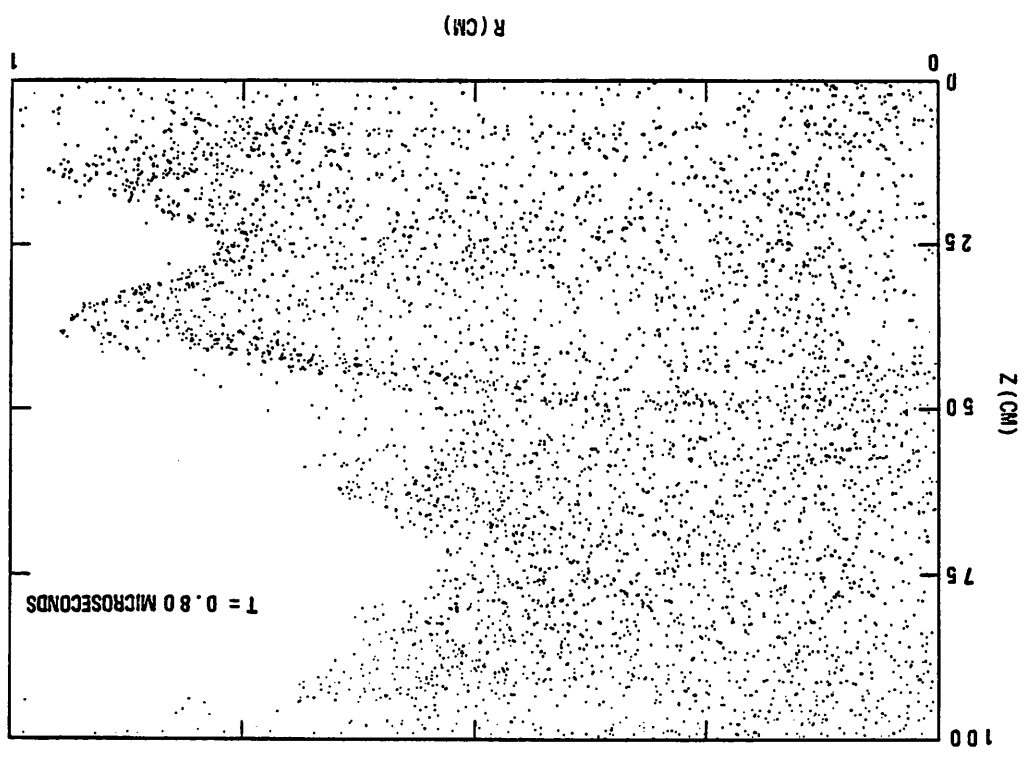
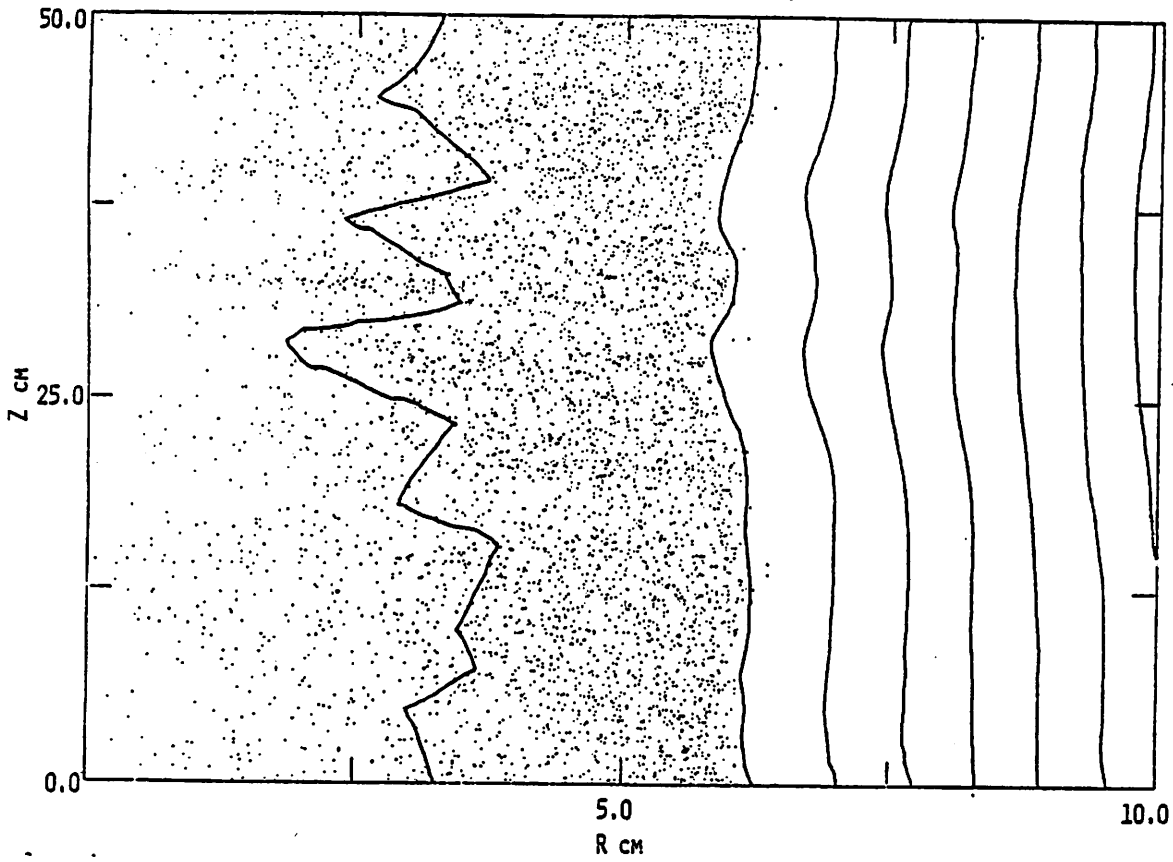


FIGURE 1

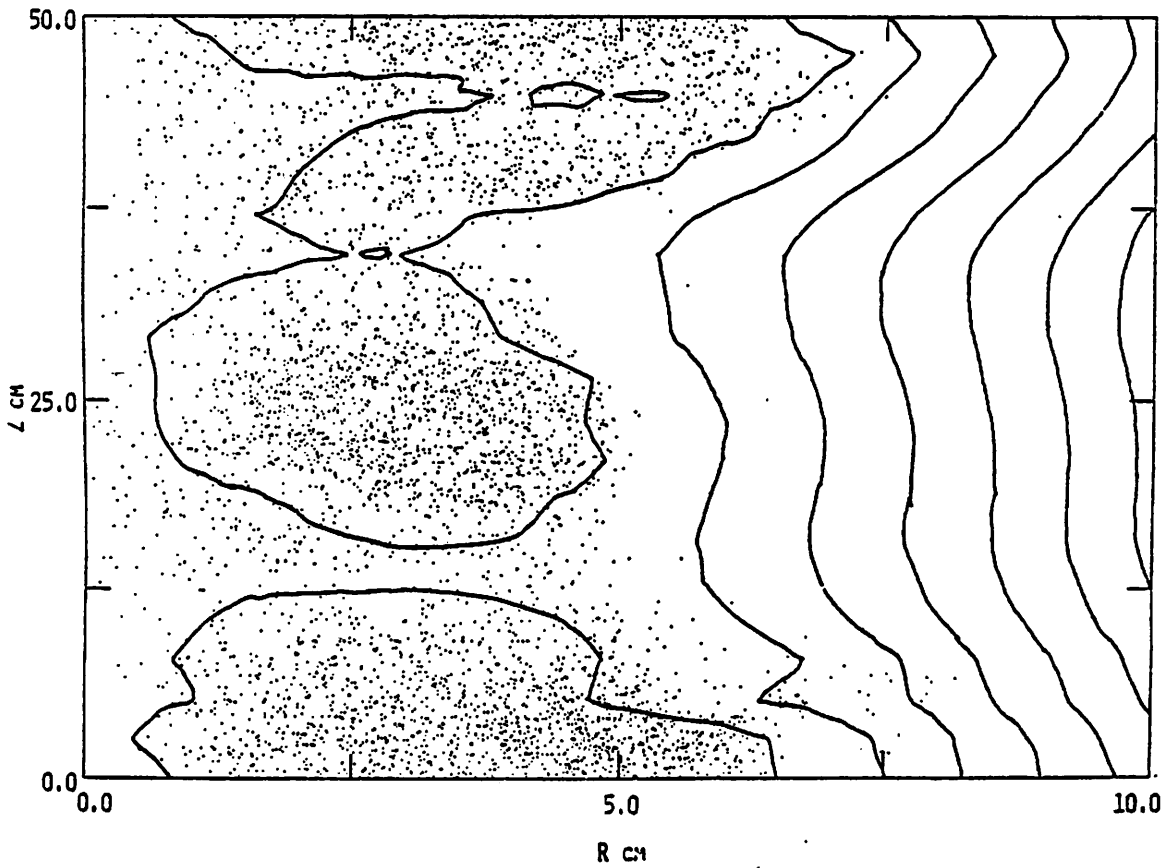
ION POSITIONS AND Ψ CONTOURS $T = 1.5 \mu s$



279

FIGURE 2

ION POSITIONS AND Ψ CONTOURS $T = 3 \mu s$

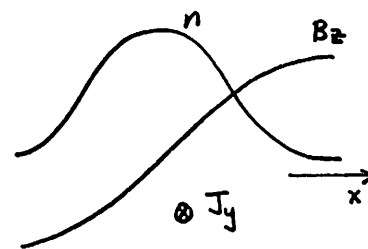


280

22 Dan Winste
U. of Maryland

Particle Simulations of
Reversed field configurations

Simplest configuration:
neutral sheet

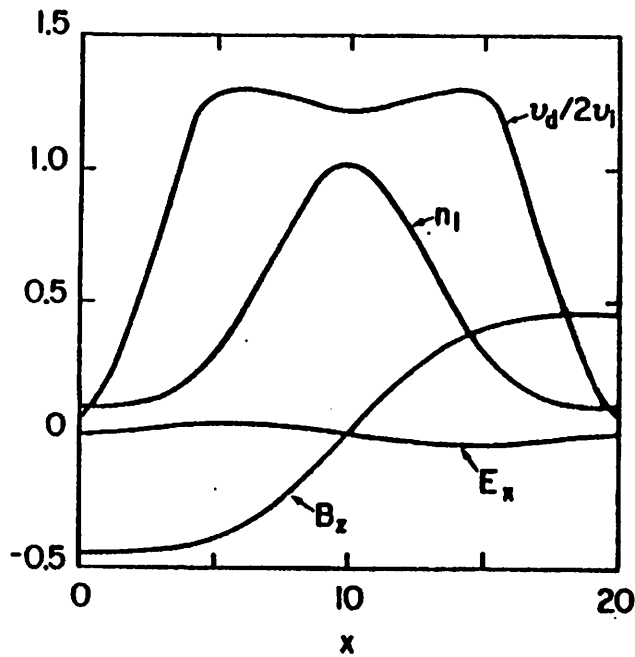


Interested in x-y plane
(\leftrightarrow current driven microinstabilities)
(x-z plane \leftrightarrow tearing modes)

- (a) "DARWIN" (C. Nielson)
2-D Darwin model particle code
- (b) Vlasov equilibrium (D. Hewett)
self consistent, high β , steep gradients

Over last several years has been used to study
micro-stability of (O-pinch) sheaths

1. Lower Hybrid Drift Instability
2. Other effects: Shear, loss-cone



Regime of interest ($T_i > T_e$ $v_d \leq v_i$) \Rightarrow

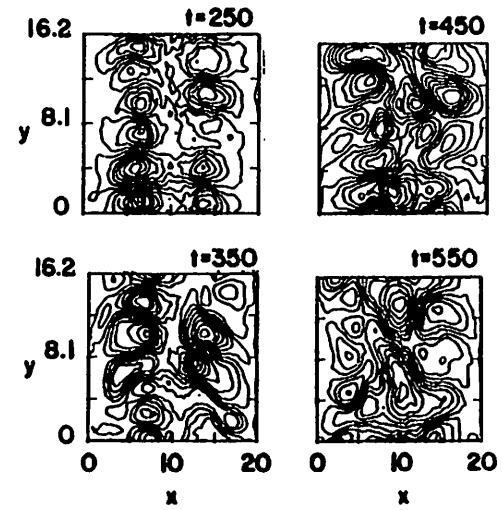
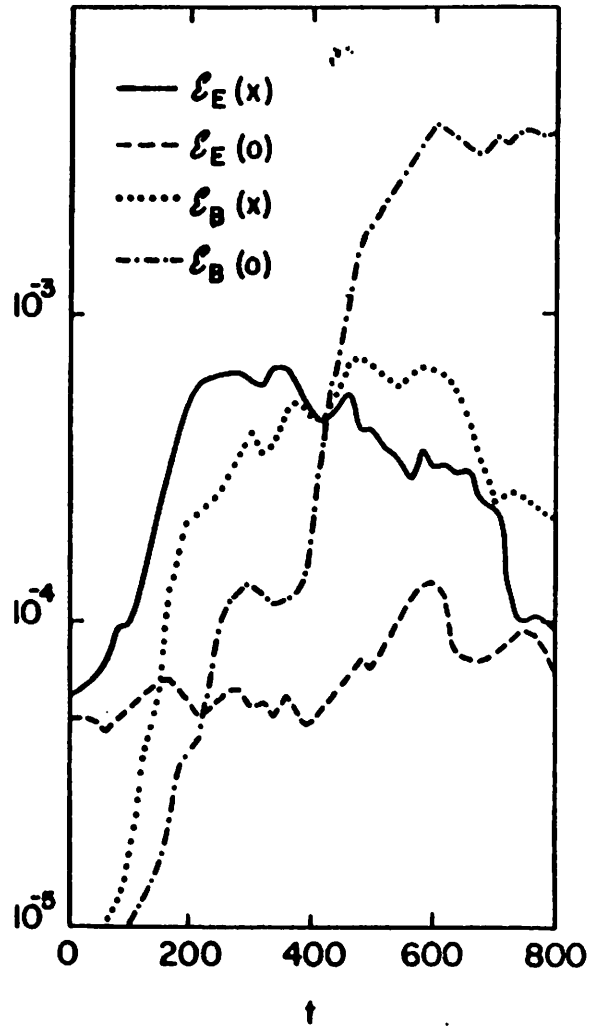
Lower Hybrid Drift Instability

Nonlocal calculations (Huba, Drake, Gladd)

1. finite β damps out mode at reversal point
2. penetrates in to $x_p \sim \lambda (T_e/2T_i)^{1/2}$ ($B_z = B_0 \tanh x/\lambda$)
3. does not treat region near $x=0$

Simulation

1. nonlocal (2b)
2. treats particle orbits exactly
3. nonlinear



Conclusions

1. LHDI grows up on outside (as expected)
2. mode penetrates in & grows to large amplitude at reversal point (surprise)
(mode is unstable because particles crossing the r.p. have no VB drift)
3. $\eta^{r.p.} \sim .1 \eta^{outside}$
4. questions
 - a. What happens in a more realistic case
 - b. Competition with tearing mode



MONTE CARLO (HYBRID) MODELLING
OF ELECTRON TRANSPORT

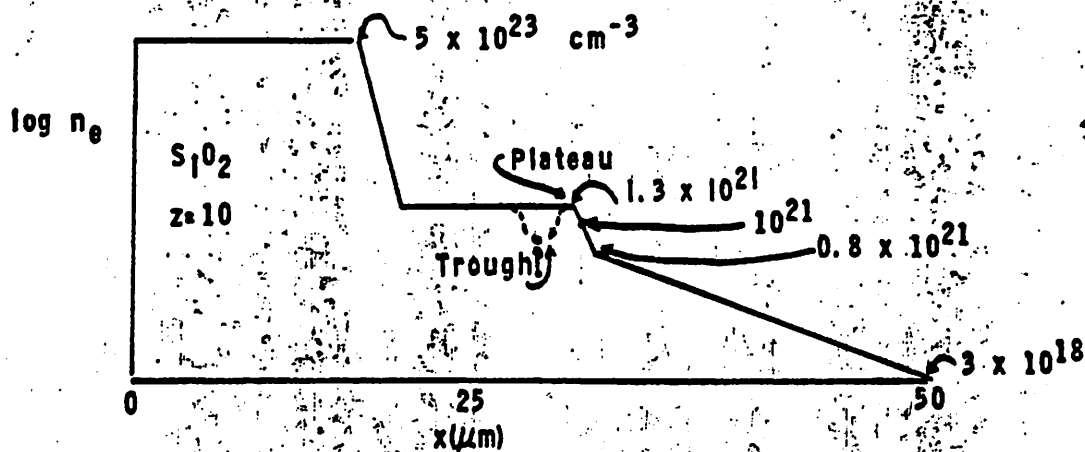
by

Rodney J Mason
Los Alamos Scientific Laboratory
Los Alamos, N.M. 87545

23

HOT e^- TRANSPORT HAS BEEN EXAMINED FOR
STATIC GEOMETRIES, AS BELOW

LASER FUSION



ANOMALOUS TRANSPORT INHIBITION CALLS FOR A
COMPREHENSIVE THEORETICAL TREATMENT

LASER FUSION

- Excessive energy loss to fast ions ($\rightarrow 50\%$)
- Late collapse times for μ -balloons
- Reduced line emissions from depths of layered targets

A M.C. - HYBRID TRANSPORT SCHEME IS UNDER DEVELOPMENT
TO PROVIDE THE REQUIRED FUNDAMENTAL VIEW




- Hot e^- - M.C. particles (w/area weighting)
- Cold e^- - fluid (or particles)
- E field - poisson eqn
(with ω_p^{-1} dilated to $O(\Delta t)$)
 Δt set by courant condition on hots
- Geometry - 1-d { 2-d extention straightforward
 $\frac{\partial B}{\partial t} = -c \text{ curl } E$

290

THE HOT ELECTRONS EXPERIENCE SCATTERING, COULOMB DRAG
AND SELF-CONSISTENT FIELDS



- Scatter -  (uniform dist azimuthal angles)
(gaussian envelope)
 $\langle e \rangle^2 = 8\pi e^4 m^{-2} c^{-3} Z(Z+1) n_i \Delta t \log \Lambda$
- Coulomb drag - $\frac{dc}{dt} = -4\pi e^4 m^{-2} n_c C^{-2} \log \Lambda$
 $c^2 = u^2 + v_t^2$
- E Field - $\frac{du}{dt} = -\frac{eE}{m}$, $\frac{dx}{dt} = u$

Subcycling with Large E
s.t. $\Delta u/u = 0.1$

291

THE SUPRATHERMAL SOURCE CAN HAVE TWO FORMS



- Resonant Absorption Fraction

$$\text{Drifting Maxwellian } g(u) ; g(u) = \frac{1}{\sqrt{2\pi}a} e^{-u^2/2a^2}$$

with arbitrary T_x/T_t (usually emission in a 20° cone towards the Laser)

- Inverse Bremsstrahlung fraction

Simple Maxwellian $g(u)$

$$T_x/T_t = 1$$

- Generally $T_H \sim a (\lambda^2)^{1/3} T_c^{1/3}$; the particles are weighted to allow this.

- The Thermal density is decreased for each suprathermal created.

292

THE COLD ELECTRONS ARE TRANSPORTED BY DONOR-CELL COLLISIONAL HYDRODYNAMICS



- Continuity

$$\frac{\partial n}{\partial t} = - \frac{\partial(nu)}{\partial x} + \dot{n}_D - \dot{n}_L$$

(convection) (Drag) (Laser) source

- Momentum

$$\frac{\partial(nu)}{\partial t} = - \frac{\partial}{\partial x} (n [T + u^2]) - \frac{enE}{m} - a(z) \nu n u$$

(convection) (resistivity)

$$+ \frac{3}{5} B(z) \nu q/T - \dot{n}_L u$$

(thermal force) (Laser source)

293

COLD TRANSPORT (cont'd)



- Energy -

$$3/2 \frac{\partial}{\partial t} (n T) = - \frac{\text{(convection)}}{3/2 \frac{\partial}{\partial x} (n u T)} - \frac{\text{(PdV work)}}{n T \frac{\partial u}{\partial x}} - \frac{\text{(heat flow)}}{\frac{\partial q}{\partial x}} + \frac{\text{(joule heating)}}{\alpha(z) \frac{1}{2} m n u^2}$$

$$= - \frac{3/5 \beta(z) \nu \mu u q / T}{\text{(thermal force heating)}} + \frac{3/2 \dot{n}_D \bar{T}_D}{\text{(drag)}} - \frac{3/2 \dot{n}_L T}{\text{(laser source)}}$$

- Limited heat flux - (diffusion) (thermo-electric)

$$q = - \frac{K}{\gamma(z)} \frac{\partial T}{\partial x} + \frac{3/2 \beta(z)}{\gamma(z)} n u T$$

$$\left[1 + \frac{|F_D|}{F_L} \right]$$

$$K \equiv \frac{5 n T}{2 m}$$

$$F_D \equiv - \frac{K}{\gamma(z)} \frac{\partial T}{\partial x}$$

$$F_L \equiv 0.6 n T^{3/2}$$

(classical limit)

α, β, γ are extended Braginskii coefficients - C. Cranfill.

294

DONOR CELL HYDRODYNAMICS WORKS IN TWO STEPS



- Update all quantities locally ignoring convection (i.e. effects of drag, sourcing, resistivity PdV work etc.)

$$n^{(m)} \rightarrow \tilde{n}, \quad u^{(m)} \rightarrow \tilde{u}, \quad T^{(m)} \rightarrow \tilde{T}$$

- Convect the tilde quantities with the flux $\tilde{n} \tilde{u}$

$$\tilde{n} \rightarrow n^{(m+1)}, \quad \tilde{u} \rightarrow u^{(m+1)}, \quad \tilde{T} \rightarrow T^{(m+1)}$$

295

$$E \leftarrow \frac{1}{\epsilon_0} \frac{\partial p_h}{\partial x} \quad (\text{CORONA})$$

$$E \leftarrow (a + 9/10 \beta^2 / \gamma) v_c n_h u_h \quad (\text{dense plasma})$$

$$\left. \begin{aligned} \omega_p^2 - \omega_p^2(m) \\ \bar{n} = n_h + n_c \\ v_{h,c} = v_{h,c} + 1/\Delta t \end{aligned} \right\} \text{Bat} = 0.2$$

$$\epsilon = \frac{\omega_p^2 \Delta t \left[\frac{v_h}{n_h} + \frac{v_c}{n_c} \right]}{(\text{Bat})^2}$$

$$\frac{\partial E}{\partial t} = 4\pi e n_h u_h + n_c u_c$$



E FIELD IS OBTAINED FROM POISSON EQN WITH ω_p^{-1} DILATED TO $\omega_p \Delta t$

with $\omega_p^2 \Delta t^2 = 0.04$
 $\Delta E = 0.2 E_{ss} / \text{cycle}$

$$\Delta E = N u_p^2 \frac{\partial^2 \Delta t^2}{\partial x^2} \cdot \frac{e n_h}{m n_h u_h^2} - N u_p^2 \Delta t^2 \frac{1}{\epsilon_0} \frac{\partial n_h}{\partial x}$$

Current condition $\Delta t = \frac{N u_h}{\Delta x}$ $N = 1.5$

$$\Delta E = \frac{4\pi e n}{m} \Delta t e n_h \cdot n_h u_h$$

$$\frac{\partial E}{\partial t} = 4\pi e n_h u_h$$

For $n_c \rightarrow 0$



THE ω_p^{-1} DILATION LIMITS $\Delta E / \text{CYCLE}$ TO A SMALL FRACTION OF THE STEADY STATE FIELD.

ALTERNATIVELY, E IS OBTAINED FROM A "MOMENT METHOD" MAKING USE OF QUASI NEUTRALITY



We use the predicted currents...

$$j_h^{(m+1)} = \frac{j_h^{(m)}}{v_h'} - \frac{1}{v_h'} \left[\frac{3P_h}{2} + en_h^{(m)} E^{(m+1)} \right] \quad (\text{same for } j_c)$$

where $v_h' = v_h + \frac{1}{\Delta t}$ and $j_h^{(m')} = j_h^{(m)} + n_h v_h$.

Add them and solve for E... ($j_h + j_c = 0$)

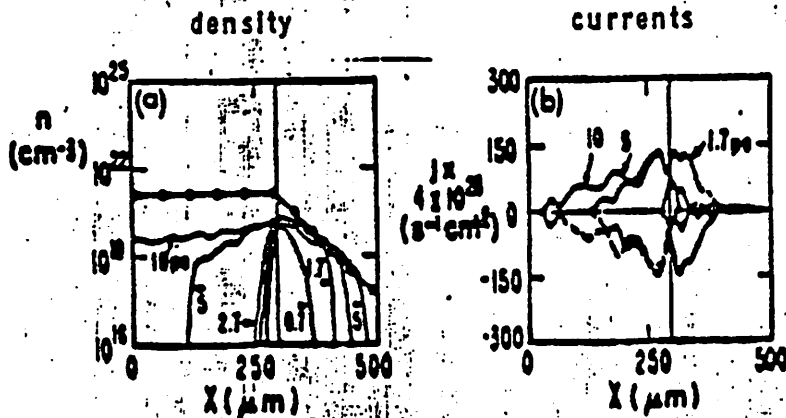
$$E^{(m+1)} = \frac{\left(\frac{j_h^{(m)'}}{v_h'} + \frac{j_c^{(m)'}}{v_c'} \right) - \frac{1}{v_h'} \frac{3P_h}{2} - \frac{1}{v_c'} \frac{3P_c}{2}}{\left(\frac{n_h}{v_h'} + \frac{n_c}{v_c'} \right)}$$

Then average with the earlier E.

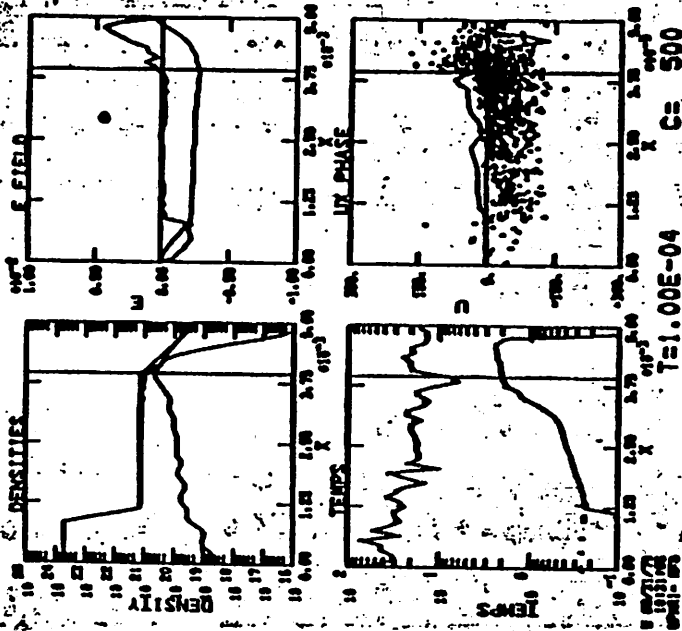
$$E^{(m+1)} = (E^{(m+1)} + (M-1)E^{(m)})/M$$

298

THE E FIELD ALGORITHM PROPERLY ESTABLISHES QUASINEUTRALITY AS INDICATED BY THE DENSITY AND CURRENT PLOTS BELOW:



299

T_c free to change

24
 Linearized Particle
 Simulation of
 Instabilities in
 Axisymmetric
 models of
 Tandem Mirrors
 + FRMs

J.A. Byers

Use $e^{im\theta}$
 Also for simplest
 applications restrict
 to a 1 dimensional grid;
 i.e., 2D prototypes for
 full 3D models

Two types of equilibria

- I. arbitrary r variation;
 uniform in z . Allows
 general θ pinch &/or
 z -pinch fields
- II. arbitrary z variation
 local-in- r

What modes can be examined?

In class I: in general have $e^{im\theta + ik_z z}$

- rotating θ pinch, both interchange and finite k_z including FLR effects
- z pinch, both interchange (k_z only-sausage mode) and kink again including FLR
- DCLC and AIC for arbitrary radial profile at high β

In class II - e^{LMS} , finite difference in z

- DCLC and its bounce orbit modifications. In particular the non-flute or localization-in-z character of this mode
- ballooning modes for axisymmetric Tandem configurations, including FLR effects

Results to date

- Quasi neutral hybrid model has been tested for nonuniform radial profiles, both for a cold plasma and for restricted versions of a hot plasma
- Electrostatic model has been successfully applied to an extreme concentric orbit equilibrium, ~~that~~ is subject to DCLC-lites modes (Agarwal et al to be pub)
- Gravity driven interchange has been modeled in the electrostatic model
- Also rotation driven interchange

Gravity-driven Interchange

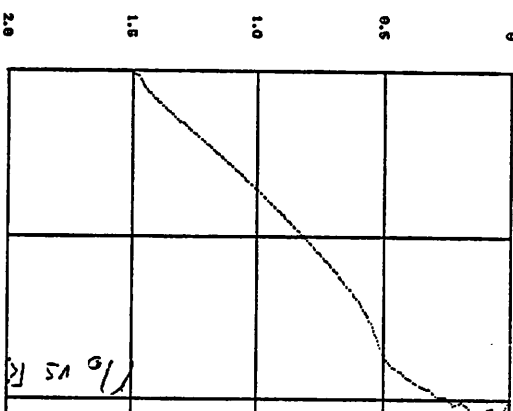
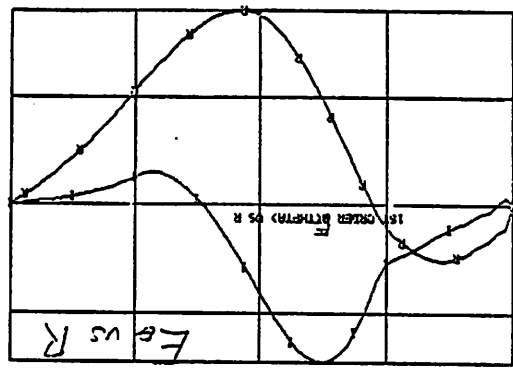
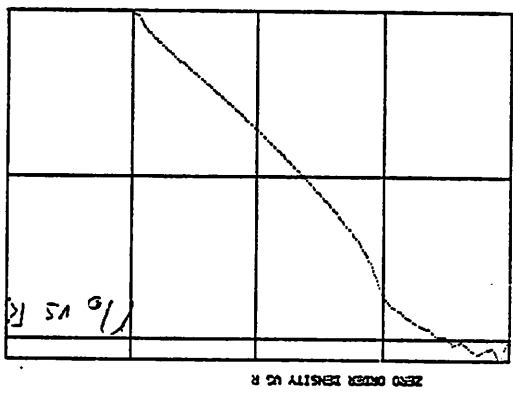
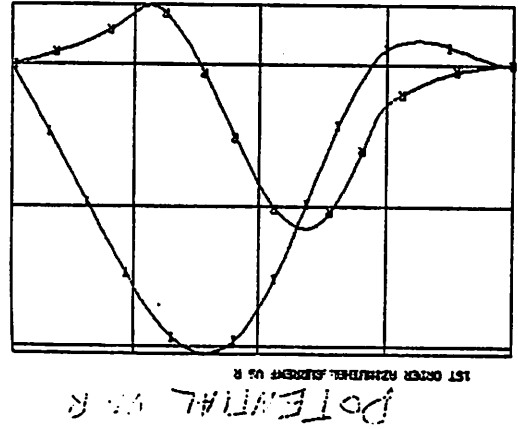
- Equilibrium: \approx Gaussian profile $\frac{\rho}{a_i} \approx 4$
- uniform B_{θ} ;
- Particle drifts in θ caused by a gravity $\vec{g} = g_0 \frac{r}{R} \hat{r}$
- Model is electrostatic using $\frac{\omega_{pi}^2}{\omega_{ci}^2} \sim 1-10$
- Typical $g \times B$ rotation frequencies are $\sim \Omega_g \approx 10^{-3} - 10^{-2} \omega_{ci}$

Results

- Instability appears to be scaling properly with g . Negative g stable
- Some FLR stabilization tendency has been observed - Scaling not yet ascertained

G Driven Unstable $\nu/a \approx 2$

DESCRIPTION
NO. 612



1112

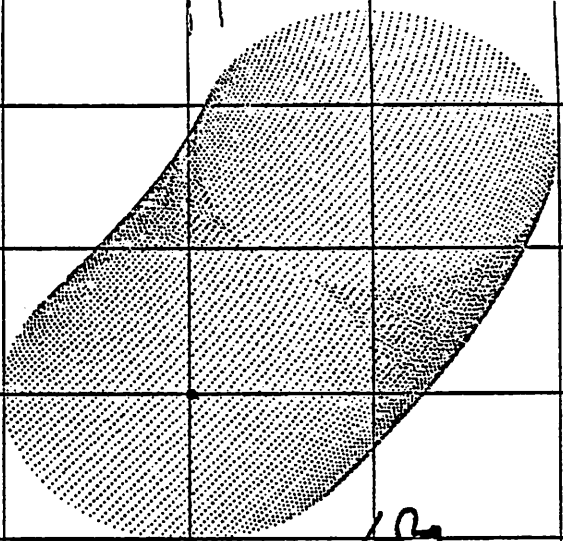
PHASE SPACE

TY VS TX HIT IS 512

Particle Positions
Late in time

Y ↑

1.0
0.5
0
-0.5
-1.0
-1.5

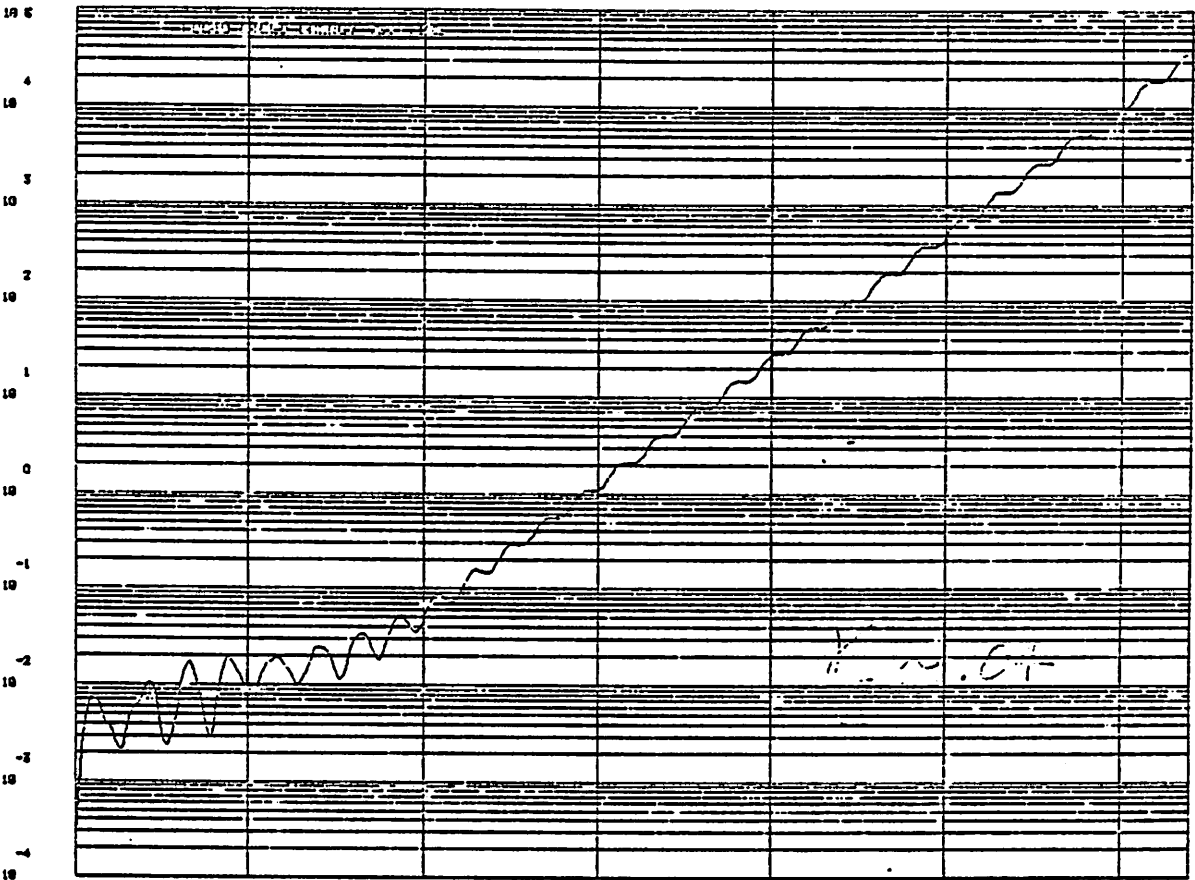


↙ Ω_g

at $\Omega_g = \frac{6\pi}{40}$

in 32 cycl periods system has
rotated $\approx \frac{3}{4}$ of 1 full rotation

-1.5 -1.0 -0.5 0 0.5 1.0
X →



Field energy vs time

311

Rotation driven interchange

Γ_p/a_i ranging from .03 up to .5

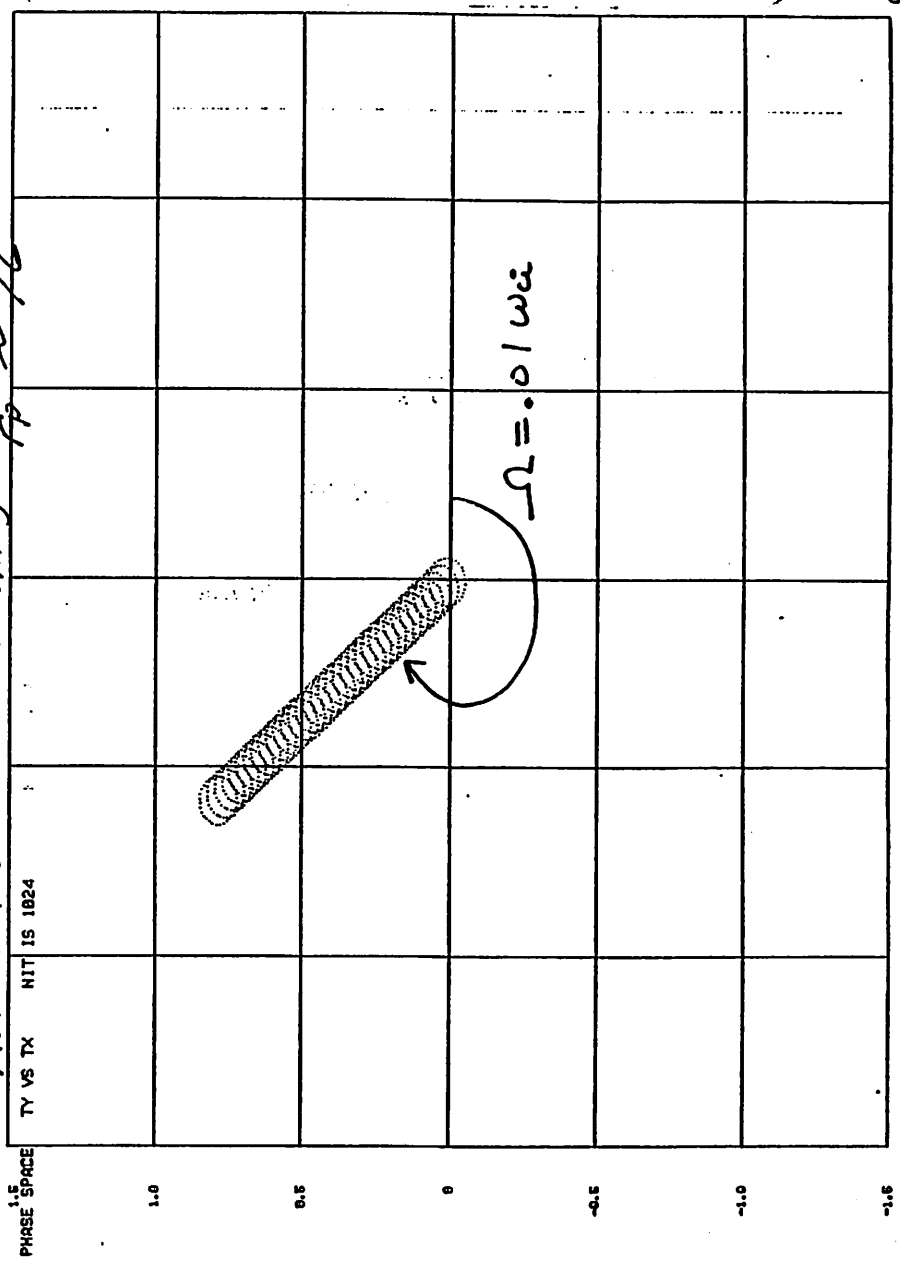
Typical rotation $\Omega \approx .01 \rightarrow .1 \omega_{ci}$

Results:

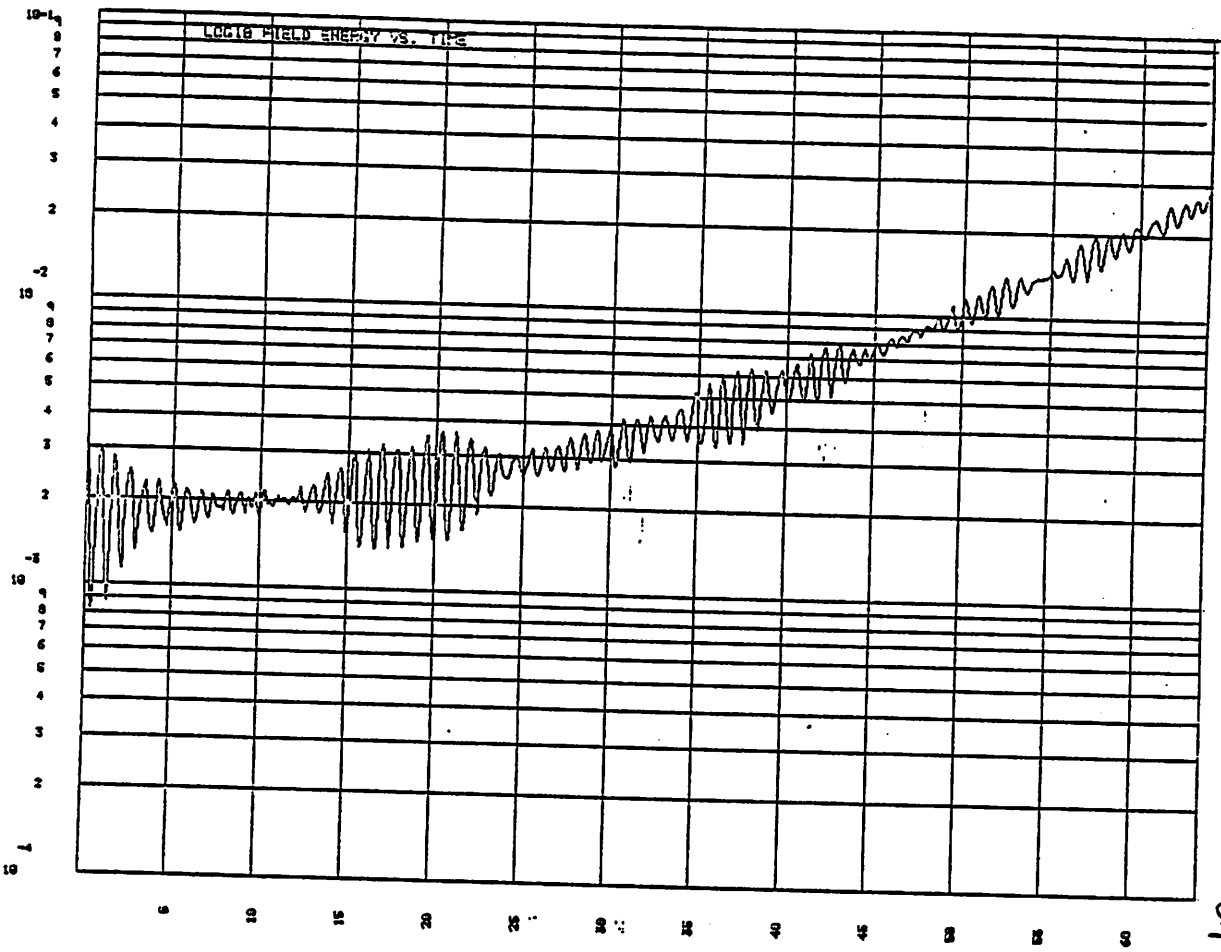
growth cleanly observed with $\gamma \sim \Omega$ in es model

FLR stabilization also observed

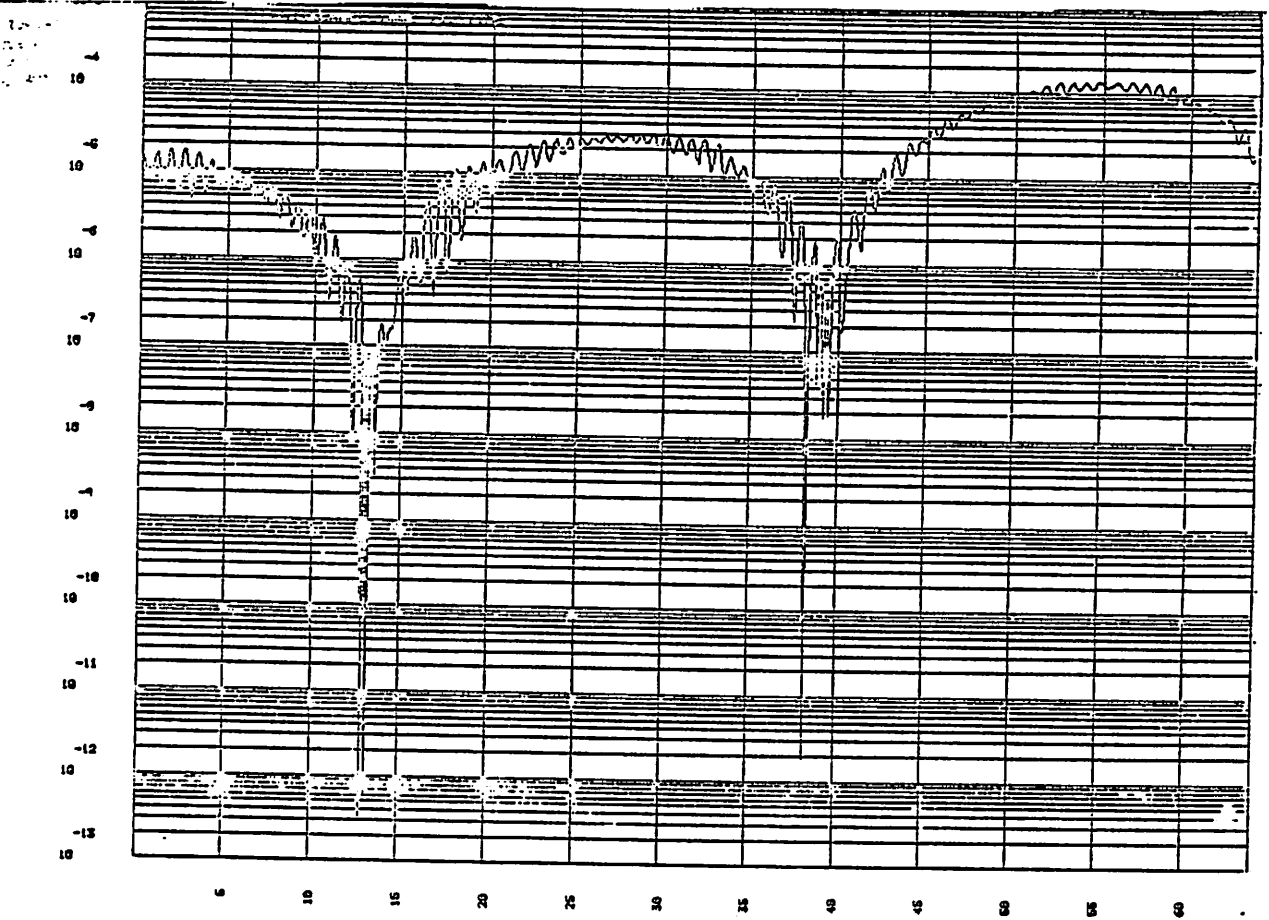
Rotation driven instability $\frac{\gamma}{\Gamma_p} \approx \frac{1}{16}$



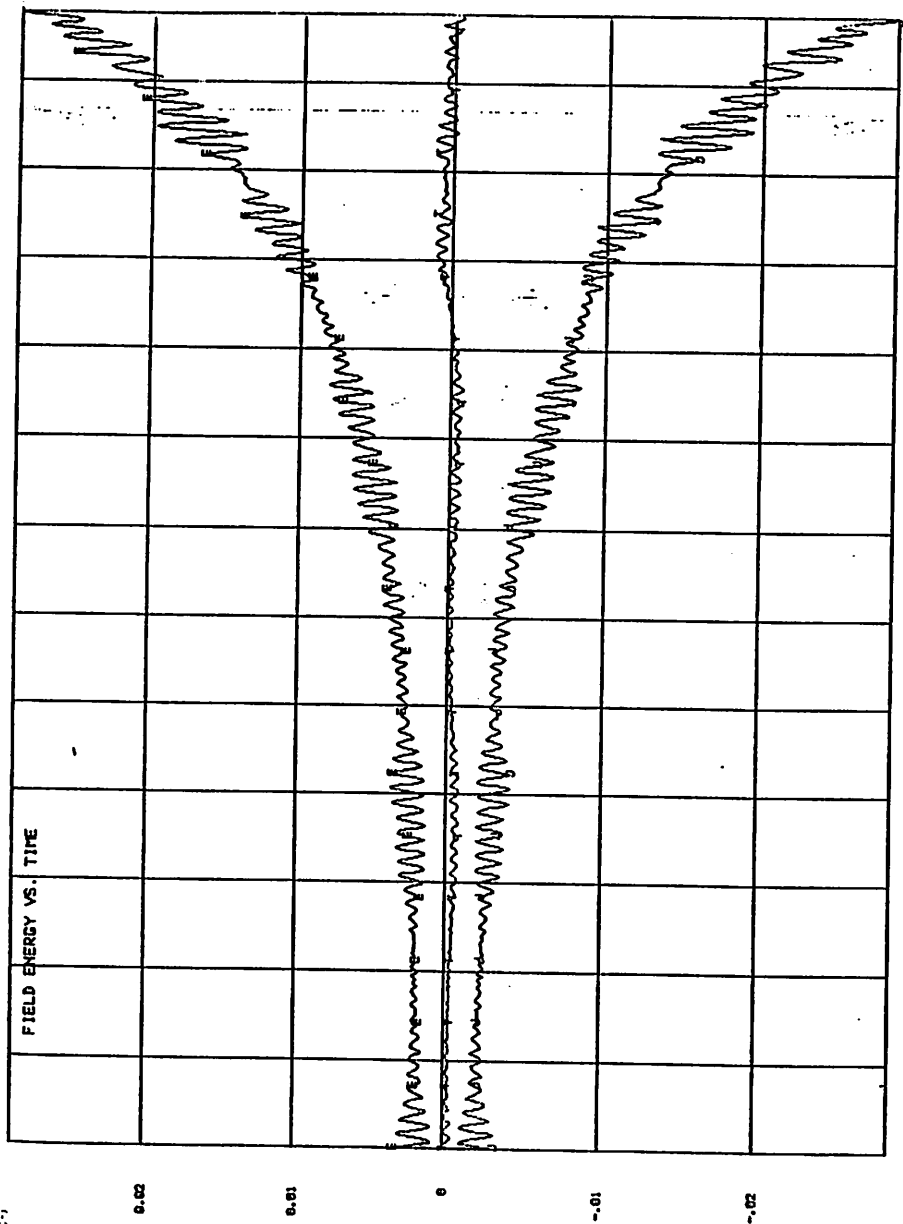
3:1
3:1
3:1
0
3:0
0:1
3:1



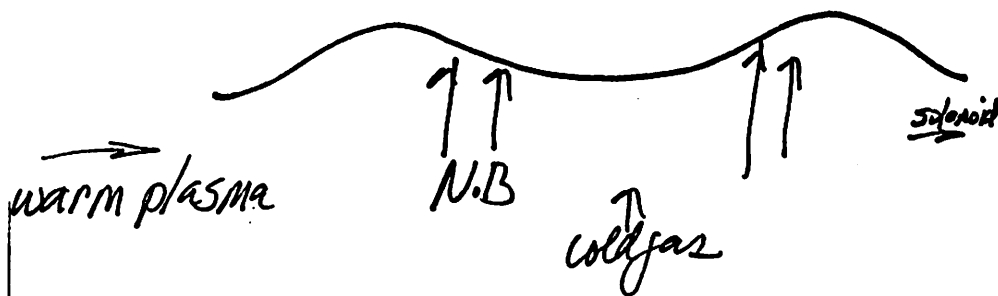
314



315



Axisymmetric Tandem Plug



Features: arbitrary N.B.
axial profile, cold gas etc -
essentially an arbitrary $f_i(z, v)$
is required to be modeled

For axisymmetric Tandem: 318

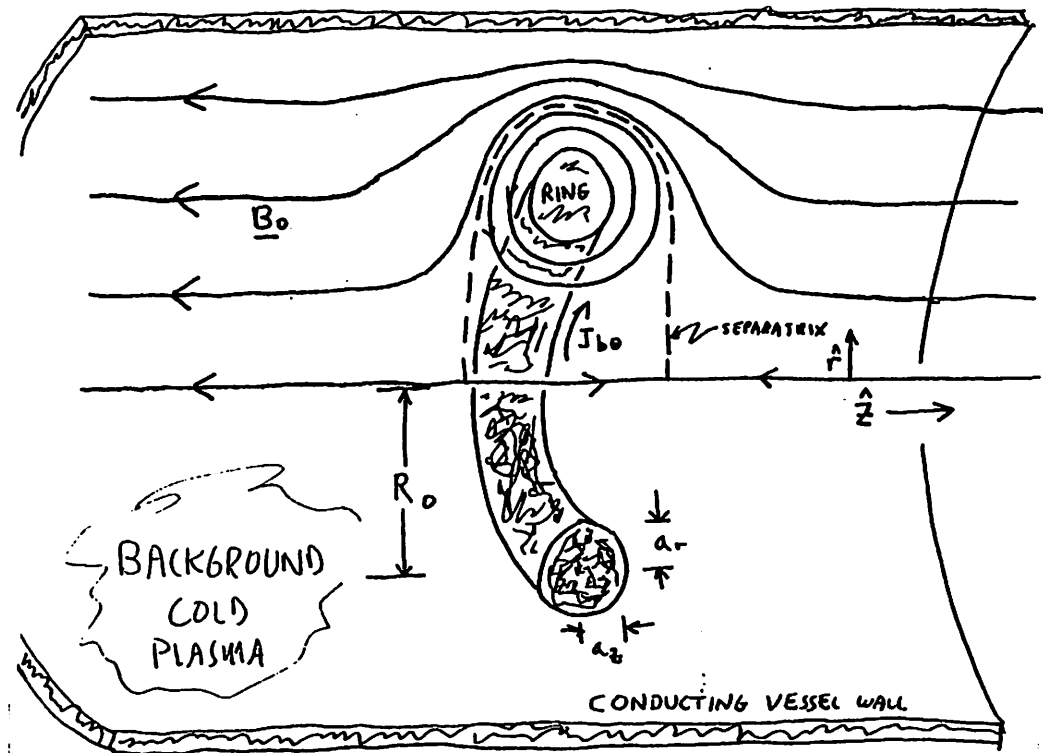
A local-in-r, arbitrary z variation simulation should be applicable to both:

- 1) W_i instability - i.e. DCLC and all of its variations due to: bounce orbits $W_i(z)$; warm plasma effects; localization in z effects, i.e. flute vs ballooning issues.
- 2) low frequency interchange + ballooning

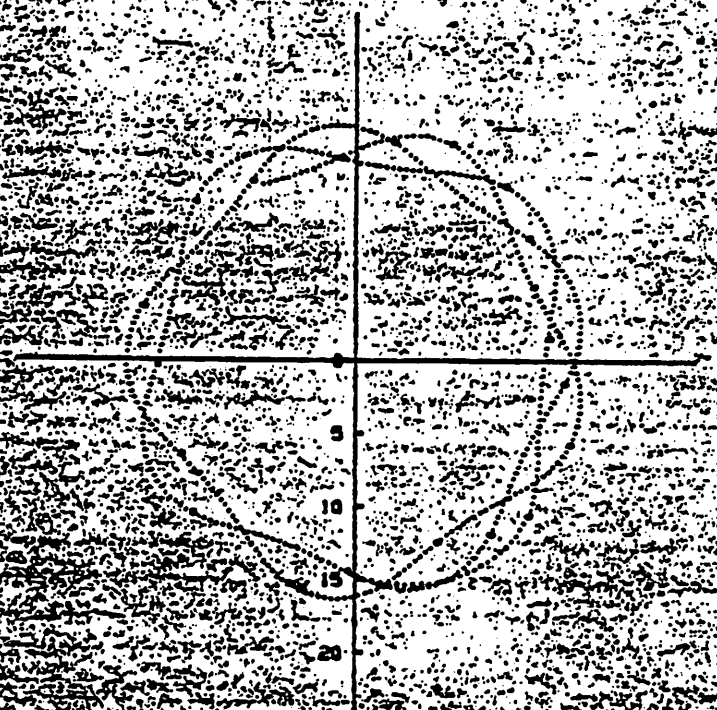
319
Numerical Issues:

- 1) beaming instabilities
worse at high R_{ai}
Desired: Technique to smooth out effects of discrete particle effects on microstability while retaining gross $f_i(v)$
- 2) Orbit averaging
- maybe a cure for 1)
- can greatly reduce # of particles needed for low frequency modes

- 25 I. LINEARIZED 3D HYBRID
SIMULATIONS: RINGHYBRID
- II. ERGODIC ORBIT EFFECTS
ON SIMULATIONS
- III. STABILITY OF A FIELD-REVERSED
ION RING IN A DENSE
BACKGROUND PLASMA
-
- A. FRIEDMAN
J. DENAVIT
R. N. SUTAN

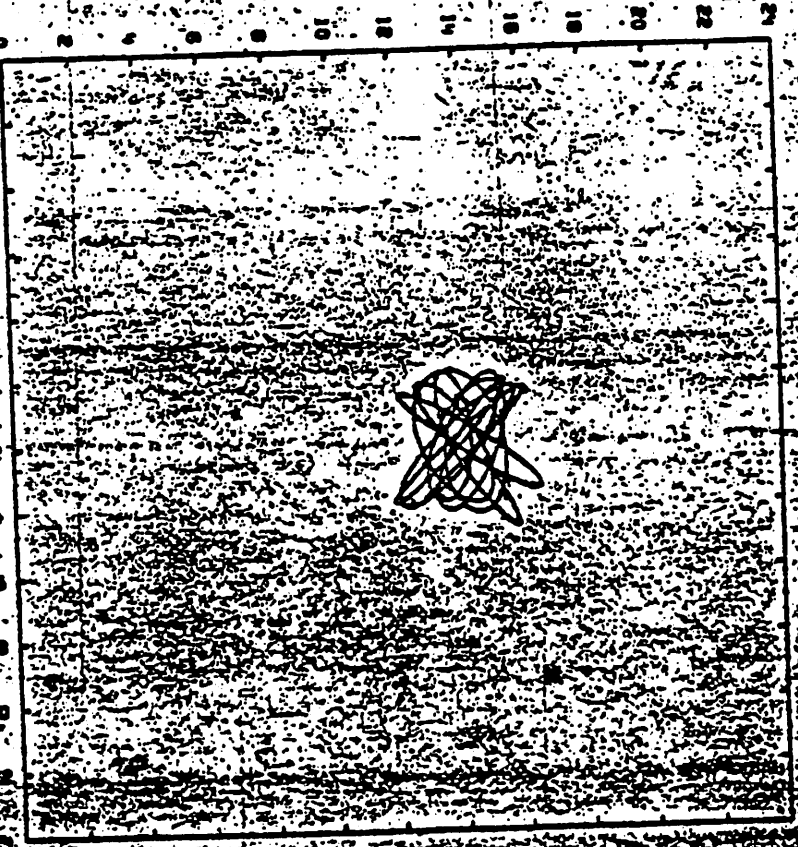


TRACER 2 R0 VS. THE10



STATISTIK

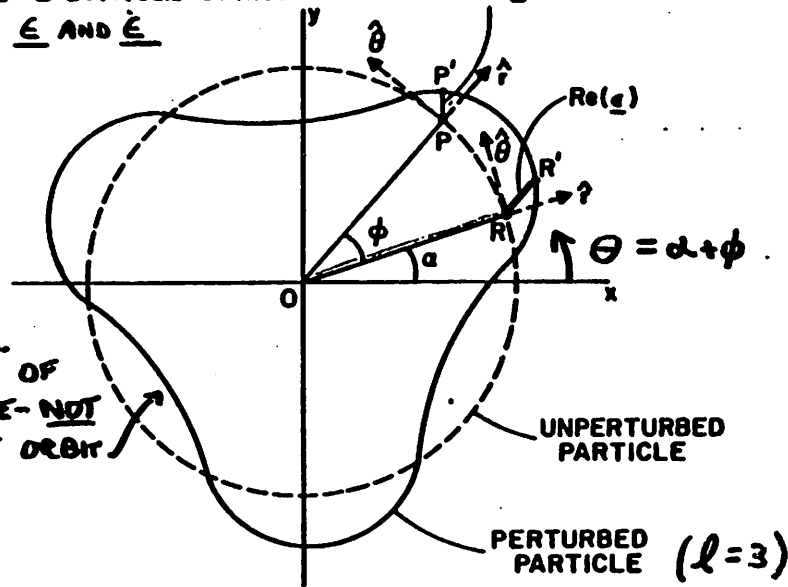
TRACER 1 R0 VS. Z0



STATISTIK

PARTICLE REPRESENTATION

ZERO ORDER: $2D3V$ ($r, z, \dot{r}, \dot{\theta}, \dot{z}$)
 INCLUDES CHAOTIC AXIAL & RADIAL MOTION, & CYRATION
 FIRST ORDER: DISPLACEMENT $\underline{\epsilon} e^{iR\phi}$ FOLLOWING
 ALL 6 COMPLEX COMPONENTS $Re(\epsilon e^{iR\phi})$
 OF $\underline{\epsilon}$ AND $\dot{\underline{\epsilon}}$



"SNAPSHOT" OF
 1 PARTICLE - NOT
 A PARTICLE ORBIT

FOLLOW MOTION OF "REFERENCE POINT" \underline{R} AND
 DISPLACEMENT $\underline{\epsilon}$. STABILITY FOR EACH l
 IS EXAMINED SEPARATELY.

ref: Cornell C.P.S. 268
 (sub. to JCP)

ZERO-ORDER EQNS:

$$\ddot{\underline{R}} = \frac{q}{mc} \dot{\underline{R}} \times \underline{B}_0(\underline{R}(t), t) + \frac{q}{m} \underline{E}_0(\underline{R}(t), t)$$

$$\nabla \times \nabla \times \underline{A}^0 \hat{\theta} = \frac{4\pi}{c} \underline{J}_0^0 \hat{\theta} \quad \left[\frac{q_0}{c} \frac{\partial}{\partial t} \underline{A}^0 \hat{\theta} \right]$$

"RELAX" TO EQUILIBRIUM FOR ~ 1000 STEPS
 (SEE 3RD PAGE FOLLOWING)

NOTE: \underline{R} (AND $\underline{\epsilon}$) ARE ADVANCED IN CARTESIAN
 COORD. - FIELDS STORED IN (r, z) COORD.

"FREEZE" ZERO-ORDER FIELD:

$\ddot{\underline{R}} = \frac{q}{mc} \dot{\underline{R}} \times \underline{B}_0(\underline{R}(t))$ MOVES PARTICLES
 ON THEIR ZERO ORDER TRAJECTORIES
 IN THE EQUILIBRIUM FIELD.
 INITIALIZE PERTURBATION; THEN

FIRST-ORDER EQN. OF MOTION:

$$\ddot{\underline{\epsilon}} = \frac{q}{m} \underline{E}' + \frac{q}{mc} \dot{\underline{R}} \times [\underline{B}' + (\underline{\epsilon} \cdot \nabla) \underline{B}_0] + \frac{q}{mc} \dot{\underline{\epsilon}} \times \underline{B}_0$$

$\underline{E}', \underline{B}'$ FUNCTION OF $\underline{R}(t), t$

\underline{B}_0 FUNCTION OF $\underline{R}(t)$

FIRST-ORDER CURRENT

$$\underline{J}'_b = N^0 \left[\frac{\partial \underline{\epsilon}}{\partial t} + (\dot{\underline{R}} \cdot \nabla) \underline{\epsilon} - (\underline{\epsilon} \cdot \nabla) \dot{\underline{R}} \right] - \dot{\underline{R}} \cdot \nabla (N^0 \underline{\epsilon})$$

PLASMA MODEL - ALONG WITH THE
HOT-ION DYNAMICAL EQUATIONS, THE
SIMULATIONS SOLVE THE FOLLOWING:

ELECTRON MOMENTUM EQ. (OHM'S LAW)

$$0 = -n_e e (\underline{E}' + \underline{v}_e' \times \underline{B}/c)$$

ION MOMENTUM EQ.

$$n_i m_i \frac{\partial \underline{v}_i'}{\partial t} = n_i z e (\underline{E}' + \underline{v}_i' \times \underline{B}/c)$$

QUASINEUTRALITY

$$n_e = \sum n_i + n_b$$

AMPERE'S LAW

$$\nabla \times \underline{B}' = \frac{4\pi}{c} (\underline{J}_e' + \underline{J}_i' + \underline{J}_b')$$

FARADAY'S LAW

$$\nabla \times \underline{E}' = -\frac{1}{c} \frac{\partial \underline{B}'}{\partial t}$$

"b" - hot ions ("beam")

"i" - cold background ion fluid

"e" - inertialess electron fluid.

(ALSO - COLLISIONS BETWEEN i, e INCLUDED
IN CODE - SCALAR ν_{ei})

from zero-order
field solution
(frozen)

$\left\{ \begin{array}{l} n_i = \text{constant} \\ n_b \text{ from zero-order} \\ \text{particle code} \\ \text{"frozen"} \end{array} \right.$

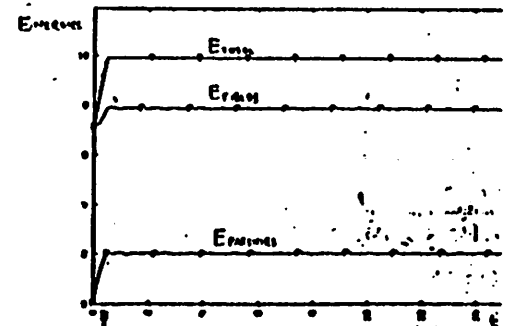
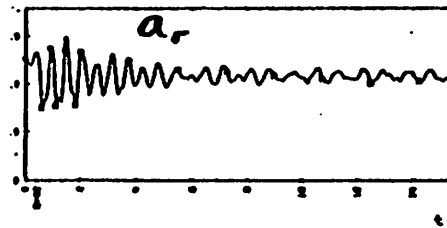
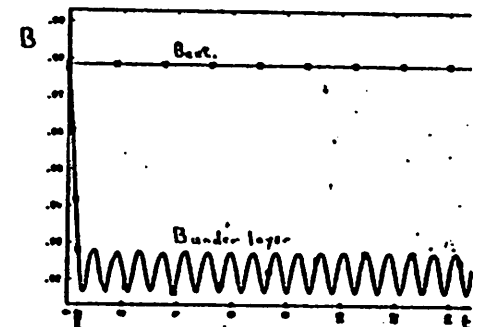
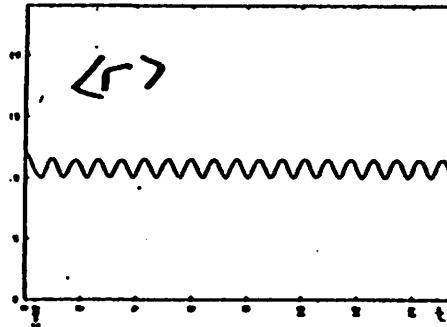
from first-order
particle code
(dynamic)

INJECTION OF PARTICLES TO FORM AN INFINITE LAYER

NO DAMPING TERM INCLUDED ($\sigma_0 = 0$)

(POOR RELAXATION TO EQUILIBRIUM)

- $\sigma_0 \dot{A}$ ACTS (VIA LENZ'S LAW) TO DAMP COLLECTIVE OSC.
- GOES AWAY AS $\dot{A} \rightarrow 0$

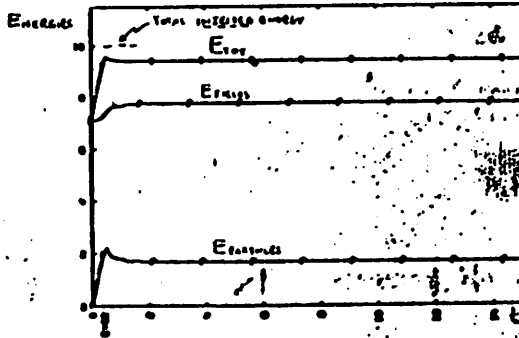
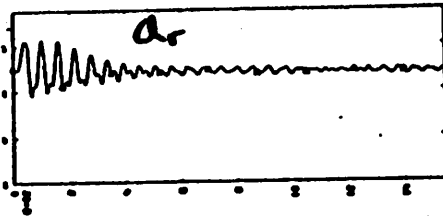
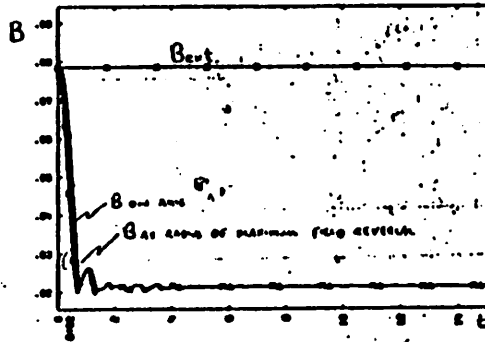
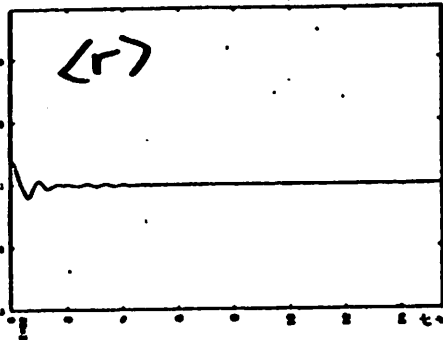


SEE CORNELL
L.P.S. #237

IMPROVED CONVERGENCE TO EQUILIBRIUM

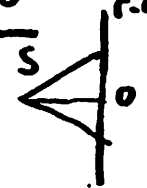
WHEN DAMPING IS INCLUDED ($\sigma=1$)

GOOD RELAXATION



RADIAL GEOMETRY: ρ, J SHARING - r_0

$$n(r) = \frac{\delta(r-r_0)}{2\pi r} \rightarrow \frac{S(r-r_0)}{2\pi r}$$



S IS A SYM. FUNCTION OF $r-r_0$ FOR SIMPLICITY IN LINEARIZED CODE: $\partial/\partial r \leftrightarrow -\partial/\partial r_0$

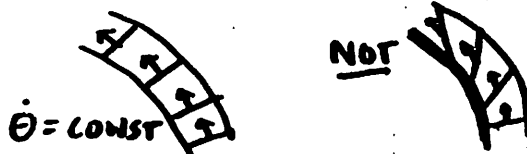
$$\int 2\pi r n(r) dr = 1 \Rightarrow \int dr S(r-r_0) = 1$$

NO SHEAR $\rightarrow \dot{\theta}(r) = \dot{\theta} = \text{CONST}$; $V_\theta(r) = V_\theta(r_0) \frac{r}{r_0}$

SO EACH ELEMENT OF THE SUPERPARTICLE RETAINS ITS INTEGRITY:

$$J_\theta(r) = n(r) V_\theta(r)$$

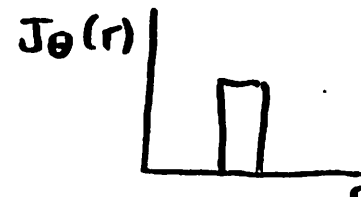
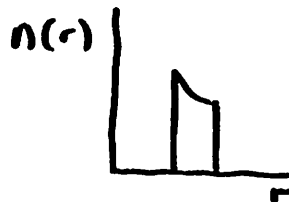
$$= \frac{S(r-r_0) V_\theta(r_0)}{2\pi r_0}$$



\therefore ALGORITHMS FOR ρ, J_θ DIFFER -

FOR ρ WE DIVIDE BY CELL RADIUS, FOR

J_θ WE DIVIDE BY PARTICLE RADIUS



(USES HIGHER-ORDER SPLINE, ACTUALLY.) 330

PREVIOUSLY, RINGHYBRID (& MANY OTHERS)

USED SAME ALGORITHM FOR ρ , J_{θ} [oops].

DIVIDING BY r NOT r_0 MAKES J_{θ} MORE

PEAKED TOWARD AXIS Γ WHICH MAY

BE UNDESIRABLE AT SMALL r .

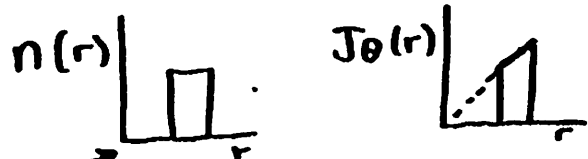
BIRDSALL & COHEN SUGGEST $n(r) = \frac{S^*(r-r_0)}{2\pi r_0}$;

THIS REQUIRES S (EFFECTIVE) = $S^* r/r_0$

NOT SYM. IF S^* IS SYM., AND $\int dr \frac{r}{r_0} S^*(r-r_0) = 1$.

TO GET J_{θ} MUST MULTIPLY BY r (COH),

IF NO SHEAR!



UNIFORM DENSITY CLOUD, CONCEPTUALLY NICE

$V_{\theta} = V_{\theta}(r)$ LEADS TO NEW TERMS IN $J_{\theta}^{1,2}$;
ALSO HAVE TO DIVIDE $J_{\theta}^0, J_{\theta}^{1,2}$ BY r_0 NOT r .

ERGODIC ORBITS AND PARTICLE SIMULATIONS

331

- NONLINEAR 2D3V (ZERO-ORDER OF RINGHYBRID, SUPERLAYER, ETC.)
- LINEARIZED 3D

REF: A. FRIEDMAN, U.C. BERKELEY
ERL REPORT M79/41, JUNE 1979

REF. FOR ERGODIC ORBITS IN STRONG
ION RINGS:

J.M. FINN, PLASMA PHYS. 21, 405 (1979).

NON-ERGODIC PARTICLES

- CONSTRAINED BY AN EXTRA CONSTANT OF MOTION, e.g.

P_{poloidal} , BICYCLE-TIRE RING

P_z , INFINITE LAYER

μ , SMALL LARMOR RADIUS

- ORBIT FALLS ON CURVE IN SURFACE-OF-SECTION PLOTS.

ERGODIC PARTICLES

- ONLY CONSTANTS OF MOTION ARE H, P_θ

- SWEEP OUT NONZERO "AREA" IN SURFACE-OF-SECTION PLOTS

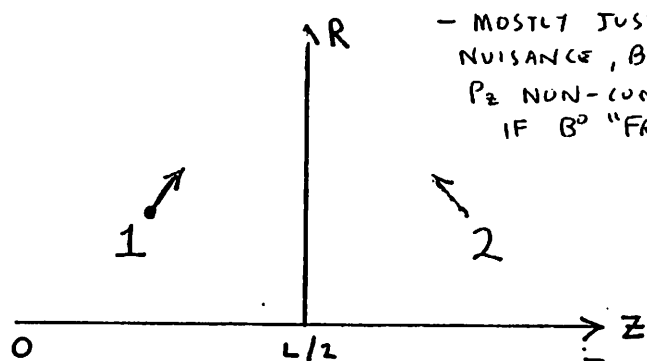
- NEIGHBORING ORBITS DIVERGE EXPONENTIALLY WITH TIME.

NONLINEAR 2 & 3v CODE MANIFESTATIONS

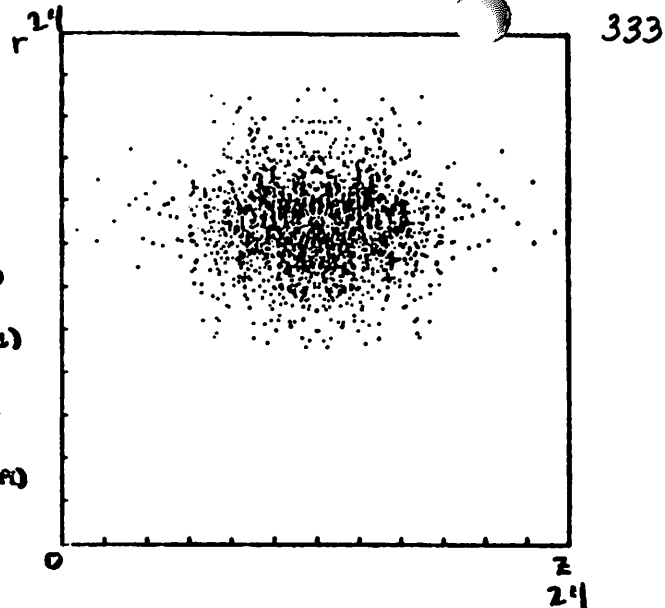
OF ERGODIC ORBITS - VIOLATION OF LEFT-RIGHT

MIRROR SYMMETRY DUE TO EXPONENTIAL

DIVERGENCE OF "NEIGHBORING" MIRROR-IMAGE ORBITS:



- MOSTLY JUST A
NUISANCE, BUT
 P_z NON-CONSERVED
IF B^0 "FROZEN"



$r_0 = 15$ (CELL)

$a_r = 2.0$

$a_z = 2.8$

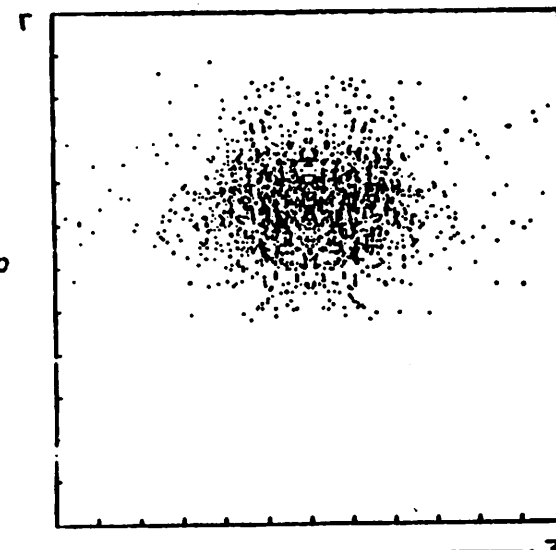
$\tau_{Li} = 40$ (STEPS)

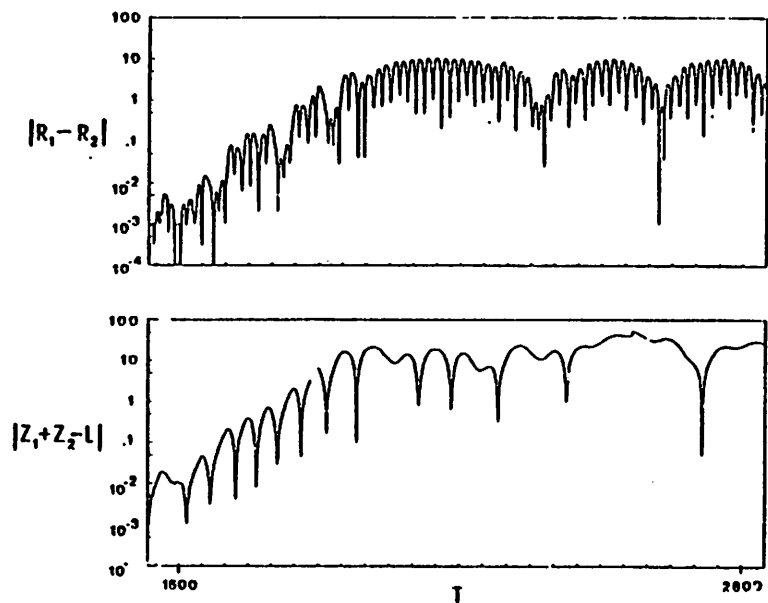
$\tau_g = 42$

$\tau_\beta = 52$

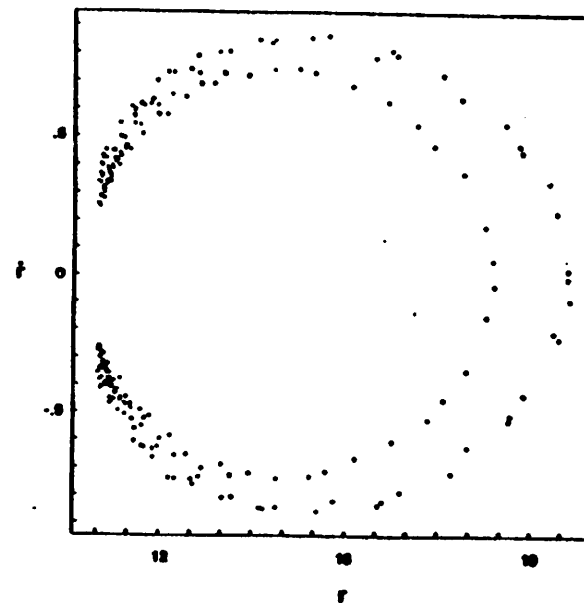
$\mathcal{S}_{\text{MAX}} = .25$

$\mathcal{S}_{\text{AXIS}} = .18$

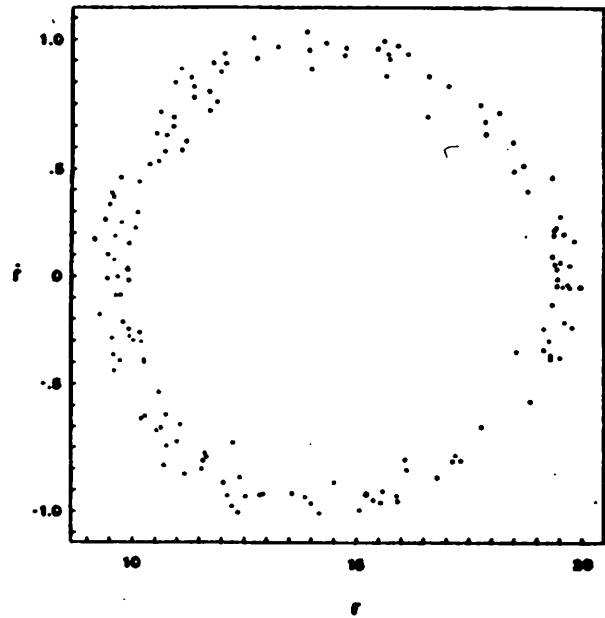




Plot of $|r_1 - r_2|$ and $|z_1 + z_2 - L|$ as functions of time
 for a run with $L = 96$. The maxima of these quantities are seen to be
 of order the system size. $\gamma/\omega_{ci} \approx \dots$



Surface-of-section,
 non-ergodic ptl.



Surface of section,
ergodic particle

LINEARIZED 3d CODE MANIFESTATION OF ERGODIC ORBITS - RINGHYBRID

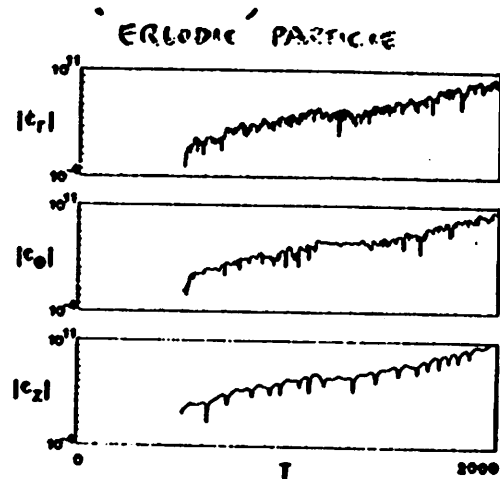
WITHOUT PLASMA RESPONSE, THE CODE
FOLLOWS DISPLACED SINGLE-PARTICLE ORBITS
IN THE EQUILIBRIUM MAGNETIC FIELD.

$\underline{\epsilon}_k$ IS THE SEPARATION OF TWO TRAJECTORIES
WHICH ARE FOREVER INFINITESIMALLY
CLOSE TOGETHER.

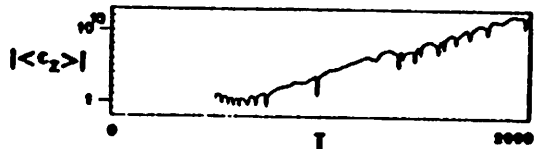
$$\ddot{\underline{\epsilon}}_k = \frac{q_k}{m_k} \left\{ \underbrace{\underline{E}^1}_{\text{NO PLASMA RESPONSE}} + \frac{v_k^0}{c} \times \left(\underbrace{\underline{B}^1}_{\text{SAME AS ZERO-ORDER FORCE}} + [\underline{\epsilon}_k \cdot \nabla] \underline{B}^0 \right) + \frac{\underline{\epsilon}_k}{c} \times \underline{B}^0 \right\}$$

MAKES ORBIT OF DISPLACED
POINT R' A "NEIGHBORING" ORBIT
OF UNPERTURBED POINT R 'S.

- MORE SERIOUS IMPLICATIONS
THAN 2d 3V.



$$\frac{\gamma}{\omega_{ci}} \sim .09$$



$$\frac{\gamma}{\omega_{ci}} \sim .09$$

FOR EQUILIBRIA WITH ERGODIC ORBITS, THE FASTEST-GROWING "SINGLE-PARTICLE MODES" CAN SWAMP THE COLLECTIVE MODES WHICH ARE THE OBJECTS OF STUDY.

- THERE ARE NOT ENOUGH PARTICLES FOR THE RANDOM PHASES OF SINGLE-PARTICLE MODES TO CAUSE "CANCELLATION" (NO MEAN $\underline{\epsilon}$). ANY MOMENT OVER THE $\underline{\epsilon}_x$ 'S REFLECTS ONLY THE FEW "FASTEST-GROWING PARTICLES".

- THE GROWTH CAN'T "SATURATE" SINCE THE CODE IS LINEARIZED.

- A SIMILAR MECHANISM MIGHT MASK THE LINEAR GROWTH PHASE OF INSTABILITIES MODELED WITH ANY NONLINEAR 3d CODE, IF PARTICLES ARE INITIALLY LOADED ON AXISYMMETRIC RINGS (A VARIANT OF "QUIET START" INITIALIZATION).

- \therefore MUST CHOOSE EQUILIBRIA W/O STRONG "ERGODIC" GROWTH (AN EXAMPLE FOLLOWS)

FIELD-REVERSED ION RING -

EQUILIBRIUM CONFIGURATION

- AN EQUILIBRIUM w/o RAPID ORBIT SEPARATION

$$\tau_{ci} = 40$$

$$\tau_j = 79$$

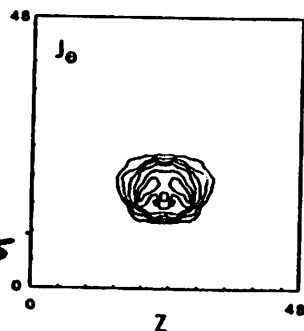
$$\tau_{\beta 2} = 35$$

$$\gamma_{max} = 1.8$$

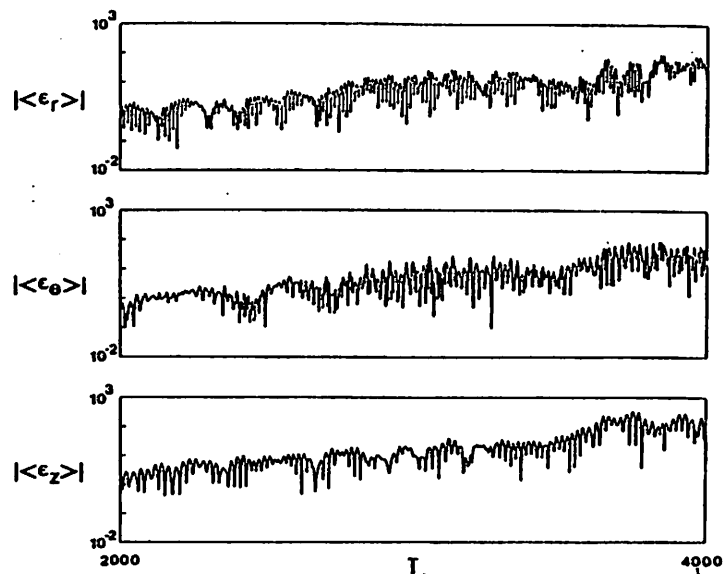
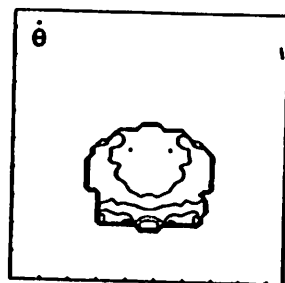
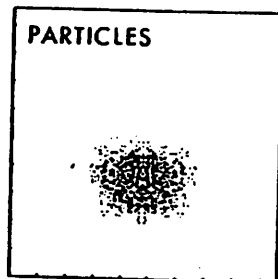
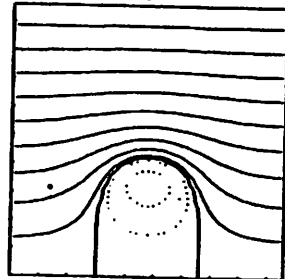
$$\gamma_{AMS} = 1.35$$

$$\frac{n_b}{n_i} \leq 0.02$$

$$\frac{v_0}{v_A} \approx 20$$

2400 SIM.
PARTICLES

FIELDLINES



GROWTH IN COMPONENTS OF MEAN DISPLACEMENT
 $\langle \epsilon \rangle$ DUE TO "ERGODIC" ORBIT SEPARATION IN
 ZERO-ORDER FIELD ($E' = B' = 0$)

(SLOW ENOUGH, WITH $\gamma/w_{ci} \approx .015$,
 THAT FOR THIS RING MEANINGFUL CONCLUSIONS
 CAN BE OBTAINED REGARDING COLLECTIVE BEHAVIOR.)

THEORETICAL PREDICTIONS - STABILITY WITH RESPECT TO KINK MODES

REF: R.V. LOVEACE, P.F. 19, 723 (1976).

R.N. SUDAN & M.N. ROSENBLUTH P.F. 22, 252 (1979).

AXIAL MODE - NO MEAN RADIAL DISPLACEMENT:

SUFFICIENT CONDITION FOR STABILITY IS
 $l\Omega > \omega_{pe}$, SUGGESTS $l=1,2$ UNSTABLE; $l \geq 3$ STABLE.

RADIAL MODE - NO MEAN AXIAL DISPLACEMENT:

FOR $l > 1$, $l\Omega > \omega_{pe}$ IS SUFFICIENT FOR STABILITY;
SUGGESTS $l=2,3$ UNSTABLE; $l \geq 4$ STABLE.

INFINITE LAYER TREATMENT BY LOVEACE - P.F. 22, 708 (1979)

INDICATES $\eta_{ext} > 0$ (POSITIVE MAGNETIC FIELD GRADIENT)

SUFFICIENT FOR STABILITY OF $l=1$ "MHD PRESSION".

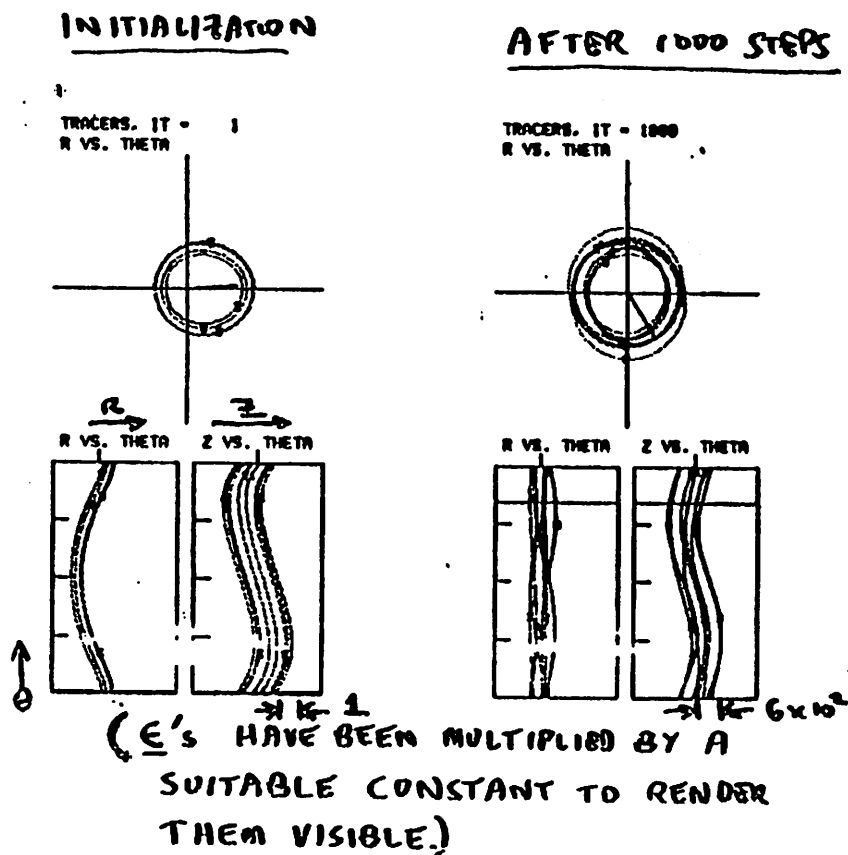
SINCE " η_{ext} " INCLUDES IMAGE FIELD EFFECTS, THE

IMPLICATION IS $l=1$ IS STABLE.

BETATRON RESONANCE EFFECTS ($l\Omega \sim \omega_{pe}$)

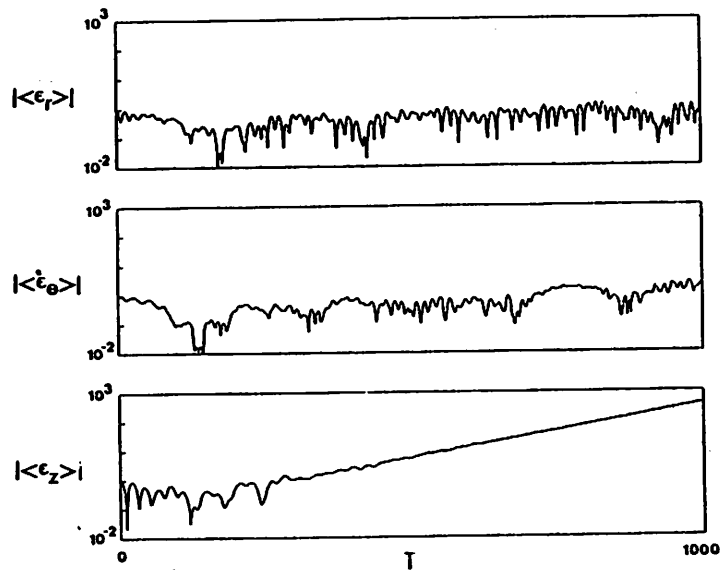
MAY LOWER INSTABILITY THRESHOLD FOR MODES
WITH PHASE VELOCITY IN THE DIRECTION OF RING
GYRATION. REF: J.M. FINN AND R.N. SUDAN,
P.F. 22, 1148 (1979).

($l=1$)



AVERAGE AMPLITUDES vs. TIME

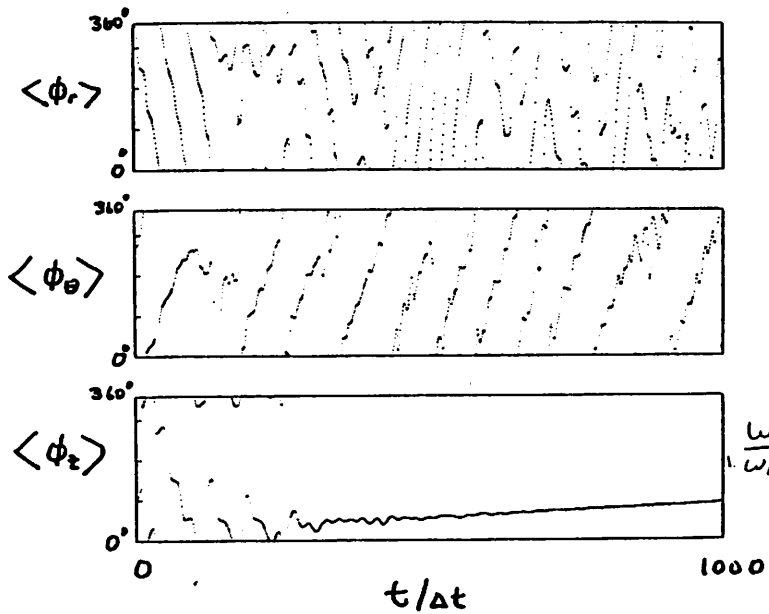
($l=1$)



$\gamma \approx 0$

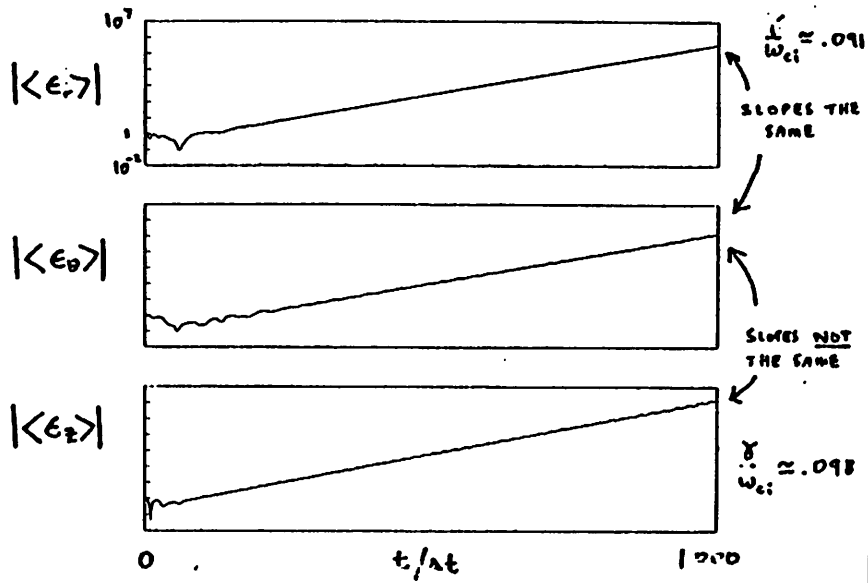
$\frac{\gamma}{\omega_i} \approx .053$

AVERAGE PHASES ($l=1$)

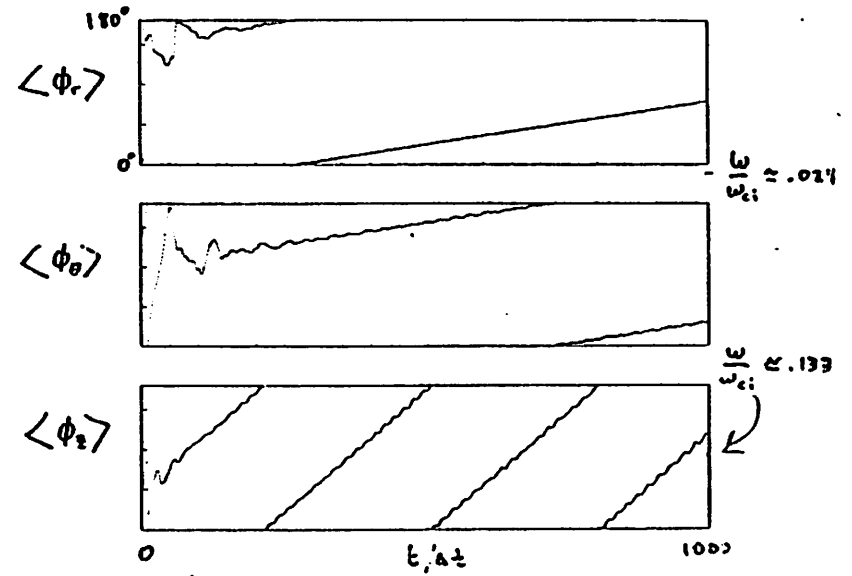


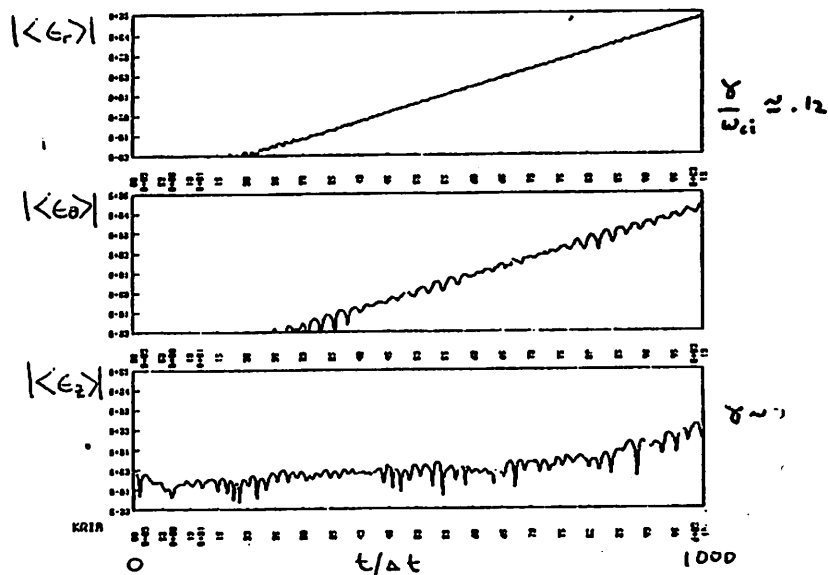
$\frac{\omega}{\omega_i} \approx .0076$

AVERAGE AMPLITUDES ($l=2$)



AVERAGE PHASES ($l=2$)



AVERAGE AMPLS. (LOG) ($l=3$)

SUMMARY, K.R. - SERIES

RUN	DESCRIPTION	γ_r/ω_{ci}	γ_z/ω_{ci}	ω_r/ω_{ci}	ω_z/ω_{ci}
KRAA,B	$l=1$	0	.053	-	.0076
KRDA,B	$l=1$, DENIER B' GROUND	0	.028	-	.002
KRBA	$l=2$.091	.098	.024	.133
KRCA,IA	$l=3$.12	~0	.165	-
KREA	$l=4$	$\leq .037$	$\leq .018$	-	-
KRFA	$l=4$ SINGLE-PARTICLE	.015	.018	-	-
KRGA	$l=5$	$\leq .022$	$\leq .029$	-	-

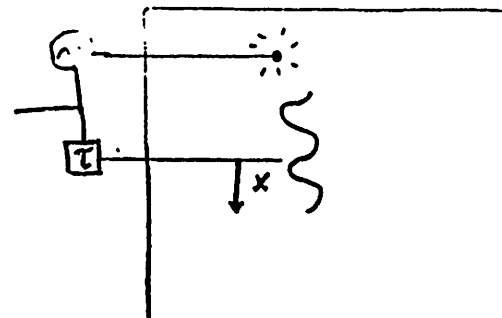
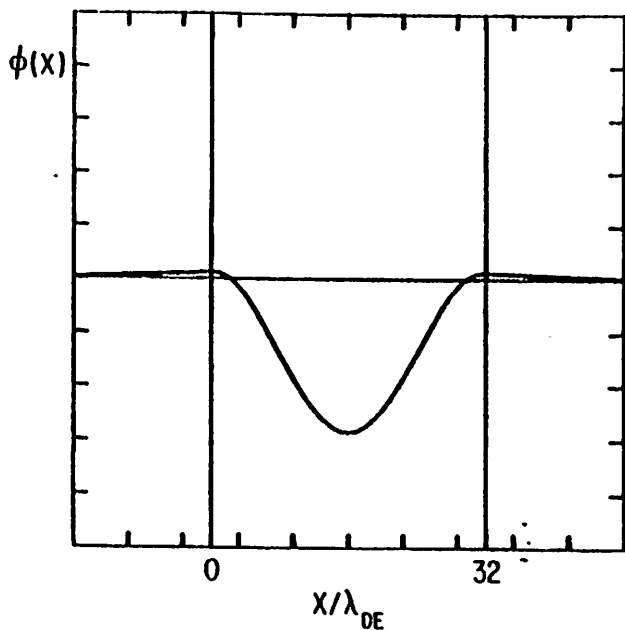
ie. $l=1, 2$ AXIAL } RAPID INSTABILITY
 $l=2, 3$ RADIAL }

$l=1$ RADIAL ("MHD PREC.") STABILIZED
 BY IMAGE CURRENTS
 IN OUTER WALL

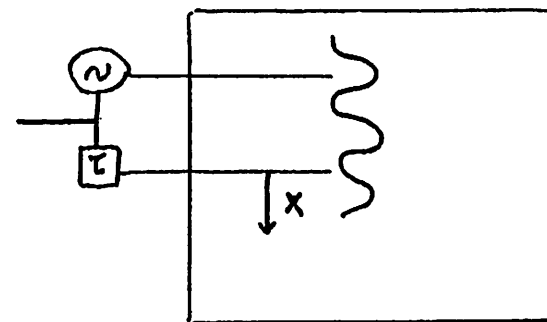
$l=4$ RADIAL, POSSIBLY OTHERS, SHOW
 EVIDENCE OF BETATRON-RESONANCE
 INSTABILITY.

26

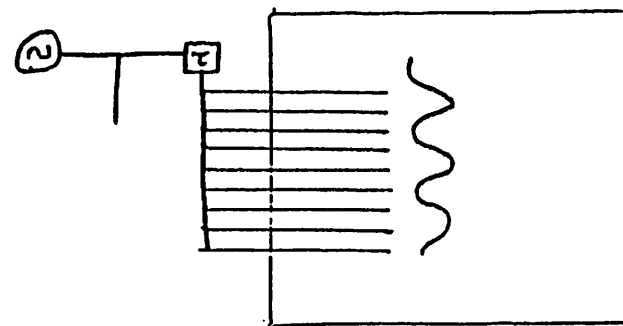
Viktor Deryzh UCIA

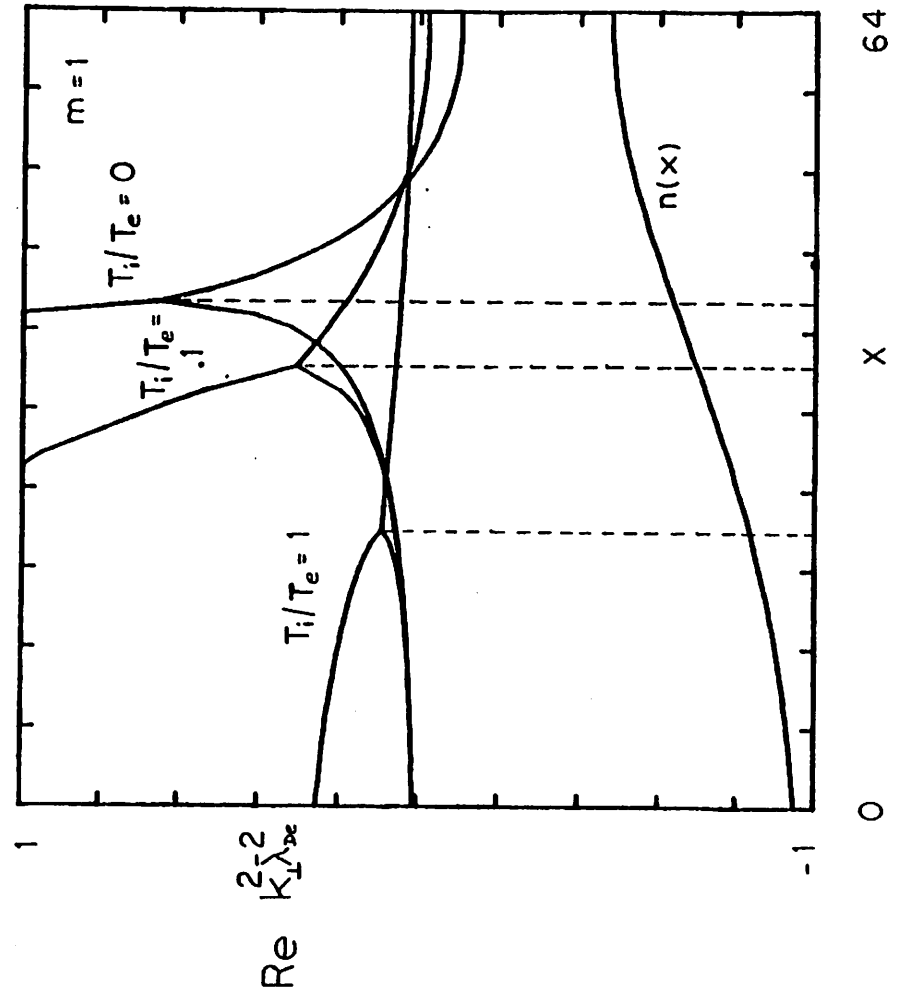
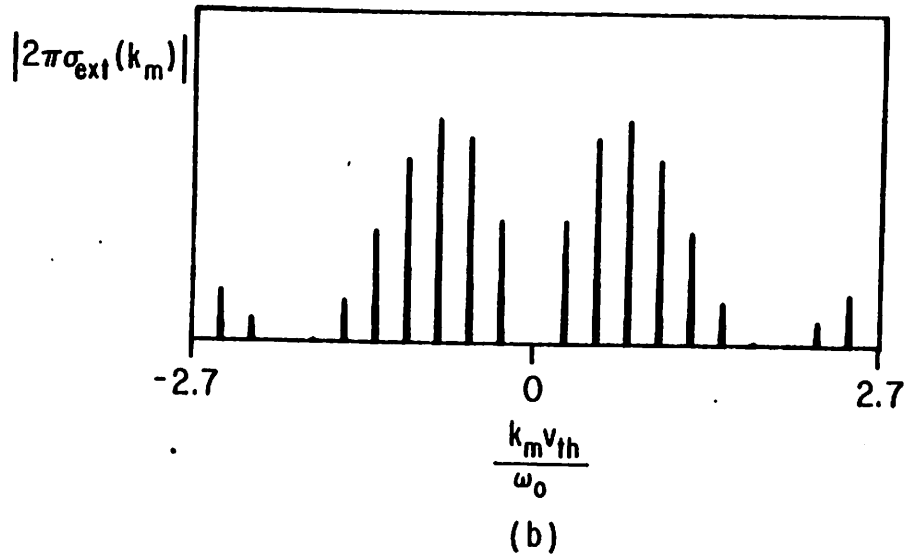
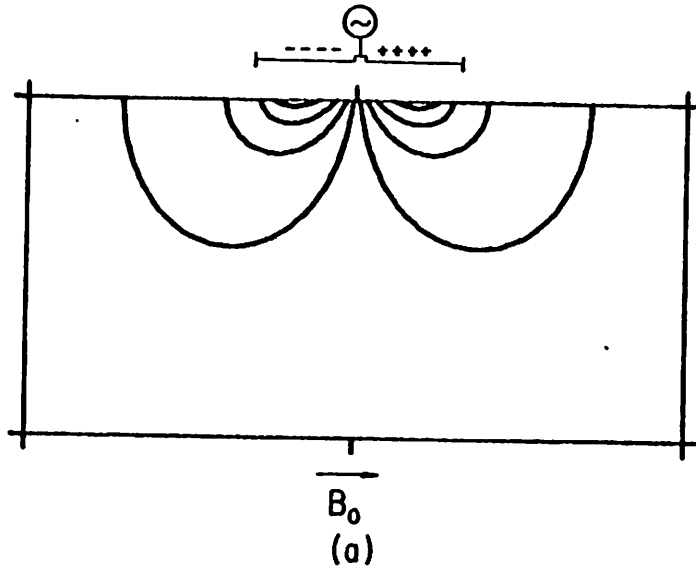
"Diagnostics for Bounded Plasmas,
with Applications"

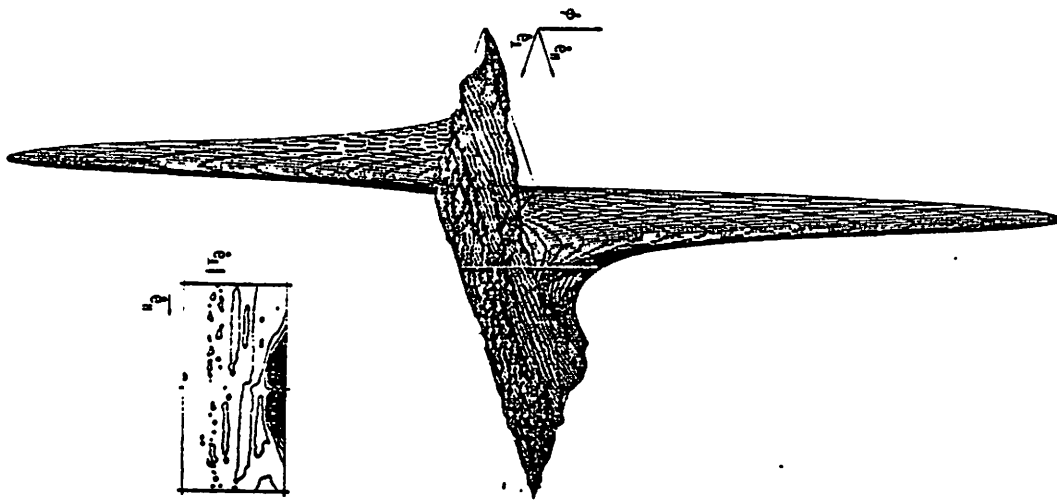
$$C(x, \tau) \equiv \frac{1}{T} \int_0^T \sin(\omega_0 t) \phi(x, t + \tau) dt$$



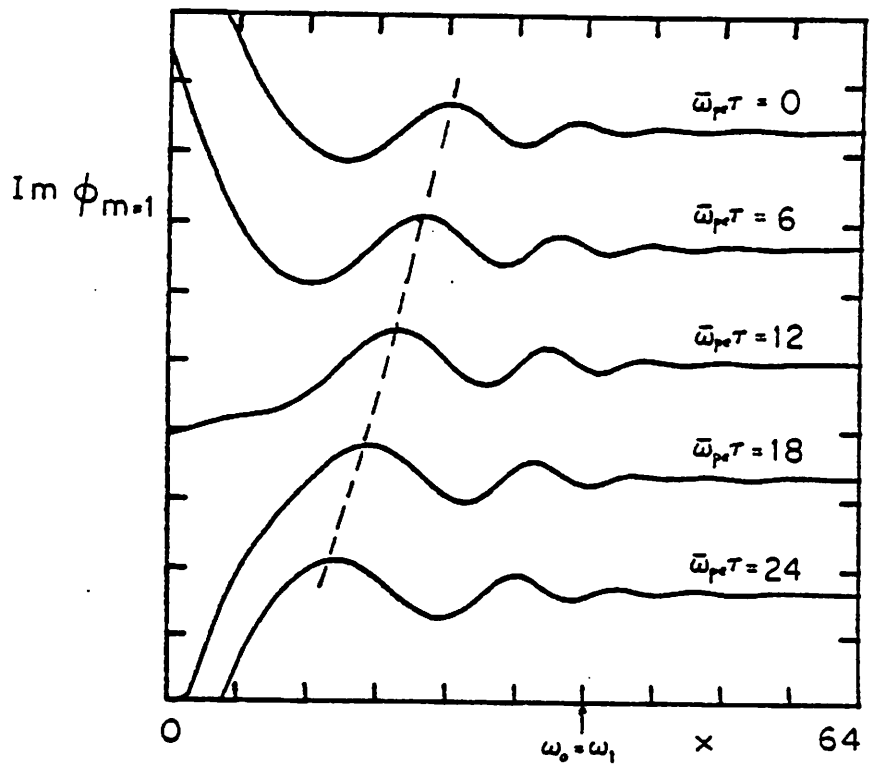
$$\tilde{C}(x, \tau) \equiv \frac{1}{T} \int_0^T \tilde{\phi}(x_0, t) \phi(x, t + \tau) dt$$



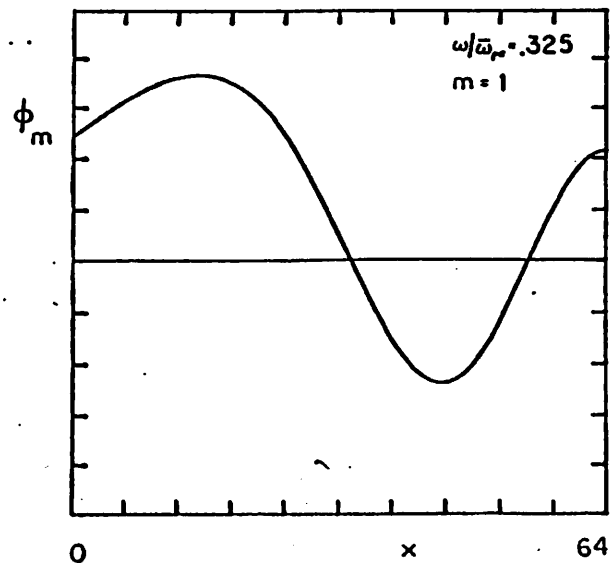
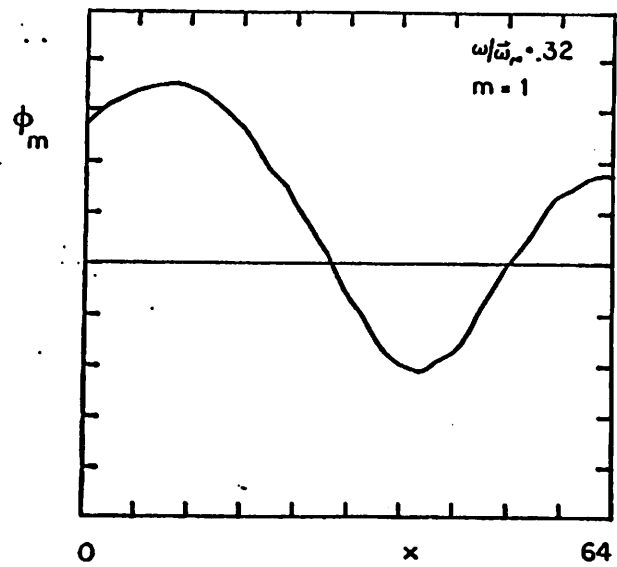
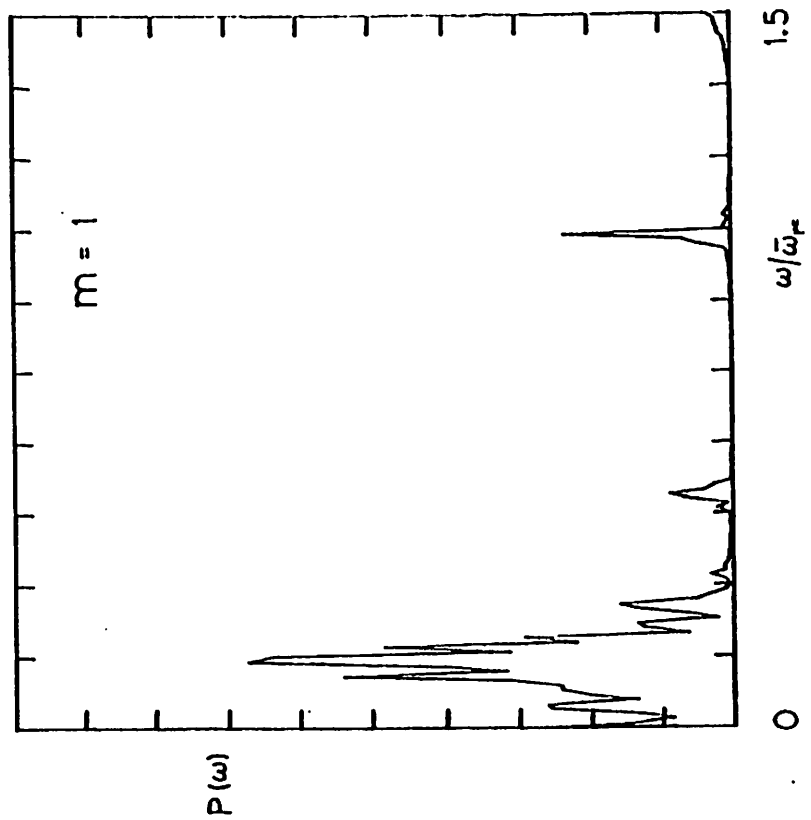




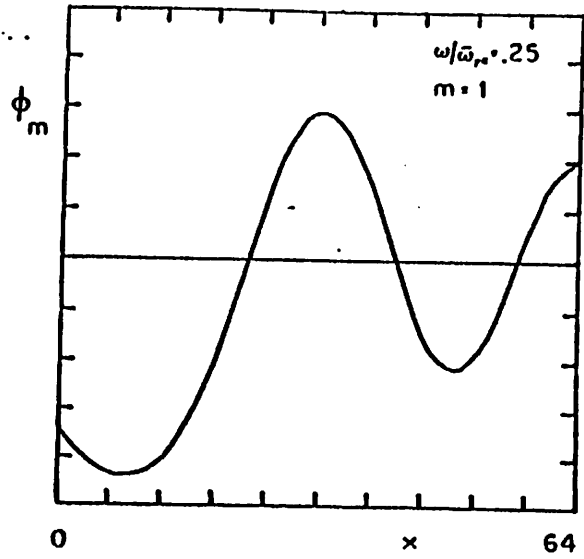
354



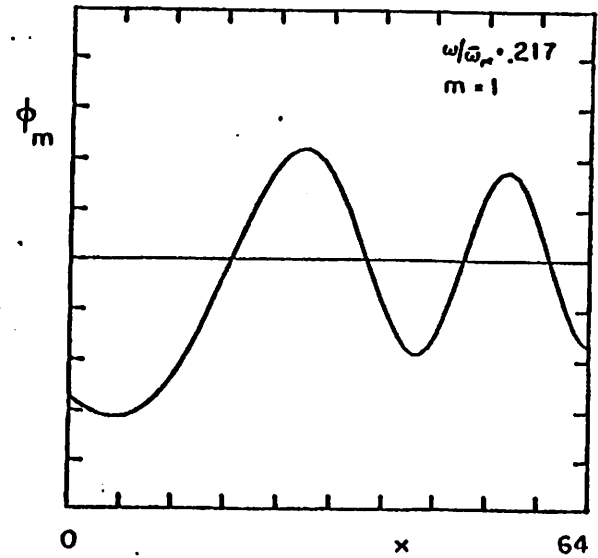
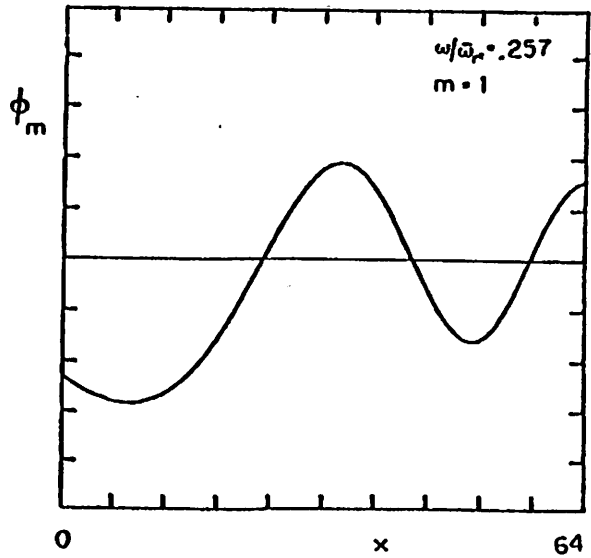
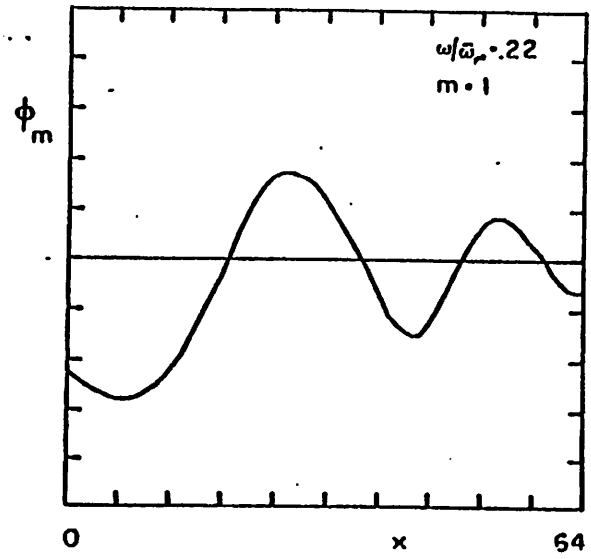
355



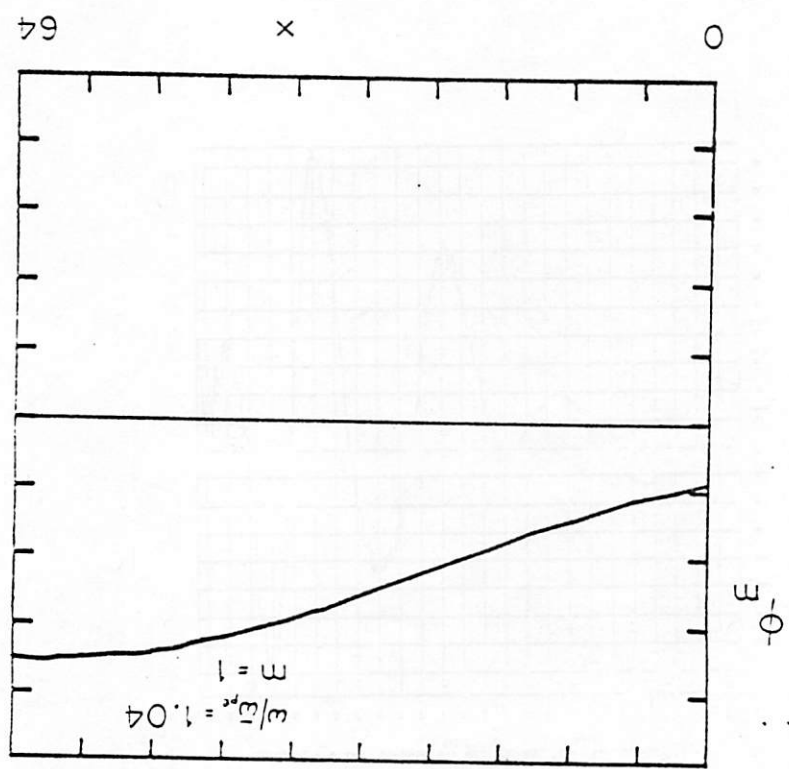
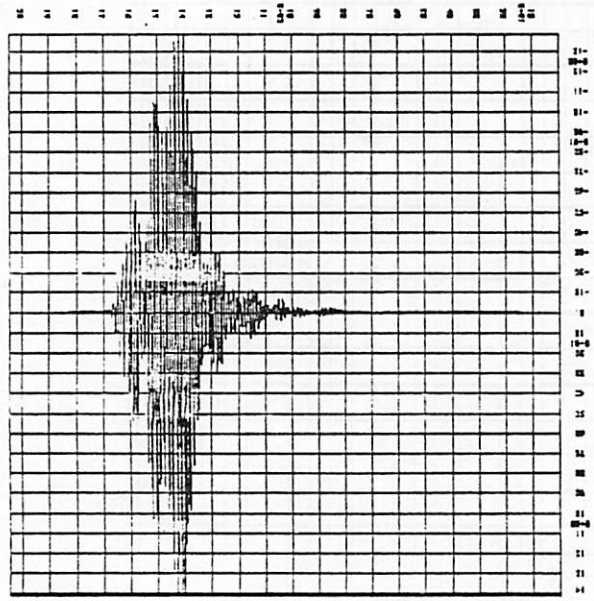
358

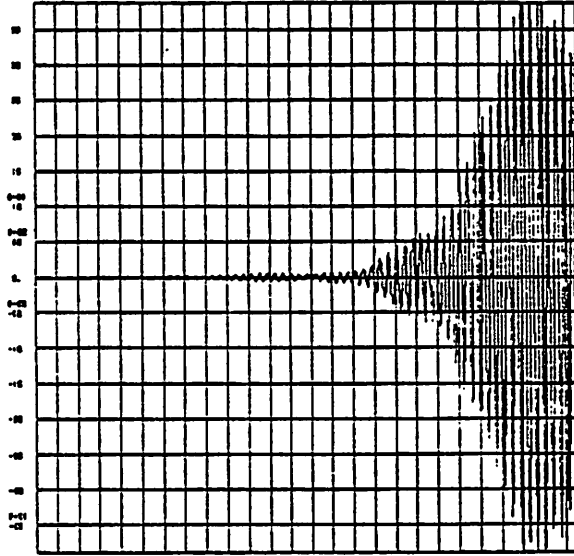


359



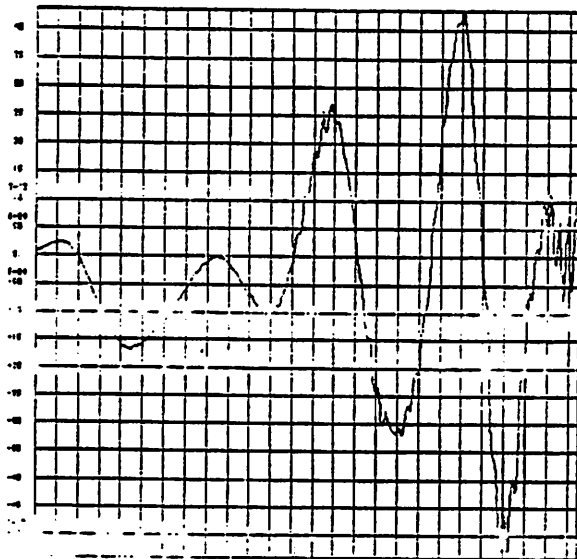
MODE 0 40.00000
ERNY = 1.00E+00 NTRYX = 2.04E+03 YMIN = -1.20E+01 YMAX = 1.43E+01





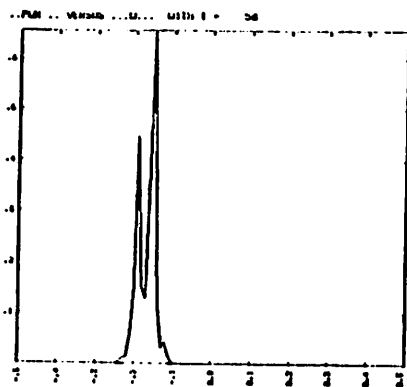
REM U X MODE 1 0.000000
 000000.0 1.000000
 MIN = 1.000E-09 MAX = 5.120E-02 MIN = 3.000E-09 MAX = 3.000E-09

362

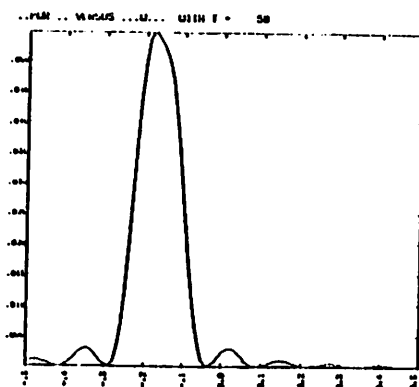


REM U X MODE 1 0.000000
 000000.0 1.000000
 MIN = 1.000E-09 MAX = 5.120E-02 MIN = 3.000E-09 MAX = 3.000E-09

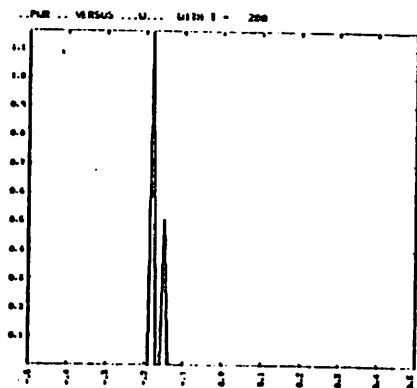
363

27 B Cohen et al. Stretched Ad Code

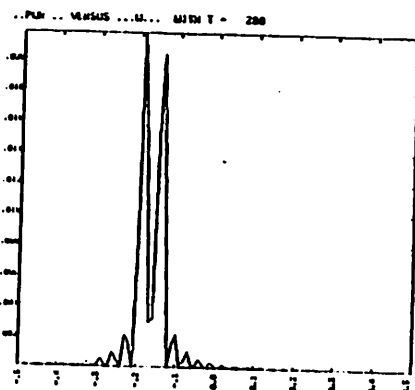
PWR PWR SPECTRUM AVERAGED OVER N= 1 TO 1 FOR PWR = 3.0



PWR SPECTRUM AVERAGED OVER N= 1 TO 4 FOR PWR = 3.0



PWR PWR SPECTRUM AVERAGED OVER N= 1 TO 1 FOR PWR = 3.0



PWR SPECTRUM AVERAGED OVER N= 1 TO 4 FOR PWR = 3.0

Mirror-Machine-Microinstability Simulations Including Ion Bounce Motion.* BRUCE I. COHEN, NEIL MARON, and GARY R. SMITH, Lawrence Livermore Laboratory--Simulations of drift-cyclotron-loss-cone (DCLC) instability in a uniform magnetic field have shown agreement with the nonlinear theory of R. Myer and A. Simon (for a single DCLC mode in weakly unstable plasma) and with a theory that invokes ion trapping and a simple free-energy argument (for a spectrum of modes in strongly unstable plasma). We study modifications to these results as well as effects due to nonuniformity of the magnetic field using a new code that includes ion bounce motion. In particular, we study effects of ion bounce resonances, namely, stochasticity and quasilinear diffusion in velocity space. The new code employs a one-dimensional electrostatic slab model: drift waves propagate and electric fields vary only in a direction mutually perpendicular to the magnetic field and to a density gradient. Ions are treated as particles, and electrons as a cold fluid that responds linearly to the wave fields.

*Work supported by U.S. DOE contract #W-7405-ENG-48.

Mirror-Machine - Microinstability Simulations Including Ion Bounce Motion

Bruce I. Cohen, Neil Maron and Gary R. Smith
Lawrence Livermore Laboratory

- Simulations of drift-cyclotron-loss-cone (DCLC) in a uniform magnetic field \vec{B}_0
 1. Saturation of a single unstable mode near marginal stability due to weak modification of orbits and $f_i(v_{\parallel})$
 2. More unstable plasmas exhibited ion trapping
- Simulations of DCLC and ion bounce modes in a nonuniform magnetic field $\vec{B}_0(\vec{r})$
 1. Ion bounce mode \Rightarrow "modified negative-mass instability" driven by $df_i(v_{\parallel})/dv_{\parallel} > 0$ and requires ion parallel bouncing.
 2. Linear (and nonlinear) modification of DCLC due to inclusion of ion bouncing
 3. Overlap of ion-bounce resonances \rightarrow quasilinear diffusion competition with nonlinear $\Delta\omega_{ci}$ and ion trapping.

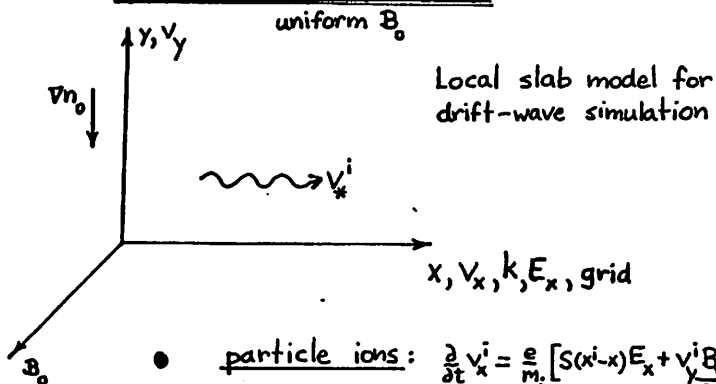
Introduction

- ion Bernstein wave ($\omega \sim N\omega_{ci}$) + ion diamagnetic-drift wave ($\omega \sim \omega_{*i}^i$)
 \longrightarrow unstable drift-cyclotron or DCLC mode
 these modes can be driven unstable by steep density gradients and loss-cone velocity distribution functions in hot dense plasma.
- If ion bouncing is included, a mode may exist that is absent in uniform $\vec{B}_0 \longrightarrow$ unstable ion-bounce mode.
 Driven, primarily, by loss-cone velocity distribution function.

Experimental motivation:

1. Observations of large-amplitude ion-cyclotron waves due to DCLC and drift-cyclotron turbulence in mirror machines, multi-poles, Q-machines, etc.
2. At steeper gradients and higher frequencies, these modes transform into the lower hybrid drift and related instabilities (sheaths of θ -pinches, Tormac, etc.)
3. Observations of ion-cyclotron flute modes in mirror experiments, e.g. PR-5 and DCX-2, propagating in the ion diamagnetic direction in highly anisotropic plasma $\langle v_{\perp}^2 \rangle \gg \langle v_{\parallel}^2 \rangle$ — modified negative-mass instability.

Hybrid Simulation Model



- particle ions: $\frac{\partial v_x^i}{\partial t} = \frac{e}{m_i} [S(x^i-x)E_x + v_y^i B_0]$ $\frac{\partial x^i}{\partial t} = v_x^i$

$\frac{\partial v_y^i}{\partial t} = -\frac{e}{m_i} v_x^i \frac{B_0}{c}$ $\frac{\partial y^i}{\partial t} = v_y^i$

$S(x^i-x)$ = linear interpolation/finite-sized ion

$n_i(x, y=0) = \sum_i S(x^i-x) W [Y_{GC}^{ghost}(0)/L_n]$ L_n = density scale length = κ^{-1}

$Y_{GC}^{ghost} = Y_{GC}^{test}(0) - y(t)^{test}$ W = density profile = $\begin{cases} \text{linear} \\ \text{exponential} \\ \text{tanh} \end{cases}$

- linearized fluid electrons, $\vec{E} \times \vec{B}$ and $\frac{d\vec{E}}{dt}$ -polarization drifts

- Poisson equation:

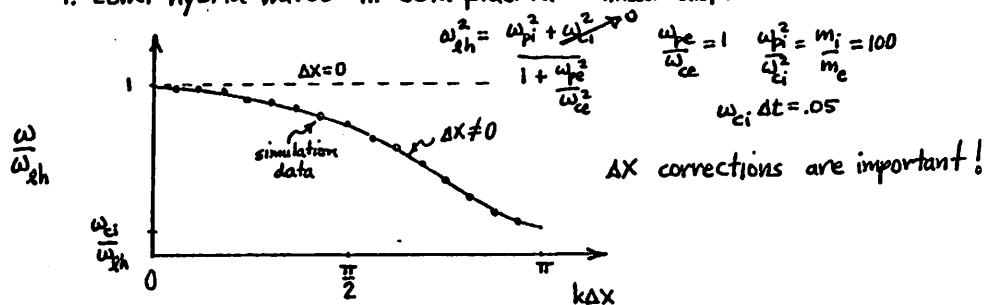
$$\left(1 + \frac{\omega_{pe}^2}{\omega_{ce}^2}\right) i \frac{\partial}{\partial t} \phi_k - \frac{\omega_{pe}^2}{\omega_{ce} k L_n} \phi_k = \frac{4\pi e}{k^2} i \frac{\partial}{\partial t} n_{i,k}$$

$n_i \rightarrow n_{i,k}$ $ik\phi_k \rightarrow E_x$ using FFT

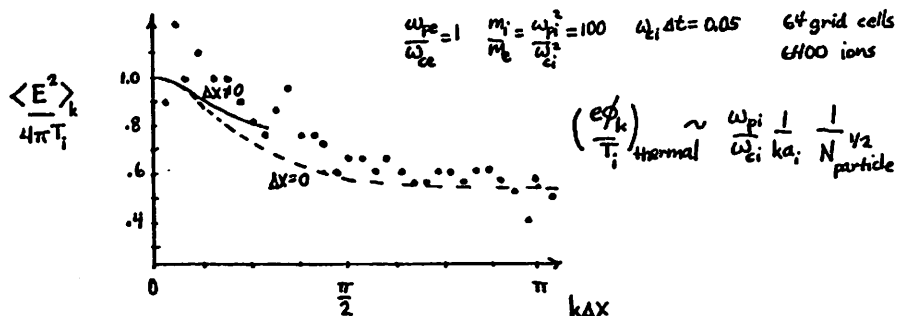
This code is a modification of N. Maron's version of Bruce Langdon's ES1 code.

Uniform plasma test cases:

- Lower hybrid waves in cold plasma - linear dispersion relation



- Ion Bernstein Waves - fluctuation spectrum



Drift waves in nonuniform plasmas

- Maxwellian $f_i(v_{\perp})$: drift-cyclotron instability
- Loss-cone $f_i(v_{\perp})$, either $\delta(v_{\perp}-v_0)$ or subtracted Maxwellian initially: drift-cyclotron-loss-cone (DCLC) modes

DCLC simulations
uniform B_0

• $f_i(v_i) = (2\pi v_i)^{-1} \delta(v_i - v_0)$ at $t=0$

DCLC linear dispersion relation
 $\omega_{pi}/\omega_{ci} = 2$ $ka_i = 2.5$
 $m_i/m_e = 1836$

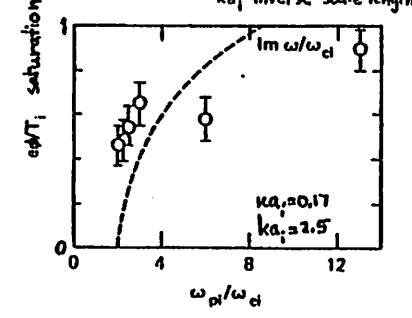
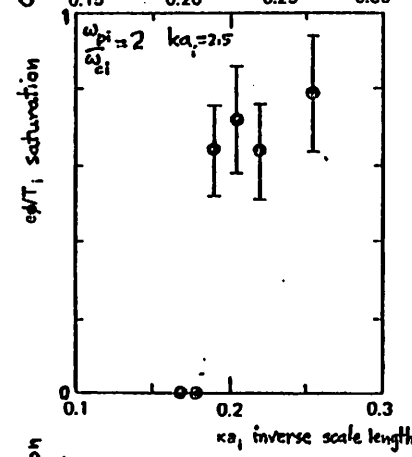
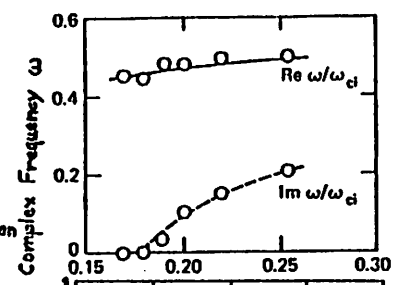
Saturation by ion trapping

$\frac{e\phi}{T_i} \approx \left(\frac{2\pi}{ka_i}\right)^{1/2} \left| \frac{\omega - N\omega_{ci}}{N\omega_{ci}} \right| \sim 0.8 - 1$

ref. Sigmar & Callen PF 14, 1423 (1971)

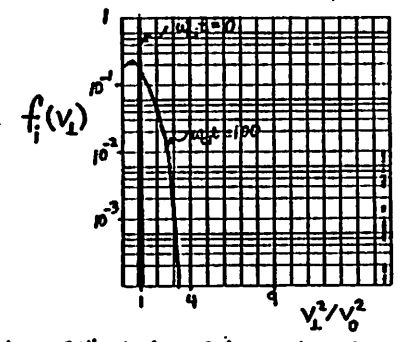
< 1% implied density profile change

$\omega_{ci}\delta t = .05$ $\Delta x = .2 a_i$ 6400 ions 64 grid cells $\Delta ka_i = .5$ $T_i \approx \frac{1}{2} m_i v_0^2$



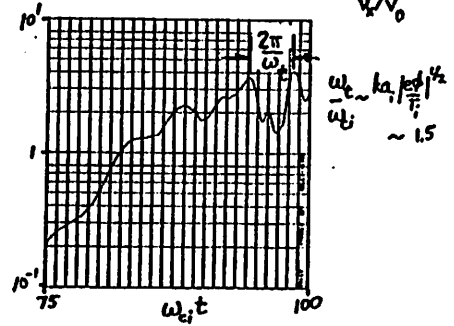
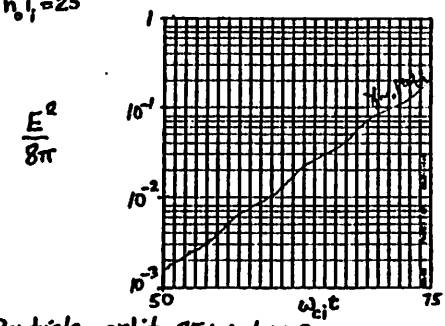
DCLC for $f_i(v_i, t=0) = \delta(v_i - v_0)$ (cont'd)

• Ion distribution function

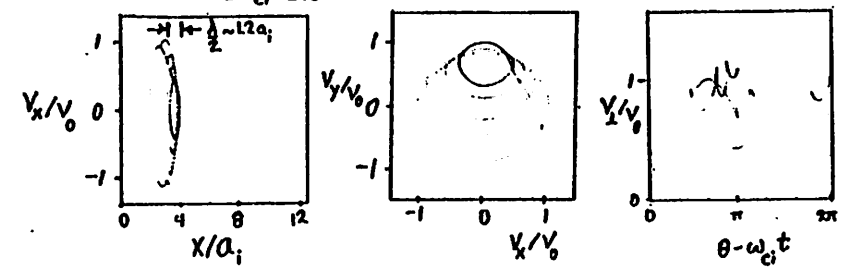


$a_i/L_n = .204$ $m_i/m_e = 1836$ $\omega_{pi}/\omega_{ci} = 2$
 $ka_i = 2.5$ most unstable

• Electric field energy density vs. $\omega_{ci}t$
 $n_0/T_i = 25$



• Particle orbit $75 \leq \omega_{ci}t \leq 100$



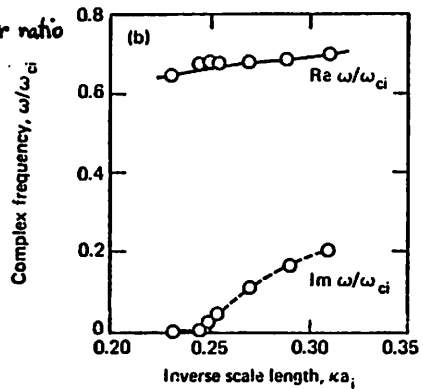
DCLC simulations
uniform B_0

• $f_i(v_{\perp}, t=0) = \frac{R}{2\pi v_i^2 (R-\Gamma)} [\exp(-v_{\perp}^2/2v_i^2) - \Gamma \exp(-Rv_{\perp}^2/2v_i^2)]$

$R = T_{hot}/T_{hole}$ = related to mirror ratio
 Γ = relative density of hole

DCLC linear dispersion relation

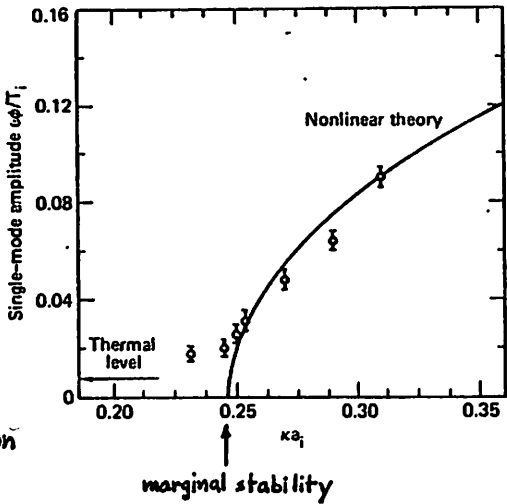
$R=9 \quad \Gamma=1 \quad \omega_{pi}/\omega_{ci}=3 \quad ka_i=3$



• Single-mode nonlinear saturation due to perturbative shift in ion orbits and $f_i(v_{\perp})$ near marginal stability:

$\frac{e\phi}{T_i} \propto \text{Im} \omega_{\text{linear}} \propto \left(\frac{\delta v}{R}\right)^{1/2}_{\text{marg. stab.}}$

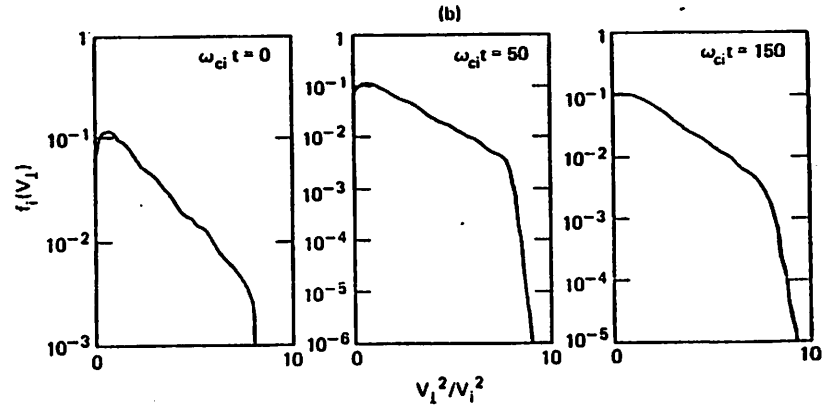
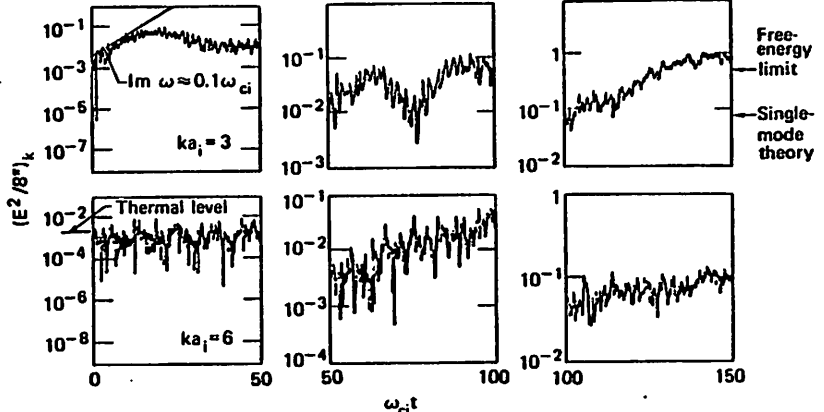
single-mode theory of Myer and Simon



$\omega_{ci}\Delta t = 0.1$ 50,000 ions 64 grid points

DCLC simulations
uniform B_0

• Two-mode simulation with $f_i(v_{\perp}, t=0) = \frac{R}{2\pi v_i^2 (R-\Gamma)} [\exp(-v_{\perp}^2/2v_i^2) - \Gamma \exp(-Rv_{\perp}^2/2v_i^2)]$
 $R=9 \quad \Gamma=1 \quad u_{a_i}=0.27 \quad u_i/\omega_{ci}=3 \quad m_i/m_e=1836$ (a)



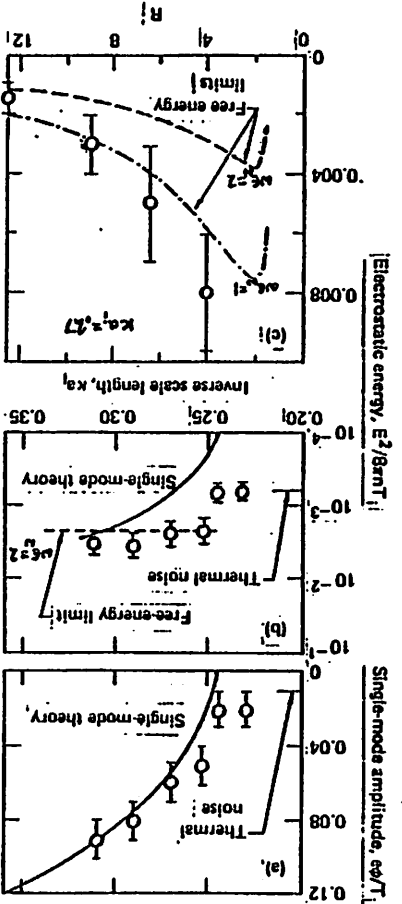
Most unstable mode $ka_i=3$ grows and saturates at Myer-Simon. Second harmonic is nonlinearly destabilized, as is the fundamental subsequently which ultimately traps ions and fills the loss-cone.

DCLC simulations

uniform B₀

• Multi-mode with $f_1(v, t=0) = \frac{1}{R} [\exp(-v^2/2v_1^2) - \exp(-Rv^2/2v_1^2)]$

$\omega_p/\omega_{ci} = 3 \quad R=1 \quad m_i/m_e = 1836$



early saturation of most unstable mode $ka_1=3$

ultimate saturation due to ion trapping and filling of loss-cone

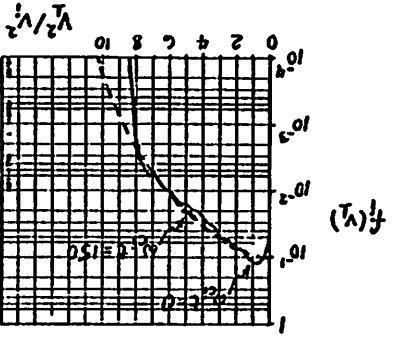
free energy balance:

$\Delta KE = \omega_{pe}^2 \frac{\Delta u}{8\pi}$

DCLC simulations (cont'd)

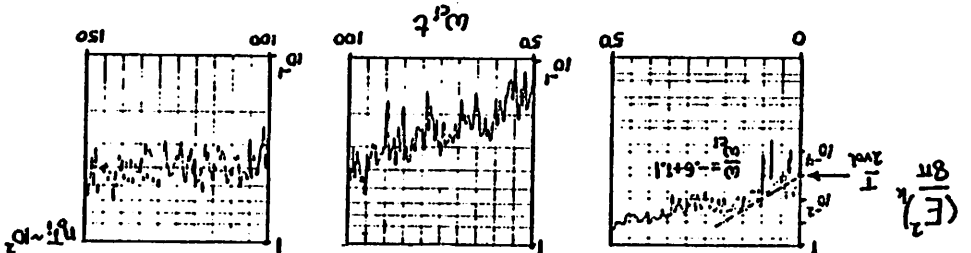
• $f_1(v, t=0) = \frac{1}{R} \frac{\exp(-v^2/2v_1^2)}{2\pi v_1^2 (R-1)} - \exp(-Rv^2/2v_1^2)$

$R=9 \quad R=1 \quad m_i/m_e = 1836 \quad \omega_p/\omega_{ci} = 3 \quad a_1/L_n = 2.7$

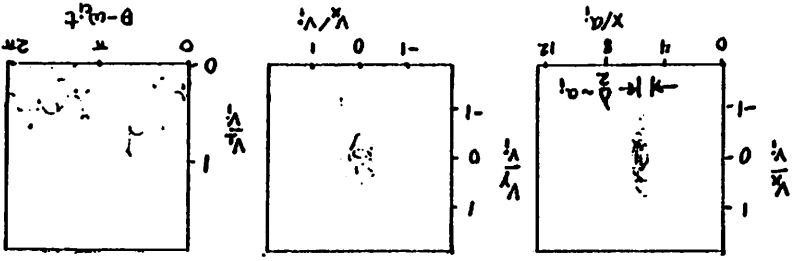


Unstable modes grow, trap ions, and fill in loss cone so $\partial f_1/\partial v_1^2 \leq 0$. $-\Delta L_n^2/L_n^2 \leq 0.01$ or 0.02 accompanies trapping. Results are insensitive to density profiles: linear, exponential, tanh.

• Electrostatic field energy density - most unstable mode, $ka_1=3$

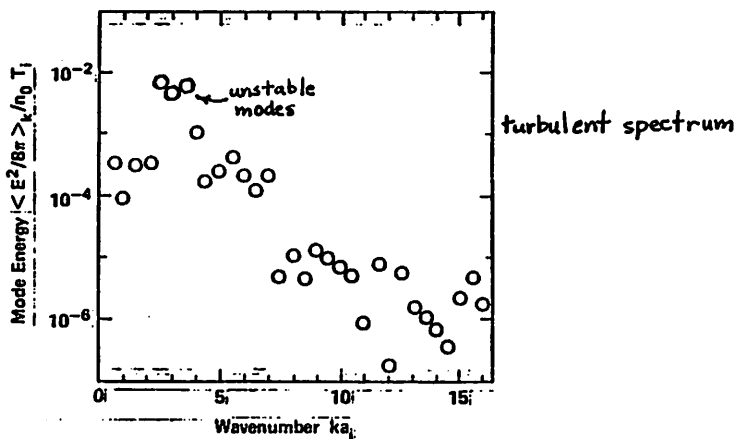
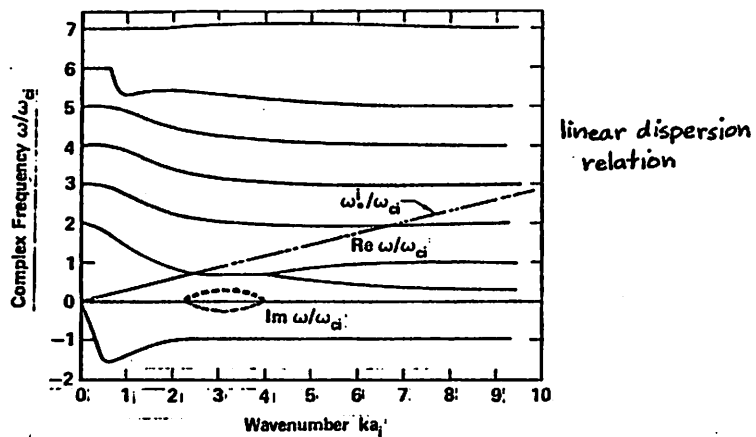


• Test ion orbit for $50 \leq \omega_{ci} t \leq 100$



uniform B_0

• multi-mode for $f_i(v_{\perp 1}, t=0) = \frac{R}{2\pi v_{\perp 1}^2 (R-\Gamma)} [\exp(-v_{\perp 1}^2/2v_{\perp 1}^2) - \Gamma \exp(-Rv_{\perp 1}^2/2v_{\perp 1}^2)]$ (a)



$R=9 \quad \Gamma=1 \quad \omega_{p1}/\omega_{c1}=3 \quad m_i/m_e=1836 \quad \kappa_{\perp 1}=0.29 \quad \Delta \kappa_{\perp 1}=0.5$

DCLC Saturation

- ion trapping in a single cyclotron harmonic flute mode $\omega \approx N\omega_{ci}$

trapping threshold: $\frac{Ne_0^2 k p J_N'(kp)}{m_i v_{\perp 1}^2} \geq |1 - \omega/N\omega_{ci}|$ $\rho \equiv v_{\perp 1}/\omega_{ci}$
 ref. Timofeev, Asmodt

e.g. $f_i(v_{\perp 1}) \propto d(v_{\perp 1} - v_0)$ $kp=2.5 \quad J_1'(2.5) \approx 1/2 \approx |1 - \omega/\omega_{ci}|$ $\frac{e_0^2 k^2}{2 \gamma_0} \geq O(1/2)$

e.g. $f_i(v_{\perp 1}) \propto$ subtracted Maxwell $\kappa_{\perp 1}=3 \quad |1 - \omega/\omega_{ci}| \approx 0.3$
 $0.1 T_i \leq m_i v_{\perp 1}^2 \leq 0.2 T_i \quad 0.1 \leq e_0^2 k^2 / T_i \leq 0.2$

- weakly nonlinear orbit and $f_i(v_{\perp 1})$ modification
 $\Delta \omega_{ci}^{nlr}, \Delta v_{\perp 1}^{nlr}, \Delta f_i^{nlr} \propto \phi_k^2$ single-wave theory (Myer-Simon)

$\frac{e_0^2 k^2}{T_i} \propto \gamma^{linear} \propto (dk/\kappa)^{1/2}$

- free energy balance estimate of saturation amplitude

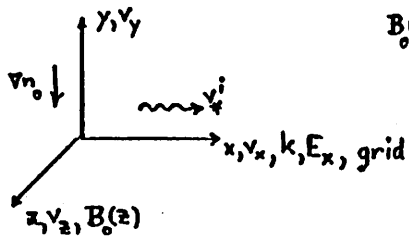
free energy $\Delta KE = KE(f_{v_{\perp 1}}^{unstable}) - KE(f_{v_{\perp 1}}^{stable}) \geq \omega \frac{\partial \epsilon}{\partial \omega} \frac{E^2}{8\pi}$ wave energy

$\rightarrow \omega \frac{\partial \epsilon}{\partial \omega} \frac{E^2}{8\pi} \leq O(1) KE_{loss-cone}$

$KE \equiv$ kinetic energy density

DCLC and Ion Bounce Mode Simulations
nonuniform \vec{B}_0

- "stretch" code to 6 phase-space dimensions $(x, y, z; v_x, v_y, v_z)$



$$B_0(z) = B_0 (1 + z^2/L_B^2)$$

$$m_i \frac{d\vec{v}_i}{dt} = e [\vec{E}_x \hat{x} + \vec{v}_i \times B_0(z) \hat{z}] c^{-1}$$

$$m_i \frac{dv_z}{dt} = -\mu \nabla B = -m_i \frac{v_z^2}{L_B^2}$$

$$\frac{d(x, y, z)}{dt} = (v_x, v_y, v_z)$$

flute-averaged ($k_z=0$) charge collection $\bar{n}_i(x, y=0) = \sum_{ions} S(x-x) V \left[\frac{Y_i^{just}(0)}{L_n} \right]$

- These equations only model mirror geometry approximately.

Note conservation laws in simulation code:

$$\frac{1}{2} m_i v_z^2 + \frac{1}{2} \frac{m_i v_\perp^2}{B_0} \frac{B_0^2}{L_B^2} = \text{const.}$$

not $v_\perp^2(z=0)$ as in lab. expt.

"particle energy"
in magnetic mirror

$$\sum_{ions} \frac{m_i v_\perp^2}{2} + \int dx^2 \frac{E_x^2}{8\pi} = \text{const.}$$

not $v_\perp^2 + v_\parallel^2$

total system "perpendicular energy"

Stretched ESI Code Performance on CRAY

typical parameters

$$\omega_{ci} \Delta t = 0.1 \quad \omega_{pi} \Delta t \leq 2 \quad \omega_{pi} / \omega_{ci} \leq 20$$

$$N_{ion} = 200,000 \quad n_{grid} = 128$$

$$\omega_{ci} t_{final} \leq 150-250 \quad \tau_{CRAY}^{final} \leq 1 - 1\frac{1}{2} \text{ hr.}$$

$$\langle \omega_{bounce} \rangle / \omega_{ci} \sim 0.2 \quad \langle \omega_{bounce} \rangle \frac{t_{final}}{2\pi} \lesssim 5-8$$

one disc record = $\frac{6400 \text{ ions} \times 6 \text{ phase-space variables}}{2 \text{ packed words per stored word}} = 19,200 \text{ words}$

$$200,000 \text{ ions} = 32 \text{ records}$$

CRAY vectorized particle push — 5 μsec / particle Δt
move & accel.
pack/unpack

needs improvement \rightsquigarrow 15 μsec / particle Δt
I/O
not overlapped

total 20 μsec / particle Δt

- In theory, one writes the flute-averaged dispersion relation

$$0 = \int_{-L_\phi/2}^{L_\phi/2} \frac{ds}{B} \left[1 + \frac{\omega_{pe}^2(s)}{\omega_{ce}^2(s)} - \frac{\omega_{pe}^2(s)}{\omega_{ce}(s)\omega} \frac{1}{kL_n} - \frac{4\pi e n_{i,k}}{k^2 \Phi_k} \right],$$

$L_\phi \equiv$ length over which mode is flute-like.

With

$$\omega_{pe}^2(s) = \omega_{pe}^2(0) \exp(-s^2/L_p^2)$$

$$\omega_{ce}(s) = \omega_{ce}(0) (1 + s^2/L_m^2)$$

$$L_p = \sqrt{2} \Delta L_m, \quad \Delta^2 = T_{||} / T_{\perp} \ll 1,$$

dispersion relation is

$$0 = \frac{L_\phi}{B_0} \left\{ 1 + \frac{\sqrt{\pi} L_p}{L_\phi} \left[\frac{\omega_{pe}^2(0)}{\omega_{ce}^2(0)} - \frac{\omega_{pe}^2(0)}{\omega_{ce}(0)\omega} \frac{1}{kL_n} - \frac{4\pi e \bar{n}_{i,k}}{k^2 \Phi_k} \right] \right\}.$$

Poisson equation in simulation code (see p. 3)

is consistent with theory if we let $\sqrt{\pi} L_p / L_\phi = 1$

and set $[\omega_{pe}^2(0)]_{\text{theory}} = [\omega_{pe}^2]_{\text{code}}$.

Why must we include ion bouncing in linear theory?

- In simulations we choose a relatively large value of

$$\frac{\omega_{bi}}{\omega_{ci}} = \frac{\text{bounce frequency of typical ion}}{\text{ion cyclotron frequency}}$$

because we want (run time) = many bounce periods

- Thus, we violate condition for neglect of bouncing [Berk & Pearlstein, Phys. Fluids 14, 1810 (1971)], which is

$$1 \lesssim \frac{\Delta \xi}{\pi} = \frac{1}{4} \frac{\omega_{ci}}{\omega_{bi}} \frac{T_{||}}{T_{\perp}},$$

where $\Delta \xi$ is thermal spread in

$$\xi \equiv \int_0^{\pi/2\omega_b} dt [\omega_{ci}(t) - \text{Re } \omega]$$

↑ integral along ion trajectory

Dispersion relation (flute-avg'd, local approx.)

$$0 = D = 1 + \frac{\omega_{pe}^2}{\omega_{ce}^2} - \frac{\omega_{pe}^2}{\omega_{ce}^2} \frac{1}{\omega k L_n} + \chi_i$$

$$\chi_i = \frac{\omega_{pi}^2}{k^2} \frac{B_0}{L_\varphi} \iint dE d\mu \frac{(2\pi)^2}{\omega_b} \sum_{l,p} J_l^2\left(\frac{k v_\perp}{\omega_{ci}}\right) J_p^2\left(\frac{l \tilde{\omega}_{ci}}{4\omega_b}\right) \times$$

$$\frac{\left[\frac{k}{L_n \omega_{ci}} + \left(\frac{l \omega_{ci}}{B_0}\right) \left(\bar{B} \frac{\partial}{\partial E} + \frac{\partial}{\partial \mu} \right) + 2p \omega_b \frac{\partial}{\partial E} \right] f_i(E, \mu)}{\omega - l \bar{\omega}_{ci} - 2p \omega_b}$$

$\omega_b = v_\perp / L_m$, ω_{ci} = ion cyclotron frequency at midplane

$$\frac{\tilde{\omega}_{ci}}{\omega_{ci}} = \frac{B_{\text{turning point}}}{B_0} - 1 = \frac{v_\parallel^2}{v_\perp^2}, \quad \bar{\omega}_{ci} = 1 + \frac{\tilde{\omega}_{ci}}{2\omega_{ci}}$$

$$f_i = F(v_\perp) G(\varphi), \quad \varphi \equiv v_\parallel / v_\perp$$

$$F(v_\perp) \propto \exp(-\alpha v_\perp^2) - \exp(-R \alpha v_\perp^2)$$

$$G(\varphi) \propto \exp(-\varphi^2 / 2\Delta^2), \quad \Delta^2 = T_\parallel / T_\perp$$

In limit $\Delta \rightarrow 0$, $L_\varphi = \sqrt{\pi} L_p$, the dispersion relation reduces to the infinite-medium DCLC result

$$\chi_i = \frac{\omega_{pi}^2}{k^2} \frac{2\alpha}{1-R^{-1}} \sum_l \frac{l}{(\omega/\omega_{ci}) - l} \left[e^{-b} I_l(b) - e^{-b/R} I_l(b/R) \right]$$

$$b \equiv (k/\omega_{ci})^2 / 2\alpha.$$

Nonlinear effects in DCLC/ion bounce mode simulations

- Ion trapping as described by Timofeev, Nucl. Fusion 14, 165 ('74), can occur for ions with
$$\frac{J}{\mu} = \frac{W_\parallel}{W_\perp} \frac{\omega_{ci}^0}{\omega_b} \lesssim \frac{4}{L}.$$

Trapping threshold:

$$\frac{L e \Phi_k k p}{m_i v_\perp^2} J_L(k p) J_0(LJ/4\mu) \geq \left| \frac{\omega}{L \omega_{ci}^0} - 1 \right|, \quad \rho \equiv v_\perp / \omega_{ci}^0.$$

Uniform- B_0 limit recovered for $J = W_\parallel = 0$. In simulations, trapping behavior similar to earlier uniform- B_0 simulations has been observed.

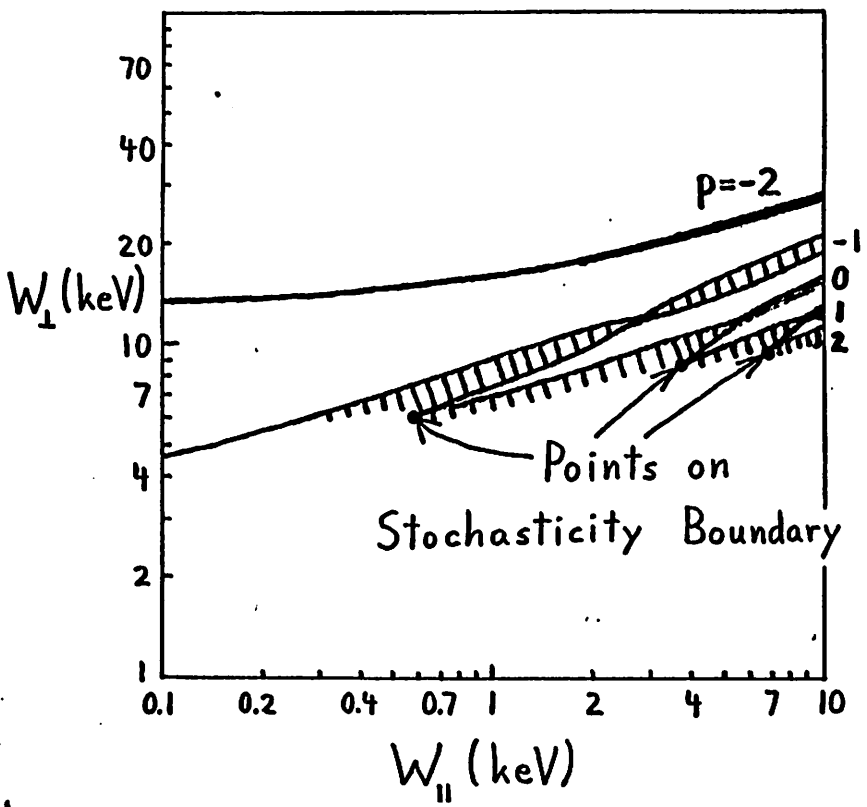
- Weakly nonlinear orbit and $f_i(v_\perp)$ modification
$$\Delta \omega_{ci}^{nlr}, \Delta v_\perp^{nlr}, \Delta f_i^{nlr} \propto \Phi_k^2 \text{ single-wave theory}$$

$$e \Phi_k / T_i \propto \gamma^{\text{linear}} \propto (\delta k / k)^{1/2}$$
 Bouncing modifies these effects.

- Quasilinear diffusion of $f_i(v_\perp)$
 - (1) Saturation has been observed to occur by $\Delta \omega_{ci}^{nlr}$ or ion trapping effects. Accompanying amplitude oscillations of unstable modes and thermal fluctuations diffuse ion v_\perp 's, filling loss cone.
 - (2) Overlap of resonances $\omega - L \bar{\omega}_{ci} + 2p \omega_b = 0$ due to a single mode leads to stochasticity. See Smith, Byers, & LoDestro, Phys. Fluids (Jan, '80).

Plot of Finite-Width Resonances

Parameters: $l=1$, $\omega = \Omega_0 = 2.8 \times 10^7 \text{ sec}^{-1}$,
 $L=60 \text{ cm}$, $R_g=30 \text{ cm}$, $q\Phi_0 = 100 \text{ eV}$,
 $k = 1 \text{ cm}^{-1}$, $M = M_{\text{Deuteron}}$



Above plot illustrates this conclusion (verified by calculating trajectories of single ions):

[high-energy ions move superadiabatically
 low-energy ions move stochastically]

Conditions for observing superadiabaticity in simulation:

1. Unstable mode must saturate at amplitude significantly above thermal level
2. This mode, in saturated state, must not exhibit large amplitude oscillations with period $< \pi/\omega_{bi}$

Conditions for observing quasilinear diffusion due to a single mode in simulation

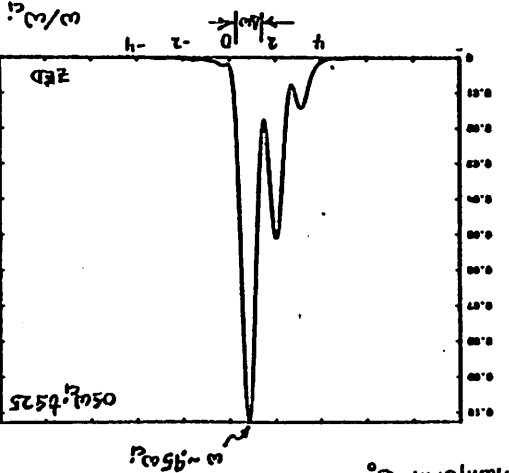
1. If $\omega < \omega_{ci}$, the mode causes exponentially small jumps Δv_{\perp} unless

$$|\omega - \omega_{ci}| < (\omega_{ci} v_{\parallel}^2 / L_m^2)^{1/3} \sim \omega_{ci} (T_{\parallel} / T_{\perp})^{1/3} (\rho / L_m)^{2/3}$$
2. For any ω , the mode must cause larger Δv_{\perp} than the thermal fluctuations with $\omega \approx \omega_{ci}$

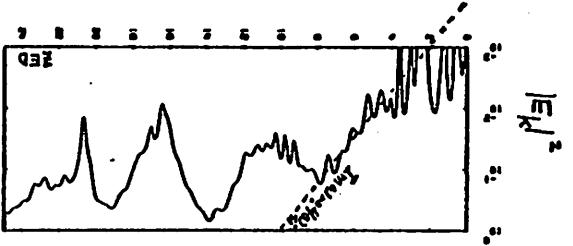
With care, these conditions can be met.

DCLC/ion bounce mode simulations

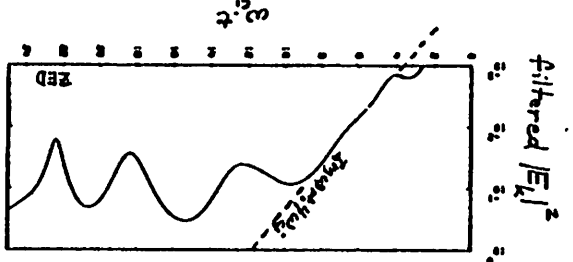
nonuniform B₀



$f(\nu) = F(\nu) G(\nu/V)$
 loss cone question
 $\omega_p/\omega_c1 = r_1 a_1 = 1.4 a_1 = 5$
 $m_i/m_e = 3672$ $R = 2$
 $T_1/T_2 = 0.1$ $F = 1$
 • single mode $k_{\perp} = 3.5$
 $\omega_{DCLC} \text{ theory} = 0.91 + i.41$



unfiltered field energy



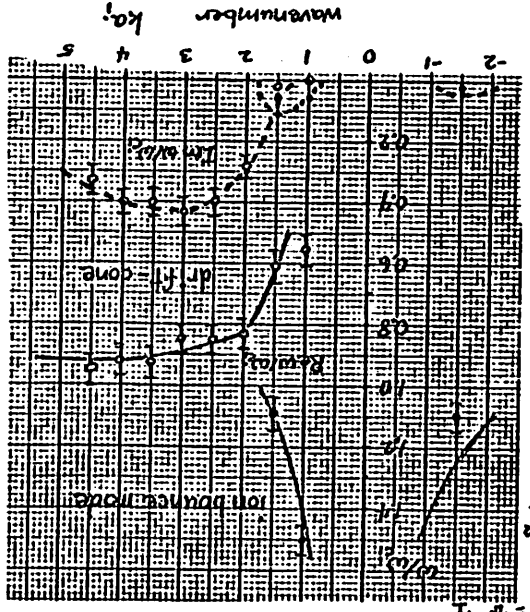
frequency filtered field energy
 $\int d\omega |E(k, \omega)|^2$

ZED (20MAR editor and post-processor, A.B. Langdon) implemented and exercised by Bill Nevins

Simulation of DCLC/ion bounce modes

• $f(\nu) = (\pi)^{-1} \Delta^{-1} \exp(-\phi^2/2\Delta^2) R [E \pi \nu^2 (E-N)] [E \phi (-\nu^2/2\nu^2) - \text{Exp}(-R \nu^2/2\nu^2)]$
 nonuniform B₀

$\omega_c1/\omega_c2 = 0.2$ $m_i/m_e = 3672$
 $\nu_1/\nu_2 = 5$ $R = 2$ $T_1/T_2 = 0.1 = \Delta^2$
 $\phi = \nu_1/\nu_2$



linear dispersion relation

Ion bounce modes have frequencies ω_c1 , lower growth rates ($\text{Im} \omega < \omega_p$), and longer wavelengths, and they can propagate in $\pm \nu_1$ directions.

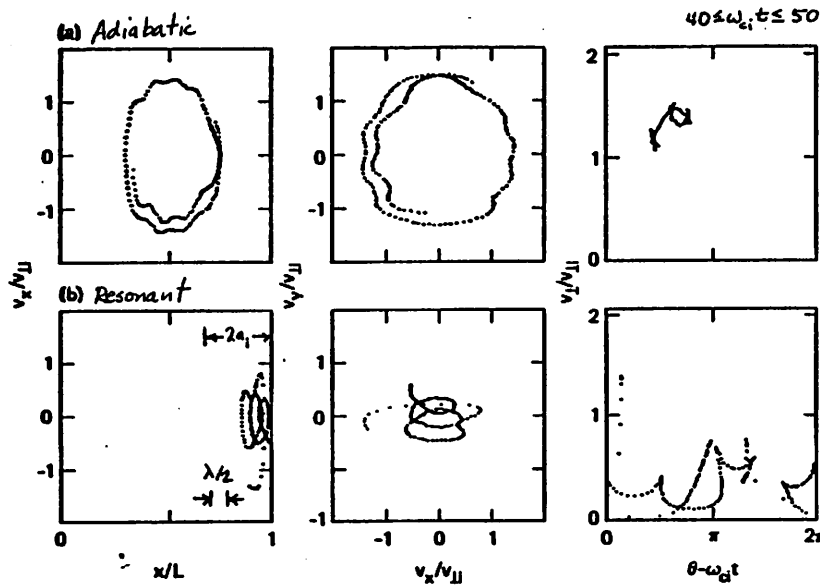
Particle Orbits in a Single-Harmonic Ion Cyclotron Wave: $\omega \sim \omega_{ci}$

28 The COT Computers:

A High-Performance Low-Cost System for Particle and Hybrid Simulations

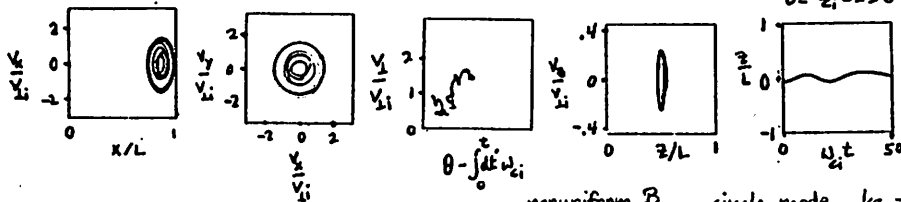
Robert W. Huff

John M. Dawson



$40 \leq \omega_i t \leq 50$

(c) Resonant with ion bouncing



$0 \leq \omega_i t \leq 50$

uniform B_0 $\frac{m_i}{m_e} = \frac{\omega_{pi}^2}{\omega_{ci}^2} = 100$ $\frac{L_n}{a_i} = 4.4$ $ka_i =$

nonuniform B_0 single mode $ka_i = 2.5$

$\omega_{pi}/\omega_{ci} = 5$ $m_i/m_e = 3672$ $T_{ii}/T_{ie} = 0.1$ $a_i/r_p = a_i/r_B = 0.2$ $P=1$ $R=2$

PRINCIPAL CHARACTERISTICS

OF THE

CHI COMPUTER SYSTEM

HIGH COMPUTING EFFICIENCY

Large-scale problems
High Speed
Comparable to CDC 7600

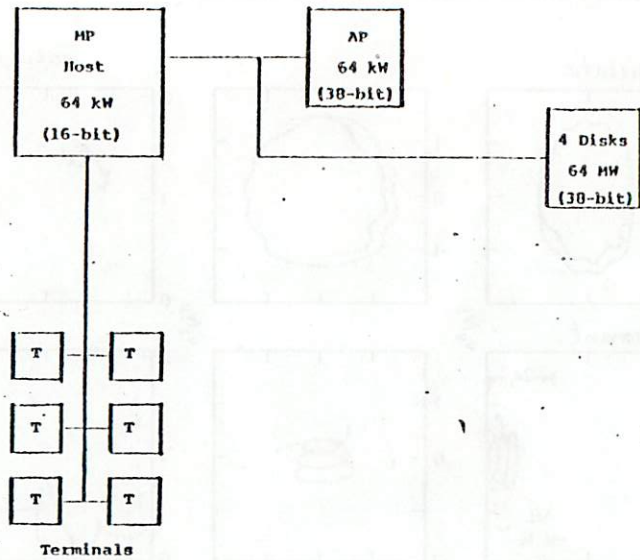
HIGH PROGRAMMER EFFICIENCY

Simple and natural language
Convenient graphics
Interactive access
Usable directly by the physicist

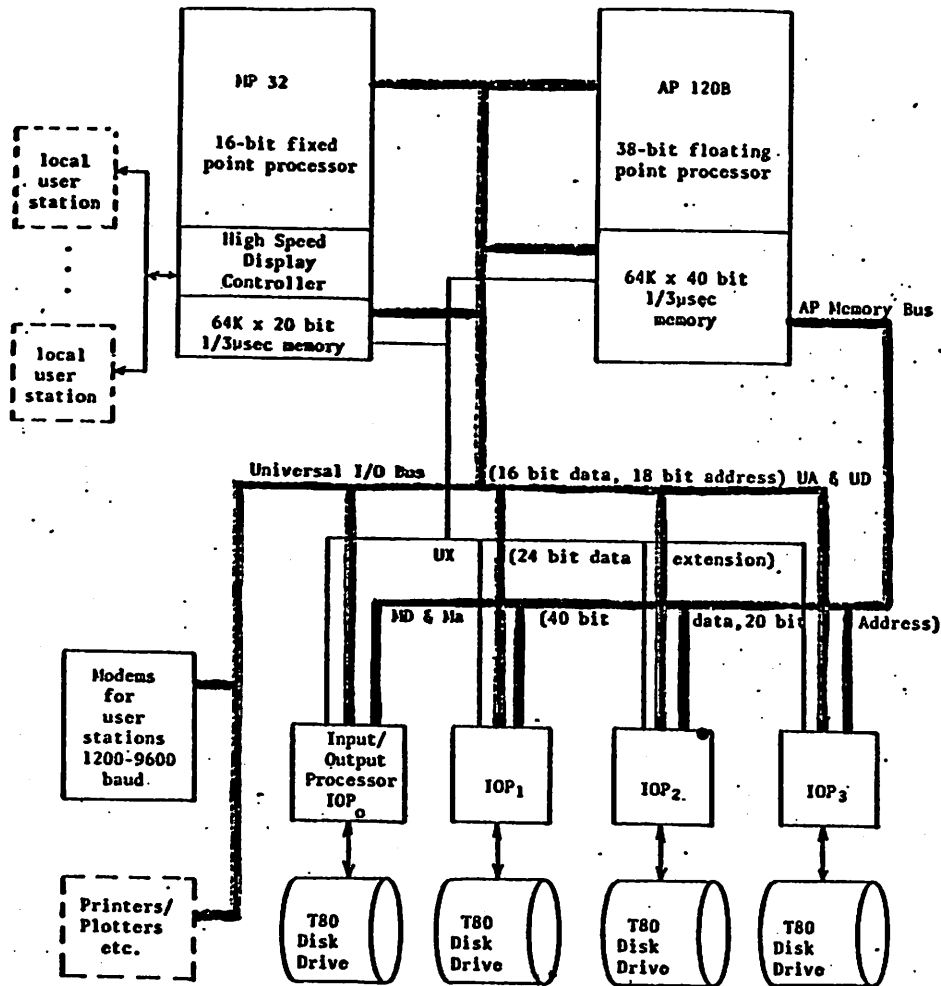
LOW COST

Comparable to minicomputers
3% of CDC 7600

CHI COMPUTER STRUCTURE



STRUCTURE OF CHI COMPUTER SYSTEM



DATA THROUGHPUT AND CAPACITY

Macro Processor (MP-32A)

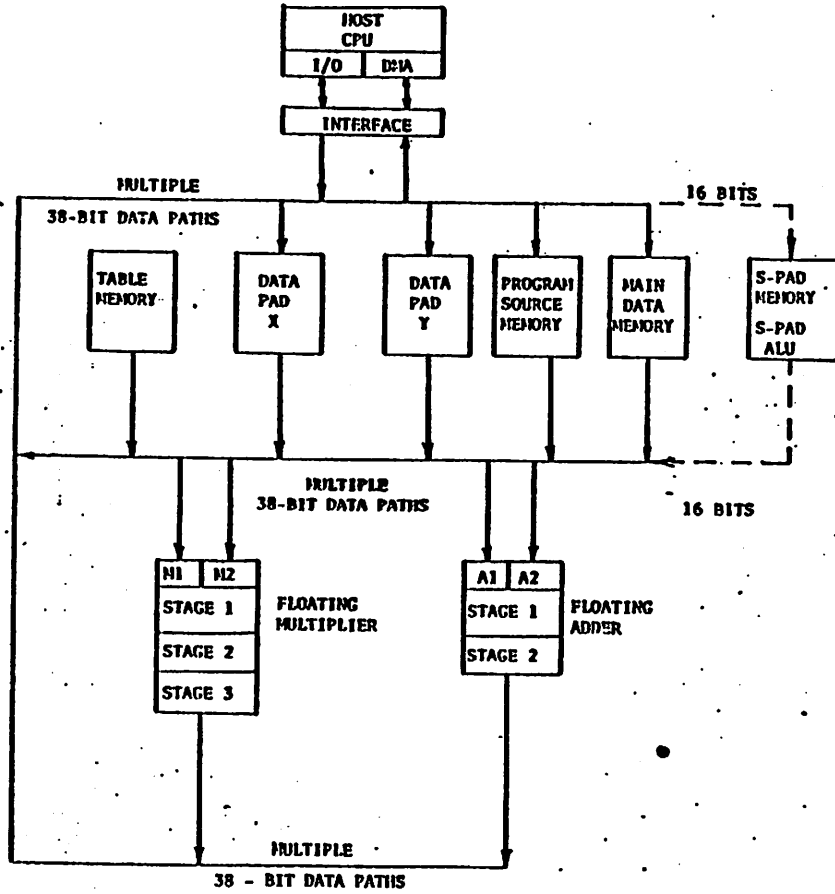
16-bit fixed point processor 167 nanosecond cycle

64 words scratch pad data memory
 512 words fixed instruction memory
 64 words writeable instruction memory
 65,536 words of 1/3μsecond instruction and data memory (CD)

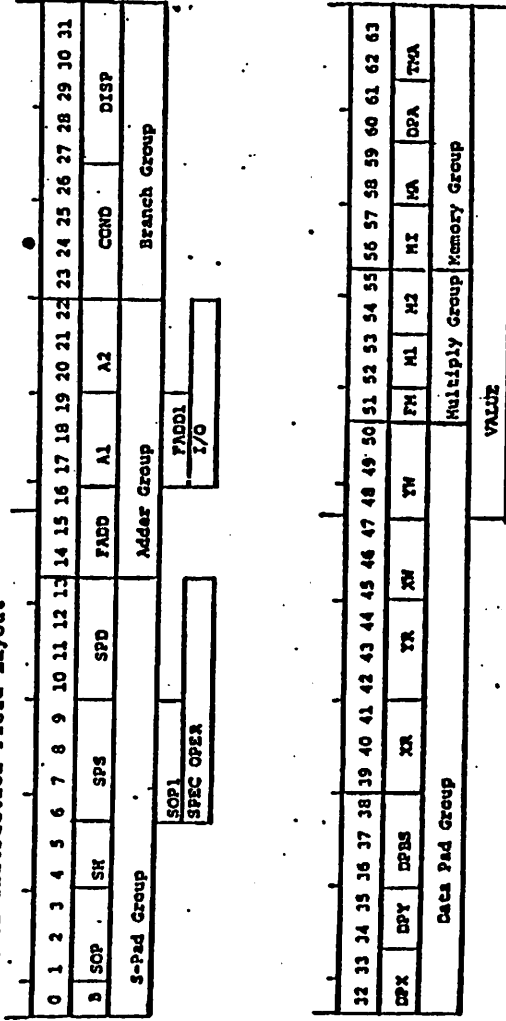
16 x 16 multiply in 333 nanoseconds

- Controls high-speed local station displays
 - Display rate: 2μsec/point
 - <2μsec for longest line
 - >4000 characters/second
- Schedules IOPs and Array Processor
- Controls data transfer to modems (1200-9600 baud) and other PDP-11 compatible I/O devices over Universal I/O bus

AP 120 B BLOCK STRUCTURE



AP-120B Instruction Field Layout



DATA THROUGHPUT AND CAPACITY

Disk - IOPs

4 Trident T80 drives -- over 16 million 38-bit words each

All four can be simultaneously transferring data to/from AP-MD or MP-CD, each at 250,000 words/second.

Any IOP can be used for memory transfer between AP-MD and MP-CD at 1,000,000 words/second.

Array Processor (AP-120B)

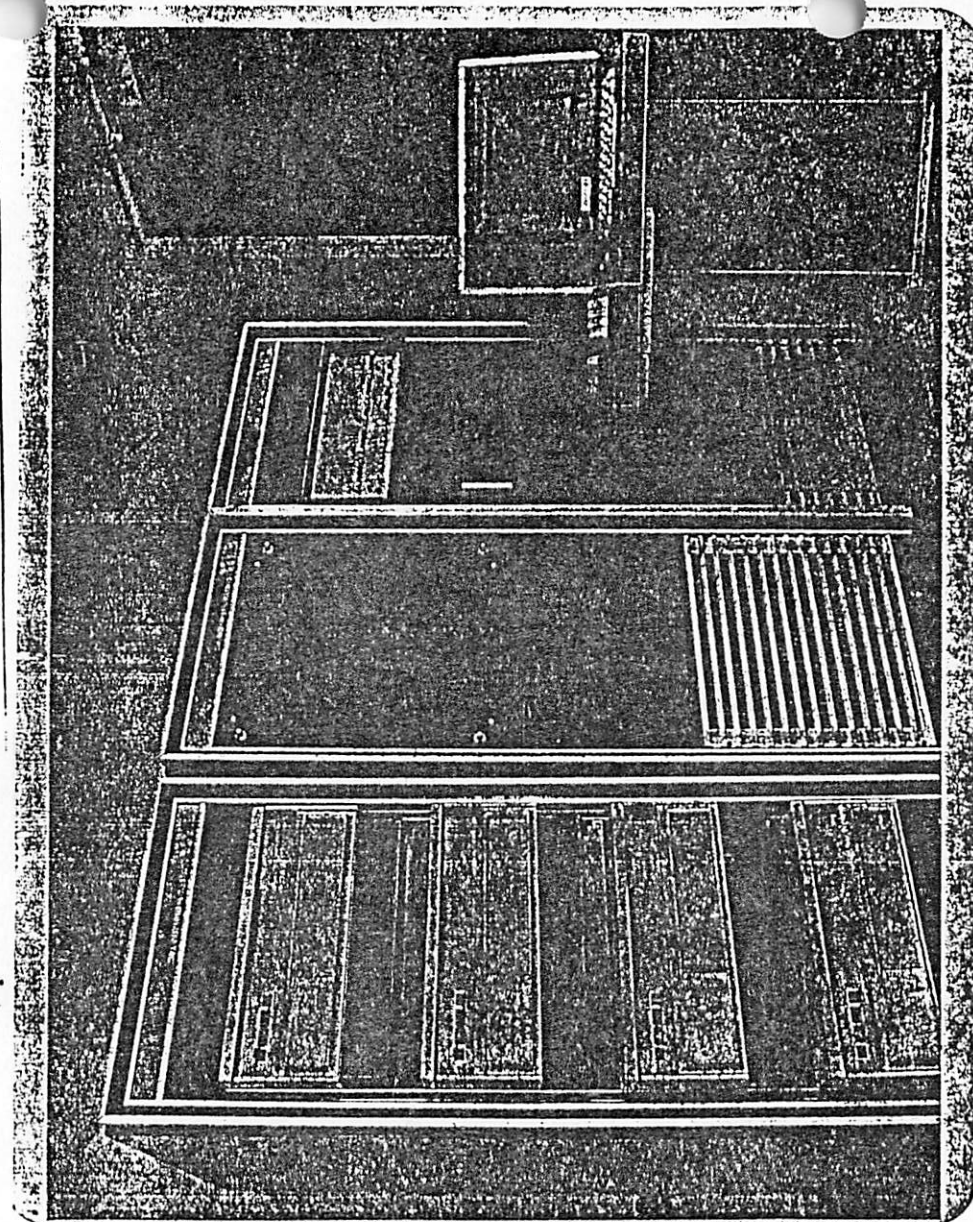
Very high-speed 38-bit floating point arithmetic unit

Two 32-word scratch pad data memories,
2560 words $1/3\mu\text{sec}$ fixed table memory
65536 words $1/3\mu\text{sec}$ data memory (MD)
512 words instruction memory

All memories can be referenced in one 167 nanosecond machine cycle.

Operation Times:

Vector add, multiply, subtract	$1\mu\text{sec/point}$
Vector SQRT, divide	$1.8\mu\text{sec/point}$
Vector EXP, LOG, SIN	$5-6\mu\text{sec/point}$



EXAMPLE OF CH1 MATH SYSTEM LANGUAGE

For the Vector Calculation: $C_i = \text{SIN}(A_i + B_i)$ Keypushes

⊕ A, B → C

SIN

DISPLAY

Operations Performed $C(i) = A(i) + B(i)$ for all i $C(i) = \sin C(i)$ for all i plot $C(i)$ versus i SECTION OF MATH SYSTEM PROGRAM
TO
INTERLEAVE DISK TRANSFERS WITH COMPUTATIONMath System Program

```

. . .
. . .
. . .
. . .
MOVE INDISK → BUFF3
MOVE BUFF1 → OUTDISK
OP PUSH BUFF2
MOVE INDISK → BUFF1
MOVE BUFF2 → OUTDISK
OP PUSH BUFF3
MOVE INDISK → BUFF2
MOVE BUFF3 → OUTDISK
OP PUSH BUFF1
. . .
. . .
. . .

```

Processors Involved

```

IOP1, Disk 1
IOP2, Disk 2
AP
IOP1, Disk 1
IOP2, Disk 2
AP
IOP1, Disk 1
IOP2, Disk 2
AP

```

```

FORCE COMPUTATION, DIPOLE SCHEME

INCLUDE DIPOLE CORRECTIONS TO CHARGE ARRAY

MULT HALF,C+FY SUBT CX,FY MULT HALF SUBT CY,FY MULT HALF
RS CX+FY LS FY+X,0+ ADD C,FY LS CX+FY RS FY+X,NX-1+ SUBT C,FY
MOVE CY+CX ADD C,CYR SUBT CYL

COMPUTE FOURIER TRANSFORM OF CHARGE ARRAY

OP FFTR C,KY,NX,NY

GET FACTOR ARRAYS FROM DISK, AND COMPUTE FIELD ENERGY

MOVE FFE+CX FF+F SQ C MULT CX OP SUM C,FE

COMPUTE FORCE COMPONENTS & DERIVATIVES VIA INVERSE FOURIER TRANSFORMS

N MULT FC+INF+,CXC OP IFTER FC+INF+,KY,NX,NY INC INF GO TO N
END

```

STRUCTURE AND TIMING - ELECTROSTATIC PARTICLE SIMULATION
1,000,000 Particles - 32 x 32 Grid

Data:

6 Words/particle x, y, z, v_x, v_y, v_z
8 Words/gridpoint: $E_x, E_y, E_{xx}, E_{xy} = E_{yx}, E_{yy}, C, D_x, D_y$

The particle descriptors are on disk, 667 particles/track, 1500 tracks, or 750 tracks on each of two disks for input, and the same for output, with the two pairs of disks being interchanged with respect to I/O at each timestep.

AP-Memory Allocation:

Electric Field arrays (5)	5k
Charge and dipole arrays (3):	3k
Particle buffers (12)	<u>48k</u>
Total	56k

Data Transfer Timing:

60 disk rotations/second or 16.7 ns/track, for a transfer rate of 25 μ s/particle for each of two disks, or an overall rate of 12.5 μ s/particle on a track-by-track basis. Loss of one rotation at the cylinder boundary (5 tracks/cylinder) increases this by 20%, giving 15 μ s/particle on a cylinder-by-cylinder basis.

Processing Time:

Dominated by the particle-push AP routine for this system size. Present AP code estimated at 13 μ s/particle. Thus the AP processing is slower than the I/O on a track-by-track basis, but is faster than the I/O on an overall basis.

Overall Timing:

15 μ s/particle overall, or 15 seconds/timestep.
16 hours for a run of 4000 timesteps (to $\omega_p t = 1000 @ \Delta t = 0.25/\omega_p$)

SPEED COMPARISONS

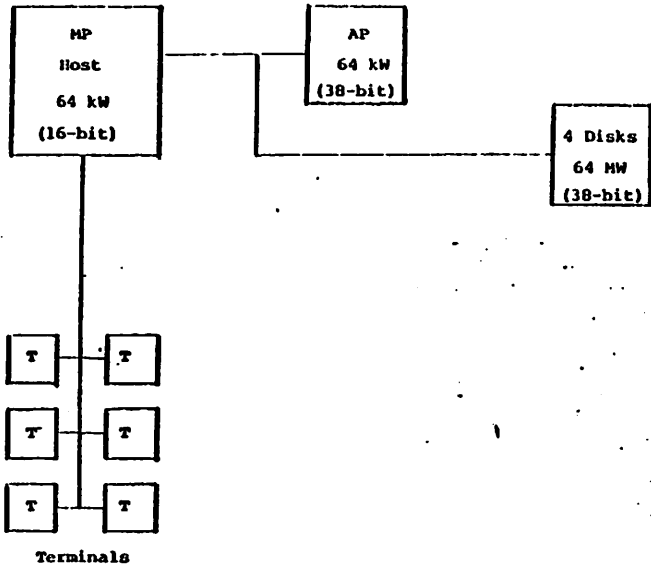
	IBM360/91	CII SYSTEM
PARTICLE CODE		
Time/Particle Push	Assembly Code	
CPU	55 μ s	13 μ s
I/O	--	0.6 x 25 μ s
Overall	55 μ s	15 μ s
RUN: 10 ⁶ Particles, 4000 Timesteps		
Total Time	<u>61 hr</u>	<u>16 hr</u>
2-1/2D MHD CODE		
Time/Gridpoint	Fortran Code (H-Compiler)	
	130 μ s	50 μ s
3D MHD CODE		
Time/Gridpoint	Fortran (H-Compiler)	
	230 μ s	100 μ s
RUN: 64 ³ System, 4000 Timesteps		
Total Time	<u>33 hr</u>	<u>14 hr</u>

CII APPLICATION CODES as of NOVEMBER 1979

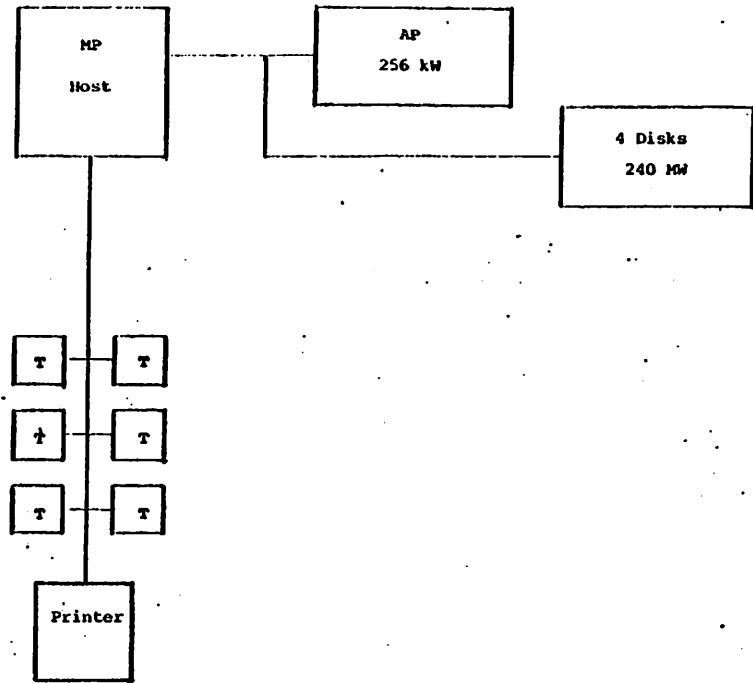
Types: MS = Math System language only, AP = some portion in AP microcode
 Status: W = Working Code, D = Under Development, P = Planned

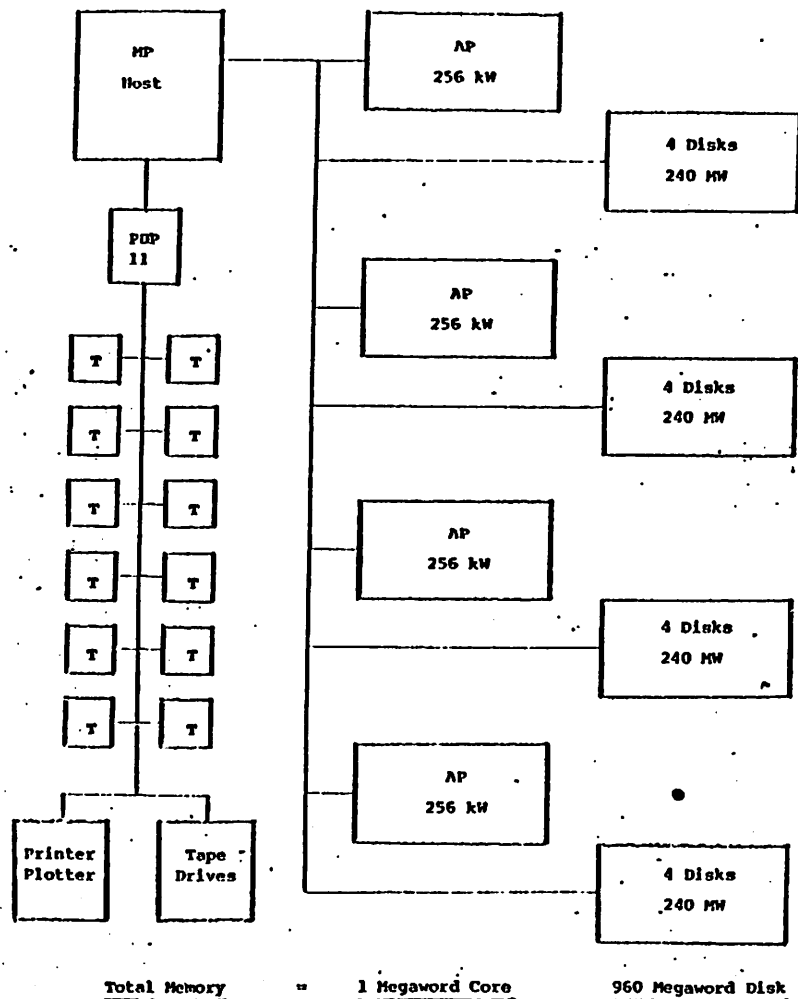
Code	Type	Status	Applications
2½D Electrostatic Particle Simulations (bounded and unbounded)	AP	W D	Transport Studies Heating Studies (with TRW) Non-equilibrium fluctuations (with MIT) Stochasticity studies Surface Bernstein modes
2½D Fluid MHD (Linear & Nonlinear)	AP	W	Tearing mode Coalescence of magnetic islands
3D Fluid MHD	AP	W P	Field reversal Toroidal-geometry tearing mode Toroidal-geometry magnetic-island coalescence
2½D Hybrid	AP	D	Kelvin-Helmholtz instability (Interchange instability) Ballooning modes in Surmac
3D Hybrid	AP	P	Tokamak studies NASA Astrophysical studies
MHD Equilibrium	AP	D	GA Doublet III equilibrium analysis
Molecular	AP	W D	Chemical molecular dynamics
Landau Damping	AP	W	Spatial Landau Damping
Two Stream	MS	W	Effects of DC electric field on beam instability Explosive instability in multipoles
Thin Sheath	MS	W	Drift-waves in thin sheaths
Trajectory Integration	MS	W	Tokamak particle orbits
Adiabatic-Invariant Integration	MS	W	Stochasticity onset in mirrors
Real & complex analysis library	MS	W D P	Variety of smaller problems whose on-line, interactive analysis develops the users' intuition
Display library	AP	W D P	Advanced displays, e.g. 3D projections Contour plots Field plots Phase-space plots

CHI COMPUTER STRUCTURE



CHI COMPUTER STRUCTURE -- First Expansion





29 ZED-

W.M. Morris

A Post processor for
Analyzing time histories

written by A.B. Langdon

Used on MFE Computer for
analyzing data from

EZOHAR (Y. Matsuda, K. Matsuda...)

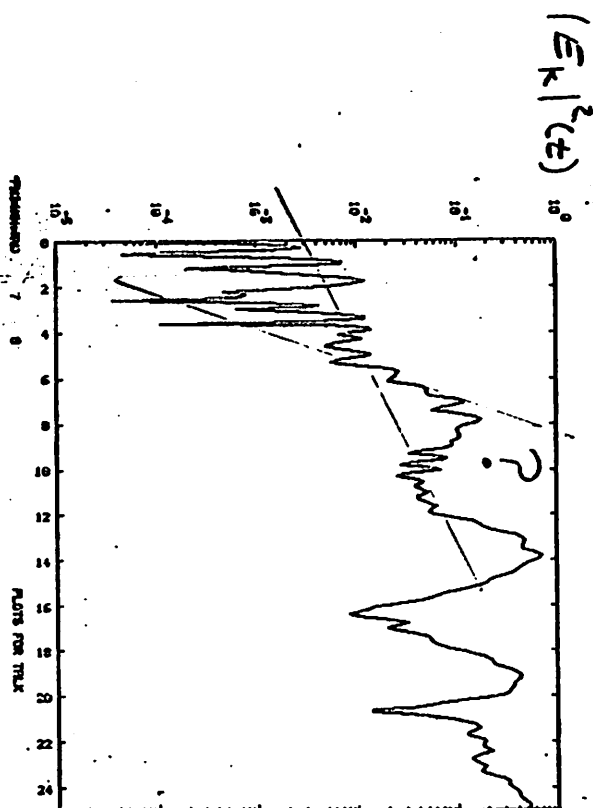
Princeton 2 1/2 d Electrostatic
Particle Code (ev. w. Lee)

Princeton 2 1/2 d Magnetostatic
Particle Code (w. w. Lee)

ESI (Birdsall + Students, B. Fairley)

Strachan ESI (B. Cohen)

a linearized Gyro-kinetic Code



Two Tools

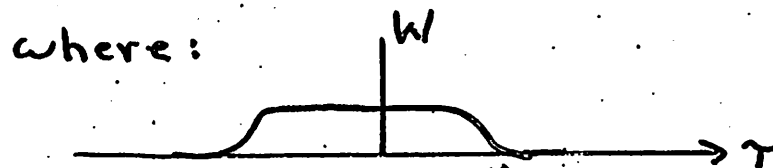
1) correlation functions / spectral densities

$$C_{AB}(\tau) \equiv \frac{1}{(t_2 - t_1)} \int_{t_1}^{t_2} A(t+\tau) B^*(t) dt$$

$$S_{AB}(\omega) \equiv \int d\tau C_{AB}(\tau) e^{i\omega\tau}$$

2) Digital Filtering:

$$\tilde{A}(t) = \int d\tau A(t+\tau) W(\tau) e^{i\omega_0\tau}$$



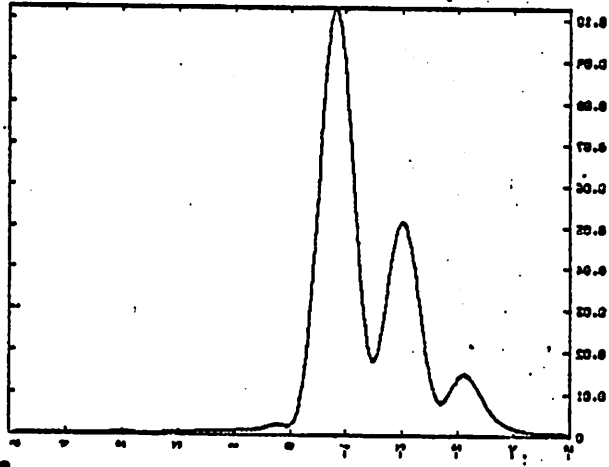
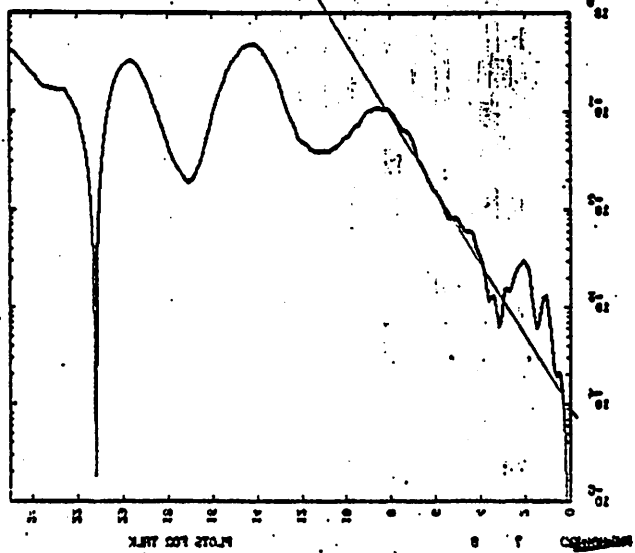


FIGURE 1 8
 PLOTS FOR DATA
 NUMBER: 100
 10.00 MIN 10
 1.00 TIME INTERVAL
 20.00 MAX RANGE

410

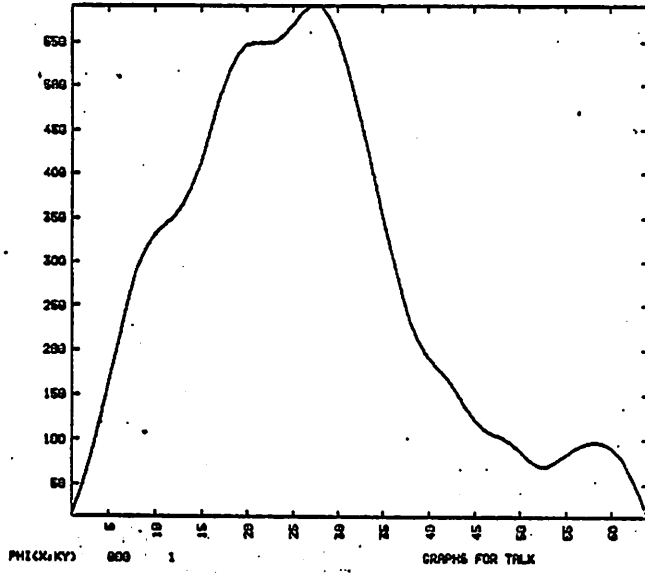


$\frac{dI}{dt}$

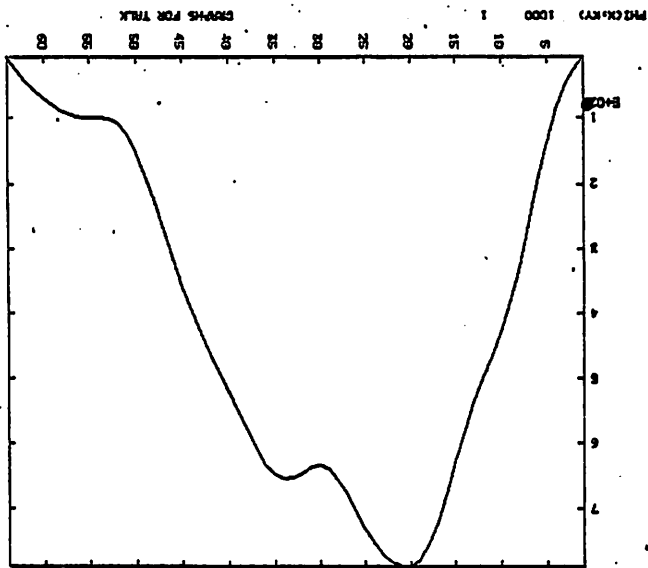
411

413

7/17



214



6/16

(15)

414

415

Mode Structures

1) Calculate the cross-correlation

$$C_{\phi(x)\phi(x')}(\tau) = \int dt \phi(x, t+\tau) \phi^*(x', t)$$

Transform to cross-spectrum:

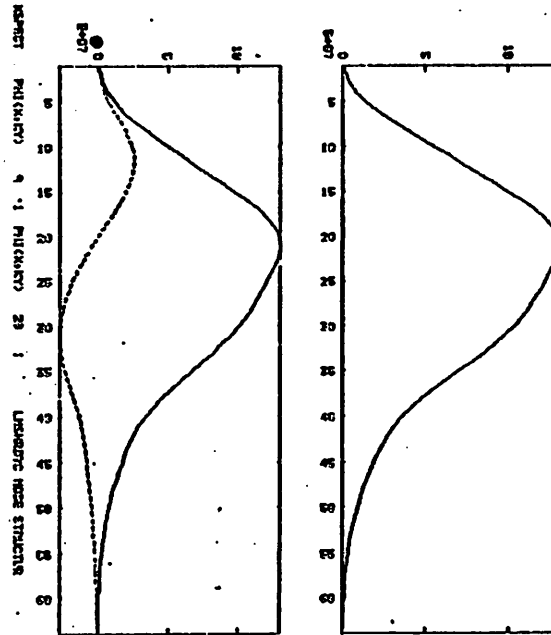
$$S_{\phi}(x, x', \omega) = \int d\tau C_{\phi}(x, x', \tau) e^{i\omega\tau}$$

Note that

$$S_{\phi}(x, x', \omega) \doteq \phi(x, \omega) \phi^*(x', \omega)$$

hence a plot of S_{ϕ} vs. x

at fixed (x', ω) gives the normal mode structure.



Fluctuations in an Inhomogeneous Plasma

① Usual Tools for evaluating fluctuation levels, i.e.

$$\frac{|E_k|^2}{8\pi} \approx \frac{\frac{1}{2} T}{1+k^2 \lambda_d^2} \quad \left(\begin{array}{l} \text{fluctuation -} \\ \text{response theorem} \end{array} \right)$$

$$\frac{|E_{k,z}|^2}{8\pi} = \frac{\frac{1}{2} T}{\omega_z \frac{\partial \epsilon}{\partial \omega_z}} \quad \left(\begin{array}{l} \text{fluctuation -} \\ \text{dissipation} \\ \text{theorem} \end{array} \right)$$

Assume Thermal Equilibrium

⇒ Must BE Discarded

IN AN INHOMOGENEOUS
PLASMA!

How to Calculate The fluctuation level of normal modes in an inhomogeneous Plasma?

Use Test particle Theorem.

Liu Chen + I have done for

- Electrostatic
- 1 non-ignorable coordinate
- Differentially response, i.e. mode Eqn is

$$\phi'' + k^2 \phi = 0$$

- convectively unstable plasma

418

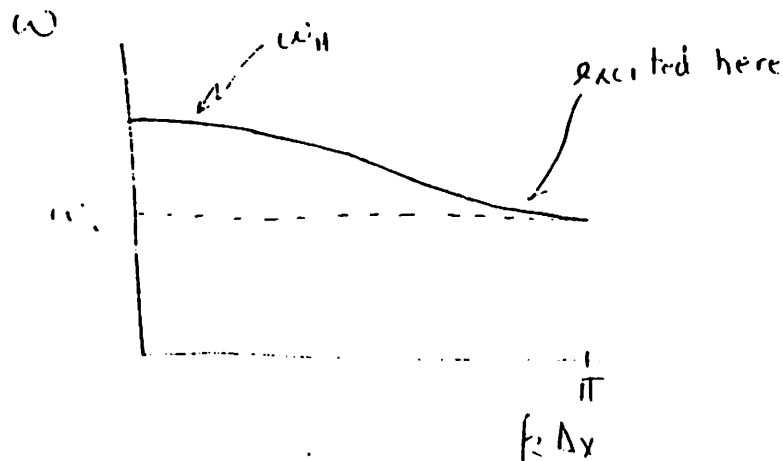
30 Alias Growth of Hybrid Oscillations ³⁰Due to Initialization at $k \Delta x \rightarrow \pi$

Vince Thomas (K. Birdsall)

A 1-D, periodic, electrostatic code ESE was used to simulate hybrid oscillations in a cold uniform plasma. Linear weighting was used.

$$\begin{aligned} N_p &= 2048 & \omega_p &= 5.0 & x_i &= 10^{-6} \\ N_s &= 32 & \omega_i &= 0.5 & l &= 32 \\ \omega_p &= 1.0 & k \Delta x &> \pi/2 \end{aligned}$$

One expects ω_p to decrease toward ω_c as $k \Delta x$ is increased toward π . This did happen, but together with the aliasing energy non-conservation was observed.



In Addition to $\omega_e = (\Omega_e, \delta_e)$ and $\phi_e(x)$
Must Calculate

$$A_e \sim e^{i \int_{x_0}^{x_m} k dx}$$

$$T_e = \oint \frac{dx}{v_g} ; v_g = \left(\frac{\partial k}{\partial \omega} \right)^{-1}$$

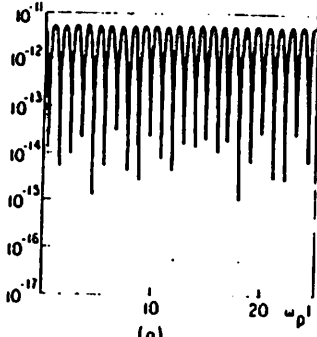
Then we find

$$\left\langle \frac{e \phi_e(x)}{\pi} \frac{e \phi_e^*(x')}{\pi} \right\rangle \sim \frac{1}{\underbrace{n_p \rho_s^2 L_n}_{\text{\# of particles in box. l. wave length on n sides}}} \frac{|A_e|^2}{\chi_e |T_e|^2}$$

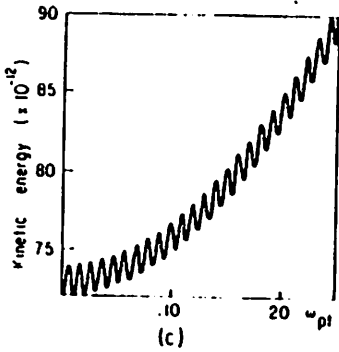
of particles
in box. l. wave
length on n sides.

for details see P.PPL-1600.

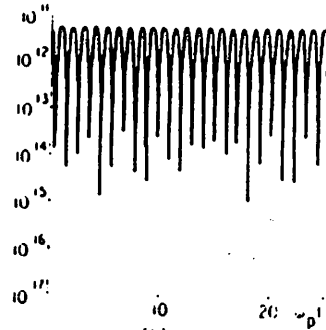
mode Not observable if $\delta_e T_e \geq 1$.



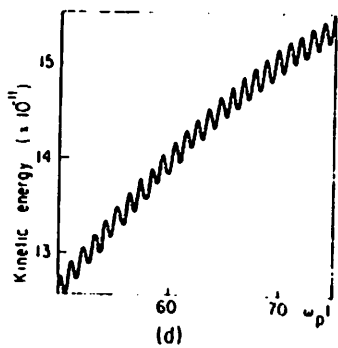
(a) Total ESE.



(c)

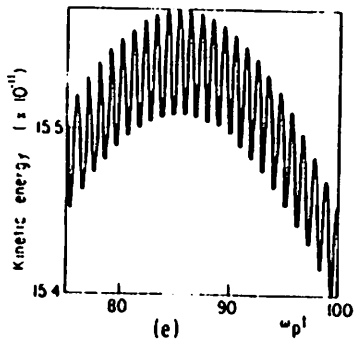


(b) Mode 11 ESE.

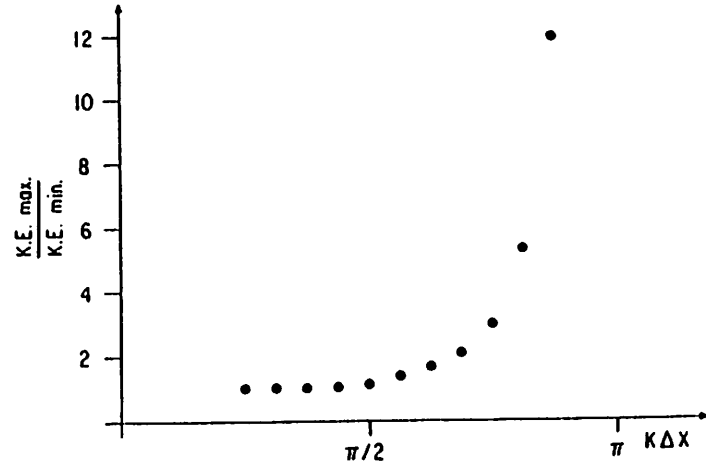
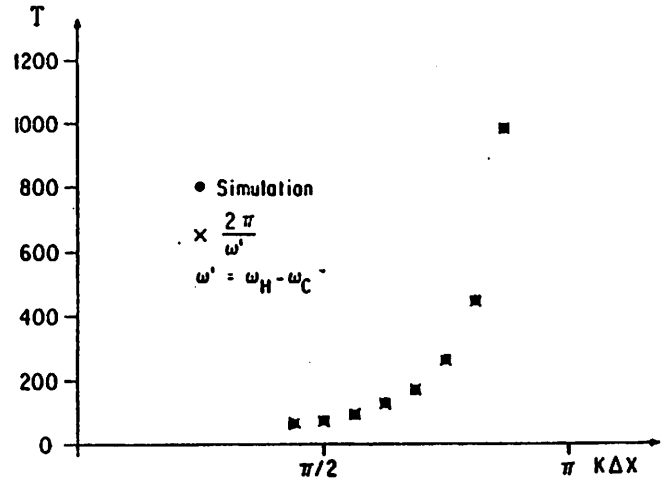


(d)

excited with mode = 11

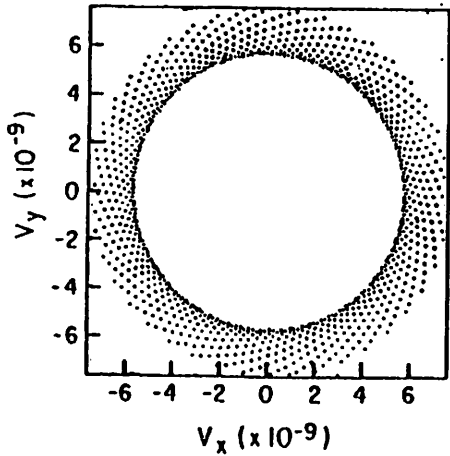
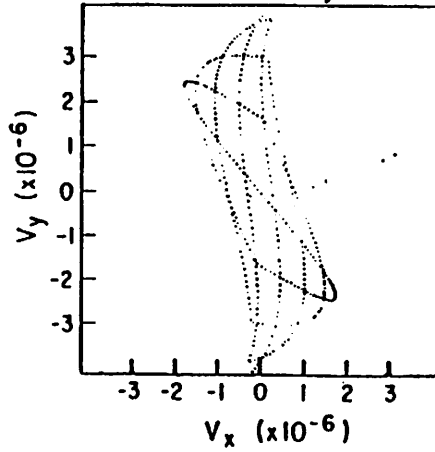
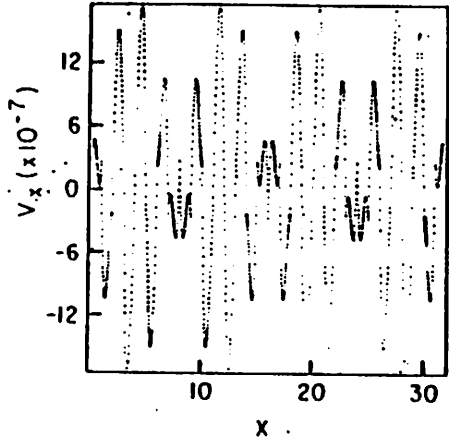


(e)

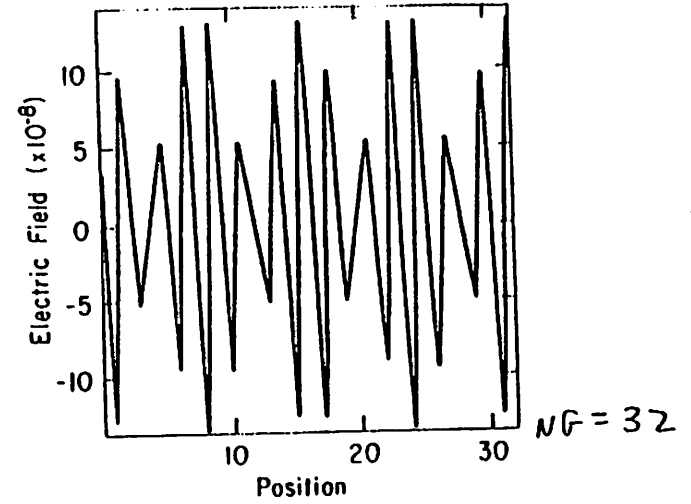


MODE 14 EXCITED

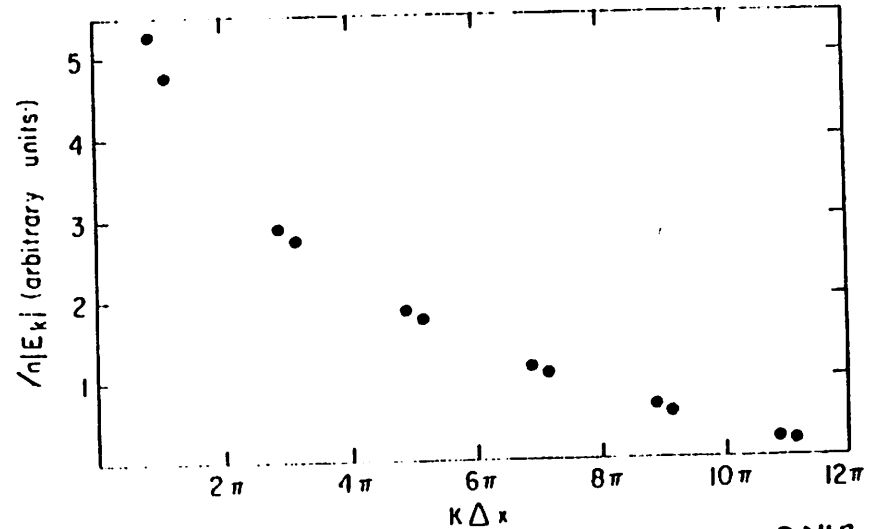
SNAPSHOTS OF ALL PARTICLES AT $\omega_p t = 50$.



History of 1 particle
from $\omega_p t = 0$ to 50.



MODE = 14 TIME = 0.



NG = 2048

For hybrid oscillations, the equations of motion with $\underline{B} = \frac{1}{2} B_0$, are

$$\ddot{y} = -\omega_c \dot{x} \quad (1)$$

$$\ddot{x} = \frac{qE}{m} + \omega_c \dot{y} \quad (2)$$

Integrating (1) with the special initial conditions of $y(0) = -\omega_c x(0)$, $\dot{x}(0) = 0$ gives

$$\dot{y} = -\omega_c x \quad (3)$$

Putting (3) into (2) yields

$$\ddot{x} + \omega_c^2 x = \frac{qE}{m} \quad (4)$$

Fourier transforming this equation in x yields

$$\ddot{x}_k + \omega_c^2 x_k = \frac{qS(-k)}{m} E(k, t) \quad (5)$$

Here k is to be treated as a continuous variable going from 0 to ∞ .

From the simulations we have observed that $E(t) \sim \cos \omega_H t$. Therefore we take $E(k, t) = A_k \cos \omega_H t$. The most general solution to (5) using the initial condition $\dot{x}_k(0) = 0$ is

$$x_k(t) = c_1 \cos \omega_c t + \frac{qS(-k)A_k}{m(\omega_c^2 - \omega_H^2)} \cos \omega_H t \quad (7)$$

For those mode where $x_k(0) = 0$, this becomes

$$x_k(t) = \frac{A_k q S(-k)}{m(\omega_c^2 - \omega_H^2)} \{ \cos \omega_H t - \cos \omega_c t \}$$

which can be rewritten as

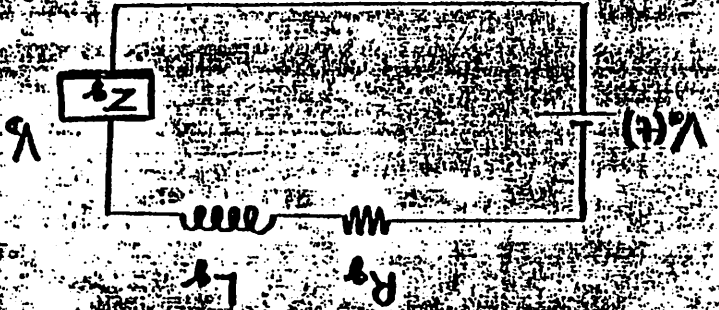
$$x_k(t) = \frac{A_k q S(-k)}{m(\omega_c^2 - \omega_H^2)} \left\{ \sin\left(\frac{\omega_H + \omega_c}{2}\right)t \sin\left(\frac{\omega_H - \omega_c}{2}\right)t \right\}$$

To find the kinetic energy of a mode, use $\dot{x}_k = Q(-\omega_H \sin \omega_H t + \omega_c \sin \omega_c t)$ and $\dot{y}_k = \omega_c Q(-\cos \omega_H t + \cos \omega_c t) = -\omega_c x_k$. The frequencies one obtains are $2\omega_H$, $\omega_H + \omega_c$ and $\omega_H - \omega_c$.

However, if $x_k(0) = \frac{qS(-k)A_k}{m(\omega_c^2 - \omega_H^2)}$ then $x_k(t) = \frac{qS(-k)A_k}{m(\omega_c^2 - \omega_H^2)} \cos \omega_H t$. For this case x_k has only 1 frequency instead of 2. The kinetic energy has the frequency $2\omega_H$.

Now $\frac{qS(-k)A_k}{m} = \frac{q}{m} E(k)$ and if $k \Delta x$ is small enough, then $\frac{q}{m} E(k) = -\omega_p^2 x$. So for $k \Delta x$ small enough $x_k(0) = \frac{qS(-k)A_k}{m(\omega_c^2 - \omega_H^2)}$ is satisfied.

$$V_o(t) = R_3 I_c + L_3 \frac{dI_c}{dt} + V_0$$



1. Field Solution
2. Particle Motion
3. Particle Emission and Absorption
4. Boundary Conditions (losses, dielectrics)
5. External Circuit

428

SIMULATION TECHNIQUES FOR
 SELF-CONSISTENT TREATMENT
 OF
 ELECTRON DYNAMICS IN HIGH
 POWER MICROWAVE DEVICES

429

POST PROCESS RUN DATA FOR DIAGNOSTICS

RESTART DATA FOR CONTINUATION

EXTERNAL FIELD ADVANCEMENT

FIELD PROPAGATION

CHANGE AND CURRENT DENSITY

PARTICLE ORBIT ADVANCEMENT

PARTICLE EMISSION

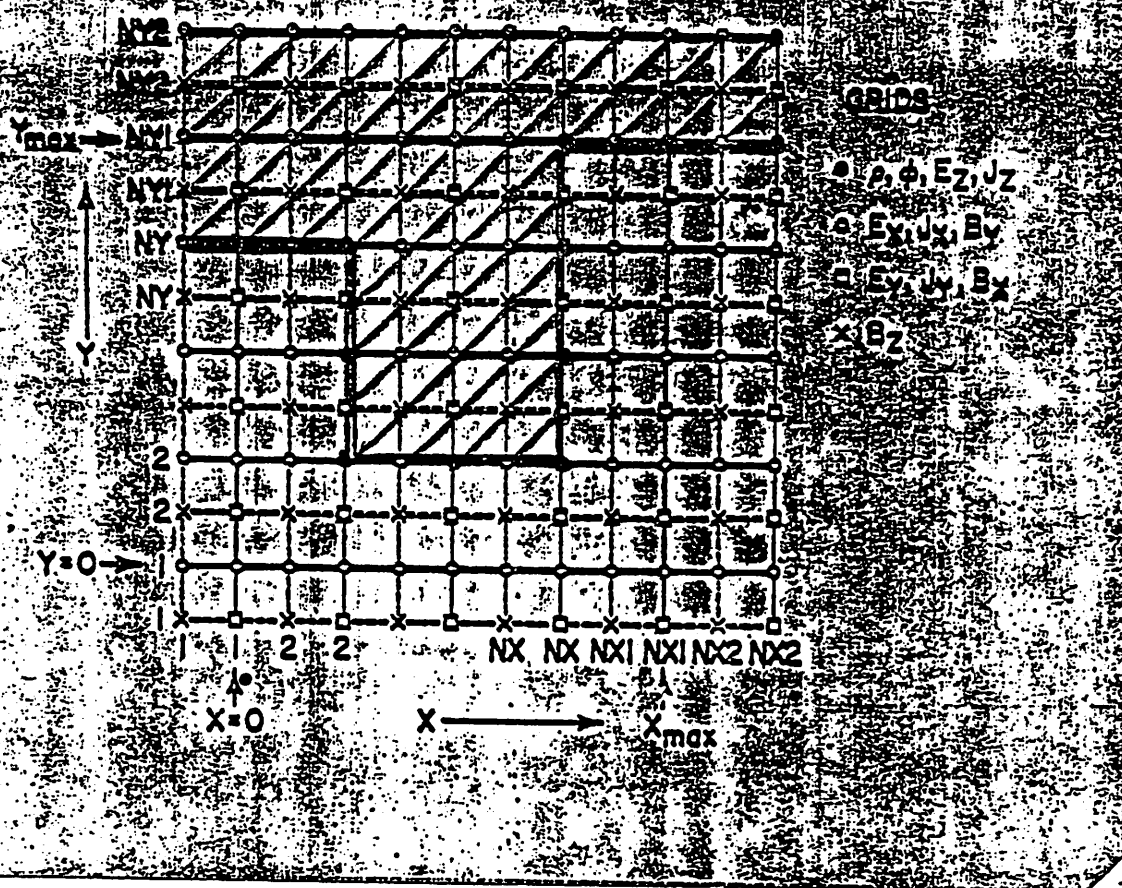
CODE INITIALIZATION

LEAP - FROG FIELD PROPAGATOR

1. $\vec{D}_{N+1} = \vec{D}_N + c\Delta t \cdot (\vec{\nabla} \times \vec{H}_{N+1/2} + \vec{J}_{N+1/2})$
2. $\vec{E}_{N+1} = \vec{D}_{N+1} / \epsilon$
3. $\vec{b}_{N+1/2} = \vec{H}_{N+1/2} / \mu$
4. $\vec{b}_{N+3/2} = \vec{b}_{N+1/2} + c\Delta t \cdot (\vec{\nabla} \times \vec{E}_{N+1})$
5. $\vec{H}_{N+3/2} = \vec{b}_{N+3/2} / \mu$

with $\vec{\nabla} \cdot \vec{E} = \rho / \epsilon$
 $\vec{\nabla} \cdot \vec{b} = 0$

• as initial conditions and all spatial operators defined on a staggered mesh.



431

Y.F. NO. 42-1985

MODIFICATION

1.0 O_{N-1} , O_{N+1} AND MASK

432

Energy Balance - Macroscopic

$$\dot{E}_{in} = \int_0^t \dot{V}(t) I dt$$

$$\dot{E}_{out} = \int_0^t \dot{V}(t) R_g I dt$$

$$\dot{E}_{out} = \dot{V} I R_g$$

$$\dot{E}_{D} = \int_0^t \dot{V}(t) V_D I dt$$

$$\dot{E}_{D} = \dot{V} I V_D + \dot{E}_{D} + \dot{E}_{D}$$

ADVANTAGES

1. SIMPLE DESIGN
2. OPERATION CAN BE AUTOMATIZED
3. WAX CAN ALSO BE USED TO CHECK PARTICLE ROUNDRY CONDITIONS
4. COOLING IS VERY COMPACT

Energy Balance Microscopic

$$\frac{\partial}{\partial t} (\rho \mathbf{r} + \mathbf{q}_r) + \nabla \cdot (\mathbf{T} - \mathbf{r} \otimes \mathbf{p})$$

$$= - \int_{c \partial \tau} \frac{1}{c} \Delta (\nabla \phi_{ext})$$

Integrate over volume of device

$$\int - \int_{c \partial \tau} \frac{1}{c} \Delta (\nabla \phi_{ext}) dV = V_b I_c$$

but $I_c = \frac{dQ}{dt}$

$$= \frac{1}{c} \int \Delta \nabla \phi_{ext} \cdot d\vec{A}$$

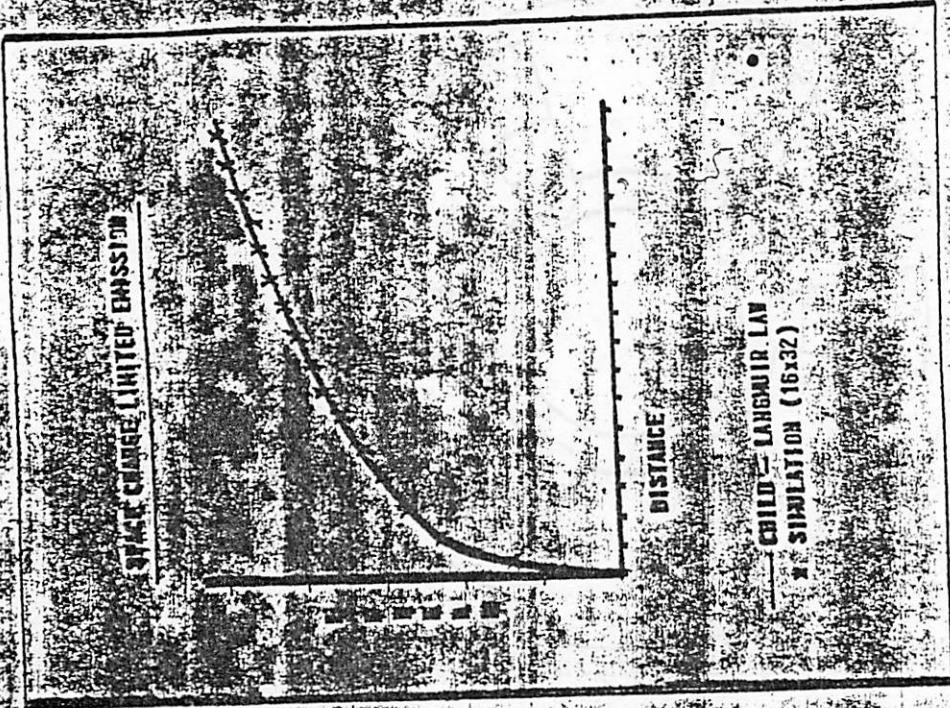
$$V_b = \int \sum \dot{E}_{ext} d^3V$$

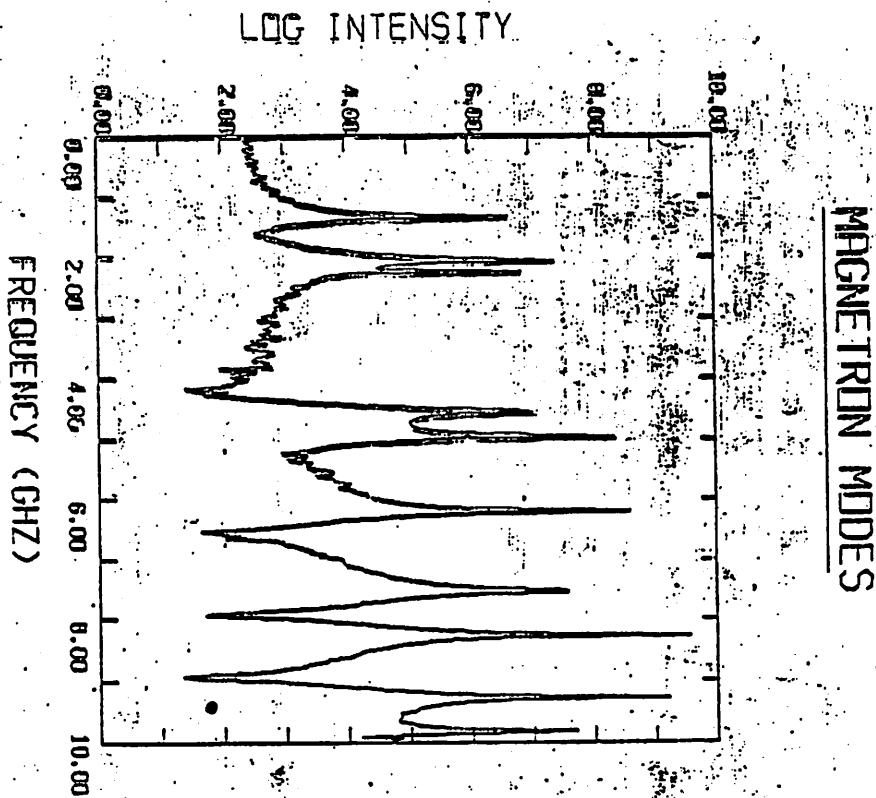
$$\phi \dot{E}_{ext} dA$$

where $\dot{E}_{ext} = \frac{\partial}{\partial t} \nabla \cdot (\Delta \phi)_{ext}$

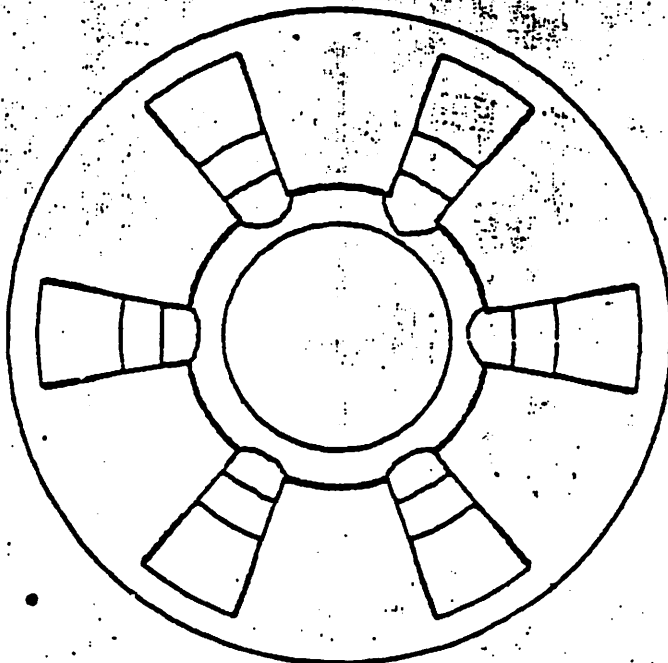
Cold Testing of a Structure

- Set up Geometry Specify Boundaries Loss Elements Dielectric Elements
- Initialize Current Impulse
- Run code for large number of timesteps ~32000
sawing field data at impulse point at every timestep.
- Fast Fourier Transform the field data to form the frequency spectrum
- Identify frequency of mode of interest and use to drive a current element for half cycle
- Field arrays contain the mode structure and can be used for graphic output.
- Rate of field energy decay determines Q for mode.





TIME = 1.747E-03 STEP = 1782

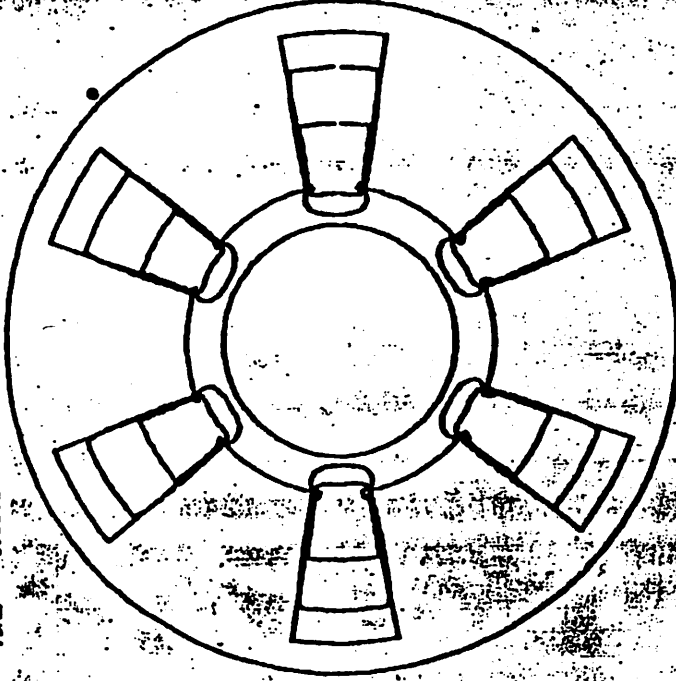


K3 MAGNETIC FIELD

87

490

TIME = 1.663E-09 STEP = 1798



01 ELECTRIC FIELD

441

SIMULATION

PARAMETERS

32x32 cells

$B_0 = 0.172T$

$V_0 = 600kV$

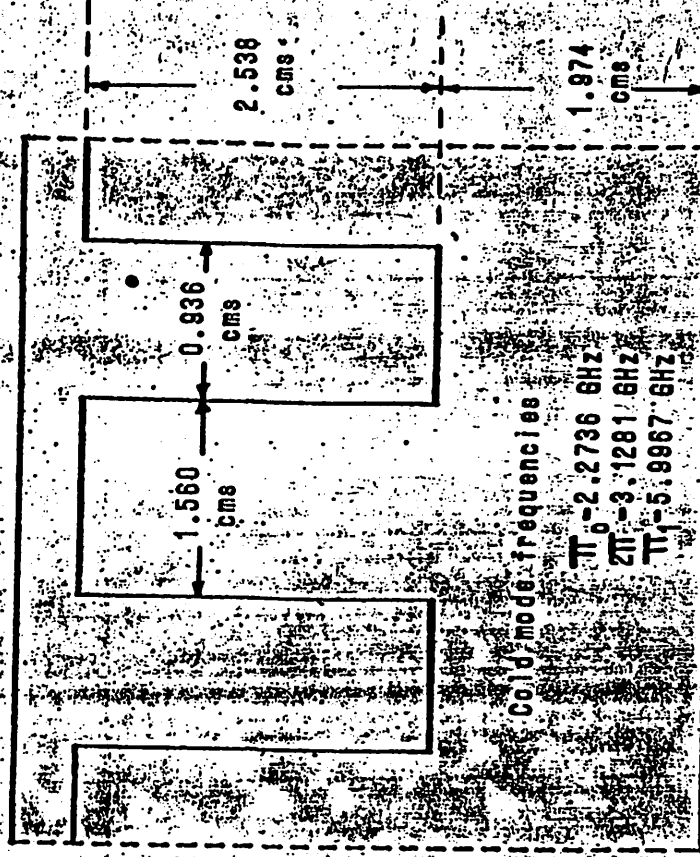
$DT = 2.0psec$

$DX = 1.56mm$

$DY = 1.41mm$

$t_p = 3nsec$

$R_g = 75\Omega$



Cold mode frequencies

$\pi_0 = 2.2736 GHz$

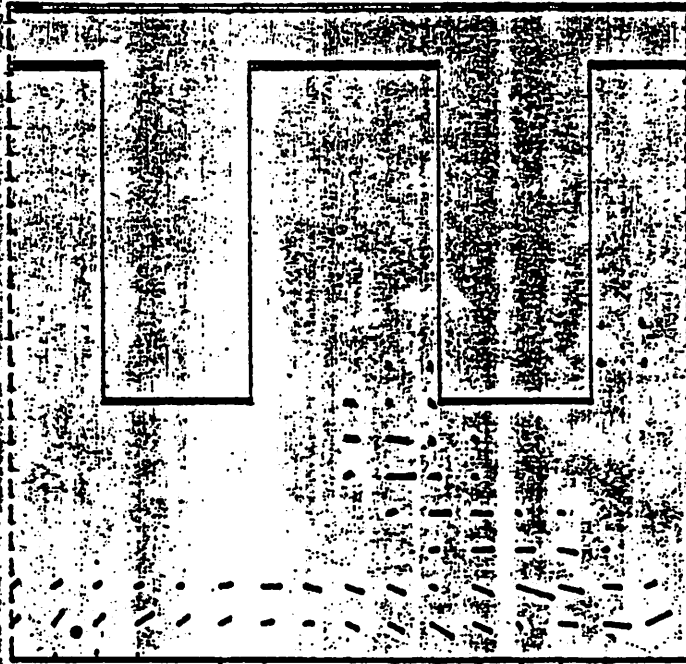
$2\pi = 3.1281 GHz$

$\pi_1 = 5.9967 GHz$

Two cell planar magnetron simulation

442

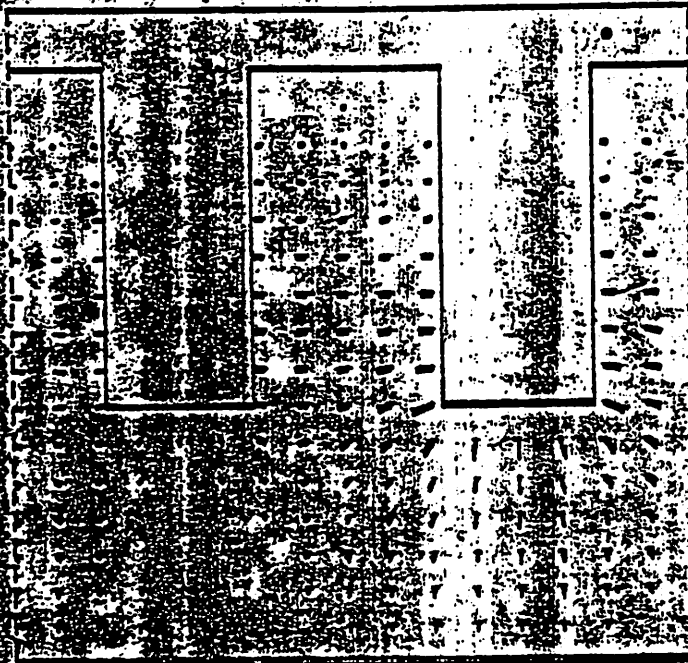
TIME = 1.700E-08 STEP = 8000



J1.2 CURRENT

493

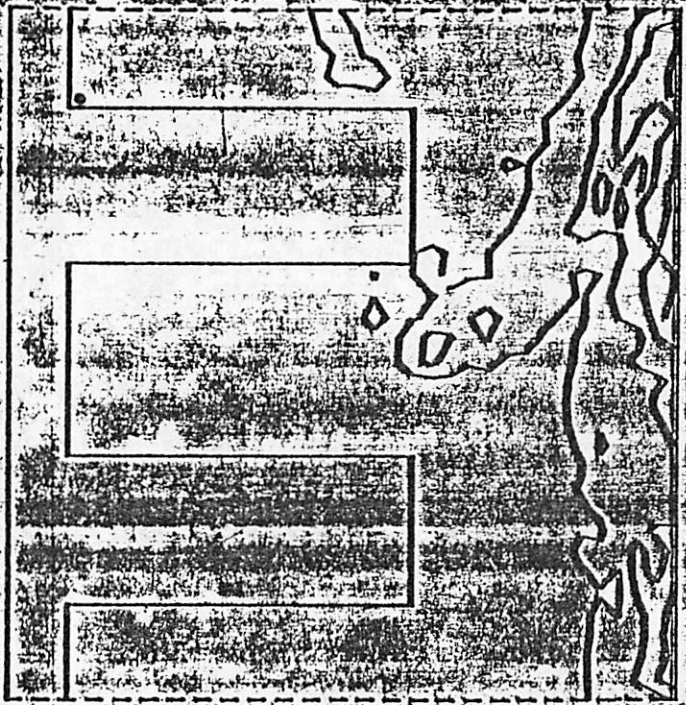
TIME = 1.700E-08 STEP = 8000



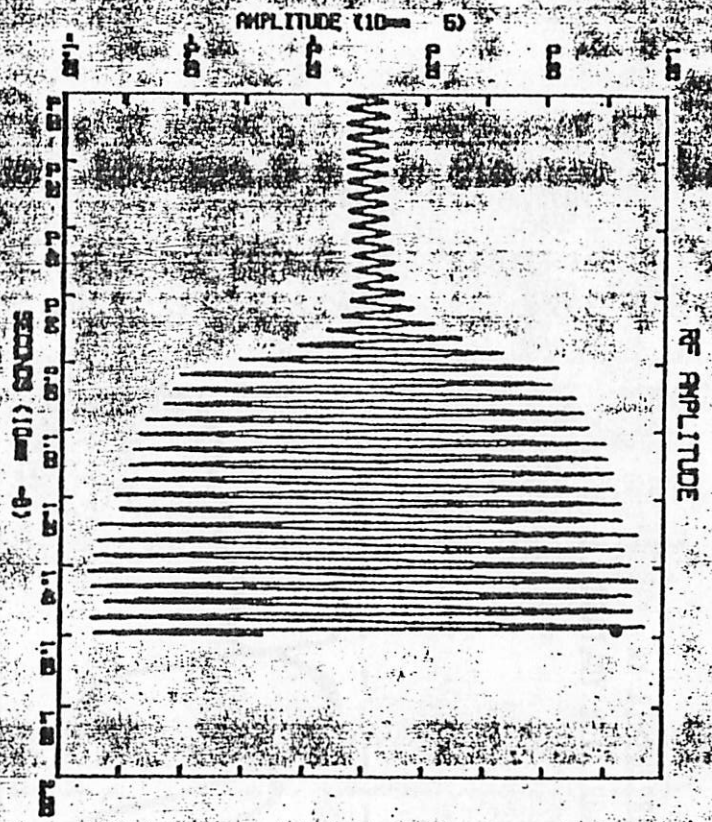
E1.2 ELECTRIC FIELD

494

TIME = 1.785-08 STEP = 0000



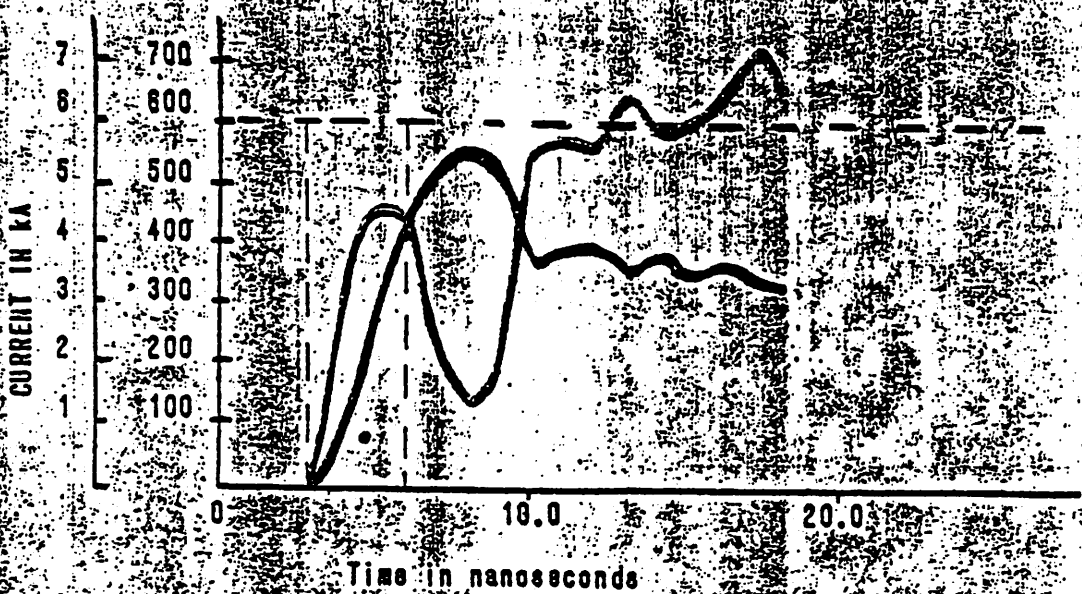
00 0000



REF AMPLITUDE

TWO CELL MAGNETRON SIMULATION

— CURRENT IN KA
 - MAGNETRON VOLTAGE IN KV



447

Application

1. RT Servos

Magnetrons

Cathodes

Klystrons

2. Inverse grids - acceleration
 E.M.I. I

E.M.I. I

Ring Formation / Mirrors

EBT

Central Accelerator

Design

3. ICF

Diode Studies

Magnetic insulation

448

32

CONFERENCE ON PARTICLE AND HYBRED CODES FOR FUSION
10-11 DECEMBER 1979

ELECTROMAGNETIC, STRICTLY TWO-DIMENSIONAL
NUMERICAL INSTABILITY IN PARTICLE CODES*

BRENDAN B. GODFREY
MISSION RESEARCH CORPORATION

*WORK SUPPORTED BY THE U.S. DEPARTMENT OF ENERGY

MRC

INSTABILITY ARISES IN RELATIVISTIC BEAM SIMULATIONS AND IS MOST SERIOUS
WHEN LAMINAR FLOW REQUIRED.

- OCCURS AT MAXIMUM k_{\perp} AND LARGE k_{\parallel}
- GROUP VELOCITY RELATIVELY SMALL
- DISRUPTS BEAM STREAM LINES
- STABILIZED BY BEAM TEMPERATURE
- SATURATES AT LOW AMPLITUDES
- PREVENTS BEAM QUALITY MEASUREMENTS

44

450

COLD BEAM NUMERICAL DISPERSION RELATION SHOWS SOURCE OF INSTABILITY

$$\left\{ [\omega]^2 - [k_{\parallel}]^2 - [k_{\perp}]^2 - \frac{\omega_p^2}{\gamma} \sum s^2(\omega) s^4(\bar{k}_{\parallel}) s^2(\bar{k}_{\perp}) \right\}$$

$$\cdot \left\{ 1 - \frac{\omega_p^2}{\gamma^3} \sum s^2(\bar{k}_{\parallel}) s^4(\bar{k}_{\perp}) (\bar{\omega} - \bar{k}_{\parallel} v)^{-2} \right\}$$

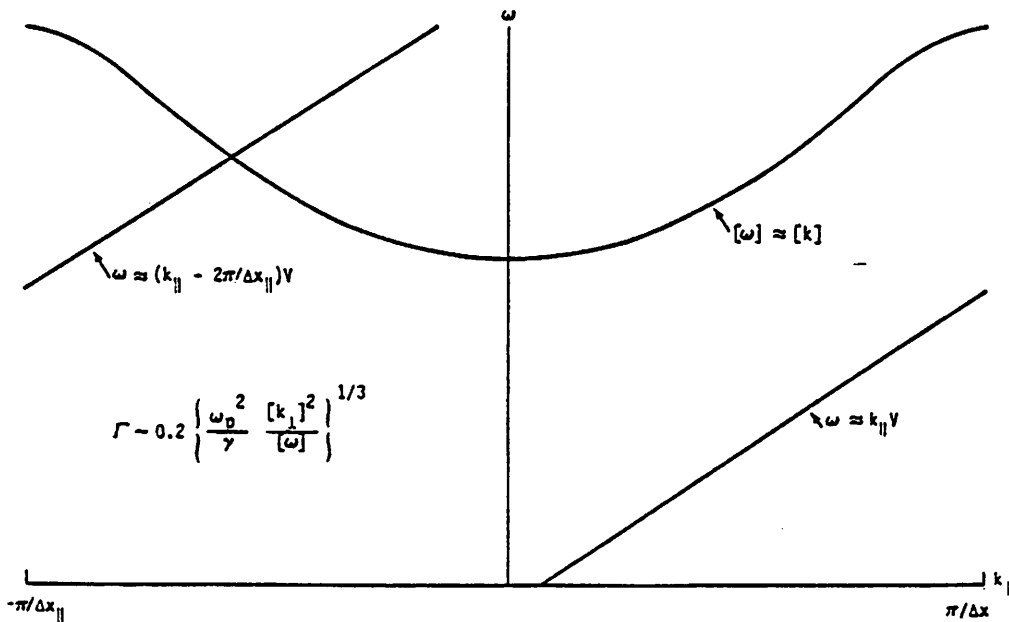
$$= \frac{\omega_p^2}{\gamma^3} [k_{\perp}]^2 \sum \left\{ \gamma^2 v^2 s^2(\bar{\omega}) s^2(\bar{k}_{\parallel}) s^2(\bar{k}_{\perp}) \right.$$

$$\left. + s^2(\bar{k}_{\parallel}) s^4(\bar{k}_{\perp}) - \gamma^2 s^4(k_{\parallel}) s^2(k_{\perp}) \right\} (\bar{\omega} - \bar{k}_{\parallel} v)^{-2}$$

- EXPRESSIONS HAVE USUAL MEANINGS
- DERIVED FOR GALERKIN ALGORITHM, BUT QUALITATIVELY UNCHANGED IN OTHER CASES
- ONLY DOMINANT TERMS KEPT

451

INSTABILITY OCCURS AT INTERSECTION OF BEAM MODE ALIAS WITH LARGE k_{\perp} LIGHT MODE



452

INSTABILITY WEAKENED BY SEVERAL METHODS, BUT NONE FULLY SATISFACTORY.

- WAVE-TRANSMITTING DOWNSTREAM BOUNDARY
- $\Delta x_{\parallel} \lesssim \Delta x_{\perp}$
- CURRENT SMOOTHING AT LARGE k_{\parallel} AND k_{\perp}
- CURRENT FILTERING IN k_{\parallel}
- HIGH FREQUENCY LIGHT WAVE DAMPING
- HIGHER ORDER DIFFERENCING SCHEME

453

33

A. Sternlieb, Shyke A. Goldstein* and Roswell Lee**

Technical Report Number 79-060
Physics Publication Number 79-134

January 1979

COMPUTER SIMULATION MODEL OF 1-D DIODE
COUPLED TO AN EXTERNAL ELECTRIC CIRCUIT*

by

COMPUTER SIMULATION MODEL OF 1-D DIODE
COUPLED TO AN EXTERNAL ELECTRIC CIRCUIT[†]

A. Sternlieb
Department of Physics and Astronomy, University of Maryland,
College Park, MD. 20742

Shyke A. Goldstein^{*}
Science Applications, Inc., McLean, VA. 22101

Roswell Lee^{**}
JAYCOR, Alexandria, VA. 22304

January 1979

28 Pages

7 Figures

ABSTRACT

A computer simulation model has been devised for the purpose of following the time-dependent behavior of electron and ion generation from 1-d reflex diodes driven by pulsed power sources. The power generator is represented by a lumped, equivalent circuit driven by a voltage source. This circuit is coupled in series to a 1-d, relativistic particle simulation model of the diode. Basically, particles collected at the electrodes contribute to the diode current, which is coupled back into the external circuit. The emission in the diode is assumed to be space-charge limited. The new scheme is able to explain and predict experimental results obtained with reflex diodes and can optimize circuit and diode parameters for specific purposes. As a basic test, results for a nonrelativistic Child-Langmuir diode are found to agree closely with exact numerical solutions. Good agreement is obtained with experimental results for reflex diode cases. Some recent analytical results in reflex diode theory are well corroborated by our simulations.

I. INTRODUCTION

Recently experiments have been performed with reflex diodes for the purpose of generating intense electron and ion beams [1-3,8]. Several basic steady-state theoretical and computational models of the reflex diode operation are available [2,4,5]. In all of them the diode voltage is artificially fixed. In reality, there is dynamic interaction between the diode and the external inductive electric circuit to which it is coupled. This interaction is experimentally apparent in oscilloscope traces, describing the diode current and voltage as functions of time. Thus, there is a need for a self-consistent coupling scheme between a diode model and an appropriate description of the external electric circuit. Such a scheme should be able to describe the time-dependent behavior of the diode current and voltage in experimental set-ups.

In this paper we describe a coupling model which is the first of its kind to our knowledge. First, the generator is represented by a lumped, equivalent circuit driven by a pulsed voltage source. Then, this circuit is coupled in series to a 1-d relativistic particle simulation model of the diode (see Fig. 1). No assumption is made concerning the relationship between the diode current and voltage. As we shall see, the constraints of both the diode physics and the external inductive circuit are self-consistently taken into account.

With our model we were able to corroborate some recent analytical results concerning conditions for steady-state reflex diode operation [6,7]. In a test case, we obtained remarkable

quantitative agreement with exact numerical solutions for a normal, unipolar Child-Langmuir nonrelativistic diode. We were also able to explain the main features of the oscilloscope traces obtained from reflex diode experiments. We intend to use our model in providing guidance for future experiments with reflex diodes, by optimizing circuit and diode parameters for better current and voltage characteristics.

The plan of this paper is the following. In section II we present some basic features of a 1-d electrostatic simulation code for a reflex diode and we also describe our basic external circuit. In section III we present the details of the coupling model between the diode code and the external electric circuit. In section IV we compare simulation results with exact numerical solutions for a simple Child-Langmuir unipolar diode and also with results for a characteristic reflex diode case. Next, in section V we mention some computational problems connected with the present model. Finally, in section VI we summarize the main achievements and potential benefits of our model.

II. SOME REMARKS ON DIODE CODES AND EXTERNAL CIRCUITS

A. The Diode Simulation Code without External Circuit ("The Uncoupled Code")

The electrostatic, relativistic and 1-d code follows the orbits of many simulation electrons and ions in the self-consistent electric field derived from both space-charge and the applied diode voltage. The dynamic emission of the electrons and ions is assumed to be space-charge limited. The flow chart of this code is presented in Fig. 2. First, the electrostatic potential distribution $\phi(z)$ is found from Poisson's equation, using as boundary condition the externally given diode voltage $V_D(t)$: $\phi(A) = V_D(t)$ ($\phi(K)$ is always zero), where the symbols A and K stand for anode and cathode, respectively. Then, the electric fields at the electrodes, $E_z(A)$, $E_z(K)$ are calculated. Using a gaussian emission law, enough electron and ion charges are emitted (at K and A, respectively), to make the electric fields zero at the electrodes. The system is thus globally charge-neutralized. Next, the potential $\phi(z)$ is corrected to take into account the emitted charge (the boundary values are not affected by this correction). Then, the electric field in the system, $E_z(z)$ is calculated (it is zero at the electrodes) from the corrected potential distribution and it is used to push the emitted particles to their new positions. The new charge distribution $\rho(z)$ and the four absorbed current density components are found (electrons or ions can be absorbed at anode or cathode) and the code proceeds to the next time step.

Initially, for a few time steps, this uncoupled code gives big emitted currents because it starts with a vacuum diode and the inductive effect is not taken into account (this effect is not present in a diode coupled to an external inductive circuit because the inductance forces the current to start from zero). After a short transient period, the simulation results do follow closely the steady-state theoretical predictions, whenever available (e.g., they follow the Child-Langmuir law, for a non-relativistic diode case).

Once a particle has been emitted (usually with negligible kinetic energy), it is accelerated across the gap and is eventually collected by one of the electrodes. Since for a reflex diode the electrons may pass several times through the anode foil before being absorbed by it, a foil-scattering model has been developed which includes energy loss and accumulated multiple small-angle elastic scattering. The model uses tabulated charts of electron ranges for various energies and materials. Any simulation electron that reaches the anode is scattered by the foil if its range is greater than the foil thickness. An electron whose range is less than the foil thickness is absorbed by the anode, as well as all the ions that reach the cathode. The absorbed particles, together with the emitted ones, contribute to the diode current.

There are usually six current density components in a bipolar diode (see Fig. 1): $i_{el}^{em}(K)$, $i_1^{abs}(K)$, $i_{el}^{abs}(K)$, $i_1^{em}(A)$, $i_{el}^{abs}(A)$ and $i_1^{abs}(A)$, where el, em, i, abs, A and K represent electron, emitted, ion, absorbed, anode and cathode, respectively. No emission of electrons at the anode or of ions at the cathode is

assumed. The electron current absorbed at the cathode and the ion current absorbed at the anode are usually small. The various current components are defined as:

$$i_{el,i}^{em,abs}(A,K) = Q_{el,i}^{em,abs}(A,K) \cdot S/\Delta t \quad (1)$$

where Q is a surface charge density, S is the cathode (or anode) area, and Δt is the simulation time step.

The total cathode and anode current densities are given by the following expressions (all the quantities are positive):

$$\begin{aligned} i_K &= i_{el}^{em} + i_1^{abs} - i_{el}^{abs} \\ i_A &= i_1^{em} + i_{el}^{abs} - i_1^{abs} \end{aligned} \quad (2)$$

During a very short initial transient period, $i_K \neq i_A$, because $\bar{v} \cdot \vec{i} = \partial \rho / \partial t \neq 0$, but in the steady-state, i_K is very nearly equal to i_A in all our uncoupled code runs. For our simulation purposes we define the diode current to be: $i_D = i_K$.

The following notations are used in connection with the flow chart of the uncoupled diode code (Fig. 2):

d = A-K gap

$V_D(t)$ = diode voltage (externally fixed)

$\Delta \phi_e(z)$, $\Delta \phi_i(z)$ = functions used to correct the potential distribution by including the effect of the emitted charges.

Δz = simulation space step

NZ = number of simulation cells: $d = NZ \cdot \Delta z$.

The following constants are used to match the boundary conditions to the finite grid system:

$$D = 1 - 0.5/NZ$$

$$B = 0.5/NZ$$

$$C = D^2 - B^2$$

The following are Green-like functions which represent the correction which should be added to the potential distribution $\phi(z)$, due to one unit of emitted surface charge density. They do not alter the potential boundary values and they cause the electric field to be zero at the electrodes:

(a) For electrons (emitted at the cathode):

$$\Delta\phi_e(z) = -2\pi \Delta z(z-d)/d, \quad +\Delta z/2 \leq z \leq d$$

$$\Delta\phi_e(z) = -4\pi (\Delta z/2-d)z/d, \quad -\Delta z/2 \leq z \leq \Delta z/2$$

(b) For ions (emitted at the anode):

$$\Delta\phi_i(z) = 2\pi \Delta z \cdot z/d, \quad 0 \leq z \leq d - \Delta z/2$$

$$\Delta\phi_i(z) = 4\pi(d-\Delta z/2)(1-z/d), \quad d - \Delta z/2 \leq z \leq d + \Delta z/2$$

The following expressions represent the usual gaussian laws used for space-charge limited emission ($E_z(K)$ and $E_z(A)$ are the boundary values of the electric field before charge emission):

(a) Emission of only electrons:

$$Q_{e1}^{em}(K) = E_z(K)/4\pi D$$

$$Q_i^{em}(A) = 0$$

(b) Emission of only ions:

$$Q_{e1}^{em}(K) = 0$$

$$Q_i^{em}(A) = -E_z(A)/4\pi D$$

(c) Emission of both electrons and ions:

$$Q_{e1}^{em}(K) = [D \cdot E_z(K) + B \cdot E_z(A)]/4\pi C$$

$$Q_i^{em}(A) = -[D \cdot E_z(A) + B \cdot E_z(K)]/4\pi C$$

(3)

(d) No emission from any electrode:

$$Q_{e1}^{em}(K) = 0$$

$$Q_i^{em}(A) = 0$$

The corrected potential which takes into account the emitted charge is therefore given by:

$$\phi^C(z) = \phi(z) + Q_{e1}^{em}(K) \cdot \Delta\phi_e(z) + Q_i^{em}(A) \cdot \Delta\phi_i(z) \quad (4)$$

Finally, the electric field is calculated as:

$$E_z(z) = [\phi^C(z) - \phi^C(z+\Delta z)]/\Delta z \quad (5)$$

[$E_z(A) = E_z(K) = 0$, when using $\phi^C(z)$ for the derivation.]

B. Basic Reflex Diode Operation

Several early models of the reflex diode operation are available [2,4,5]. In Fig. 1 a sketch of a 1-d symmetric reflex diode is drawn, of which only one half is simulated. The diode is coupled to an external electric circuit consisting of an impedance R_G , an inductance L_G ("G" stands for generator) and a pulsed voltage source, $V_{ext}(t)$. If the anode foil thickness is only a fraction of the electron range in the given anode foil material, the electrons will reflex several times through the foil before being absorbed by it. If the foil is an ion source, the accumulation of negative charge near the anode foil which occurs during the steady state regime will draw enhanced ion currents which in turn will cause enhanced electron currents from the cathode. Thus, in a reflex diode, the total diode current may largely exceed the Child-Langmuir value for normal bipolar flow.

The ion current efficiency, $i_1^{em}(A)/i_D$ is also enhanced over the usual bipolar ratio, because of the increased electron lifetime. No law similar to the Child-Langmuir law is available for

a reflex diode. However, some recent theoretical results [6] have shown that the reflex diode current is "resonant" for $N_r \geq 4$, where N_r is the number of reflexions of an electron through the anode foil. In an inductive circuit the current will not be allowed to resonate. Therefore, an inductive reflex diode will probably operate at a voltage corresponding to $N_r \approx 4$ for the given foil thickness τ . This predicted operational diode voltage $V_D^{OP}(\tau)$ can be found from suitable electron "energy vs. range" charts for the specific foil material, and is given approximately by $V_D^{OP}(\tau) = a\tau^{2/3}$ where "a" depends mainly on the foil materials [1].

C. Some Remarks on Expected Reflex Diode Behavior in External Circuits

As shown in Fig. 1, both cathodes are coupled together to the negative polarity, and the anode to the positive polarity of the external pulsed power generator. The circuit equation is:

$$V_{ext}(\tau) = V_D(\tau) + L_G \frac{di_D(\tau)}{dt} + R_G i_D(\tau) \quad (6)$$

The diode current and voltage should start from zero because of the inductance. This solves the big initial transient current problem of the uncoupled code. Because of the high initial impedance, the diode voltage rises quickly to its maximum value, and then follows a plateau period which lasts until a critical amount of electron energy is deposited in the anode foil. When this happens, an ion source is formed at the anode and the current starts to exponentiate, if the plateau value is higher than $V_D^{OP}(\tau)$ (the operational diode voltage, corresponding to

approximately 4 reflexions through the given foil of thickness τ). Because of the $L_G \frac{di_D(\tau)}{dt}$ term in Eq. (6) and because of the "resonant" current behavior for $N_r \geq 4$, the diode voltage is expected to collapse and stabilize at an average value $V_D^{OP}(\tau)$. The saturation current i_D^{sat} is given by:

$$i_D^{sat} = (V_{ext}^{sat} - V_D^{OP}(\tau)) / R_G, \quad (\langle L_G \cdot \frac{di_D}{dt} \rangle^{sat} \approx 0)$$

The diode current tends to i_D^{sat} according to:

$$i_D(\tau) \approx (1 - e^{-(R_G/L_G)(\tau - \tau_s)}) \cdot [i_D^{sat} - i_D(\tau_s)] + i_D(\tau_s),$$

where τ_s is the time at which the diode voltage stabilizes.

An estimate of the current gain over the usual bipolar Child-Langmuir value can be found from:

$$V_{ext}^{sat} = R_G \cdot M \cdot i_{C.L.}^{b.p.} + V_D^{OP}(\tau) \quad (\text{steady-state}),$$

where M is the gain factor, and $i_{C.L.}^{b.p.}$ is given by:

$$i_{C.L.}^{b.p.} \approx 4.6 \cdot 10^{-6} V_D^{OP}(\tau)^{3/2} \cdot S/d^2 \quad (\text{in M.K.S. units})$$

We see that M is determined by V_{ext}^{sat} , R_G , S, d, τ and foil material. $V_D^{OP}(\tau)$ can be estimated from electron "range" charts to give $N_r \approx 4$.

Thus, we expect the steady-state diode current and voltage to be relatively insensitive to parameters such as S, d, L_G and m_i/m_e (ion to electron mass ratio). This fact allows us to choose simulation values for these parameters which greatly increase the computational speed and stability; lower L_G and m_i/m_e decrease the computation time, while higher S and d increase the code numerical stability by reducing the current density (higher

current densities require higher-order time-centering of the difference equations for the same Δt).

From the above picture it is clear that the diode voltage cannot be externally fixed in a realistic code but should be self-consistently determined at any time, including the inductive effect of the external circuit.

467

III. THE COUPLING PROCEDURE

In the uncoupled code the diode voltage is externally fixed. In the present code, coupled to an external inductive circuit, the diode voltage is found self-consistently at each time step. An i_D - V_D relationship is not assumed, so we look for a general coupling technique while keeping the number of assumptions at a minimum. The main assumptions in our simulation model are the following:

- a. The circuit equation (6) is valid at any time.
- b. The potential distribution is found from Poisson's equation:

$$\nabla^2 \phi(z) = -4\pi\rho(z) . \quad (7)$$

- c. A gaussian law is used for space-charge limited emission at the electrodes [Eq. (3)].
- d. We assume zero initial currents and zero initial charge distribution.
- e. The boundary conditions are:

$$\phi(K) = 0$$

$$E_z(A) = E_z(K) = 0$$

- f. For a bipolar diode we assume

$$i_D = i_K = i_A \quad (8)$$

In Fig. 3 we present the flow chart of a particle simulation code, coupled to an external circuit. The notations are as in the previous section.

The integration cycle starts by assuming that the emitted electron and ion currents, the total diode current and the charge

48

distribution function are all zero, at $t=0$. Then, by using the gaussian emission laws [Eq. (3)] one finds the uncorrected (before emission) electric field at the cathode (it is zero, at $t=0$). Using a recursion formula to solve the Poisson equation (7), one finds the potential distribution function $\phi(z)$ throughout the system by taking as left-hand side boundary conditions the electric field at the cathode and the potential at the cathode (defined to be zero). At $t=0$, $\phi(z)=0$, because $\rho(z,t=0)$ is defined as zero. Having found $\phi(z)$, the cycle continues along two parallel channels. In one of them, the instantaneous, self-consistent diode voltage $V_D(t)$ is simply found from:

$$V_D(t) = \phi(z=d) \equiv \phi(A),$$

where d is the cathode-anode gap. Therefore, the process is in a way opposite to that used in the uncoupled code (see Fig. 2). Then, from the circuit equation (6), the total instantaneous diode current time rate change $di_D(t)/dt$ is found (at $t=0$, di_D/dt is simply equal to $V_{ext}(t=0)/L_C$. The current is then advanced to the next time step. The simplest way to do that is by using:

$$i_D(t+\Delta t) = i_D(t) + \frac{di_D(t)}{dt} \cdot \Delta t \quad (9)$$

We found that this simple method was quite satisfactory in a variety of cases. Problems arose in cases in which the current densities and the electric fields became relatively high or too rapidly varying in space and time. In these cases, higher order time centerings of the circuit equation, and careful choice of Δt and Δz are necessary (see discussion in Section V).

In the parallel channel, $\phi(z)$ is corrected, as in the uncoupled code, to take into account the emitted charges at the

electrodes [Eq. (4)]. This correction does not affect the boundary values of $\phi(z)$, because the correcting Green-like functions $\Delta\phi_e(z)$ and $\Delta\phi_i(z)$ are zero at the boundaries (see definitions in section II-A). Therefore, the value of $V_D(t)$ is unchanged as it should be. From the corrected potential distribution $\phi^C(z)$, the corrected electric field distribution $E_z(z)$ is found [Eq. (5)]; (it is zero at the electrodes). In the meantime the necessary charges are emitted at the electrodes [$Q_{e1}^{em}(K)$, $Q_1^{em}(A)$] and the newly found electric field is used to push the emitted particles to their new positions during the timestep Δt . The new charge distribution function $\rho(z)$ is then calculated by usual grid-weighting methods. The code also calculates at this time the various absorbed currents. There are four different absorbed currents, electrons, or ions being absorbed at cathode or anode.

At this point the two parallel channels converge, the total diode current $i_D(t+\Delta t)$ and the various absorbed currents being used to find the necessary emitted currents at the next time step, $t+\Delta t$. These currents are Q_{e1}^{em} (at the cathode) and Q_1^{em} (at the anode). For this purpose equations (1), (2), and (8) are employed. Then, the time-integrating cycle restarts for the new time $t+\Delta t$.

As a remark, we mention that for a simple diode emitting, for example, only electrons, all ion currents Q_i should be equalled to zero.

As can be seen from the above description of the coupling code, the necessary emitted electron and ion currents at any time are determined, as it should be, by a close dynamic interaction between the intrinsic diode physics and the electric circuit

parameters. The presence of the inductance gives to this model, even when using a non-centered equation like (9) an enhanced measure of stability, both numerically and physically, because the inductive term opposes any change in the current. For extreme cases (high current density or long simulation times) better numerical procedures are needed. Indeed, as we shall see in section V, the current behaves in a relatively stable way even when the time-dependent behavior of the voltage becomes numerically unstable.

471

472

IV. RESULTS AND DISCUSSION

As a basic test, results of computer simulations using our model as described in section III were compared with an exact numerical solution for a simple unipolar diode (only electrons emitted at the cathode). In the numerical solution, the usual Child-Langmuir law was assumed to be valid at all times. Thus, the system of equations to be integrated was the following:

$$i_D(t) = 2.34 \cdot 10^{-6} \cdot v_D(t)^{3/2} \cdot S/d^2 \quad (\text{in MKS units}), \quad (10)$$

$$\frac{di_D(t)}{dt} = [v_{\text{ext}}(t) - R_G i_D(t) - v_D(t)]/L_G.$$

$$i_D(t=0) = 0$$

The saturation values of the diode current and voltage, i_D^{sat} and v_D^{sat} can be estimated from:

$$v_{\text{ext}}^{\text{sat}} = R_G \cdot i_D^{\text{sat}} + v_D^{\text{sat}}, \quad (11)$$

where i_D^{sat} is found from Eq. (10).

For both the numerical solution and the simulation, we used the following physical parameters:

v_{ext} = square pulse of 1 MV and 4 nsec, beginning at $t=0$.

$L_G = 2\text{ nH}$

$R_G = 2\Omega$

$d = 1 \text{ cm}$

$S = 100 \text{ cm}^2$

From Eqs. (10) and (11) we find:

$$i_D^{\text{sat}} = 140 \text{ KA}; \quad v_D^{\text{sat}} = 720 \text{ KV}.$$

These values are actually attained in the numerical solutions.

The simulation results are:

$$i_D^{\text{sat}} = 132 \text{ KA} ; \quad V_D^{\text{sat}} = 735 \text{ KV} .$$

The results are presented in Figs. 4a and 4b. As one can see, the agreement between the numerical and simulation results is very good, thus giving us additional confidence in our model.

Next, we used our model to simulate several reflex diode cases [6]. A typical simulation result is presented in Fig. 5a. For comparison, a typical experimental result is also reproduced [9] in Fig. 5b. There appears to be good qualitative and in several respects quantitative agreement between the two [3,9]. A major difference between the simulation and the experiment is in the time scale of the current and voltage development. The externally applied pulse rises more slowly in the experiment. The ion source is also formed only after approximately 20 nsec (in the simulation the ion source is assumed to be available from the beginning). In the simulation we used lower than real values for L_G and m_i/m_e to speed up computation. The current saturation time in both simulation and experiments corresponds closely to:

$$t^{\text{sat}} \approx t_g + (2.2L_G/R_G), \text{ which is expected to be true for any } L_G.$$

Concerning the simulation results, more study is needed to find the dependence of $i_D(t)$, $V_D(t)$ and i_1^{cm}/i_D on L_G , m_i/m_e , S and d . Alternatively, a better time-centering of the circuit equation is needed to handle longer simulation times and higher current densities. In our simulations we use realistic values for V_{ext} , τ and R_G , because i_D^{sat} and V_D^{sat} depend mainly on these parameters. Also d is close to the experimental values. The cathode area S

cannot be made too small, because it may increase the current density to values which presently make the code unstable numerically.

In general, however, both simulation and experimental results display the same functional relationship for $V_D(t)$ and $i_D(t)$.

Other similar features are:

- a. The diode voltage collapses and stabilizes at a value corresponding to $N_T^{2/3}$, as required by theory [6];
- b. The diode current first exponentiates and then saturates at the predicted value;
- c. The diode voltage displays coherent fluctuations still to be investigated;
- d. Significant current density gains over the Child-Langmuir value are present in both simulation and experiments.

In future simulations we plan to include the energy threshold for ion source formation at the anode and the diode closure effect which is present in all the experiments. Because of possible 2-d effects in the experiments (when B_z is not high enough), we could not expect a better agreement between simulation results and experiments.

V. NUMERICAL REMARKS

Previous attempts to provide a coupling scheme between a diode code and an external circuit proved to be unstable numerically. For example, a non-self-consistent model trying to directly subtract from the external voltage the $R_G i_D$ and $L_G \frac{di_D}{dt}$ terms as taken from the uncoupled code runs did not succeed because of the following reasons: (a) the requirement that $V_D(t)$ be essentially non-negative would pose unnatural restraints on the time dependence of $V_D(t)$, which may or may not be satisfied [it is easy to see this by using the circuit equation and the Child-Langmuir law (Eqs. 6 and 10)]; (b) the inductive, current-noise generated term $L_G \frac{di_D}{dt}$ is most of the time much larger than $V_{ext}(t)$ in the uncoupled code, because of the discreteness of the charge emission mechanism (a few particles are emitted at each time step); even averaging the current over many time steps at a time could not reduce the inductive term below the externally applied voltage.

Our new coupling model, as described in Section III, is quite stable both physically and numerically, because of the $L_G \frac{di_D}{dt}$ term, which opposes any change in the current. The current noise is much lower than in the uncoupled model, satisfying in the steady-state regime: $|L_G \frac{di_D}{dt}| \ll V_D$.

The choice of the simulation parameters should fulfill some basic requirements. First, the time step should be small enough to allow rapid time variations of the physical quantities. For example, we require $\Delta v_{el} < v_{el}^{max} (v_e/c)$ at any time, where v_{el} is the electron speed and c is the light speed. Taking the maximum possible value for the electric field (when the A-K voltage spans

across a few simulation cells), we get: $\Delta t < (\Delta z/v_D^{sat})(m_e c/e)$. This is formally similar to a Courant-type condition, $\Delta z > c\Delta t$, in which the fastest electrons are not allowed to travel over more than one cell during one time step in order to correctly sample the space-varying field. In reflex diode cases with high current densities, situations with high and rapidly space and time varying electric fields often occur, especially after diode voltage stabilization, when electrons accumulate near the electrodes. Thus, quite small time steps must be used in these cases. On the other hand, very short time steps cause prohibitively long computation times or large accumulation errors. A higher order time centering of the circuit equation can improve the accuracy of the model, for long simulation times and high, rapidly varying electric fields.

A separate condition exists on Δz , to ensure that the system can accommodate the highest physically attainable currents in the system. This can be estimated from: $i_D^{sat} < K(V_D^{sat})^{3/2} \cdot S/\Delta z^2$, where K is the Child-Langmuir constant. This condition poses an upper limit on Δz , which together with d , determines the minimum number of simulation cells NZ to be used ($d = NZ \cdot \Delta z$) for given v_{ext} , R_G and S .

The problems which arise in choosing Δz and Δt are illustrated in Figs. 6 and 7. In Fig. 6, the parameters are similar to those in Fig. 5a, except for S , which is 1 mm^2 . The current density and the electric fields become very high, and both Δt and Δz (as used in Fig. 5a) become insufficiently small. To make Δt small enough would cause too long computation times. So we reduced Δz , by increasing NZ from 128 to 1024. As one can see, the stability is better, but still unsatisfactory, for the smaller Δz . In Fig. 7 the parameters

are similar to Fig. 5a, except for S which is 10 mm^2 , and NZ which is 1024. The numerical stability of the results is still not sufficient, although the maximum current density is reduced by a factor of 10 in comparison with Fig. 6. This means that Δt is still too big.

A different problem exists concerning the physical parameters of the simulations. In all our simulations we used realistic values for V^{ext} , R_G and τ , because i_D^{sat} and V_D^{sat} depended mainly on them. However, for L_G and m_i/m_e we chose values much lower than in the experiments. We did this in order to reduce the computational times to acceptable levels. A study of the scaling-up of the simulation results with these and other parameters is necessary. While the dependence of the current time development on L_G is more obvious ($\tau^{\text{sat}} \sim \tau_S + 2.2 L_G/R_G$), the effect of m_i/m_e on the various current components in the diode is critical and should be carefully investigated.

VI. CONCLUSIONS

This is the first successful attempt to our knowledge to provide a self-consistent computer simulation model for the time-dependant behavior of a 1-d diode coupled to an external inductive circuit. A current-voltage relationship similar to the Child-Langmuir law is not assumed. The emitted electron and ion currents are determined by both the total diode current, which is advanced according to the circuit equation and by the absorbed electrodic currents, which are calculated by the simulation code.

For the first time, a direct comparison can be made between simulation results and experimental oscilloscope traces describing the diode current and voltage as functions of time. The agreement is quite encouraging. Some recent analytical predictions are also corroborated by the simulation results. More technical improvements are necessary in order to deal with long simulation times and very high current densities.

In the absence of a self-consistent time-dependent and inductive analytical theory, it seems to us that our computer simulation model provides an indispensable tool for the explanation and guidance of future reflex diode experiments.

ACKNOWLEDGEMENTS

†Work done under the auspices of the University of Maryland - NRL
Joint program in Plasma Physics.

We are grateful to Adam Drobot for critically reading the
manuscript.

REFERENCES

1. D. S. Prono, J. W. Shearer and R. J. Briggs, Phys. Rev. Lett. 37, 21 (1976).
2. J. Golden, C. A. Kapetanakis, Roswell Lee and Shyke A. Goldstein, Sandia Laboratory Report No. SAND76-5122, Vol. I, p. 635 (1976).
3. D. S. Prono, H. Ishizuka, B. Stallard and W. C. Turner, Bull. Amer. Phys. Soc. 23, 903 (1978).
4. J. M. Creedon, I. D. Smith and D. S. Prono, Phys. Rev. Lett. 35, 91 (1975).
5. T. M. Antonsen, Jr. and E. Ott, Phys. Fluids 19, 52 (1976).
6. A. Sternlieb, Shyke A. Goldstein and Roswell Lee, Bull. Amer. Phys. Soc. 23, 816 (1978); also University of Maryland Technical Report #79-059, December 1978.
7. A. Sternlieb, Shyke A. Goldstein and Roswell Lee, 1979 IEEE International Conference on Plasma Science, June 4-6, 1979.
8. G. Cooperstein, Shyke A. Goldstein, J. J. Condon, D. D. Hinshelwood, D. Mosher and S. J. Stephanakis, Bull. Amer. Phys. Soc. 23, 800 (1978).

FIGURE CAPTIONS

Fig. 1. A symmetric reflex double diode coupled to an external circuit:

i_{el}^{em} = emitted electron current

i_{el}^{abs} = absorbed electron current

i_i^{em} = emitted ion current; i_A = anode current

i_i^{abs} = absorbed ion current; i_K = cathode current

R_G, L_G = generator impedance and inductance

ϕ = potential; V_D = diode voltage (= anode potential)

E = electric field (=0, at all electrodes)

V_{ext} = external voltage source

τ_r = rise time of the external pulsed voltage $V_{ext}(t)$

\oplus = a typical ion; \ominus = a typical electron

R.H.S. of diode has same currents (not represented).

Fig. 2: Flow-chart of the uncoupled code (Section II-A).

Fig. 3: Flow-chart of the coupled model (Section III).

Fig. 4: Numerical solutions vs. simulation results for a normal unipolar Child-Langmuir diode: (a) currents; (b) voltages.

Fig. 5: (a) Simulation results for a reflex diode:

$S = 10 \text{ cm}^2$; $\tau = 5 \text{ mil}$; $m_i/m_e = 25$; $NZ = 128$; $L_G = 0.5 \text{ nH}$;

$R_G = 0.6 \Omega$; $d = 0.5 \text{ cm}$; $\tau_r = 75 \text{ psec}$; $V_{ext}^{max} = 500 \text{ KV}$;

$V_f = 5\%$; polyethylene anode foil.

Note: 5 mil + 300 KV correspond to ≈ 4 reflexions

$$500 \text{ KV} = R_G \cdot i_D^{sat} + V_D^{sat} \begin{cases} i_D^{sat} \approx 330 \text{ KA} \approx 10 \cdot i_{C.L.} \\ V_D^{sat} \approx 300 \text{ KV} \end{cases}$$

(b) Experimental results for a reflex diode:

$S = 2 \text{ mm}^2$; $\tau = 2.5 \mu$ of Gold

$R_G = 1.5 \Omega$; $d = 0.5 \text{ cm}$

$\tau_r = 20 \text{ nsec}$; $V_{ext}^{max} = 700 \text{ KV}$

$L_G = 50 \text{ nH}$; $V_D^{OP}(\tau) = 240 \text{ KV}$

$m_i/m_e = 1836$; $V_f = 0$

Fig. 6: Same as Fig. 5a, but $S = 1 \text{ mm}^2$ and NZ is 128 and 1024.

Fig. 7: Same as Fig. 5a, but $S = 10 \text{ mm}^2$, $NZ = 1024$.

Note: The fluctuations in $V_D(t)$ are mainly due to the $L_G \frac{di_D(t)}{dt}$ term.

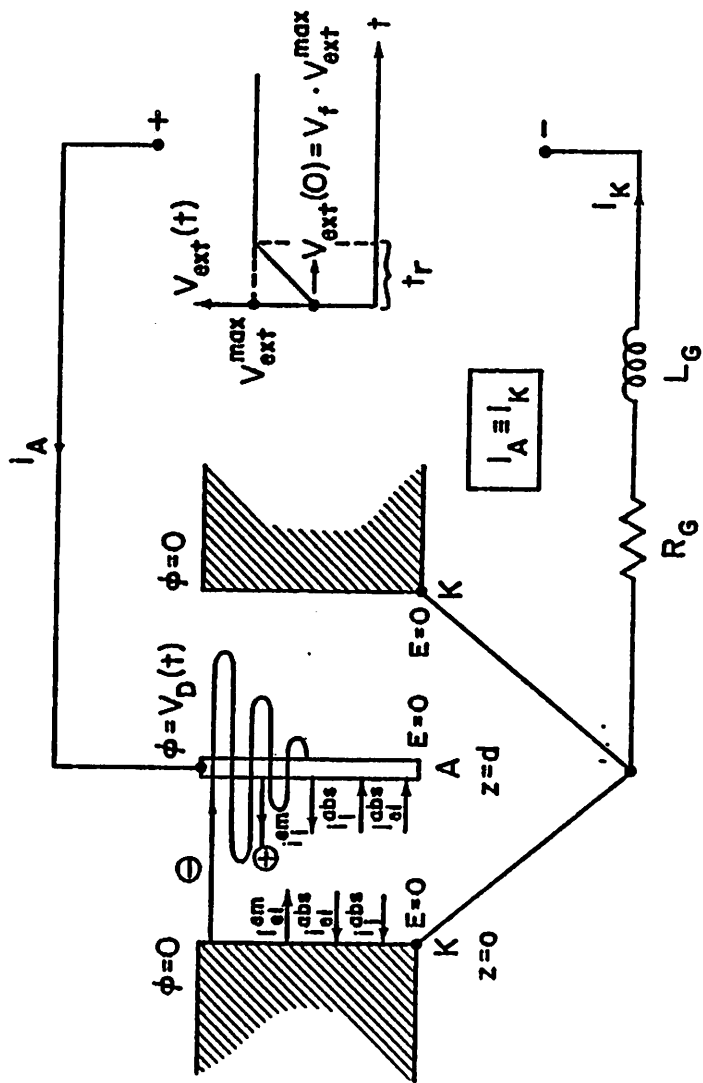


Figure 1

FLOW CHART OF THE UNCOUPLED 1-D CODE

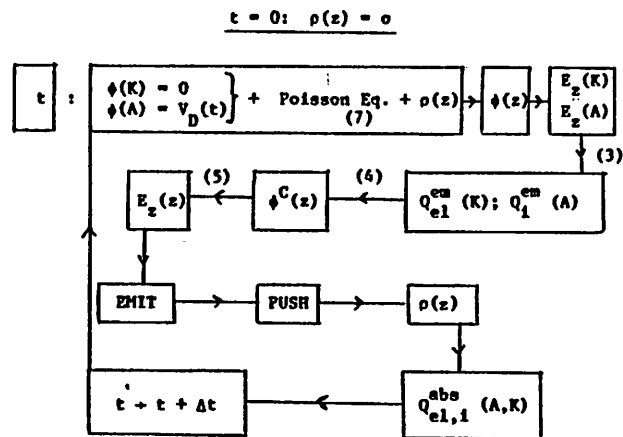


Figure 2

FLOW CHART OF THE COUPLED MODEL

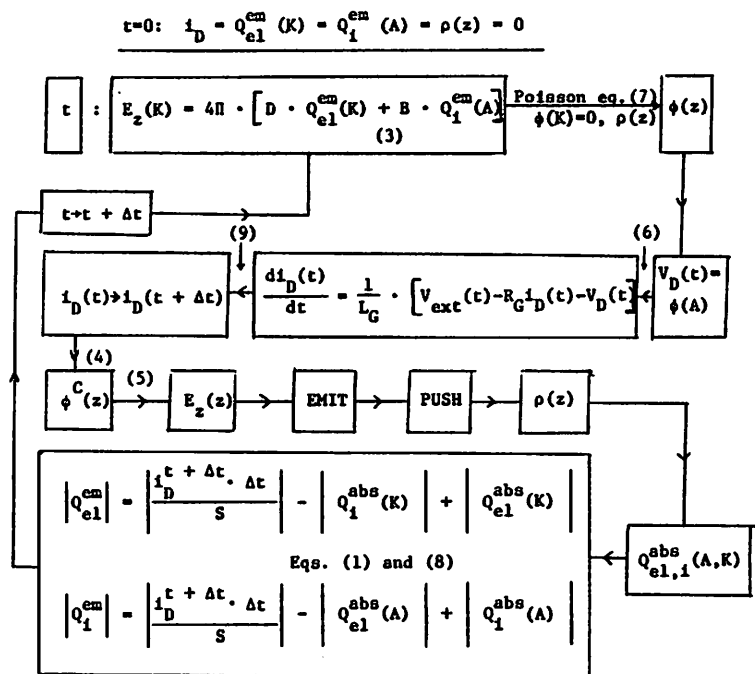


Figure 3

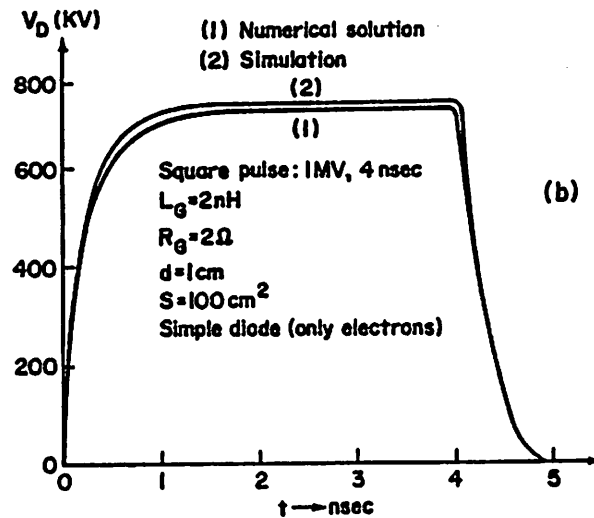
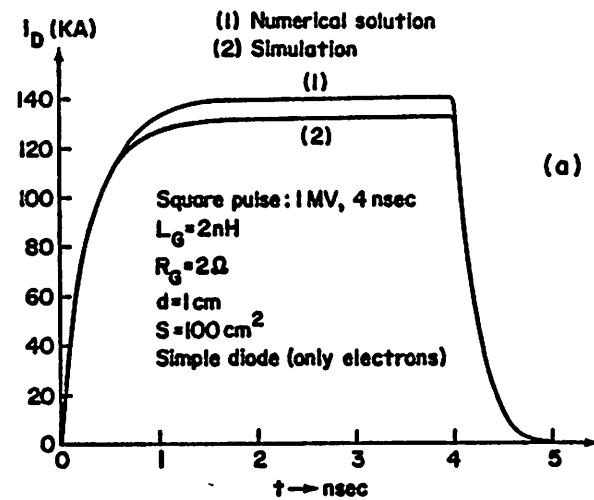


Figure 4

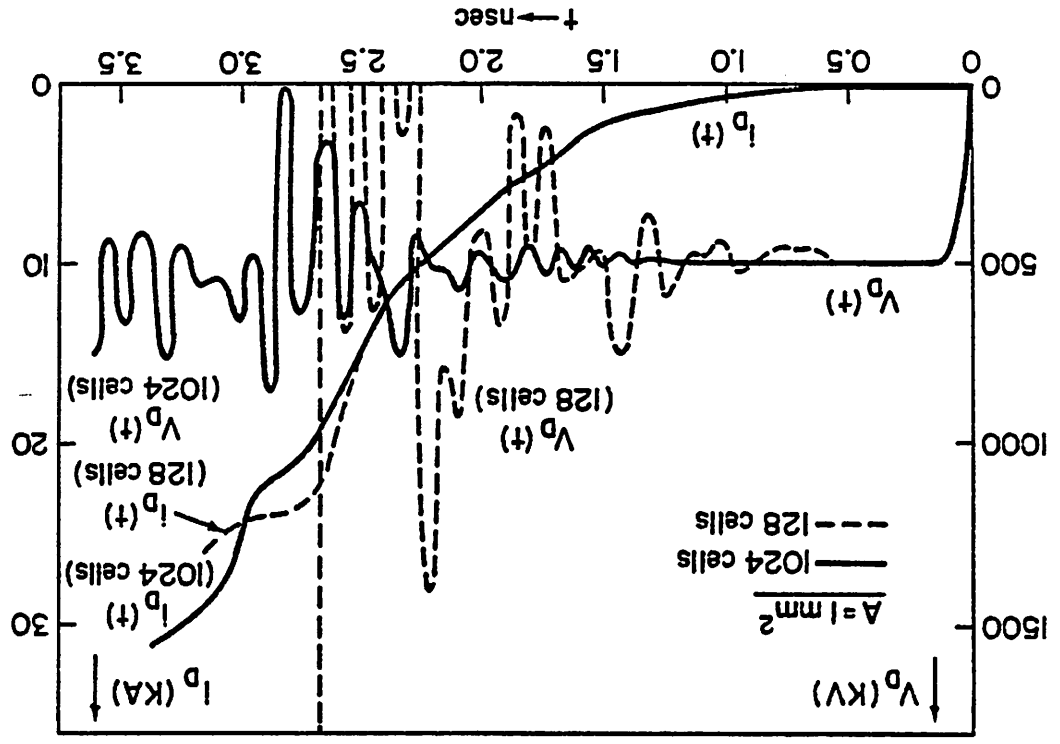


Figure 6

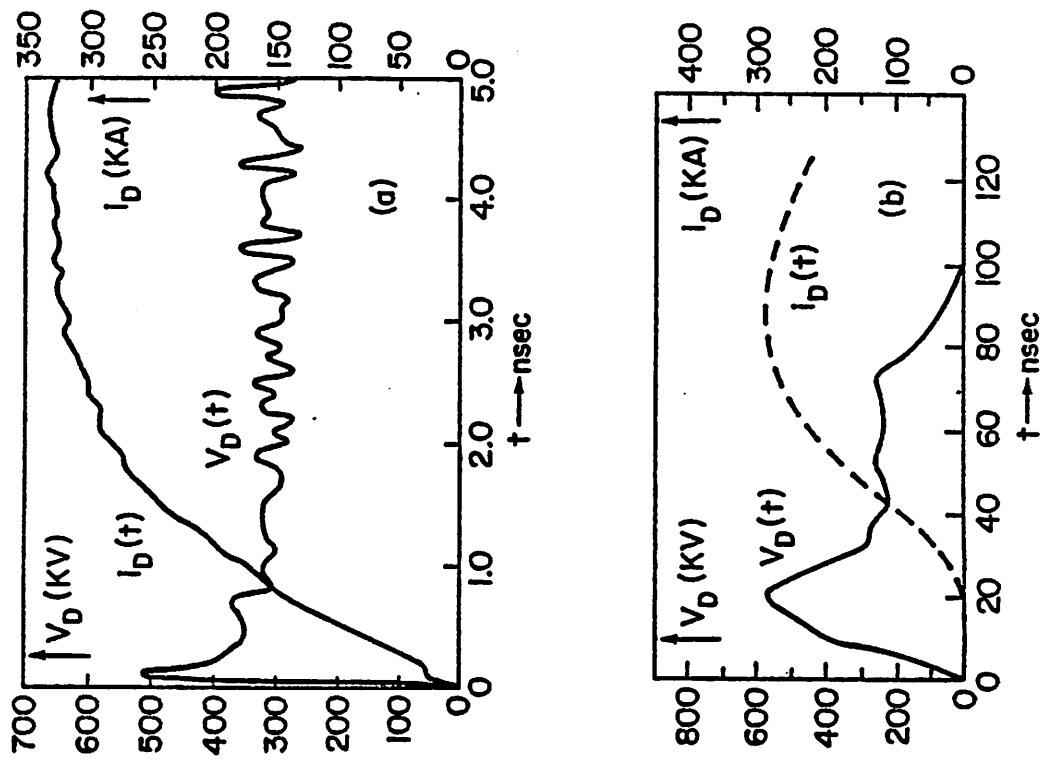
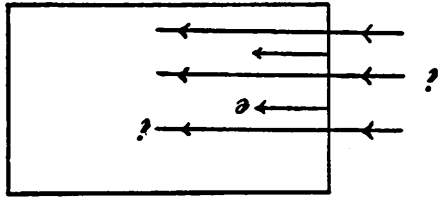


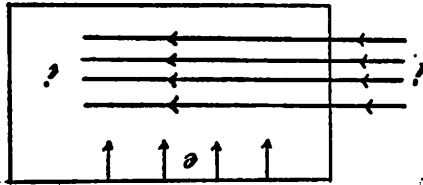
Figure 5

EXAMPLES: REACTOR CHAMBER, COLLECTIVE ION ACCELERATION



B. LONGITUDINAL

EXAMPLES: PULSELAC, ION DIODES



A. TRANSVERSE

SIMULATION OF SPACE CHARGE NEUTRALIZATION OF BEAMS

34



Handwritten notes:
 2.2. 1974
 J. J. ...
 ...

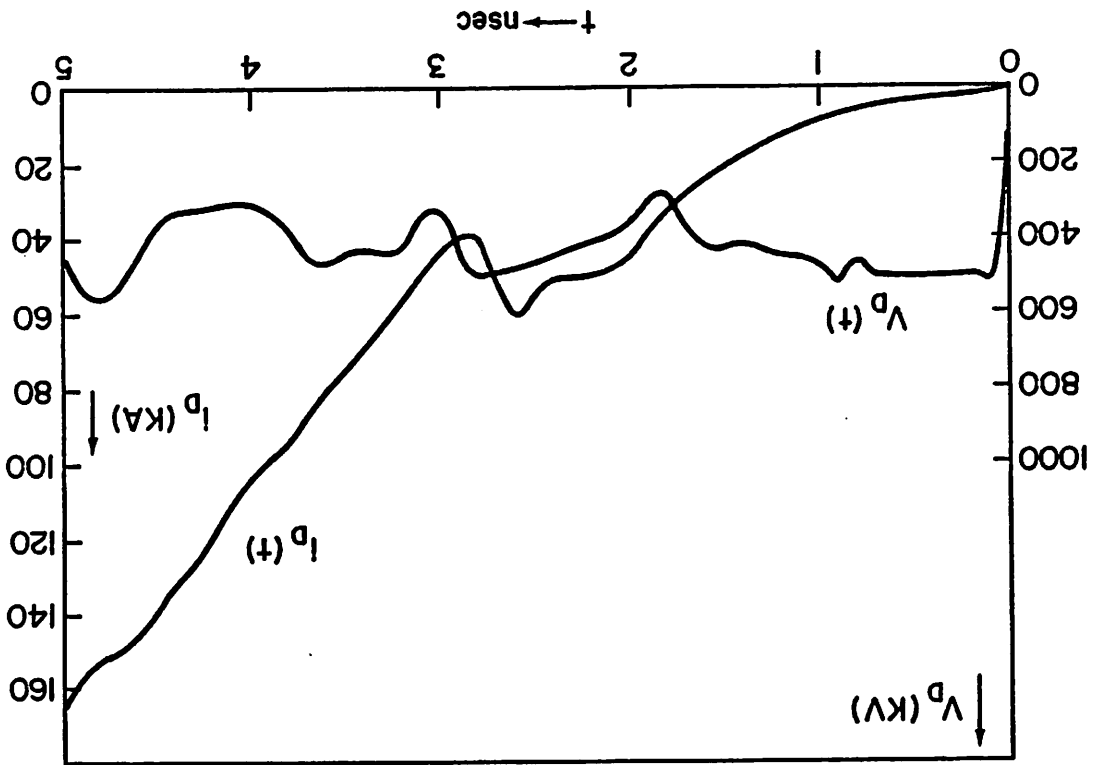


Figure 7



PROBLEM

FIND TIME DEPENDENT DENSITIES AND FIELDS
(MAY HAVE APPLIED B)

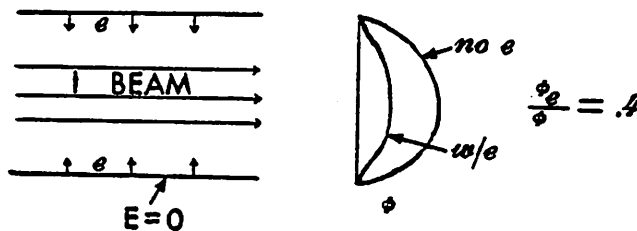
APPROACHES

1. ANALYTIC 1-D MODELS
2. QUASI-STATIC CODES, 1-D AND 2-D
 - A. FLUID I, PARTICLE E
 - B. PARTICLE I, $n_e = \exp(-e\phi/kT)$
 - C. PARTICLE I, PARTICLE E
 - D. SUGGESTED BY GODFREY: PARTICLE I, $F_e(H,P)$
3. EM CODES

492

IS SC NEUTRALIZATION AUTOMATIC?

NO: 1-D ANALYTIC EXAMPLE, TRANSVERSE



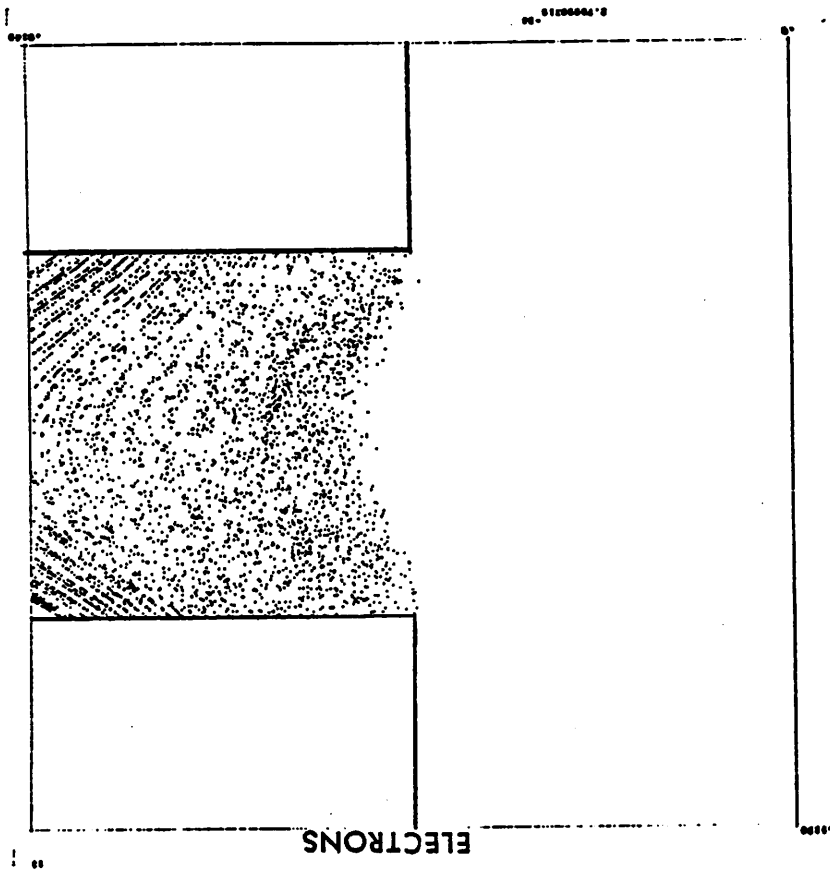
WHO CARES?

UNLESS SC NEUTRALIZATION OBTAINS TO "HIGH" DEGREE IN
"SHORT" TIME, MANY ICF SCHEMES FAIL.

493

56h
91

87-11 dmf

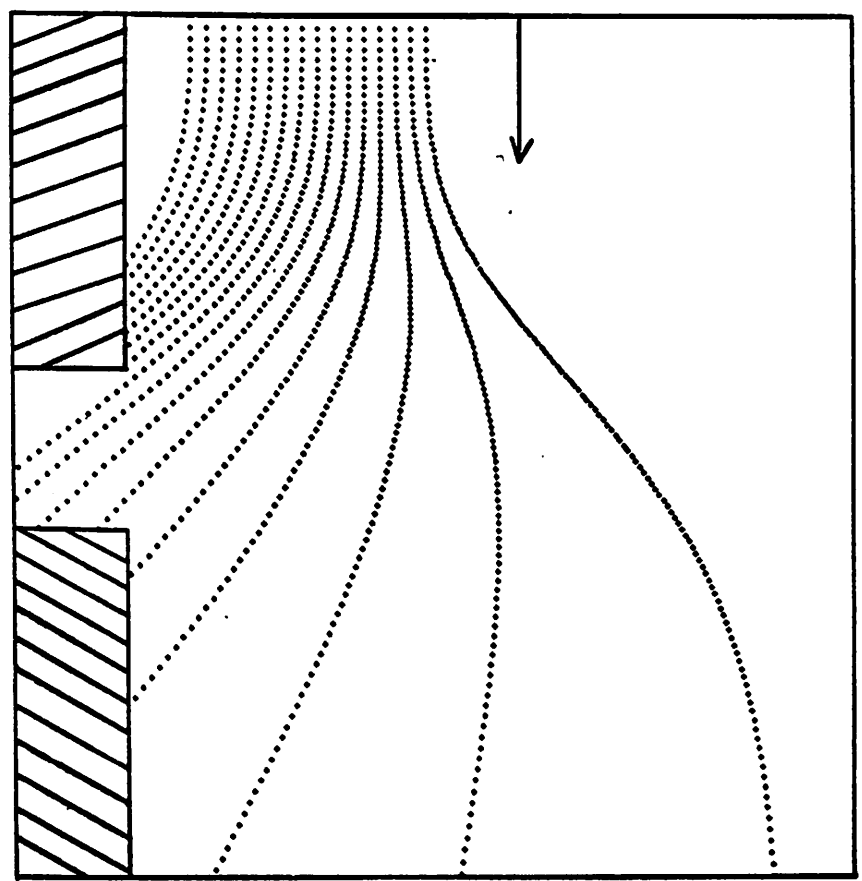


ELECTRONS

499

 Sandia Laboratories

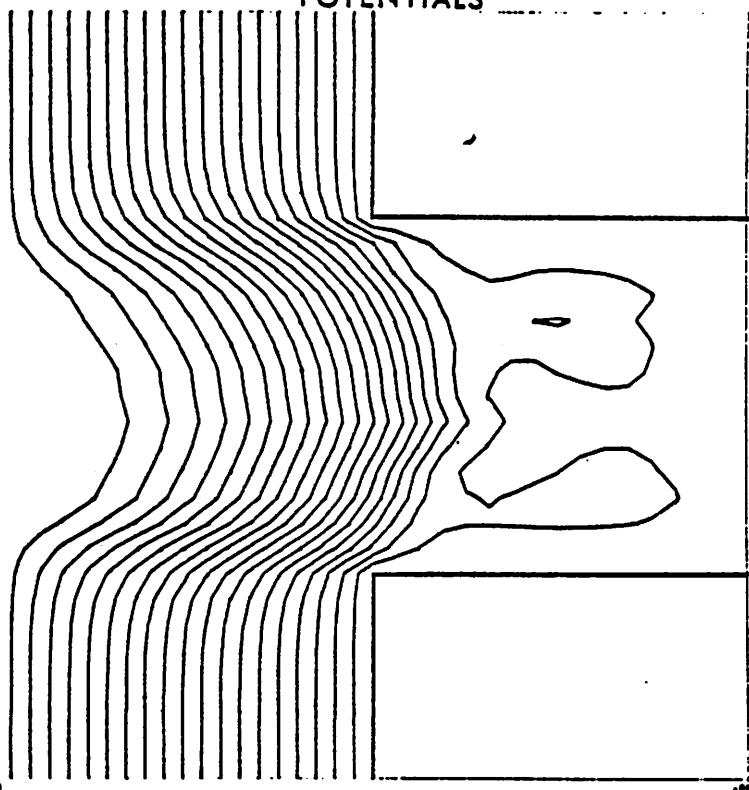
NONNEUTRAL ION BEAM



Z

4

POTENTIALS

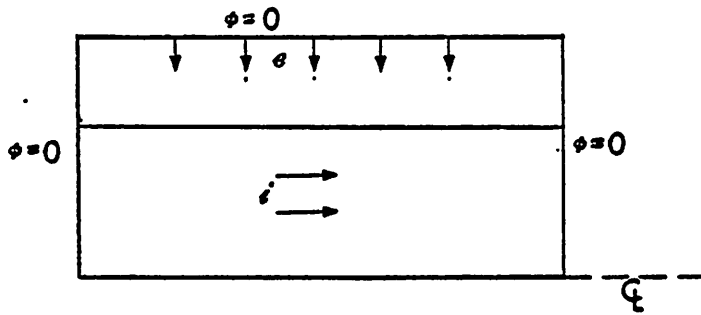


57

jwp 11-79

496

PERFECT NEUTRALIZATION IMPOSSIBLE

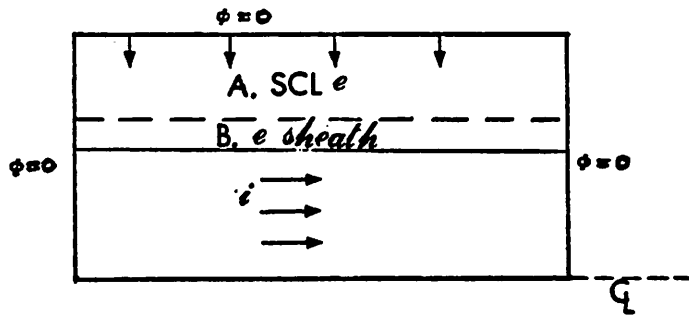


$$\rho = 0 \rightarrow \nabla^2 \phi = 0; \phi_p = 0 \rightarrow \vec{E} = 0$$

REAL SYSTEM $\left\{ \begin{array}{l} \rho \neq 0 \rightarrow \epsilon \text{ FREE STREAM TO WALLS} \\ n_1 \text{ NONUNIFORM} \rightarrow \text{NEED } \vec{E} \rightarrow \text{HAVE } \rho \end{array} \right.$

497

PARTIAL NEUTRALIZATION



A. SCL e FROM WALLS, $E_{BDY} = 0$,
 IGNORE ENDS $\rightarrow Q = 0$

\rightarrow I BEAM UNDERNEUTRALIZED

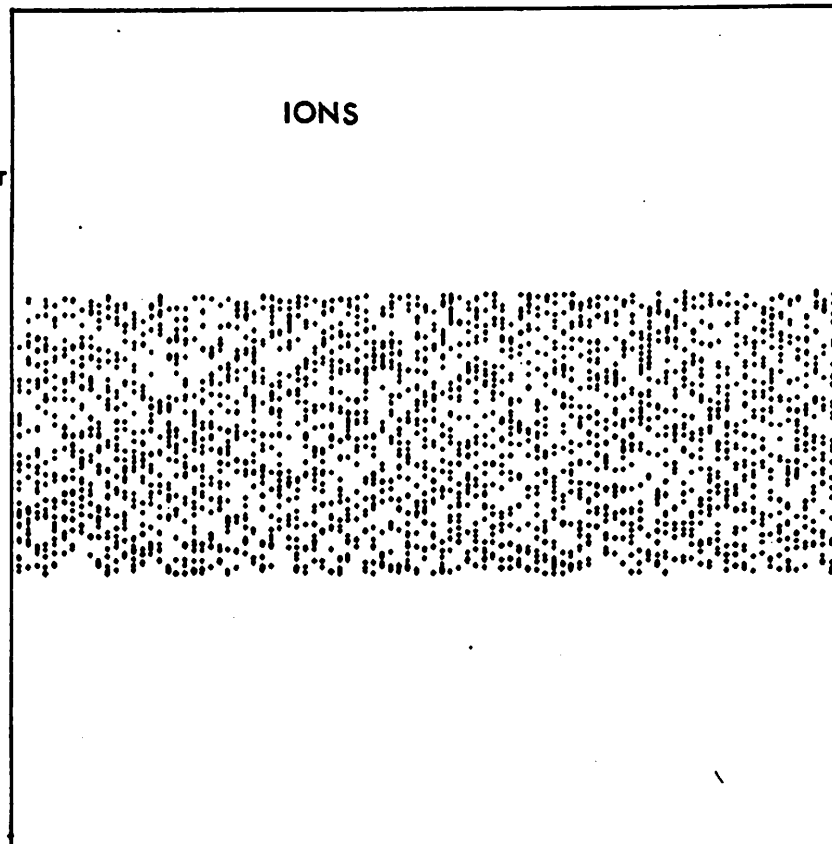
(CODE RESULT)

B. NO e FROM WALLS IN SS $\rightarrow e$ SHEATH λ_D

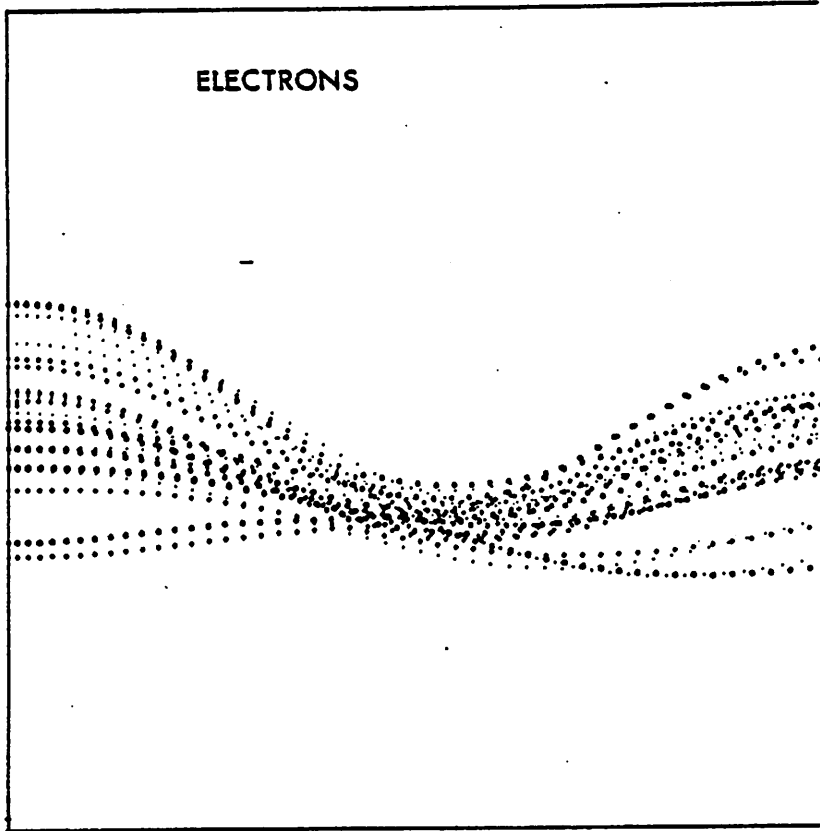
$n_e = n_i \exp(e\phi/kT)$ QUASINEUTRAL

CAN THE APPROACH TO QUASINEUTRALITY BE SIMULATED?

PULSELAC EXPERIMENT: NEUTRAL TO .2%, FEW ns

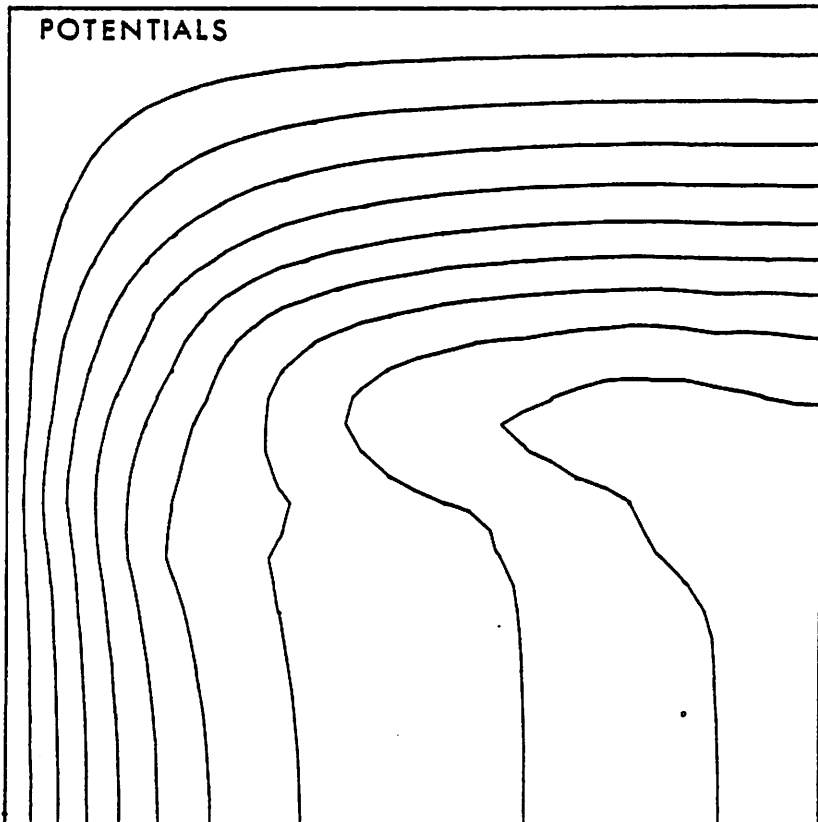


bh



z

505



506

The dispersion:
 $1 + \chi_e + \chi_i = 0$

$$\chi_i(k, \omega) = \sum_{j=1}^{N_b} \frac{N_j e^2}{m_i} \frac{1}{(\omega - k V_j)^2}$$

V_j, N_j - beams' velocity and density, respectively

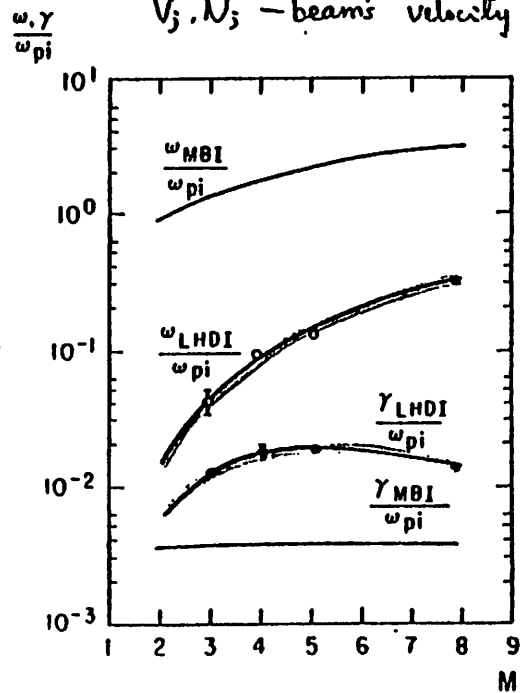


FIG. 1 Dispersion curves of the lower-hybrid drift mode and the fastest growing multibeam mode for the choice of parameters: $N = N_b = 16384$, $m_i/m_e = 1600$, $\omega_{pe}^2/\omega_{ce}^2 = 1$, $V_E/v_{te} = 0.424263$, $T_e = 0$, $L_n/L_s = 0$, and $L_n/L_T = 0$. Simulation data are denoted by circles ($\omega_{LHDI}/\omega_{pi}$) and dots ($\gamma_{LHDI}/\omega_{pi}$). $M = kL/2\pi$ is the mode number.

How to measure the growth rate and frequency of LHDZ from this E-field energy history plot?

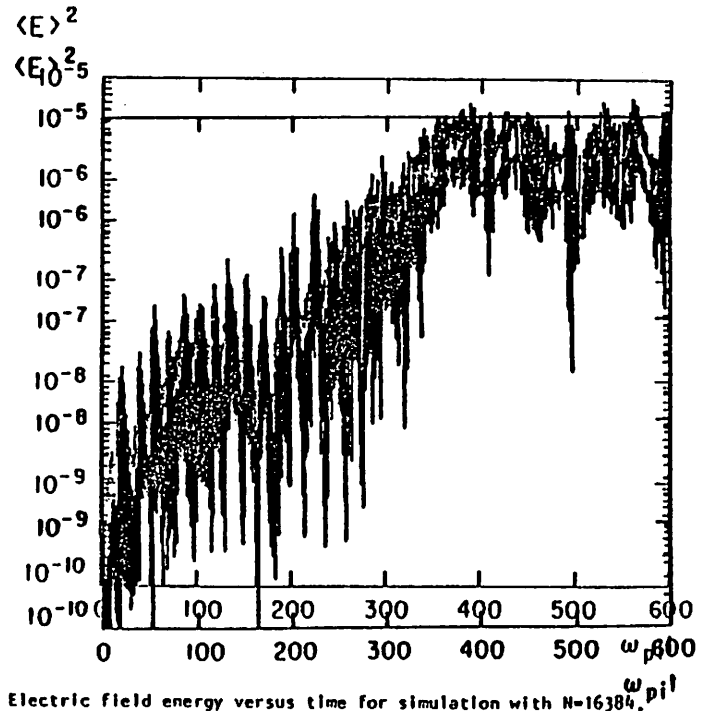


FIG. 2 Electric field energy versus time for simulation with $N = 16384$.
 FIG. 2 Electric field energy versus time for simulation with $N = 16384$, $T_e = 0$, $L_n/L_s = 0$, and $L_n/L_T = 0$, and $m_i/m_e = 1600$, $\omega_{pe}^2/\omega_{ce}^2 = 1$, $V_E/v_{te} = 0.424263$, $T_e = 0$, $L_n/L_s = 0$, and $L_n/L_T = 0$, and $M = 5$.



SUMMARY

1. SPACE CHARGE NEUTRALIZATION (SCN) CANNOT BE TAKEN FOR GRANTED.
2. SIMULATIONS OF SCN ARE IMPORTANT TO ICF AND HAVE THEIR OWN CLASS OF PROBLEMS, ASSOCIATED WITH TRANSITION FROM UNNEUTRAL BEAM TO QUASINEUTRAL PLASMA.
3. WORK IN PROGRESS TO DEVELOP NEW OR BETTER SIMULATION TECHNIQUES FOR SCN PROBLEMS. THE MOST PROMISING SEEM TO BE HYBRID APPROACHES.

504

5M multibeam. Instability Interference with

503

Lower Hybrid Drift Instability

(LHDI Simulation with hybrid ES1 Code)

Yu-Jivan Chen & C.K. Birdsall
(U.C. Berkeley)

Simulation of LHDI by using 1d particle-hybrid ES1.

ion - particle, unmagnetized ($k_{\perp} r_D \gg 1$)

$U_{Te} = 0$. (quasi static Maxwellian loader)

e^- - fluid, linear susceptibility χ_e

$$\chi_e = \chi_e(k, \omega; U_e, U_x)$$

$U_e =$ external $E \times B$ drift + e^- diamagnetic drift

$$\Rightarrow [1 + \chi_e(k, i\frac{\omega}{\Omega_e})] \hat{k}^2 \Phi_k = 4\pi \hat{P}_k$$

Objectives:

1. In the linear regime: _____ separate LHDI from MBI, _____ and measure LHDI's growth rate and frequency.

2. In the nonlinear regime: _____ study the saturation mechanism: a. constant U_e & T_e , b. readjust χ_e for $U_e(t)$ and $T_e(t)$.

1.

The growth rate is calculated by using

$$\gamma = \frac{\ln |\phi^2|_k(t_1) - \ln |\phi^2|_k(t_2)}{t_1 - t_2}$$

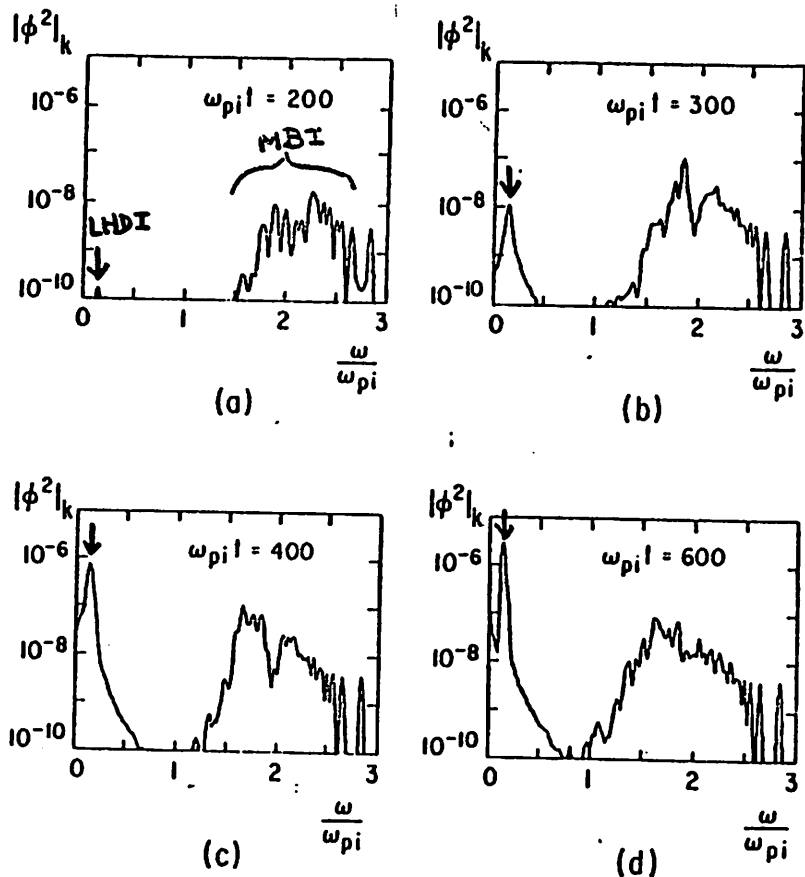
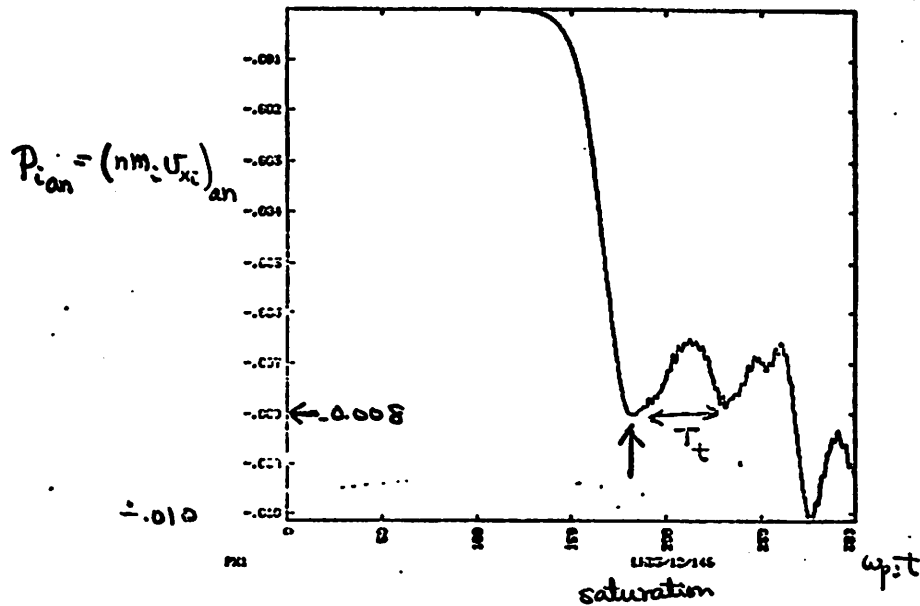


FIG. 3 Power spectrum $|\phi^2|_k(\omega)$ at (A) $\omega_{pi} T=200$, (B) $\omega_{pi} T=300$, (C) $\omega_{pi} T=400$, and (D) $\omega_{pi} T=600$ for $m_i/m_e=1600$, $\omega_{pe}^2/\omega_{ce}^2=1$, $V_E/v_{ti}=0.424263$, $T_e=0$, $L_n/L_T=0$, $L_n/L_T=0$, and $M=kL/2\pi=5$. The sharp peak at $\omega/\omega_{pi} \approx 0.136$ corresponds to the lower-hybrid drift instability. (by using ZED) 4

So, the LHD I tends to saturate at very high $\omega_{pi} T$ for $\omega_{pi} T$ large U_{de}/U_{ti} (= const. int.) It is shown that there are anomalous transport in P_i and $(k.E)_i$ momentum conservation:

$$P_i(t) + m_e U_{de}(t) = 0 + m_e U_{de}(0) \Rightarrow U_{de} = U_{de}(t)$$

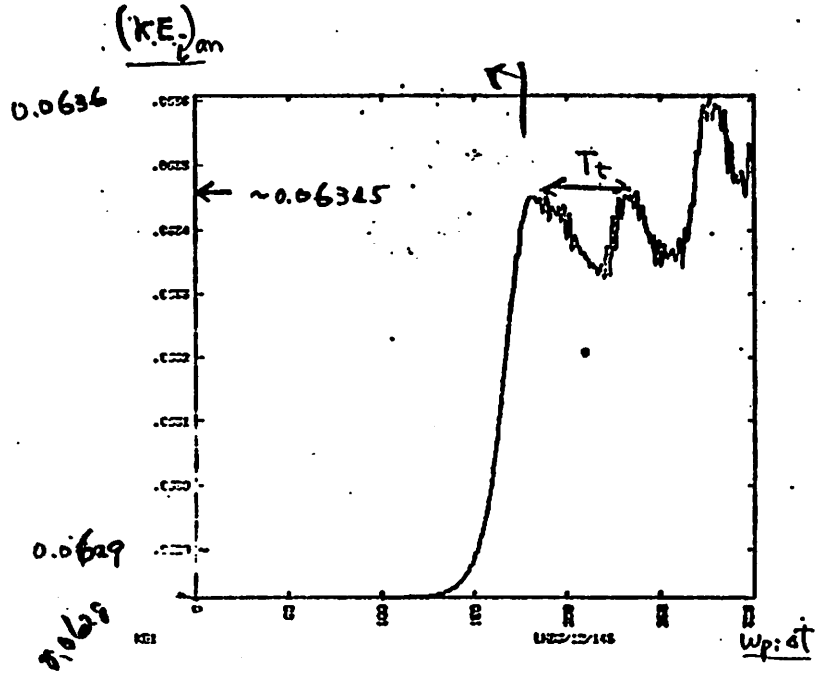


$N=16384$, $\omega_{pi} \omega t = 0.2$, $\lambda_{z}/\lambda_x = 1.44$, $m_i/m_e = 1600$
 $\omega_{pe}^2/\omega_{ce}^2 = 1$, $T_e=0$, $L_n/L_T=0$, $L_n/L_T=0$, $kL_D=0.70$
 $v_e/U_{ti} = 0.85 = \text{constant}$

energy conservation:

$$(KE_p)_{an}(t) + \langle E^2 \rangle(t) + \frac{1}{2} n m_e U_{de}^2(t) + \frac{T_e}{2}(t)$$

$$= \frac{1}{2} T_e(0) + \langle E^2 \rangle(0) + \frac{1}{2} n m_e U_{de}^2(0) + \frac{T_e}{2}(0)$$



$N = 16384$, $w_p t = 0.2$, $\lambda_{De}/\Delta x = 1.44$, $m_i/m_e = 1600$.

$w_{pe}/w_{ce} = 1$, $T_e = 0$, $L_n/L_0 = 0$, $L_n/L_T = 0$.

$k\lambda_D = 0.707$, $U_E/U_{ci} = 0.85$.

508

Change $U_E(t)$ and $T_e(t)$

509

1. as $n \leq n_{th}$

U_E^n, T_e^n — constant

2. as $n > n_{th}$

a. predictor

$\chi_e(U_E^{n+1}, T_e^{n+1}) = \chi_e(U_E^n, T_e^n)$

$\Rightarrow \begin{pmatrix} \phi_p^{n+1} \\ \langle E^2 \rangle_p^{n+1} \end{pmatrix} \Rightarrow \text{push } U^{n+1/2} \rightarrow U^{n+3/2}, \begin{pmatrix} P_i^{n+1/2} \\ KE_{ci}^{n+1} \end{pmatrix}$

b. corrector

momentum conservation

$U_{de}^{n+1} = U_{de}^0 + \frac{1}{nm_e} (P_{ip}^{n+1} - P_i^0)$

$P_{ip}^{n+1} = \frac{1}{2} (P_{ip}^{n+1/2} + P_i^{n+1/2})$

energy conservation

$\frac{1}{2} T_e^{n+1} = \frac{1}{2} T_e^0 + KE_{ci}^0 + \langle E^2 \rangle^0 + \frac{1}{2} n m_e U_{de}^0{}^2$
 $- KE_{ci}^{n+1} - \langle E^2 \rangle_p^{n+1} - \frac{1}{2} n m_e U_{de}^{n+1}{}^2$

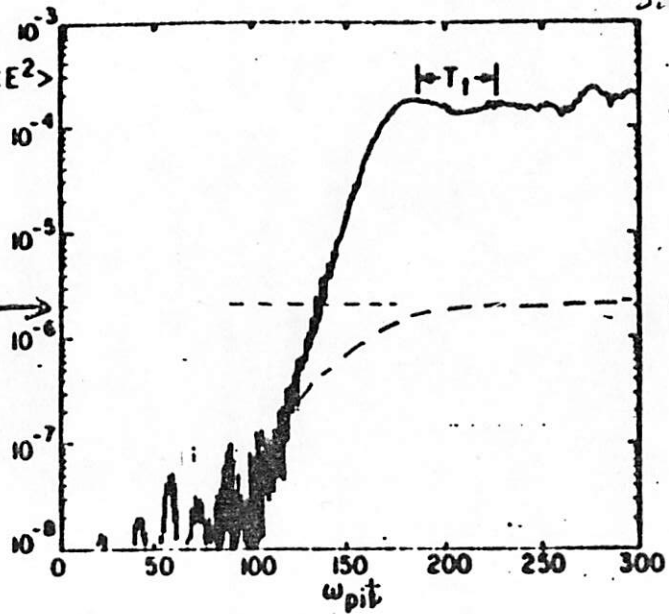
c^- drift velocity

$U_E^{n+1} = U_{de}^{n+1} - \frac{T_e^{n+1}}{U_{ce}} \left(\frac{\partial h}{\partial n} \right)$

$\chi_e(U_E^{n+1}, T_e^{n+1}) \Rightarrow \phi^{n+1}, \langle E^2 \rangle^{n+1} \dots$

(a) Keep U_E and $T_e \langle E^2 \rangle$
constant in time

the saturation level
predicted by the
anomalous transport
theory. (Davidson
and Gladd)



(b) $U_E(t)$ and $T_e(t)$

